University of Zagreb

FACULTY OF SCIENCE
DEPARTMENT OF BIOLOGY

Pavel Ankon

THE EFFECT OF TEMPERATURE ANOMALIES ON THE CORALS (ANTHOZOA) IN THE ADRIATIC SEA

DOCTORAL THESIS

Zagreb, 2026

University of Zagreb

FACULTY OF SCIENCE

DEPARTMENT OF BIOLOGY

Pavel Ankon

THE EFFECT OF TEMPERATURE ANOMALIES ON THE CORALS (ANTHOZOA) IN THE ADRIATIC SEA

DOCTORAL THESIS

Supervisor:

Petar Kružić, PhD, Full Professor

Zagreb, 2026

Sveučilište u Zagrebu

PRIRODOSLOVNO – MATEMATIČKI FAKULTET
BIOLOŠKI ODSJEK

Pavel Ankon

Utjecaj temperaturnih anomalija na koralje (Anthozoa) Jadranskog mora

DOKTORSKI RAD

Mentor:
Prof. dr. sc. Petar Kružić

Zagreb, 2026

This doctoral thesis was made at the *University of Zagreb, Faculty of Science, Department of Biology, Division of Zoology*, under the supervision of *Prof. Petar Kružić, PhD* as a part of the Doctoral programme of Biology at the University of Zagreb, Faculty of Science, Department of Biology. The research was financed by Croatian Science Foundation as part of the project UIP 2019-04-3389 „Utjecaj klimatskih promjena na bioraznolikost koralja – istraživanje slučaja masovnih ugibanja u Jadranskome moru (ADRICOR)“ and “Young Researchers’ Career Development Project – Training New Doctoral Students” (DOK-2020-01).

SUPERVISOR INFORMATION

Prof. Petar Kružić, PhD

Petar Kružić finished elementary and high school in Zagreb and graduated in biology, majoring in ecology, in 1996 from the Division of Biology of the Faculty of Science in Zagreb. He defended his master's thesis in 2001, and then in 2005, his doctoral dissertation in the field of Oceanology with a topic in the field of coral biology and ecology. Since 2016, he has been working as an associate professor, and since 2023 as a full professor at the Division of Biology, Faculty of Science in Zagreb. Since 1997. To this day, he participates in undergraduate and graduate teaching at the Faculty, first as a practicum leader, and then as a lecturer in the courses Biological Oceanography, Marine Management and Protection, Marine Biodiversity, and Diversity of Fauna of Croatia. At the doctoral study of Oceanology, he is the lecturer of the course Conservation and Protection of Marine Biodiversity and Zoobenthos. Since 2013, he has been participating in graduate teaching at the University of Primorska (Koper, Slovenia). He underwent scientific and professional training in the field of marine biology, especially coral biology and ecology, at the Institut für Zoologie at the Universität Wien, Vienna, Austria; Station Marine d'Endoume, Centre d'Oceanologie, Université de la Méditerranée, Marseille, France; Marine Reserve "Miramare" in Trieste; ENEA Marine Research Centre, La Spezia, Italy, and at the Piran Marine Biology Station in Slovenia. Since 2020, he has been an associate of the GFCM EU (General Fisheries Commission for the Mediterranean FAO), participating in the work of the commission for the protection of red coral (*Corallium rubrum*) in the Mediterranean Sea. He has been the president of the Croatian Biological Society (HBD) since 2024. Scientific and professional activity of Petar Kružić includes the study of macrozoobenthos in the Adriatic, especially the Cnidaria group; biological and ecological characteristics of isolated habitats in the Adriatic (estuaries, sea lakes, underwater caves, coral reefs); seagrass settlements *Posidonia oceanica*; "sea bloom" along the Adriatic coast; conservation of Adriatic biodiversity, classification and mapping of marine benthic habitats in the Adriatic, ecology of benthic habitats in the Adriatic; deep-sea coral communities in the Adriatic; and research and monitoring of coralligenic biocenosis in the Adriatic. He also deals with the impact of climate change on benthic species, primarily corals, in the Adriatic Sea.

ACKNOWLEDGEMENTS

University of Zagreb

Faculty of Science

Department of Biology

Doctoral thesis

The effect of temperature anomalies on the corals (Anthozoa) in the Adriatic sea

Pavel Ankon

Division of Zoology, Department of Biology, Faculty of Science, Horvatovac 102a, 10000 Zagreb

This doctoral thesis investigates the impacts of climate change, particularly marine heatwaves (MHWs), on four scleractinian and two octocoral species across the northern, central, and southern Adriatic over the period 2020–2023, evaluating changes in the microbiome, tissue integrity, and population condition. In situ temperature records collected along a depth gradient extending to 40 m were integrated with morphological, histological, and molecular analyses to assess species-specific responses to heat stress. The results demonstrate that thermal anomalies induce pronounced, yet species-dependent responses, in all analysed coral species. Both scleractinian and gorgonian corals revealed increased mortality and tissue degradation across all study stations, while population density remained relatively stable over the study period. Bleaching emerged as a sensitive but species-specific response restricted to symbiotic taxa. Histological analyses of all species revealed both sublethal and lethal alterations across all tissue layers, including symbionts, consistent with known cellular responses to heat stress. Microbiome assessments indicated lesion-related shifts in host–microbe associations and patterns of stress-induced dysbiosis. The recorded species-specific differences in external and internal lesions indicate that vulnerability is shaped by growth form, trophic strategy, life-history traits, and the environmental context in which species occur. Overall, these results provide novel insights into coral responses and resilience to thermal anomalies, and contribute to improved predictions of future Adriatic ecosystem dynamics under accelerating climate change.

(261 pages, 75 + 22 figures, 13 + 12 tables, 282 references, original in English)

Keywords: climate change, marine heat waves, Adriatic sea, scleractinians, octocorals

Supervisor: Prof. Petar Kružić, PhD, Full Prof.

Reviewers: Assoc. Prof. Sunčica Bosak, PhD

Lovenc Lipej, PhD, Full Prof.

Assoc. Prof. Tvrtko Dražina, PhD

Sveučilište u Zagrebu Doktorski rad

Prirodoslovno-matematički fakultet

Biološki odsjek

Utjecaj temperaturnih anomalija na koralje (Anthozoa) Jadranskog mora

Pavel Ankon

Zoologijski zavod, Biološki odsjek, Prirodoslovno-matematički fakultet, Biološki odsjek, Horvatovac 102a, 10000 Zagreb

Ova doktorska disertacija istražuje utjecaj klimatskih promjena, s posebnim naglaskom na morske toplinske valove (MHW), na četiri vrste kamenih koralja i dvije vrste gorgonija u sjevernom, srednjem i južnom Jadranu tijekom razdoblja od 2020. do 2023. godine. U radu se analiziraju promjene u mikrobiomu, integritetu tkiva i stanju populacija, pri čemu su podaci temperature mora prikupljeni *in situ* duž dubinskog gradijenta do 40 m dubine te objedinjeni s rezultatima morfoloških, histoloških i molekularnih analiza radi procjene specifičnih odgovora pojedinih vrsta na toplinski stres. Rezultati pokazuju da toplinske anomalije uzrokuju izražene, ali za vrste specifične odgovore kod svih analiziranih vrsta koralja. Kod kamenih koralja i gorgonija zabilježeni su povećana smrtnost i degradacija tkiva na svim istraživanim postajama, dok je gustoća populacija tijekom istraživanog razdoblja ostala relativno stabilna. Izbjeljivanje se pokazalo kao osjetljiv, za vrste specifičan odgovor ograničen na simbiotske taksone. Histološke analize svih vrsta otkrile su subletalne i letalne promjene u svim slojevima tkiva, uključujući i simbionte, što je u skladu s poznatim staničnim odgovorima na toplinski stres. Analize mikrobioma ukazale su na promjene u odnosima domaćin–mikroorganizam povezane s pojavom lezija, kao i na obrasce disbioze uzrokovane stresom. Uočene razlike između vrsta u vanjskim i unutarnjim lezijama upućuju na to da osjetljivost pojedinih vrsta oblikuju morfologija rasta, trofička strategija, obilježja životnog ciklusa i okolišni uvjeti u kojima obitavaju. Dobiveni rezultati donose nove spoznaje o odgovorima koralja na toplinske anomalije i njihovoj otpornosti na takve poremećaje te pridonose pouzdanijem predviđanju buduće dinamike jadranskih ekosustava u uvjetima ubrzanih klimatskih promjena.

(261 stranica, 75 + 22 slika, 13 + 12 tablica, 282 literaturnih navoda, jezik izvornika engleski)

Ključne riječi: klimatske promjene, morski toplinski valovi, Jadransko more, kameni koralji, gorgonije

Mentor: Prof. dr. sc. Petar Kružić

Reviewers: Izv. prof. dr. sc. Sunčica Bosak

Prof. dr. sc. Lovenc Lipej

Izv. prof. dr. sc. Tvrtko Dražina

Table of Contents

1. INTRODUCTION

Environmental change poses a major challenge to species with limited mobility, particularly sessile organisms that rely on pre-existing phenotypic plasticity or genetic adaptations to ensure survival (Visser, 2008). Unlike mobile organisms that may avoid unfavourable conditions through migration or behavioural adjustments, sessile invertebrates are confined to specific habitats and must endure environmental fluctuations *in situ*. Their long lifespans, slow growth, and narrow ecological tolerance make them especially vulnerable to rapid changes in temperature, chemistry, and circulation patterns. As a result, climate-driven stressors can have immediate impacts not only on individual physiology but also on population viability and ecosystem stability. Understanding the mechanisms of adaptation in different species is essential for assessing their present health status and predicting responses to ongoing climate change (Waller et al., 2018). These issues are especially pronounced in marine benthic ecosystems, where climate-induced pressures have profound ecological consequences.

The Mediterranean Sea is recognised as one of the most sensitive and fragile regions in the world, since it is a semi-enclosed basin with one of the greatest areas of biodiversity (Coll et al., 2010). Environmental stressors associated with climate change such as warming, acidification, mass inundation, etc., have a significant impact on marine ecosystems (Kružić 2015). Changes in the Mediterranean area are directly reflected to the Adriatic Sea, where they are projected to alter the hydrogeological cycle (through reduced precipitation and enhanced evaporation), nutrient dynamics and primary production, as well as seawater temperature, circulation patterns, and thermohaline circulation (Vilibić et al., 2013; Waller et al., 2018; Fader et al., 2020).

Over the past three decades, mass mortality events in the Mediterranean have been consistently associated with positive thermal anomalies (Hughes et al., 2003; Garrabou et al., 2009). During the two most severe events in 1999 and 2003, seawater temperatures increased up to 4 °C above average, affecting nearly 30 species, particularly those inhabiting colder and deeper waters such as gorgonians, down to depths of 40 m (Cerrano et al., 2000; Perez et al.,

2000; Cupido et al., 2009; Bensoussan et al., 2010; Crisci et al., 2011). Subsequent years (2006–2009) also recorded localised anomalies that negatively impacted benthic communities in several Mediterranean regions (Coma et al., 2009; Bensoussan et al., 2010; Lejeusne et al., 2010; Maldonado et al., 2010; Cebrian et al., 2011). These events varied in spatial extent and severity depending on local hydrological conditions, and species responses ranged widely, from minimal to extensive mortality, even within the same thermal regimes (Garrabou et al., 2001, 2009; Linares et al., 2005). While most mass mortality reports concern the north-western Mediterranean (Spain, France, Italy), fewer studies have addressed the eastern basin, including the Adriatic Sea, despite its vulnerability (Di Camillo et al., 2013; Kružić et al., 2016).

At the organismal level, elevated seawater temperature induces metabolic dysfunction, oxidative stress, and physiological imbalances, which can compromise growth, reproduction, and survival. Thermal stress also disrupts host–symbiont interactions, leading to coral bleaching: under elevated temperatures, photosynthetic endosymbionts produce reactive oxygen species that damage host tissues, ultimately causing their expulsion. Although bleached corals may survive temporarily, their weakened condition increases susceptibility to disease and starvation. In parallel, warming promotes the proliferation of pathogens while suppressing host immune defences, thereby exacerbating host–pathogen dynamics (Danovaro et al., 2009; Vezzulli et al., 2010). Such processes have been implicated in large-scale mortalities across multiple sessile invertebrate taxa, including sponges, bivalves, bryozoans, ascidians, and corals (Cerrano et al., 2000; Perez et al., 2000; Garrabou et al., 2009; Vázquez-Luis et al., 2017).

Among sessile invertebrates, corals are particularly vulnerable because of their stenovalent nature and narrow ecological tolerance. Their structural complexity, symbiotic associations, and reliance on stable environmental conditions make them especially sensitive indicators of climate-driven stress. Despite extensive documentation of mass mortality events in the north-western Mediterranean, the eastern basin, including the Adriatic Sea, remains comparatively understudied. Investigating coral responses at multiple levels—morphological, histological, and microbial—offers a multidimensional perspective on how thermal stress compromises organismal integrity. This integrative framework provides critical insights into species resilience

and vulnerability, and is essential for predicting the trajectories of Mediterranean coral communities under accelerating climate change.

To address these challenges, this doctoral dissertation investigates the effects of elevated seawater temperatures and marine heatwaves on representative Mediterranean coral species of the eastern Adriatic Sea using an integrative multi-level approach. The study combines marine heatwave analyses with morphological, histological, and microbiome-based methods in order to assess coral responses across multiple biological levels and depth ranges.

The structure of this dissertation consists of six main chapters: Introduction, Literature Review, Materials and Methods, Results, Discussion, and Conclusion. The Literature Review chapter summarises current knowledge on climate-driven changes in Mediterranean marine ecosystems, marine heatwaves, coral morphology, anatomy, ecology, and coral-associated microbiomes, thereby providing the theoretical framework for interpreting the results of this dissertation. The Materials and Methods chapter describes the study area, field sampling procedures, and environmental datasets used for marine heatwave and oceanographic analyses. It further outlines the methodologies applied for morphological assessments, histological processing and staining, and molecular analyses of coral-associated microbiomes. Finally, the chapter presents the statistical approaches used to evaluate relationships between thermal stress and the observed biological responses. The Results chapter is organised by coral species and integrates marine heatwave dynamics, physicochemical conditions, morphological assessments, histopathological analyses, and microbiome composition in order to evaluate species-specific responses to thermal stress across different habitats and depth ranges. The Discussion integrates these findings within the broader context of climate-driven degradation of Mediterranean benthic ecosystems and evaluates the implications of recurrent marine heatwaves for coral resilience in the Adriatic Sea. The Conclusion synthesises the main findings of the dissertation and evaluates the effects of marine heatwaves and elevated seawater temperatures on Mediterranean coral species in the eastern Adriatic Sea.

Results presented in Chapters 5.1 and 5.3 were partially published as: Kružić, P., Guić, R., Lipej, L., Mavrič, B., Gračan, R. and Ankon, P. (2025) 'A *Cladocora caespitosa* bank (National Park Mljet, Adriatic Sea) under climate and anthropogenic impacts: a 20-year survey',

Mediterranean Marine Science, 26(1), pp. 156–174, doi:10.12681/mms.37029. The published study focused on long-term changes in the *Cladocora caespitosa* bank within Mljet National Park under combined climatic and anthropogenic pressures. Within this dissertation, these results were expanded through additional analyses of marine heatwave dynamics, histopathological alterations, and microbiome responses, and integrated into a broader multi-species assessment of climate-driven coral degradation in the eastern Adriatic Sea.

The scientific contribution of this dissertation lies in providing one of the first integrative assessments of climate-driven coral degradation in the eastern Adriatic Sea, combining marine heatwave analyses with morphological, histological, and microbiome-based approaches across multiple coral taxa and depth ranges. The study provides novel insight into hidden tissue deterioration, microbial dysbiosis, and species-specific vulnerability associated with chronic thermal stress, while also evaluating the potential refuge role of deeper coralligenous habitats under ongoing climate change.

1.1. Aims and hypotheses of the doctoral thesis

The general aim of this study is to identify and characterize the negative impacts of climate change on marine benthic ecosystems, in particular the coralligenous biocoenosis of the eastern Adriatic Sea, by combining multidisciplinary methods on different biological organisation levels, at a specific location and time.

Specific objectives of this doctoral dissertation are as follows:

1. Evaluation of the impact of temperature anomalies on individuals and communities on damage to the visible morphological changes in particular coral species.
2. To determine the amount of observable tissue abnormalities in corals using histological analyses and their relationship to elevated water temperatures.
3. To idenfity whether elevated temperatures affects microbiome of hosts (corals) and their environment in order to assess the impact of elevated temperatures on the diversity of microbiota.

The hypothesis that this doctoral dissertation investigates are as follows:

Temperature anomalies (long-term elevated sea temperatures) negatively affect corals, causing stress that leads to:

H1. Increased number of visible morphological damages

H2. Increased number and more extensive tissue damage and necrosis

H3. Differences in the diversity of coral microbiota and the surrounding seawater

2. LITERATURE REVIEW

2.1. Marine heat waves and mass mortality events

Climate change represents one of the most pressing global challenges of the present century, with profound impacts on marine ecosystems. The ongoing climate crisis has emerged as a dominant environmental driver, strongly affecting marine biodiversity and ecosystem functioning, and often interacting with other human-induced stressors (Smale et al., 2019; Gissi et al., 2021). Rising sea temperatures, ocean acidification, and altered circulation patterns are reshaping the structure and dynamics of marine systems, particularly in coastal and semi-enclosed seas such as the Mediterranean. Moreover, ecosystems in this region are increasingly subjected to additional anthropogenic pressures, including destructive fishing practices, anchoring, unregulated diving, coastal urbanisation, increasing tourism pressure, and localised pollution (Harmelin & Marinopoulos, 1994; Mistri & Ceccherelli, 1996; Bavestrello et al., 1997; Coma et al., 2004; Garrabou et al., 2009; Cebrian et al., 2011). Taken together, these pressures reduce ecosystem resilience and amplify the effects of climate-driven variability, thereby increasing the influence of extreme oceanographic conditions. Among these, marine heatwaves stand out as a critical factor demanding closer examination.

Heat waves can affect both terrestrial and marine ecosystems (Jentsch et al., 2007; Halpern et al., 2008; Gugliotti et al., 2019). A marine heat wave (MHW) can be defined as a "prolonged discrete anomalously warm water event that can be described by its duration, intensity, rate of evolution, and spatial extent" (Hobday et al., 2016) and has a strong effect on marine ecosystem structure and functioning (Rose et al., 2012; Caputi et al., 2016; Smale et al., 2019; Thomsen et al., 2019). MHWs presence and characteristics differ between regions and across years, and are primarily related to local hydrological conditions. In recent decades, the frequency of MHWs has risen dramatically and has been characterised by longer duration, higher intensity, and broader distribution (Collins et al., 2019). Species and their populations respond differently to these events at the local and regional levels (Garrabou et al., 2009). The rising occurrence of MHWs has been closely linked to the accelerated incidence of mass

mortality events in marine ecosystems across the globe (Garrabou et al., 2009; Thomson et al., 2015; Wernberg et al., 2016; Hughes et al., 2017).

Mass mortality events (MMEs) are defined as sudden, large-scale episodes of population decline that affect multiple species or entire communities over relatively short time frames, often leading to severe alterations in ecosystem structure and functioning (Garrabou et al., 2009; Hughes et al., 2017). Such events are typically associated with acute environmental stressors, among which anomalous increases in seawater temperature have emerged as the dominant driver in marine ecosystems. Reports of climate-related MMEs have increased substantially since the 1980s, paralleling the intensification of marine heatwaves at regional and global scales (Wernberg et al., 2016; Rivetti et al., 2014). Mass mortality events are primarily caused by two different types of positive temperature anomalies: short-term anomalies (lasting up to five days) with warm average sea temperatures (reaching up to 30°C down to 10 metres depth) and long-term anomalies (lasting more than a month) with measured temperatures reaching 24°C down to 50 metres depth (Crisci et al., 2011). The Mediterranean Sea has been recognised as a hotspot for these events due to its semi-enclosed nature, strong thermal stratification, and the prevalence of habitat-forming species that are particularly sensitive to thermal stress (Cerrano et al., 2000; Garrabou et al., 2009).

Documented MMEs in the Mediterranean Sea have affected a wide range of taxa, from invertebrates such as gorgonians, sponges, and bivalves to other sessile benthic communities, with cascading effects on biodiversity and ecosystem services. Over the past few decades, the Mediterranean has experienced several large-scale MMEs directly linked to extreme thermal anomalies. The earliest documented cases of this phenomenon date back to the early 1980s, when significant die-offs were reported in both the western Mediterranean and the Aegean Sea (Harmelin, 1984; Bavestrello & Boero, 1986; Gaino, 1989; Gaino et al., 1992; Voultsiadou et al., 2011). Some of the most dramatic episodes occurred in 1999 and 2003, when unprecedented marine heatwaves triggered mortality across thousands of kilometres of coastline in the northwestern Mediterranean, affecting more than 40 species from diverse taxa including cnidarians, sponges, bivalves, bryozoans, and ascidians (Cerrano et al., 2000; Perez et al., 2000; Garrabou et al., 2009). In many populations, mortality rates exceeded 80% of

colonies, with profound consequences for benthic community structure and ecosystem functioning (Cerrano et al., 2000; Garrabou et al., 2009). These outbreaks, however, represent only the most visible manifestations of a much broader pattern, as basin-wide analyses have documented the recurrent nature and geographical spread of mortality events across the Mediterranean. According to Garrabou et al. (2019), a collaborative Mediterranean-wide database recorded 676 mortality events between 1979 and 2017, involving 93 species from nine major taxonomic groups. The majority of events were concentrated in the western Mediterranean (55.5%), while 23.5% were reported in the Adriatic and 12.7% in the Aegean Sea (Garrabou et al., 2019). In terms of taxa, cnidarians and sponges dominated, accounting for 47.4% and 37.6% of cases, respectively (Garrabou et al., 2019). Other groups such as bryozoans, bivalves, and ascidians were also affected, although with lower frequencies. Growing evidence suggests that MMEs are widespread, climate-driven ecological crises, with their frequency and severity closely linked to the intensification of marine heatwaves in the region.

2.2. Adriatic Sea – a research hotspot for climate driven ecological change

The Adriatic Sea, located in the northernmost sector of the Eastern Mediterranean, is a semi-enclosed basin approximately 800 km long and 200 km wide, with its only connection to the Mediterranean through the 72 km wide Strait of Otranto (Lipizer et al., 2014). It exhibits a highly variable bathymetric profile, with shallow waters in the north gradually deepening towards the central and southern regions. The basin is commonly divided into three areas: the northern Adriatic, the largest continental shelf in the Mediterranean, characterised by extensive river input and bounded by the 100 m isobath (Cushman-Roisin et al., 2001); the central Adriatic, which has an average depth of approximately 140 m and encompasses the Palagruža Sill (170 m) and the Jabuka Pit (250 m); and the southern Adriatic, which includes the South Adriatic Pit, the deepest point of the basin (1,233 m), connected to the Ionian Sea through the Otranto Sill (780 m) (Artegiani et al., 1997). Overall, the basin encompasses more than 1,300 islands, the majority located along its eastern coastline, and is characterised by slight tidal amplitudes, although larger oscillations may occasionally occur. Compared to the

wider Mediterranean, the Adriatic exhibits lower salinity because it receives nearly one third of the total river inflow, which generates a partially positive water budget (Artegiani et al., 1997; Verri et al., 2018). Moreover, it represents a critical site for dense water formation, contributing to the renewal of deep waters in the Mediterranean.

The main nutrient inputs to the basin derive from surface runoff, groundwater discharge, urban effluents, and aeolian transport (Marini et al., 2008). Hydrographic and biogeochemical parameters such as temperature, salinity, nutrients, dissolved oxygen, and chlorophyll *a* follow a pronounced seasonal cycle and exhibit distinct longitudinal gradients (Lipizer et al., 2014). The northern Adriatic, strongly influenced by coastal processes and riverine forcing, is marked by higher nutrient levels and greater variability, largely shaped by the Po River, which can extend across the basin towards the eastern coast (Jeffries & Lee, 2007). From north to south, nutrient concentrations in the surface layer progressively decline, while the amplitude of the seasonal cycle decreases towards the middle and southern areas (Zavatarelli et al., 1998).

The ecological significance of the Adriatic Sea is strongly linked to its morphological and hydrographic heterogeneity, which supports a wide range of benthic habitats. Shallow infralittoral zones dominated by photophilic algal communities create structurally complex assemblages that provide food and shelter for numerous invertebrates and fish species (Thibaut et al., 2005). At greater depths, reduced irradiance with relatively constant conditions of temperature, strong currents and salinity favours the development of coralligenous assemblages: complex bioconstructions formed by calcareous algae and associated macroinvertebrates, which represent one of the most important biodiversity reservoirs and an endemic habitat of the Mediterranean (Ballesteros, 2006). Together, these habitats host a high diversity of sessile organisms, including numerous coral species, many of which are listed as threatened on the IUCN Red List (Kružić, 2017, Red Data Book of Corals of Croatia).

In recent decades, the Adriatic has emerged as a hotspot for climate-driven ecological change, with rising sea temperatures exerting profound impacts on benthic communities. Positive thermal anomalies, particularly in the southern basin, have been recorded with sea surface temperatures reaching up to 29 °C (Kružić, et al., 2012), while unusually high temperatures have been observed to depths of 50 m (up to 24 °C sustained for over a month). These extreme

conditions have triggered mass mortality events of sessile benthic organisms during multiple summers, including 1997, 1999, 2001, 2003, 2004, 2006, 2009, 2010, 2012, and 2016, with the most severe impacts documented in protected areas such as Mljet and Kornati National Parks, and the Nature Parks Telašćica and Lastovo (Kružić et al., 2014, 2016). Coral populations have been particularly affected, showing strong declines in abundance and altered community structures. Of a total of 116 coral species recorded in the Adriatic Sea, 84 species are currently on the IUCN Red List of Threatened Species. Of those, 66 are in the category of endangered species (8 critically endangered, 21 endangered, and 37 sensitive species), which is 56% of all recorded Adriatic species (Kružić, 2017, Red Data Book of Corals of Croatia).

Monitoring coral populations within both photophilic algal and coralligenous biocoenoses offers a valuable means of identifying which species and functional groups are most vulnerable to the combined pressures of climate change and anthropogenic disturbance. In this context, the Adriatic, shaped by distinctive thermohaline circulation, complex bathymetry and pronounced climatic gradients, is increasingly recognised as a hotspot of climate-related hazards, where the cumulative influence of human pressures and rising sea temperatures underscores the urgent need to evaluate species-specific responses of corals to ongoing environmental change.

2.3. Biological characteristics of Anthozoa (Cnidaria)

Cnidaria represent a diverse phylum of diploblastic metazoans, encompassing four major subphyla: Anthozoa, Scyphozoa, Cubozoa, and Hydrozoa (WoRMS Editorial Board (2025)). Members of this group are characterised by the presence of two primary germ layers, the ectoderm and the endoderm, which persist as epithelial monolayers throughout the organism's life cycle (Habdija et al., 2011). The ectoderm differentiates into the epidermis, the external cell layer, while the endoderm forms the gastrodermis, which lines the digestive or gastrovascular cavity. The gastrodermis originates from the archenteron, the primitive gut formed during gastrulation (Habdija et al., 2011). Between these two epithelial layers lies the mesoglea, an acellular or sparsely cellular matrix, which provides some additional structural

support. Although highly variable in thickness, being relatively thin in many sea anemones and considerably thickened in medusoid forms, it does not represent a true third germ layer (mesoderm). Rather, its cellular elements are derived from either ectodermal or endodermal lineages (Habdija et al., 2011).

Corals, belonging to the class Anthozoa, exist solely in the polyp form (lacking the medusae stage characteristic of other Cnidarians) and can exhibit two main organisational forms: solitary and colonial. Solitary species consist of a single polyp that lives attached or loosely anchored to the substratum, whereas colonial species comprise numerous genetically identical polyps integrated into a common structural and physiological unit (Fautin & Mariscal, 1991). Each polyp has a cylindrical body plan with a basal attachment and an oral disc surrounded by tentacles. High densities of cnidocytes, which each carry a cnidocyst (nematocyst), a sophisticated stinging organelle specific to the phylum Cnidaria, are commonly found at the tips of the tentacles (Beckmann & Özbek, 2012). Within the oral disc lies the mouth, which leads into the actinopharynx, a short muscular tubular passage that opens into the gastrovascular cavity. The cavity is internally partitioned by calcareous or membranous septa supporting the mesenteries, thin tissue folds that increase the digestive surface area and house the gonads (Habdija et al., 2011). In colonial forms, individual polyps are interconnected by the coenosarc, a living tissue extending over the calcareous skeleton. This tissue contains an integrated network of gastrovascular canals, lined by the same epithelial layers, which enables the translocation of nutrients, symbionts, and signalling molecules between polyps. Such integration allows coral colonies to function as modular organisms rather than as collections of independent individuals (Hughes et al., 2003).

Within the class Anthozoa, many species engage in a mutualistic symbiosis with unicellular photosynthetic dinoflagellates of the family Symbiodiniaceae. These endosymbionts inhabit the gastrodermal cells of their hosts, where they perform photosynthesis and translocate a substantial proportion of the produced organic compounds, composed of primarily carbohydrates and lipids, to the coral (LaJeunesse et al., 2018). In return, the algae receive inorganic nutrients, such as nitrogen and phosphorus, as well as access to carbon dioxide and a stable environment protected from external fluctuations. This symbiotic relationship

represents only one component of the nutritional strategy in Anthozoa. Coral polyps generally rely on a dual trophic mode, combining the autotrophic input of photosynthates provided by Symbiodiniaceae with heterotrophic feeding through tentacle-mediated prey capture (Houlbrèque & Ferrier-Pagès, 2009).

While some corals, particularly those inhabiting low-light or mesophotic environments, depend more heavily on heterotrophy, the majority of shallow-water reef-building species acquire the largest proportion of their energy budget from their endosymbiotic algae. Using their tentacles equipped with nematocysts (stinging cells), non-symbiotic corals capture and feed primarily on planktonic invertebrates and other particulate organic matter suspended in the water column (Beckmann & Özbek, 2012). When living prey, such as plankton, passes over a coral polyp, the polyp releases barbed harpoon-like nematocysts to immobilise the prey so that its tentacles can draw it back to its mouth (Habdija et al., 2011). In addition to feeding on live prey captured by their tentacles and nematocysts, coral polyps can also absorb dissolved organic matter from the surrounding ocean water and graze on suspended particles and detritus that become trapped in their mucus layer.

Many corals are hermaphroditic, whereas others are gonochoric, with polyps of separate sexes (Habdija et al., 2011). At the colony level, reproductive organisation may vary: colonies may be exclusively hermaphroditic, unisexual (male or female), or comprise a mosaic of male, female, and hermaphroditic polyps (Galloway et al., 2007). Polyps also reproduce both sexually and asexually.

Corals exibit two principal modes of sexual reproduction: broadcast spawning and brooding (internal fertilisation). In broadcast spawning species, corals simultaneously release sperm and eggs into the water column, where external fertilisation occurs; the resulting planula larvae are planktonic until they locate a suitable hard substrate for settlement (Waller, 2003). In brooding species, female polyps retain eggs internally; sperm from neighbouring individuals enters the female gastrovascular cavity, fertilises the eggs, and fully developed planulae are released, often through the polyp mouth, once larval development is complete (Waller, 2003). In Anthozoans, the larval stage exhibits a gastrula-type organisation. From the archenteron, lined with endoderm, the gastrovascular cavity develops, ultimately becoming lined by the

gastrodermis. The mouth of the animal, in turn, originates from the blastopore, a feature retained from early embryonic development (Habdija et al., 2011). Upon locating a suitable substratum, a planula settles, metamorphoses into a juvenile polyp, and initiates a new colony.

Following sexual reproduction, colony expansion may proceed via asexual means (budding or fragmentation) (Habdija et al., 2011). Budding may be intratentacular or extratentacular, yielding genetically identical clones of the founding polyp (Waller, 2003). Both the newly formed polyps and the original polyp retain the capacity for sexual reproduction in subsequent spawning events.

Mass spawning events typically occur once or twice per year in many anthozoan species; their timing is believed to be regulated by environmental cues such as the lunar cycle, diurnal (day/night) cycle, and increasing sea temperatures (or seasonal temperature rise) (Waller 2003). To reduce hybridisation, different coral species often stagger their spawning days across a species-typical time window (often over several nights) even if they spawn in the same general season (Waller, 2003). The maturation period of gametes varies among species: sperm may require approximately 3–4 months to reach full maturity, whereas ova often develop over longer periods (commonly 6 to 22 months), depending on species and environmental conditions (Waller, 2003).

Beyond their morphological, nutritional, and reproductive diversity, corals are also recognised as key bioconstructors of marine habitats. As ecosystem engineers—organisms that influence ecosystem state by modifying the physical habitats in which biological interactions occur (Cheung et al., 2021)— they create complex three-dimensional environments that provide shelter, feeding grounds, and nursery areas for numerous organisms, thereby exerting a profound influence on marine biodiversity and ecosystem functioning. Two principal types of biogenic habitats are formed by corals: coral reefs and coralligenous assemblages. The latter are endemic to the Mediterranean Sea and arise from the accumulation of encrusting coralline algae (mainly Corallinaceae) and calcifying invertebrates, including corals, on rocky substrates under low-light conditions (Ballesteros, 2006). These multi-layered formations represent one of the most species-rich habitats in the region, harbouring more than 10% of known Mediterranean marine species, many of which are endemic, threatened, or protected

(Sartoretto et al., 1996; Ballesteros, 2006; Coll et al., 2010). Coralligenous assemblages also deliver valuable ecosystem services, supporting fisheries, enhancing coastal tourism, and supplying natural resources (Ballesteros, 2006; Salomidi et al., 2012).

Coral reefs, by contrast, are globally distributed biogenic formations generated primarily by reef-building scleractinian corals (Spalding et al., 2001). As polyps secrete calcium carbonate skeletons, they produce a highly complex three-dimensional framework that supports immense biodiversity, estimated at around 25% of all marine life (including fish, crustaceans, molluscs, echinoderms, and seaweeds) (Spalding et al., 2001). Beyond their ecological importance, reef ecosystems provide critical services to human societies, including coastal protection, nitrogen fixation, sand supply, climate archives, and productive fisheries.

The subphyllum Anthozoa is divided into two major classes, Hexacorallia and Octocorallia, distinguished primarily by the number of mesenteries and tentacles in the polyp body plan: hexacorals possess these structures in multiples of six, whereas octocorals consistently display eight (Habdija et al., 2011).

2.3.1. Stony corals (Hexacorallia; Scleractinia)

The order Scleractinia, commonly referred to as stony corals, belongs to the class Hexacorallia within Anthozoa. Scleractinians exhibit considerable morphological diversity, occurring as both solitary and colonial forms (Morrissey et al., 2018). The body of the polyp is composed of three principal tissue layers: the epidermis, which mediates protection, mucus secretion, and sensory functions; the gastrodermis, responsible for digestion and harbouring symbiotic dinoflagellates; and the mesoglea, which separates the two epithelia and provides structural support (Galloway et al., 2007).

The coral polyp is a cylindrical sac organised into two main regions: the surface body wall, which interfaces with the external environment, and the basal body wall, which anchors the polyp to its calcareous skeleton. The surface body wall comprises three tissue layers: the outermost epidermis, the innermost gastrodermis, and the mesoglea, a connective layer situated between them (Hawthorn et al., 2023). The basal body wall consists of the gastrodermis and mesoglea—structurally similar to those of the surface wall—and an

additional layer, the calicodermis, a secretory epithelium responsible for skeletal formation (Hawthorn et al., 2023) (Figure 1).

The epidermis, which is in direct contact with seawater, is typically composed of simple to pseudostratified columnar epithelial cells, many of which are ciliated to assist in the movement of mucus or sediment (Hawthorn et al., 2023). This layer contains a variety of specialised cells, including mucocytes, cnidocytes, neurons, sensory cells, pigment-containing granular cells, granular amoebocytes, and epitheliomuscular cells (Palmer and Traylor-Knowles, 2012; Palmer et al., 2011; Sudek et al., 2012) (Figure 1). A continuous mucus layer covers the epidermal surface, serving as a physical and biochemical barrier that protects tissues from sedimentation, desiccation, and colonisation of microbial pathogens. In addition to its defensive role, this mucus provides a nutrient-rich microhabitat for associated microbial communities, forming an integral component of the coral holobiont by mediating host–microbe interactions and contributing to overall coral health (Hawthorn et al., 2023). The distribution and abundance of granular cells vary considerably among coral species (Hawthorn et al., 2023). While multiple morphologically distinct granular cell types have been described, their specific functions remain poorly characterised and may differ between species (Palmer and Traylor-Knowles, 2012; Palmer et al., 2011; Sudek et al., 2012).

Within the mesoglea, a predominantly acellular collagenous matrix providing structural support and elasticity, round to oval agranular amoebocytes with clear cytoplasm can occasionally be observed (Hawthorn et al., 2023). Extensions of smooth muscle fibres, derived from epidermal epitheliomuscular cells, interdigitate into the mesoglea, forming anchoring sites that enable polyp contraction and tentacle movement (Berzins et al., 2021). The overall thickness of the living coral tissue ranges from a few millimetres to several centimetres, depending largely on the thickness of the mesoglea as well as species-specific traits and environmental conditions (Hawthorn et al., 2023).

The gastrodermis lines the gastrovascular cavity and canals and is composed of columnar to cuboidal epithelial cells interspersed with variable numbers of cnidocytes, granular amoebocytes, granular gland cells, mucocytes, and pigment-containing granular cells (Hawthorn et al., 2023) (Figure 1). Gastrodermal epithelial cells commonly contain cytoplasmic

vacuoles, the symbiosomes, which house symbiotic dinoflagellates of the family Symbiodiniaceae (Hawthorn et al., 2023). These symbionts are most abundant within the gastrodermis of the surface body wall but may also occur in mesenterial filaments and the basal gastrodermis (Hawthorn et al., 2023).

The mesenteries extend from the mesoglea of the body wall into the gastrovascular cavity and are lined on both sides by gastrodermis (Peters, 2016). They serve to increase the internal surface area and provide additional structural support. In reproductive polyps, mesenteries may contain gametes (ova and spermaries). The free margins of the mesenteries form mesenterial filaments, thickened cnidoglandular bands covered by a layer of thin columnar ciliated epithelial cells, granular gland cells, mucocytes, and cnidocytes (Peters, 2016) (Figure 1). These structures play a central role in prey digestion, as they secrete digestive enzymes and deploy nematocysts to immobilise zooplankton captured by the tentacles and transported into the gastrovascular cavity (Hawthorn et al., 2023). Granular gland cells, found individually within the gastrodermis or aggregated within cnidoglandular bands and the actinopharynx, contain large secretory granules and are thought to contribute to extracellular digestion (Work and Farah, 2014; Peters, 2016; Reynolds, 2016; Wada et al., 2016). Adjacent to the cnidoglandular bands, nutrient-absorbing gastrodermal cells line the mesenterial bases and contribute to intracellular digestion and nutrient distribution (Peters, 2016).

The basal body wall is lined internally by gastrodermal epithelial cells interspersed with mucocytes and granular cells, and externally by the calicodermis, composed primarily of calicoblasts (Bertucci et al., 2013). These modified epithelial cells mediate skeletal deposition through the secretion of an organic matrix composed of collagens, laminins, fibronectin, and calcium-binding proteins that regulate aragonite crystallisation (Bertucci et al., 2013). Interspersed among the calicoblasts are desmocytes, differentiated epithelial cells that form anchoring junctions between the tissue and the skeleton, providing mechanical stability and maintaining tissue integrity (Peters, 2016) (Figure 1).

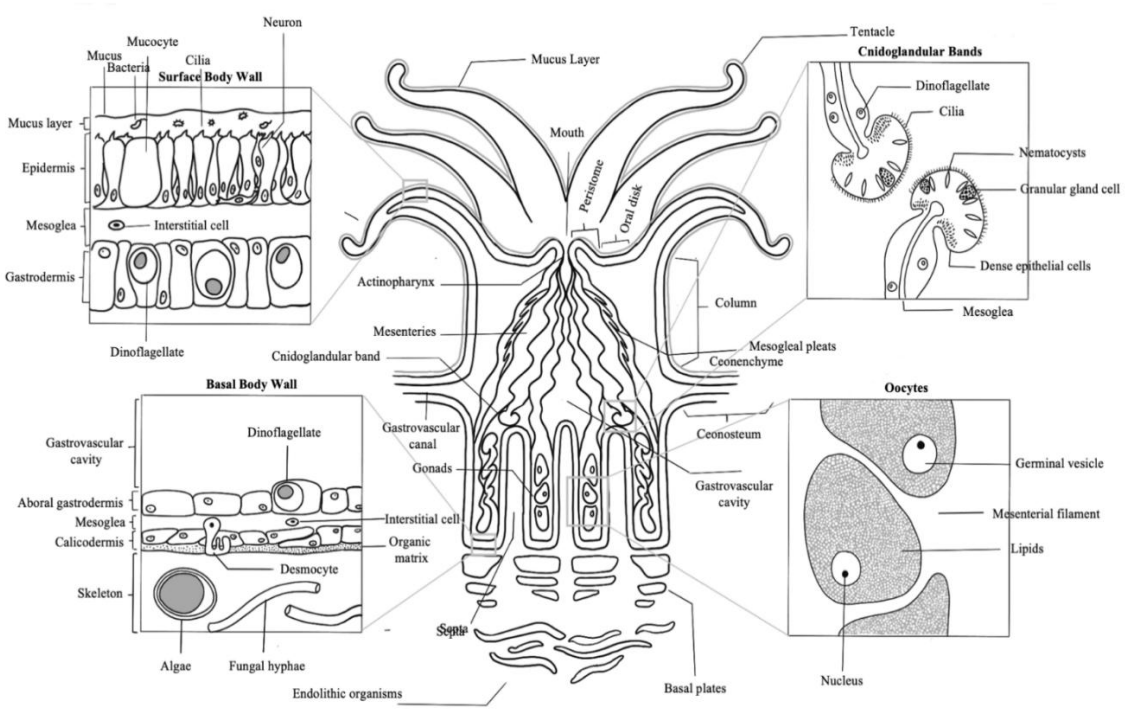

Figure 1. Detailed schematic representation of the anatomical and histological organisation of a scleractinian coral polyp. The central image depicts the gross morphology, including the oral disc, tentacles, actinopharynx, mesenteries, gastrovascular canals, septa, and basal plates. Surrounding inset panels highlight histological details of distinct tissue regions. Source: McDonald M., CDHC, NOAA, (2023)

At the level of individual polyps, each secretes a skeletal cup known as the corallite. The corallite is subdivided into three main regions: the calice, which forms the oral opening; the columella, a central projection derived from the basal plate or septal modifications; and the theca, which constitutes the wall of the cup. Radiating from the theca, calcareous septa provide internal support for the mesenteries, while their external extensions across the coenosteum form costae (Habdija et al., 2011).

In colonial scleractinian corals, individual polyps are interconnected through the coenenchyme, a living tissue complex embedded within and overlying the shared calcareous skeleton (Hawthorn et al., 2023). The coenenchyme maintains both structural and physiological continuity across the colony, linking adjacent polyps into an integrated biological unit (Galloway et al., 2007). The coenenchyme is composed of the same three tissue layers

found in the polyp body wall—the epidermis, mesoglea, and gastrodermis—but it is generally thinner, less cellular, and partly embedded with skeletal elements (Hawthorn et al., 2023).

Through the secretion of aragonitic $CaCO_3$, scleractinians are capable of rapid carbonate deposition, producing large and rigid frameworks that provide structural support at the colony level (Lalli & Parsons, 1997). In tropical shallow waters, this capacity underlies the formation of coral reefs, defined as "persistent, positive topographic biogenic structures, rising to the surface of the sea and characterised by their capability to resist hydrodynamic stress" (Lowenstam, 1950; Nelson et al., 1962; Braithwaite, 1973; Heckel, 1974). By contrast, in temperate seas and in deeper environments, scleractinians may form banks, thickets and bioherms, which contribute to seabed accretion and habitat complexity but do not meet the strict definition of a reef (Schuhmacher & Zibrowius, 1985).

To describe these forms unambiguously, Schuhmacher & Zibrowius (1985) proposed a separation of terminology:

- symbionts vs. asymbionts — presence or absence of Symbiodiniaceae symbionts;
- constructional vs. non-constructional — ability to build elevated, durable carbonate structures;
- hermatypic vs. ahermatypic — significant vs. negligible contribution to the framework of reefs (a subset of constructional growth restricted to shallow, tropical settings).

Accordingly, scleractinians in temperate regions that form banks are constructional but not hermatypic, since the term "hermatypic" should be reserved for those contributing to true reef structures. Importantly, symbiosis with Symbiodiniaceae is not a prerequisite for constructional growth: corals may be reef-building (hermatypic) or bank-forming (constructional) regardless of their symbiotic status, while presence or absence of endosymbionts can even occur within the same species depending on the environment.

Beyond their taxonomic and structural definitions, scleractinian corals are also recognised as key reef ecosystem engineers. They function as autogenic engineers through their calcification and consequent reef accretion, thereby modifying the physical, chemical, and biological

environment and creating habitats for associated reef organisms. In addition, they act as allogenic engineers, since their inorganic calcareous skeletons are gradually transformed into reef sands that sustain abundant communities of heterotrophic microbes (Wild et al., 2004; 2011).

In this PhD thesis, four scleractinian coral species that inhabit distinct biocoenoses within the Adriatic Sea are investigated. In shallow infralittoral algal assemblages (0–15 m), *Cladocora caespitosa* represents a colonial, symbiotic coral, whereas *Balanophyllia europaea* occurs as a solitary but likewise symbiotic species. At greater depths, within the deeper infralittoral and upper circalittoral zones (20–40 m), *Leptopsammia pruvoti* is a solitary, asymbiotic coral, while *Madracis pharensis* is a facultative symbiotic species exhibiting colonial growth. Given their stenovalent nature and sensitivity to environmental fluctuations, these species serve as valuable bioindicators of climate change impacts in the Mediterranean, particularly in the Adriatic basin.

Cladocora caespitosa (Linnaeus, 1767) is an endemic species of colonial and symbiotic scleractinian constructional coral to the Mediterranean Sea and is a member of the Faviidae family (Figure 2). Colonies of *C. caespitosa* can be found on stony and sandy seafloors beginning several metres below the surface of the water; however, it is rarely found below 30 metres. It is a branching coral (dendroid form), with calyces that grow parallel to one another and form colonies up to 1 m in diameter. The hemispherical bush-like colonies may be found isolated and sparse, forming 'beds' (numerous colonies living close to each other) or 'banks' (colonies connected in a large formation more than 1 m high and covering several square metres) (Zibrowius, 1980; Morri et al., 1994; Peirano et al., 1998; Kružić and Benković, 2008). The polyps are a clear maroon colour, around 5 mm in diameter and form cushion-shaped colonies, in symbiosis with dinoflagellates of the family Symbiodiniaceae. They produce deposits of calcium carbonate which form the calcite structures in which they live. It is the largest stony coral in the Mediterranean, reaching up to 50 cm in diameter. Large fossil banks of *C. caespitosa* are known in the Mediterranean from the Late Pliocene (Aguirre and Jiménez, 1998; Dornbos and Wilson, 1999), from the Early Pleistocene (Bernasconi et al. 1997), from the Middle and Late Pleistocene and the Holocene (Peirano et al., 2009). Recently large

colonies of this coral are found in the Adriatic Sea in the channel of Lim near Rovinj, near Prvić and Pag Islands, and in Veliko jezero (Island of Mljet) (Kruzic et al., 2002; Kružić and Požar-Domac, 2003; Kružić and Benković, 2008). Asexual reproduction in *C. caespitosa* may take the form of budding or fragmentation. Both extratentacular and intratentacular budding occur (Zibrowius, 1980; Kružić, 2005). Fragmentation in *C. caespitosa* is caused by the division of a colony into smaller fragments to produce additional colonies. Peripheral fragments of large colonies are broken off by wave action in shallow water or by cryptofauna that burrow into the sediment in deeper water. Typically, small fragments near the original colony will form a new colony (Schiller 1993; Kružić 2005). The sexual reproductive structures of corals are located within the polyp on the mesentery (Harrison and Wallace, 1990). The reproductive cycle in *C. caespitosa* appears to be annual, with a spawning period at the beginning of summer (Schiller 1993; Kružić 2005). Oocytes and spermaries develop on separate mesenteries (digonic) within each polyp, which indicates that the polyps are hermaphroditic (Kružić 2005).

The second investigated species, *Balanophyllia europaea* (Risso, 1827) is a solitary, non-constructional, scleractinian coral that occurs on rocky substrates in the Mediterranean Sea and off the coast of Spain (Zibrowius, 1980; Aleem & Aleem, 1992) (Figure 2). Also known as scarlet coral or pig-tooth coral, it is a small stony coral species belonging to the Dendrophylliidae family, reaching a diameter of 4 to 6 centimetres and a height of 2 cm. Due to the presence of symbiotic microalgae, the body pigmentation ranges from light brown to green-brown, and the polyp has nearly transparent tentacles with red to yellow spots. Due to its symbiosis with Symbiodiniaceae, it is restricted to depths of 0–40 m (usually down to 20 m in the Adriatic Sea) on rocky substrates (Goffredo et al., 2008), where its population density peaks at approximately 100 individuals per square metre (Zibrowius, 1980). This species is very common along the coast of the eastern Adriatic Sea (Kružić, 2002, 2007), with population densities reaching dozens of individuals per square metre (Zibrowius 1980; Kruzic et al., 2002; Kružić, 2007; Goffredo et al., 2008). *B. europaea* is the only member of the genus *Balanophyllia* and one of the few members of the family Dendrophylliidae to display hermaphroditism (Harrison 1985; Goffredo et al. 2000). This solitary coral is a brooding simultaneous hermaphrodite with a yearly reproductive cycle. Neither spatial nor temporal separation exists between male and female gametogenesis, and mature spermatozoa and oocytes are produced

by the same individual (Goffredo et al., 2002). These observations suggest that autogamy may be a strategy for reproduction in this species.

Leptopsammia pruvoti (Lacaze-Duthiers, 1897) is a non-symbiotic and solitary scleractinian coral, which is distributed in the Mediterranean basin and along the European Atlantic coast from Portugal to Southern England and Ireland (Zibrowius, 1980) (Figure 2). It is one of the most common organisms in semi-enclosed rocky habitats, under overhangs, in caverns and small crevices at 0–70 m depth, with mean abundances of 104 individuals m^{-2} (Goffredo et al., 2007). The polyp of *Leptopsammia pruvoti* resides in a calcareous cup that is broader at the bottom than it is at the top and whose shape ranges from cylindrical and short to conical and long. It grows to approximately 60 mm in height and 20 mm in diameter. The polyp is yellow or orange with approximately ninety-six tentacles that are yellow and translucent. The tentacles can retract into the skeletal cup so that they are scarcely visible. Harrison (1985) defines Dendrophylliidae, the family to which *L. pruvoti* belongs, as a gonochoric taxon. Dendrophylliidae is a cosmopolitan family comprising 148 extant species divided into 19 genera. According to some authors, the genera *Leptopsammia* and *Balanophyllia* are so closely related that the two taxa may be considered synonymous (Fadlallah, 1983a; Heltzel and Babcock 2002). Following Cairns SD (1999), authors of the most recently compiled list of scleractinian extant species, also consider *Leptopsammia* and *Balanophyllia* as two distinct taxa. The Mediterranean is inhabited by only one species, *Leptopsammia pruvoti* Lacaze-Duthiers, 1897 (Avian et al., 1995). *L. pruvoti* has also been observed along the Atlantic littoral between Portugal and southern England. The mean annual sea surface temperature varies from 12°C in southern England to 19°C in the Mediterranean along the species' distribution range. This species typically inhabits shady habitats, under overhangs, and in grottos at depths of up to 70 metres (Zibrowius, 1980). At depths between 15 and 21 metres, the species' population density averages between 4,000 and 17,000 individuals per square metre (Goffredo et al., 2005). They discovered that *L. pruvoti* are sex separated, as all examined specimens had either male or female germ cells and did not have sexual dimorphism, nor were there significant differences in average body size between males and females. There is no evidence of asexual reproduction (through polyp budding, fission, or the asexual production of planulae (Goffredo et al., 2006)). Its genetic structure is marked by heterozygote deficits at

all scales, from patches to populations, with no correlation between genetic differentiation and geographic distance (Goffredo et al., 2009).

Madracis pharensis (Heller, 1868) was described from Hvarski Kanal, Croatia, in the Adriatic. It forms small clumps or encrusting colonies often found in caves and overhangs (Morri et al., 2000) and has two cycles of ten septa with well-formed paliform lobes (Zibrowius, 1980) (Figure 2). It is found at various localities in the Mediterranean and in the Eastern Atlantic (Madeira, Canary, Cape Verde, and Azores islands) (Zibrowius, 1980; Cairns, 1999; Morri et al. 2000). *M. pharensis* is known to exhibit colour variation, with diverse colour morphs described in detail for the reefs of Curaçao (Sheppard et al., 2007). The role of these host colour morphs in controlling symbiont diversity has not been investigated. Wells (1973) in a study of the Scleractinia from Jamaica, distinguished two forms of *M. pharensis*, one he defined as lucifugous and ahermatypic with encrusting and nodular growth form, *M. pharensis f. pharensis* (Heller, 1868), and the other one luciphilous and hermatypic with laminar or encrusting growth form, *M. pharensis f. luciphila* Wells, 1973. To date, the genetic and morphological boundaries between *M. pharensis f. luciphila* and *M. pharensis f. pharensis* in the Caribbean, as well as between these two forms and the Mediterranean and West Atlantic *M. pharensis* remain unexplored (Benzoni et al., 2018).

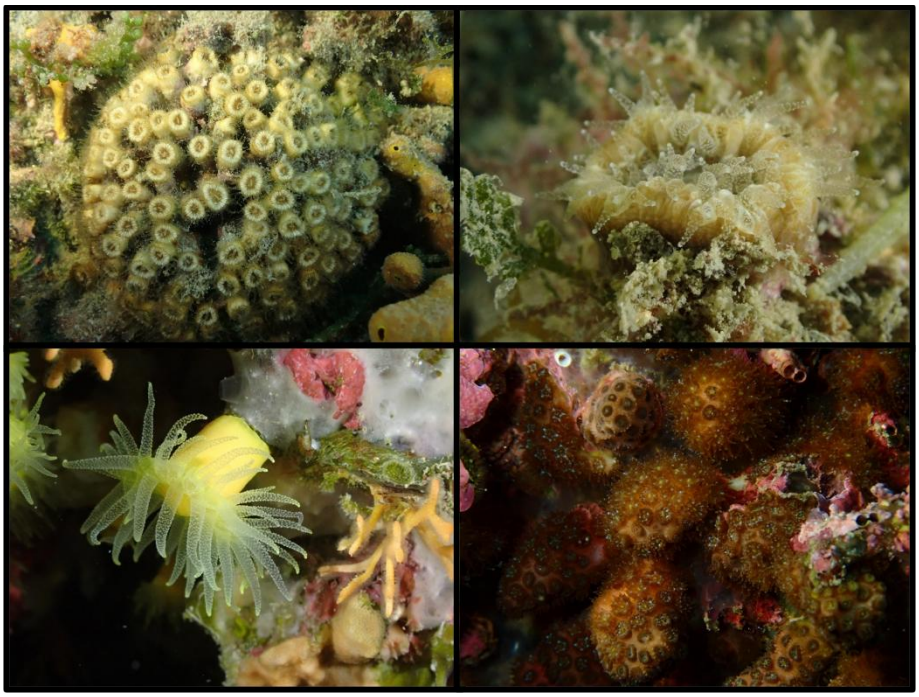

Figure 2. External appearance of scleractinian corals in the Adriatic Sea: a) colonial constructional symbiotic coral *Cladocora caespitosa* (Linnaeus, 1767), b) solitary symbiotic coral *Balanophyllia (Balanophyllia) europaea* (Risso, 1827), c) solitary scleractinian coral *Leptopsammia pruvoti* Lacaze-Duthiers, 1897, d) colonial scleractinian symbiotic coral *Madracis pharensis* (Heller, 1868).

2.3.2. Gorgonians (Hexacorallia; Octocorallia)

The Gorgonians belong to the class Octocorallia together with soft corals and sea pens, animals that are characterised by polyps possessing eight pinnate tentacles and eight mesenteries, hence their name (Habdija et al., 2011). Octocorals share the same basic epithelial and mesogleal organisation as scleractinians but differ markedly in polyp and skeletal morphology (Figure 3). The distal portion of the polyp, bearing the mouth and tentacles, is termed the anthocodia. Gorgonian tentacles are distinctive in possessing two rows of lateral side-branches, the pinnules, which give them a feather-like appearance (Habdija et al., 2011). At the aboral end, polyps are anchored into the colony axis, and in some taxa the anthocodia can retract into a rigid sheath, the anthostele. Unlike scleractinians, octocorals do not secrete massive calcareous corallites or septa. Instead, their tissues are reinforced by microscopic calcareous spicules (sclerites) and, in many gorgonians, a flexible axial skeleton composed of a central horny or calcareous core surrounded by an axial cortex and sheath (Carella et al.,

2014). The sheath contains longitudinal canals and sclerites, which also permeate the thickened mesoglea of the coenenchyme, thereby providing mechanical support and resilience. The gastrovascular system includes specialised tubular canals, the solenia, which penetrate the mesoglea and interconnect neighbouring polyps (Figure 3). This organisation results in a colony structure that is less rigid than that of stony corals but highly flexible and resilient, adapted to diverse marine environments.

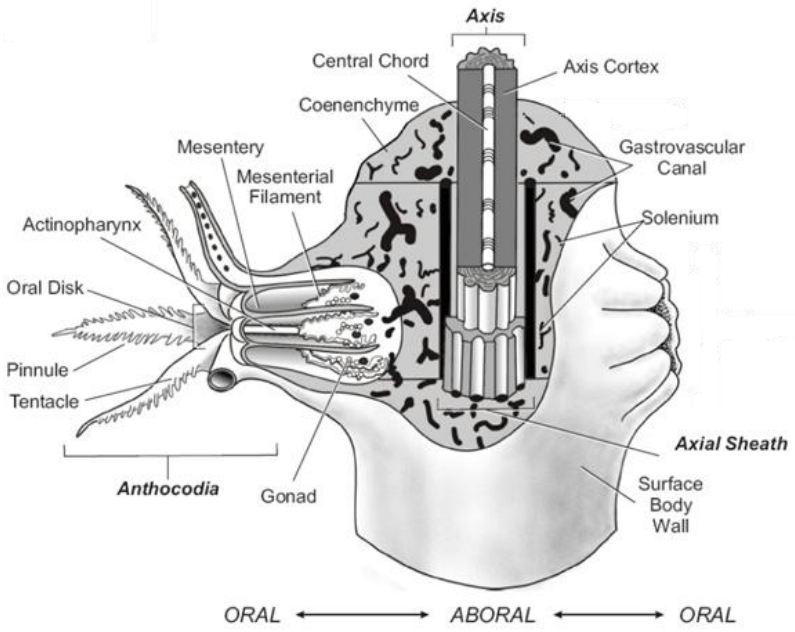

Figure 3. Detailed schematic representation of the anatomical and histological organisation of a gorgonian coral polyp. The illustration shows the overall morphology, including the main polyp structures (anthocodial: oral disk, tentacles, pinnule, actinopharynx, mesenteries, mesenterial filaments, and gonads) as well as the coenenchyme components such as the axial sheath, axis, axis cortex, central chord, gastrovascular canals, and solenia. Illustration adapted and modified from Galloway et al. (2007)

From an ecological perspective, octocorals do not form reefs, since they do not deposit extensive $CaCO_3$ frameworks capable of resisting hydrodynamic stress. Instead, they can establish structurally complex assemblages known as animal forests, which enhance benthic three-dimensionality and provide habitat for a wide range of associated species (Rossi et al., 2017). Some octocoral species harbour Symbiodiniaceae and contribute to primary production, while others are entirely azooxanthellate and rely exclusively on heterotrophic feeding. Their ecological role is therefore complementary to that of scleractinians: although

they are not reef-building, they are key ecosystem engineers in both tropical and temperate environments.

Among octocorals, gorgonians represent a particularly important group in the Mediterranean Sea. They are long-lived organisms with very slow population dynamics, including low linear growth rates (≈1.8 cm yr^{-1}), late maturity (≈13 years), low recruitment (mean of 1.9 ind. m^{-2}), and low post-settlement survival (Garrabou and Harmelin, 2002; Linares et al., 2007; Coma et al., 2009). These traits limit their demographic resilience and make gorgonians especially vulnerable to both local and global disturbances.

Because of their life-history constraints, gorgonian populations are highly sensitive to a wide range of stressors, including mechanical damage from fishing activities and recreational diving, pollution, sedimentation, mucilaginous algal aggregates, and invasive species (Cánovas-Molina et al., 2018; Piazzi et al., 2021). In addition, outbreaks of bacterial pathogens and mass mortality events linked to marine heatwaves have emerged as major drivers of decline (Linares et al., 2005; Gómez-Gras et al., 2021). When combined, these stressors often exacerbate one another, leading to more severe impacts and resulting in recovery that is both slow and usually incomplete.

As habitat-forming species, Mediterranean gorgonians exert a profound influence on community structure and benthic diversity by generating three-dimensional complexity and establishing animal forests that serve as refugia and feeding grounds for numerous associated organisms (Piazzi et al., 2021). Their conservation is therefore not only crucial for maintaining population persistence, but also for preserving the integrity and functioning of Mediterranean coastal ecosystems. In this PhD study, two widespread Mediterranean gorgonian species are analysed. The symbiotic species *Eunicella cavolini* occupies an ecological niche within the deeper infralittoral zone (15–30 m), while the asymbiotic *Paramuricea clavata* is a characteristic inhabitant of the circalittoral zone (≥30 m). Owing to their stenovalent nature and pronounced sensitivity to environmental fluctuations, both taxa are regarded as reliable indicators of ecological stress in marine habitats.

Eunicella cavolini (Koch, 1887), commonly known as the yellow gorgonian or yellow sea whip, is a symbiotic colonial soft octocoral in the family Gorgoniidae which can be observed for depths from less than 10m to more than 100m (Figure 4). It is a widespread species in the eastern Atlantic Ocean, Mediterranean Sea, and its native habitat, Ionian Sea. *Eunicella cavolini* is a much-branched soft coral growing to a height of about 50 cm. It is fan-shaped with irregular, cylindrical branches largely growing in a single plane. The stem has an enlarged base fixed to the substrate and the branches are smooth, short, and about 3 mm thick. The coenenchyma is yellowish orange, while the polyps are white to yellow, about 2 mm long and arranged in four rows. The skeleton of *Eunicella cavolini* is composed of a central axial core made of the structural protein gorgonin, which provides flexibility and support to the colony (Carella et al., 2014). Its distribution range is wide, although patchy in terms of abundance, and it is known to occur from the W Mediterranean and Tunisian coasts to the Aegean Sea, and the Sea of Marmara (Sini et al., 2015).

Paramuricea clavate (Risso, 1827), the violescent sea-whip, is a colonial soft coral in the family Plexauridae (Figure 4). It is found in shallow seas of the north-eastern Atlantic Ocean and the north-western Mediterranean Sea, as well as the Ionian Sea. Among gorgonians, *P. clavata* is the biggest sea fan inhabiting the Mediterranean Sea and it is commonly found from shallow to mesophotic depths because of the absence of endosymbiotic algae hosted in its tissues. It lives on vertical and overhanging surfaces and forms large colonies with thick, irregularly ramified branches (Bavestrello et al., 1994; Mistri and Ceccherelli, 1996). The stem and branches are stiffened by gorgonin, a complex protein that produces a horny skeleton. The coenenchyma covers the skeleton, from which the polyps protrude, each with eight feeding tentacles surrounding a central mouth. The polyps are up to 10 mm high and the whole colony is up to one metre high and 1 m across. The colonies are typically red but may occasionally display yellowish areas. Each colony contains either male or female individuals. Male colonies release sperm into the ocean, and fertilisation occurs on the surface of female colonies. The embryos are incubated there before being released into the water column as planula larvae. The larvae are photophobic and rapidly settle on the seafloor. Once there, they transform into polyps and begin to produce gorgonin, which forms the skeleton. By producing new polyps,

the colony grows further. Some fragments that become detached from existing colonies may form new colonies.

Mediterranean gorgonian populations are subjected to multiple stressors, including destructive fishing activities, anchoring damage, excessive and poorly regulated diving, mucilaginous algal outbreaks, invasive algal species, and widespread mortality events linked to abnormal increases in seawater temperature (Harmelin & Marinopoulos, 1994; Mistri & Ceccherelli, 1996; Bavestrello et al., 1997; Coma et al., 2004; Garrabou et al., 2009; Cebrian et al., 2011). *P. clavata* is an important ecosystem engineer with a sluggish growth rate, and its rarefaction and/or disappearance may produce important consequences on benthic habitat architecture, such as reducing spatial complexity and decreasing biodiversity (Ponti et al., 2014; Kipson et al., 2015).

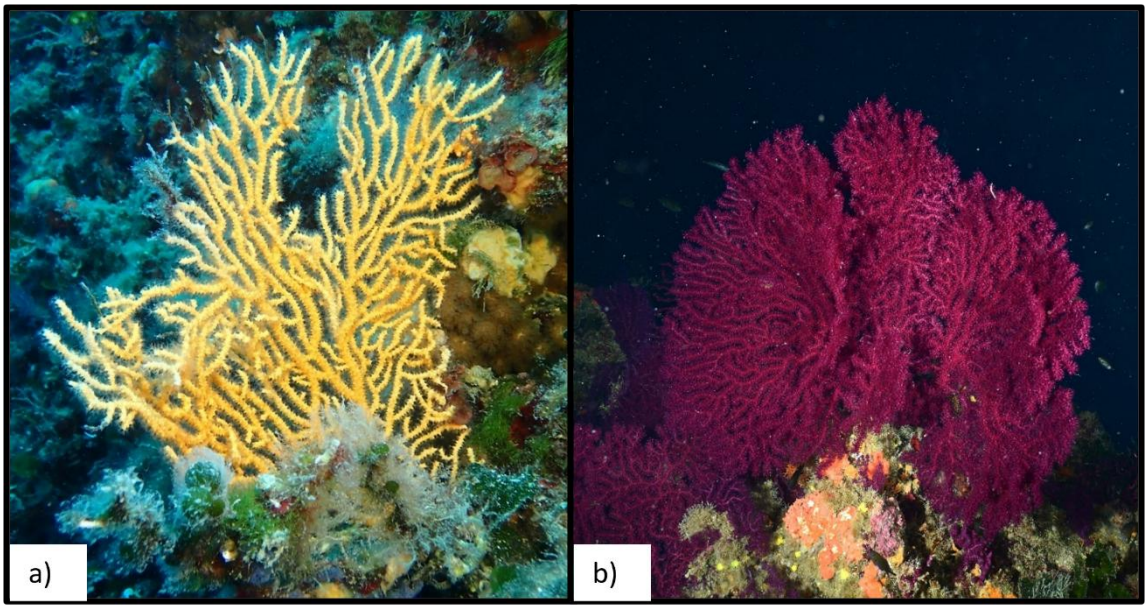

Figure 4. External appearance of a) colonial soft symbiotic coral *Eunicella cavolini* (Koch, 1887) and b) colonial soft coral *Paramuricea clavata* (Risso, 1827) in the Adriatic Sea

These six species investigated in this PhD study were selected for their pronounced sensitivity to climate change and ecological relevance as indicator species, collectively representing a gradient of ecological niches and symbiotic strategies across Adriatic depth zones and thereby

providing a comprehensive framework for assessing climate-induced stress, thermal anomalies, and community-level shifts within temperate coral assemblages.

2.4.Coral holobiont

Corals are among the most important habitat builders and often act as keystone species in marine ecosystems that harbour more than 25% of all marine biodiversity, including approximately 30% of all marine fish species (Moberg and Folke, 1999; Knowlton, 2001). This ecological complexity is deepened by the fact that are among first recognised species as holobionts—integrated biological units composed of the animal host and a consortium of associated microorganisms.

Endosymbiotic dinoflagellates of the family Symbiodiniaceae (order *Suessiales*, class *Dinophyceae*; Blackall, Wilson and van Oppen, 2015) inhabit vacuoles, or symbiosomes, within the gastrodermal cells of the coral host (Wakefield and Kempf, 2001). Corals rely heavily on these symbionts for their energy supply through the translocation of photosynthetic products such as glucose, glycerol, and amino acids (Burriesci, Raab and Pringle, 2012; Blackall, Wilson and van Oppen, 2015). In addition to organic compounds, Symbiodiniaceae provide oxygen required for host respiration and generate reactive oxygen species with potential antimicrobial roles (Banin et al., 2003). In return, the algae benefit from protection against predation and a stable, light-rich environment with access to inorganic waste released by the host (Allemand and Furla, 2018). Nitrogen, supplied primarily in the form of nitrate (Rädecker et al., 2015), and carbon dioxide produced by host metabolism sustain algal growth, while photosynthetic activity further drives the dissociation of carbonic acid and enhances calcium carbonate precipitation. This photosymbiosis underpins light-enhanced calcification, coral growth, and ultimately reef accretion (Gutner-Hoch et al., 2016; Inoue et al., 2018).

However, the holobiont also includes diverse microbial associates such as bacteria, archaea, fungi, protists, and viruses (Rohwer et al., 2002; Kimes et al., 2010; Allemand and Furla, 2018). Collectively, these organisms form the coral microbiome, with each partner playing a fundamental role in maintaining the health and functioning of the holobiont. While

Symbiodiniaceae provide oxygen and photosynthetically fixed carbon to their host (Davy, Allemand and Weis, 2012), microbes contribute to processes such as pathogen defence, nutrient acquisition, and biogeochemical cycling (González, Kiene and Moran, 1999; Lema, Willis and Bourne, 2012; Bourne, Morrow and Webster, 2016).

Beyond these overall functions, the corals establish a diversity of specialised microhabitats, each providing unique microbial communities and functional roles. These include the gastrovascular cavity, tissues, skeleton, and the surface mucus layer, each harbouring specific microbial assemblages (Rosenberg et al., 2007; Hernandez-Agreda, Gates and Ainsworth, 2017; van Oppen and Blackall, 2019). Such compartmentalisation strongly influences microbiome structure and function (Kimes et al., 2010). Within the tissue layers of the polyp (ectodermis and gastrodermis), bacteria are frequently organised into cell-associated microbial aggregates (CAMAs), often consisting of a single bacterial species (Ainsworth et al., 2006; Ainsworth and Hoegh-Guldberg, 2009; Work and Aeby, 2014; Wada et al., 2019). The endolithic community within the skeleton supports the highest bacterial diversity compared with other microhabitats, also containing fungi and green algae (Tribollet, 2008; Verbruggen and Tribollet, 2011; Ricci et al., 2019). Most coral-associated bacteria reside in the surface mucus layer covering the ectodermis (Garren and Azam, 2010), a nutrient-rich environment with high concentrations of dissolved organic and inorganic compounds, including carbon and phosphorus (Wild et al., 2010; Nakajima et al., 2015). The composition of mucus-associated bacterial communities is largely determined by the physical and chemical properties of the mucus, such as nutrient profile, viscosity, and bioactive compounds (Brown and Bythell, 2005; Jatkar et al., 2010), and host-specific receptors within the coral surface and mucus layer (Teplitski and Ritchie, 2009). Functionally, the mucus serves as a selective barrier that can promote beneficial microbes while inhibiting pathogens, either by preventing their antibiotic production required for colonisation or by altering the nutritive and physical properties of the habitat (Ritchie, 2006; Krediet et al., 2013).

Microbial partners are fundamental for sustaining coral health and the functioning of reef ecosystems (Bourne et al., 2016). Corals often display a degree of specificity in their microbial associations (Morrow et al., 2012; Blackall et al., 2015; Ziegler et al., 2017), pointing towards

adaptive co-evolution between hosts and their microbiota (O'Brien et al., 2019). Environmental factors strongly influence microbial community composition, with the same coral species harbouring distinct assemblages across habitats, reflecting local adaptation (Rohwer et al., 2002; Kelly et al., 2014; Pantos et al., 2015; Hernandez-Agreda et al., 2016). Coral-associated microbiota are recognised as among the most diverse in marine systems (Blackall et al., 2015), encompassing at least 37 bacterial phyla (Huggett and Apprill, 2019). Scleractinian corals are typically dominated by Proteobacteria (Rohwer et al., 2002)—particularly Alpha- and Gammaproteobacteria—together with Bacteroidetes (Huggett and Apprill, 2019), Cyanobacteria (Rohwer et al., 2002), and Firmicutes (Huggett and Apprill, 2019). The most consistently represented genera include *Endozoicomonas*, *Vibrio*, and *Serratia* (Huggett and Apprill, 2019), often displaying high host specificity (Blackall et al., 2015). These symbionts perform numerous critical functions within the holobiont, such as nutrient acquisition and biogeochemical cycling (Kimes et al., 2010), detoxification of reactive oxygen species (Thurber et al., 2009; Raina et al., 2010) and metals (Kimes et al., 2010), regulation of Symbiodiniaceae density and physiology (Lesser et al., 2013; Olson et al., 2009; Bernasconi et al., 2019), defence against pathogens (Shnit-Orland and Kushmaro, 2009), and enhancement of stress tolerance (Rädecker et al., 2015; Ziegler et al., 2017).

Beyond their diversity, bacterial symbionts play a crucial role in coral nutrient dynamics, particularly through regulating the nitrogen cycle. By transforming nitrogenous waste into usable or non-toxic forms, these microbes help stabilise Symbiodiniaceae densities and maintain coral homeostasis. In addition, some taxa contribute to sulphur cycling and provide antioxidant protection, further supporting holobiont resilience (González, Kiene and Moran, 1999; Thurber et al., 2009; Kimes et al., 2010; Rädecker et al., 2015).

Another fundamental function of the coral microbiota is the defence against pathogens. Protection is achieved through multiple mechanisms, including competitive exclusion, interference with pathogen metabolism, and the production of antimicrobial compounds (Ritchie, 2006; Shnit-Orland and Kushmaro, 2009). The surface mucus layer, rich in glycoproteins and lipids, acts as the first barrier to invading microbes (Brown and Bythell, 2005). Within this habitat, commensal bacteria can disrupt pathogen establishment by

competing for resources, producing antibiotics, and interfering with colonisation processes. Such antagonistic interactions reduce the risk of disease and maintain microbial balance on the coral surface. Additionally, microbial signalling via quorum sensing plays an important role in regulating physiological processes linked to symbiosis, virulence, and defence, while its inhibition may further suppress the establishment of pathogens (Teplitski and Ritchie, 2009).

The stability of the coral holobiont depends on multiple interacting factors, including biotic elements such as pathogens, prey dynamics, host physiology and genetic traits, as well as abiotic drivers such as temperature, light, pH, hydrodynamics, and nutrient availability (Ainsworth et al., 2010). When these parameters deviate from ambient conditions, holobiont homeostasis may be disrupted, leading to microbial imbalance and reduced resistance to opportunistic infections (Thurber et al., 2009). One of the most severe outcomes of such dysbiosis is coral bleaching, a stress response that can be induced by diverse external factors, including elevated temperature, cold stress, high irradiance, hypoxia, nutrient enrichment, and microbial infections. Among these triggers, heat is recognised as the primary driver of mass bleaching events worldwide (Hughes et al., 2017). Although thermal and light stress often co-occur, they act through distinct pathways and can elicit different physiological responses within the holobiont (Downs et al., 2009).

2.5. Coral bleaching

Coral bleaching is the breakdown of the symbiosis (i.e. dysbiosis) between reef-building corals and their photosynthetic dinoflagellate algal endosymbionts (family Symbiodiniaceae), resulting in symbiont loss and exposure of the white colour of the calcium carbonate skeleton through the translucent symbiont-devoid animal tissue left behind (Glynn, 1993; Baker, Glynn and Riegl, 2008). This process may be initiated by the activation of the host immune responses, involving pathways such as apoptosis, autophagy, exocytosis, cell detachment, or necrosis, all of which lead to the loss of algal partners. Alternatively, bleaching may result from pigment loss in the algae themselves, particularly when thylakoid membranes are damaged by reactive oxygen species (ROS) and oxygen radicals (Lesser, 2011). Although ROS formation within Symbiodiniaceae cells is strongly implicated as the primary mechanism for symbiont expulsion

(Bieri et al., 2016), the precise cellular and molecular basis of bleaching remains only partially understood (Nielsen, Petrou and Gates, 2018) (Figure 5).

During bleaching, multiple physiological and molecular processes are disrupted within the coral holobiont. At the cellular level, elevated temperature and high irradiance overstimulate the photosynthetic machinery of Symbiodiniaceae, leading to the excessive generation of reactive oxygen species (ROS). These ROS inflict damage on organelles such as chloroplasts and mitochondria, compromise antioxidant defence systems, and impair key metabolic functions (Smith, Suggett and Baker, 2005; Gardner et al., 2017). A cascade of stress responses follows, including the production of nitric oxide in both the algal symbionts and the coral host, which has been proposed as a signalling molecule initiating symbiont expulsion (Baker, Glynn and Riegl, 2008; Downs et al., 2009) (Figure 5). This loss of symbionts and pigments reduces the host's energy supply, driving colonies towards a state of starvation (Jones, 2008).

At the molecular level, bleaching is also associated with pronounced immune activity in the coral host. Genes regulating apoptosis, necrosis, and cell–cell adhesion show increased activity during thermal stress (Barshis et al., 2013). Heat-tolerant corals display higher expression of cell death and immunity-related genes, particularly within the Hsp family, suggesting a "frontloaded" immune preparedness that supports resilience under heat stress (Barshis et al., 2013). However, these responses are highly species-specific (Palmer et al., 2011).

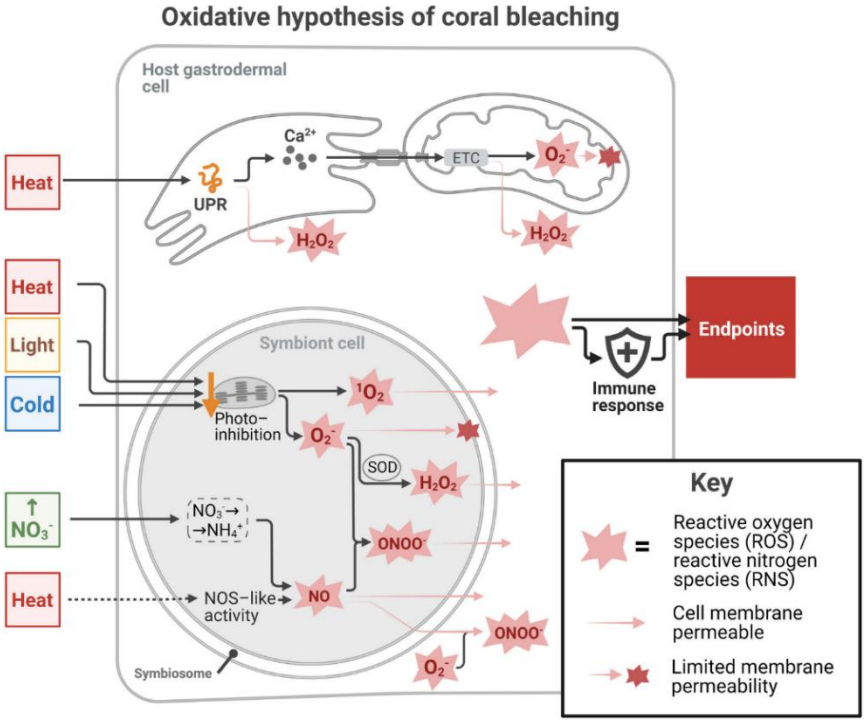

Figure 5. Overview of the oxidative hypothesis of coral bleaching. Schematic representation of the principal environmental triggers and their downstream effects on cellular pathways in both the host gastrodermal cells and algal symbionts. Reactive oxygen species (ROS) and reactive nitrogen species (RNS) include hydrogen peroxide (H_2O_2), singlet oxygen ($^1O_2$), superoxide (O_2^-), nitric oxide (NO), and peroxynitrite ($ONOO^-$). Abbreviations: ETC, electron transport chain; NOS, nitric oxide synthase; SOD, superoxide dismutase; UPR, unfolded protein response. Adapted from Suggett and Smith (2020).

In addition to the breakdown of the coral–dinoflagellate partnership, bleaching is often accompanied by marked shifts in the bacterial community composition of the holobiont (Figure 6). Typically, bleached colonies exhibit a decline in mutualistic and health-associated taxa, such as *Endozoicomonas*, which are considered key symbionts for maintaining host homeostasis (Neave et al., 2016). At the same time, there is frequently an increase in community diversity and the proliferation of opportunistic and potentially pathogenic groups, most notably *Vibrio* spp. (Bourne, Morrow and Webster, 2016; Ritchie, 2006). Experimental and field studies have reported that *Vibrio* abundances can rise dramatically during thermal stress—sometimes reaching up to 30% of the bacterial community in bleached corals—before returning to baseline levels in resilient or recovered colonies (Bourne et al., 2008). For example, the mortality of *Oculina patagonica* in the eastern Mediterranean was linked to infection by the bacterium *Vibrio shiloi* (Rosenberg & Loya, 1999), while Caribbean gorgonians

suffered epizootics caused by the fungus *Aspergillus sydowii* (Geiser et al., 1998). Such shifts are often associated with an enrichment of genes linked to virulence factors, suggesting that microbial imbalances not only accompany but may also exacerbate tissue damage and disease susceptibility. However, it remains unresolved whether increases in opportunistic bacteria like *Vibrio* directly trigger bleaching, or instead reflect a secondary outcome of holobiont destabilisation under thermal stress (Pogoreutz et al., 2020).

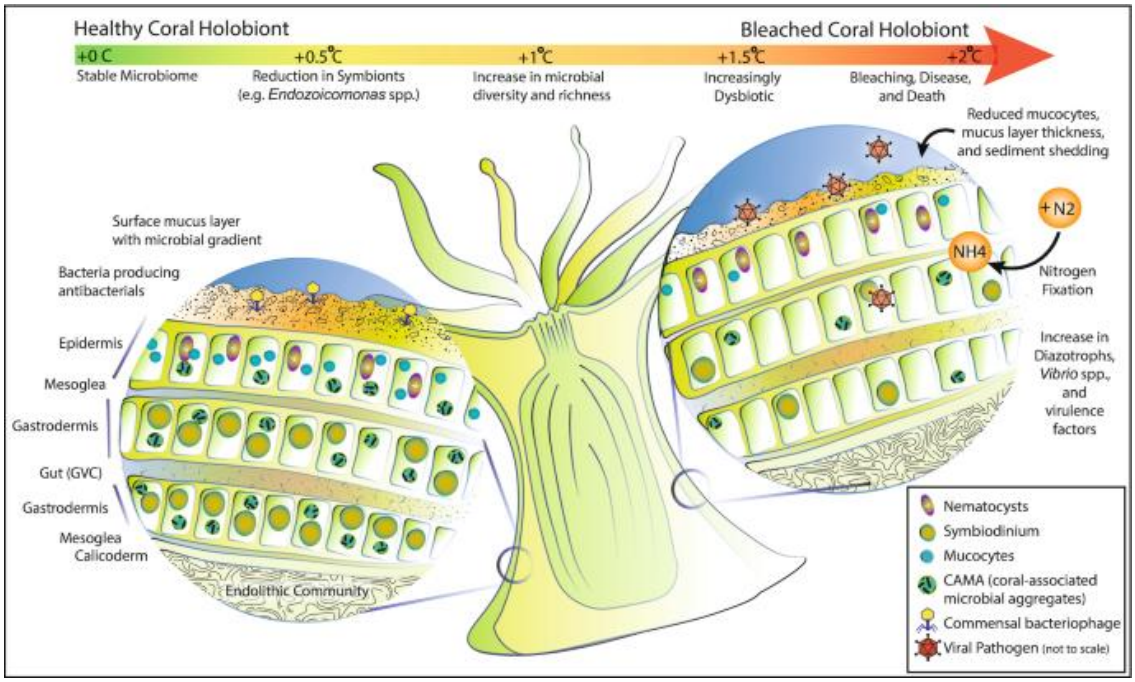

Figure 6. Schematic of host and microbial responses to thermal stress. Rising temperatures alter coral physiology and disrupt microbial homeostasis. Mucocyte density, mucus composition, and mucus layer thickness decline, weakening the protective microbial barrier. Beneficial symbionts such as Endozoicomonas within coral-associated microbial aggregates (CAMA) decrease, while potential pathogens (e.g. Vibrionales) increase. Enhanced diazotrophy relaxes nitrogen limitation of Symbiodiniaceae, stimulating algal cell division, reducing carbon translocation to the host, and heightening susceptibility to photodamage and bleaching. Adapted from Morrow, Muller and Lesser (2018).

If environmental stress persists and exceeds the buffering capacity of the microbial and dinoflagellate partners, bleaching progresses into a “traumatic” dysbiosis in which the permanent loss of symbionts makes recovery unlikely, often accompanied by the invasion of opportunistic pathogens (Smith, Suggett and Baker, 2005; Gardner et al., 2017). Recent perspectives therefore frame bleaching not solely as the collapse of a host–algal partnership,

but as a broader microbial dysbiosis within the holobiont (Pogoreutz et al., 2020). Under such conditions, microbial communities often shift from being dominated by beneficial taxa such as *Endozoicomonas* to opportunistic and potentially pathogenic groups like *Vibrio*, changes that further compromise tissue integrity and disease resistance. According to the adaptive dysbiosis hypothesis, these shifts may initially act as a buffer to environmental stress, but once thresholds are surpassed, they accelerate holobiont breakdown and culminate in bleaching (Pogoreutz et al., 2020).

The association with microbial symbionts contributes a wide array of essential functions that support holobiont stability. By sustaining balanced nutrient exchange and regulating photosynthetic efficiency, microbes can buffer corals against thermal stress and reduce the likelihood of bleaching (Rädecker et al., 2015; Pogoreutz et al., 2020). Conversely, microbial dysbiosis can destabilise photosymbiosis, disrupting the finely tuned metabolic interactions between host and Symbiodiniaceae and ultimately contributing to bleaching onset (Bourne et al., 2008; Nielsen, Petrou and Gates, 2018). Under thermal anomalies, coral persistence depends not only on the capacity of the holobiont to tolerate physiological stress, but also on its ability to recover and re-establish a stable equilibrium once conditions normalise.

Altogether, these observations highlight that the coral microbiome is not just a supporting component, but a central regulator of holobiont stability and stress tolerance. Its dynamic restructuring under MHWs underscores the need for integrative approaches that link microbial community shifts with host physiology, symbiont function, and bleaching patterns.

3. MATERIAL AND METHODS

3.1. Study area

For the purposes of research, coral investigation was conducted in 5 locations (11 stations) along the eastern Adriatic coast along the depth gradient for four years (2020 - 2023) using SCUBA diving (Figure 7). In Croatia, sampling localities included marine protected areas and Natura 2000 areas: Nature Park Telašćica (stations: Veli Garmenjak and Sestrica Vela sites), Kornati National Park (stations: Mana, Balun and Mali Obručan sites), and Mljet National Park (stations: Veliko jezero, Rt Lenga and Hrid Štit sites), while unprotected areas involved Croatian location Ljubačka vrata, as well as Slovenian locations (Ronek and rt Madona stations). The main environmental and ecological characteristics of all investigated locations and sampling stations are summarised in Table 1.

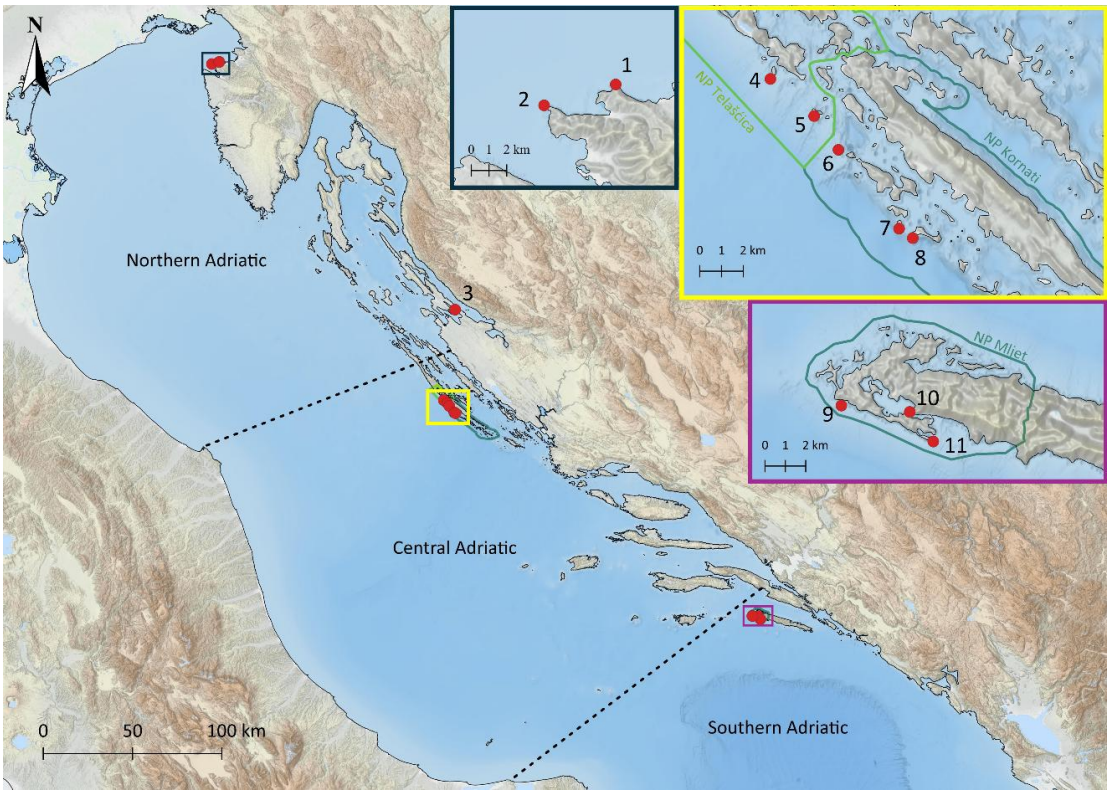

Figure 7. The map of the Adriatic Sea shows three main oceanographic sub-basins: the Northern, Central, and Southern Adriatic (Pérès and Gamulin-Brida, 1973; UNEP/MAP-RAC/SPA, 2015), and the location of 11 study sites marked with red dots and numbers. These include the Ronek (1) and rt Madona (2) stations on the Slovenian coast; Ljubačka vrata (3); Veli Garmenjak (4), and Sestrica Vela (5) in Nature Park Telašćica; Mali Obručan (6), Balun (7), and Mana (8) in National Park Kornati; and hrid Štit (9), Veliko jezero (10), and rt Lenga (11) in National Park Mljet.

Table 1. Main environmental and ecological characteristics of the investigated study locations and sampling stations across the Adriatic Sea. The table includes geographic position, depth range, habitat type, dominant biocoenoses, and the main geomorphological and hydrodynamic features of each station.

Adriatic basin	Location	Station	GPS coordinates	Depth range (m)	Station description	Marine habitat type	Dominant biocoenoses	Geomorphological characteristics and hydrodynamic exposure
North Adriatic	Slovenian coast	Cape Madona	N 45°31'50'' E 13°33'49''	0–16	Rocky coastal station near Piran with developed algal assemblages and coral presence	Rocky infralittoral reef	Infralittoral algae biocoenosis	Solid rocky bottom with gradual slope transitioning to sedimentary bottom; moderately exposed to wave action
		Ronek	N 45°32'28'' E 13°36'55''	10–16	Flat detrital seabed dominated by coral banks	Sand-detritus bottom with coral banks	Coral bank assemblages	Nearly flat sandy-detrital seabed with low to moderate hydrodynamic influence
Central Adriatic	Ljubačka vrata	Ljubačka vrata	N 44°19'07'' E 15°15'37''	0–25	Passage area with strong currents and exposed rocky coast	Rocky infralittoral reef	Infralittoral algae biocoenosis	Rugged vertical coasts and rocky reef exposed to intense currents, strong bora winds and wave action
	Nature Park Telašćica	Veli Garmenjak	N 43°51'56'' E 15°10'51''	0–70	Exposed cliff with developed coralligenous assemblages	Vertical rocky wall with coralligenous habitat	Infralittoral algae and coralligenous biocoenosis	Vertical rocky cliff with half-caves, highly exposed to open-sea wave action
	Nature Park Telašćica	Vela Sestrica	N 43°51'01'' E 15°12'21''	0–60	Rocky slope with fissures and gorgonian-dominated coralligenous habitat	Rocky slope and coralligenous reef	Infralittoral algae and coralligenous biocoenosis	Inclined rocky cliff with deep fissures and cavities under strong hydrodynamic exposure

	National Park Kornati	Mali Obručan	N 43°50'11'' E 15°13'11''	0–70	Steep rocky wall with caves and coralligenous communities	Vertical rocky wall with semi-dark caves	Infralittoral algae, coralligenous and semi-dark cave biocoenosis	Vertical cliff with half-caves strongly exposed to wave action
	National Park Kornati	Balun	N 43°48'14'' E 15°15'16''	0–60	Gradual rocky slope transitioning into Posidonia habitat and coralligenous reef	Rocky and mixed sediment bottom	Infralittoral algae, Posidonia oceanica, coralligenous biocoenosis	Rocky slope under moderate to strong exposure
	National Park Kornati	Mana	N 43°48'00'' E 15°15'44''	0–70	Highly exposed rocky wall with overhangs and caves	Vertical cliff with coralligenous habitat	Infralittoral algae, coralligenous and semi-dark cave biocoenosis	Indented vertical cliff with overhangs and half-caves, extremely exposed to waves
South Adriatic	National Park Mljet	Veliko jezero	N 42°46'08'' E 17°22'26''	0–46	Semi-enclosed marine lake	Marine lake formed by postglacial flooding of karst depressions	Infralittoral algae and coral reef assemblage	Gradual rocky slope transitioning to sedimentary bottom within a semi-enclosed low-hydrodynamic basin
	National Park Mljet	Lenga	N 42°45'21'' E 17°23'17''	0–70	Exposed rocky wall with deep coralligenous assemblages	Vertical coralligenous cliff	Infralittoral algae, coralligenous and semi-dark cave biocoenosis	Vertical rocky cliff with caves strongly exposed to wave action
	National Park Mljet	Štit	N 42°46'19'' E 17°19'58''	0–60	Exposed offshore rocky islet with caves and coralligenous habitat	Rocky coralligenous slope	Infralittoral algae, Posidonia patches and coralligenous biocoenosis	Rocky slope with numerous holes and caves under strong hydrodynamic conditions

3.2. Field survey

Research was conducted over a four-year period (2020–2023) across 11 stations distributed within five coastal locations along the eastern Adriatic Sea. Due to the multidisciplinary nature of the study, several parameters were measured at different temporal frequencies and depths. Seawater temperature was continuously recorded throughout the study period at five key stations: Ronek, Vela Sestrica, Mana, Veliko jezero, and Lenga.

Environmental parameters (nutrients, salinity, dissolved oxygen, and pH) were sampled twice annually, in July and October, between 2020 and 2022 at six representative stations (Ronek, Ljubačka vrata, Veli Garmenjak, Mana, Lenga, and Veliko Jezero).

Sampling for microbiome analysis of corals and surrounding seawater was performed during a two-year period (2021–2022) at selected stations in Mljet and Kornati National Parks and Nature Park Telašćica, encompassing depths from 2 to 40 m.

Coral colonies were sampled annually over a four-year period (2020–2023) at all stations for morphometric analyses, while histological samples were collected in 2021 and 2022 at a subset of sites and species. Not all species were present at all localities; therefore, the spatial coverage of sampling varied depending on the species distribution and habitat depth (Table 2).

Table 2. Overview of field sampling design (2020–2023) including coral species sampled for microbiom analysis, morphometric and histological analyses, and measured parameters.

Location	Station	Coral species sampled for Morphometry	Coral species sampled for Histology	Parameters measured
Slovenia	Ronek	*Cladocora caespitosa* *Balanophyllia europaea*	*Cladocora caespitosa* *Balanophyllia europaea*	Temperature
	Rt Madona	*Cladocora caespitosa* *Balanophyllia europaea*	*Cladocora caespitosa* *Balanophyllia europaea*	Nutrients
Ljubačka vrata	Ljubačka vrata	*Cladocora caespitosa* *Leptopsammia pruvoti* *Madracis pharensis* *Eunicella cavolini*	–	Nutrients
NP Telašćica	Veli Garmenjak	*Balanophyllia europaea* *Leptopsammia pruvoti* *Madracis pharensis* *Eunicella cavolini*	–	Temperature Nutrients
	Vela Sestrica	*Balanophyllia europaea* *Leptopsammia pruvoti* *Madracis pharensis* *Eunicella cavolini* *Paramuricea clavata*	–	Microbiome
NP Kornati	Mana	*Balanophyllia europaea* *Leptopsammia pruvoti* *Madracis pharensis* *Eunicella cavolini* *Paramuricea clavata*	*Balanophyllia europaea* *Leptopsammia pruvoti* *Eunicella cavolini* *Paramuricea clavata*	Temperature Nutrients Microbiome
	Mali Obručan	*Balanophyllia europaea* *Leptopsammia pruvoti* *Madracis pharensis* *Eunicella cavolini* *Paramuricea clavata*	*Balanophyllia europaea* *Leptopsammia pruvoti* *Madracis pharensis* *Eunicella cavolini* *Paramuricea clavata*	Microbiome
	Balun	*Balanophyllia europaea* *Leptopsammia pruvoti* *Madracis pharensis* *Eunicella cavolini* *Paramuricea clavata*	*Leptopsammia pruvoti*	–
NP Mljet	Veliko jezero	*Cladocora caespitosa* *Balanophyllia europaea*	*Cladocora caespitosa* *Balanophyllia europaea*	Temperature Nutrients Microbiome
	Rt Lenga	*Balanophyllia europaea* *Leptopsammia pruvoti* *Madracis pharensis*	*Leptopsammia pruvoti* *Madracis pharensis*	Temperature Nutrients Microbiome
	Hrid Štit	*Balanophyllia europaea* *Leptopsammia pruvoti* *Madracis pharensis*	*Leptopsammia pruvoti* *Madracis pharensis*	Microbiome

3.3. Oceanographic data and marine heat wave analysis

The seawater temperatures were measured using HOBO data loggers (HOBO Pendant Temperature/Light 64K Data Logger) (Onset Computers Corporation, Cape Cod, Massachusetts USA) in one-hour intervals. Temperature loggers were deployed at depths from 5 to 40 metres and secured with chrome-molybdenum bolts. Loggers were set up at 4 locations: Nature Park Telašćica, National Park Kornati, National Park Mljet and Slovenian coast. Informations were retrieved from data loggers using the HOBOware Pro program (Onset Computers Corporation, Cape Cod, Massachusetts USA) and graphs were made using Microsoft Excel.

The analysis of marine heatwaves (MHWs) in this study was conducted in accordance with the hierarchical framework proposed by Hobday et al. (2016), which offers a standardized method for detecting and characterizing these extreme thermal anomalies. An MHW was defined as a period of at least five days during which sea temperatures exceeded the 90th percentile, allowing for gaps of up to two days that were still considered part of the same event. Although the reference study recommends using a 30-year climatological baseline for percentile calculations, historical temperature records at the observed depths (5m, 10m, 20m, 30m, 40m) were not available. Consequently, I employed the longest available dataset, comprising four years of temperature observations collected between 2020 and 2023. This threshold-based approach enables cross-regional comparisons while ensuring methodological consistency with previous studies. For each depth, three descriptors have been selected to characterize the MHWs: the number of MHWs per year, the total duration (in days) of the MHWs per year and the mean intensity (in Celsius degrees (°C)) of MHWs. The intensity of MHWs is defined as the temperature above the climatological mean, so the mean intensity during a MHW is the mean of daily intensities during the MHWs (Hobday et al., 2016). In addition, cumulative intensity (relative to threshold) was used as an integrated measure of MHW severity, defined as the sum of daily temperature anomalies above the climatological threshold over the duration of each event, allowing comparison of thermal exposure among depths. To further refine the characterization of MHWs, I adopted the intensity-based categorization scheme proposed by Hobday et al. (2018). This scheme classifies MHWs into four severity levels: Category I

(Moderate), Category II (Strong), Category III (Severe), and Category IV (Extreme). The classification is based on multiples of the difference between the seasonal climatological mean and the 90th percentile threshold. This allows for the differentiation between low- and high-impact heatwaves, and facilitates ecological interpretation of their severity.

The multisensor probe (EXO3, YSI, USA) was used for environmental parameters measurements at all sites. A sampling of seawater for nutrient analysis was performed twice annually, in July and October, during the period from 2020 to 2022. The sampling in the water column at all investigated sites was carried out using a 5-liter Niskin Water Sampler (General Oceanics, Model 1010) up to 40 metres depth (depending on which depth the coral populations are located). Nutrient analysis (nitrite, nitrate, ammonium and total phosphorus) as well as salinity, dissolved oxygen, and pH were conducted at the Institute of Public Health in Zadar (Department of Water Chemistry, Sediment and Waste).

3.4. Molecular analyses of the coral microbiom

Samples of seawater and coral species for molecular analyses were collected at 3 different localities: the National Parks of Mljet, Kornati and the Slovenian coast. Seawater samples were taken from two different depths: 5m and 40m, except in Veliko jezero where samples were collected from depths of 5m and 15m. The seawater samples were filtered with a peristaltic pump on a membrane filter with a pore size of 0.2 µm. Membrane filters for eDNA analysis were stored at a temperature of -20 °C until further processing. Three branches of 5-7 cm length were sampled from each coral colony (for a total of 3 x 3 or 3 x 5 samples for each species at three depths). After fieldwork, samples of coral species were placed in artificial seawater and stored at a temperature of -20 °C until further processing. Total genomic DNA was isolated from membrane filters using the DNeasy® PowerWater® Kit (Qiagen GmbH Hilden, Germany) following the manufacturer's instructions. Coral samples were thawed, and total DNA was isolated from 0.25 g of crushed coral sample using the DNeasy® PowerSoil® Kit (Qiagen GmbH Hilden, Germany) according to the manufacturer's instructions.

The hypervariable V4 region of the prokaryotic 16S rRNA gene was amplified by polymerase chain reaction (PCR) using primer pair 515F Parada (5'- GTG YCA GCM GCC GCG GTA A -3') (Parada, Needham and Fuhrman, 2016) and 806R Apprill (5' GGA CTA CNV GGG TWT CTA AT -3') (Apprill et al., 2015). The eDNA samples were amplified, barcoded, filtered, normalized, and prepared for sequencing on the Illumina MiSeq system (v3 chemistry, 2x 300 bp) according to the protocol from Pjevac et al., 2021. Individual amplicon pools were extracted from the raw sequencing data using the FASTQ workflow in BaseSpace (Illumina) with default parameters and demultiplexing of each amplicon pool library into single amplicon libraries was performed with BBDuk (BBTools, Bushnell B) and python package demultiplex (Laros JFJ). Amplicon sequence variants (ASVs) were inferred using the DADA2 R package version 1.14.1 (Callahan et al., 2016a) with R version 3.6.1 (R Core Team, 2021), applying the recommended workflow (Callahan et al., 2016b). The taxonomy of prokaryotic ASVs was assigned using the SILVA SSU Ref NR 99 database version 138.1 (HTTP: //www.ncbi.nlm.nih.gov / PubMed / 23193283).

3.5. External examination and morphological analyses

Morphological analyses and external examinations of all investigated coral species were performed through *in situ* photosampling along established transects, followed by image analysis on a computer. Depending on the species and habitat depth, different photographic sampling protocols were applied, while using the same photographic equipment. All images were taken with a Nikon D810 underwater camera (Nikon Corporation, Japan) enclosed in a Sea&Sea MDX-D810 waterproof housing (Sea&Sea Sunpak Co., Ltd., Japan), and subsequently processed using Adobe Photoshop Lightroom Classic CC (Version 8.2.1.10; Adobe Systems Incorporated, 2019).

For the scleractinian species *Cladocora caespitosa*, *Balanophyllia europaea*, *Leptopsammia pruvoti*, and *Madracis pharensis*, coral condition was assessed based on photographs taken along a minimum of three randomly placed 5-m transects at each sampling station, using 25 x 25 and 50 × 50 cm metal quadrats (Figure 8). Transects were positioned within the depth range and benthic community characteristic of each species, encompassing shallow infralittoral algal

assemblages for *C. caespitosa* and *B. europaea*, and deeper infralittoral to upper circalittoral coraligenous habitats for *L. pruvoti* and *M. pharensis*. Each quadrat corresponded to a single photograph. Within each quadrat, all visible polyps were classified according to their condition. For *Balanophyllia europaea* and *Leptopsammia pruvoti*, two categories were distinguished: healthy (normally pigmented) and dead (white skeleton devoid of coral tissue). For *Cladocora caespitosa* and *Madracis pharensis*, an additional category of bleached/necrotic (partial tissue loss or change in tissue pigmentation) was included.

Each image was analysed separately on a computer to identify and count individuals within these categories. Based on the total number of healthy, bleached/necrotic, and dead polyps recorded across all images for a given site and year, polyp density (number of healthy polyps per square metre), bleaching rate (percentage of bleached polyps relative to the total population), and mortality rate (percentage of dead polyps relative to the total population) were calculated for each location and sampling year (Figure 8). Quantification of healthy, bleached/necrotic and dead polyps was performed followed the protocol of Kružić *et al*. (2008, 2012, 2013, 2014, 2016) to assess the condition of coral populations at each sampling station.

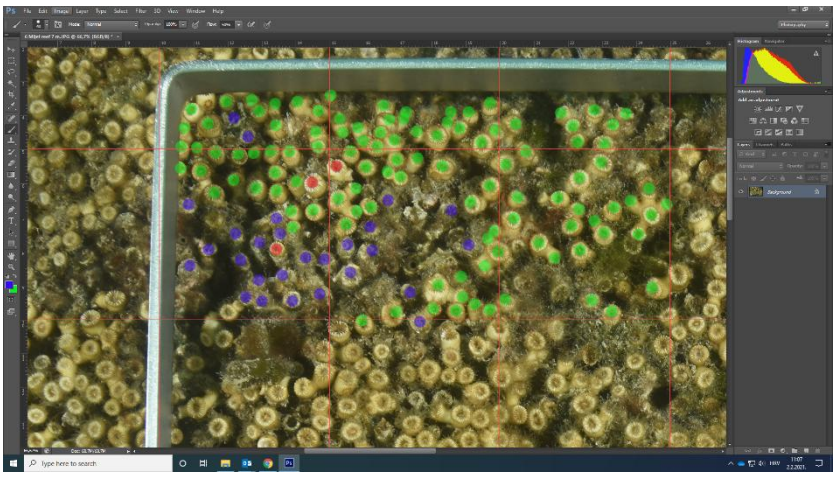

Figure 8. Counting live, necrotic and dead individuals of *Cladocora caespitosa* within one photo - a segment from larger 50x50 cm metal square using Photoshop SC software

For the gorgonians *Paramuricea clavata* and *Eunicella cavolini*, photosampling was performed at stations within deeper infralittoral and circalittoral coraligenous assemblages, between 20 and 40 m depth. At each station, a minimum of three randomly selected areas of 2.5 m² (each

composed of ten contiguous photographs of 50 × 50 cm quadrats) were photographed to ensure accurate species identification and quantification (Figure 9).

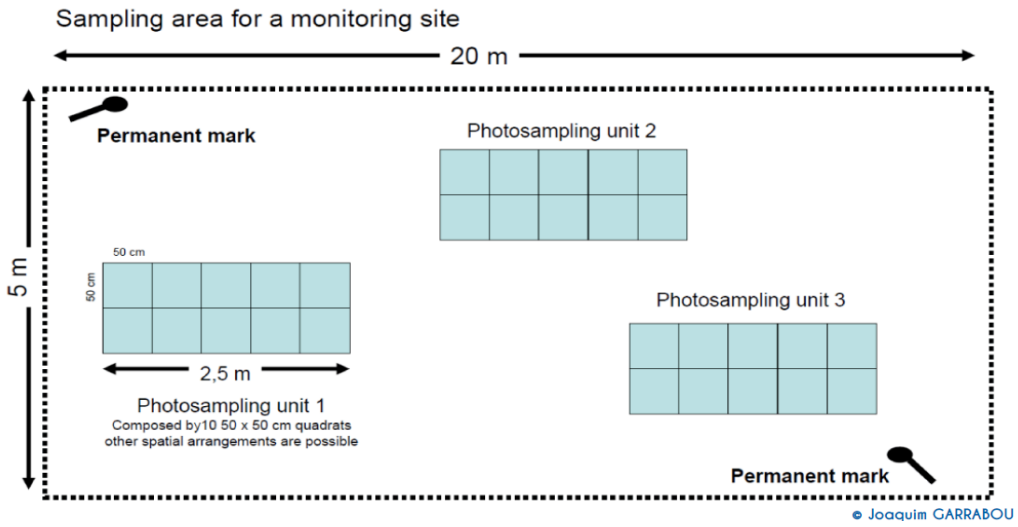

Figure 9. Sample scheme for morphological analysis of gorgonian species, adopted and modified from Garrabou et al. 2015

Along each transect, the percentage of affected colonies was determined from photo analyses. A colony was considered affected when the necrosis rate exceeded 10 % of its total surface area (Figure 10). For affected colonies, necrosis was classified as recent (presence of denuded axes or colonisation by pioneering species such as hydrozoans), old (axes covered by long-lived species such as bryozoans or calcareous algae), or mixed, following the classification by Garrabou et al. (2015). Quantification of necrosis and colony condition was conducted to evaluate the status of gorgonian populations at each sampling station.

Figure 10. Estimation of the colony's extent of injury (adopted and modified from Perez et al., (2000)), according to the proposed protocol, colonies with >10 % injured surface are considered as affected (Garrabou et al., 2015)

3.6. Histological analyses

All coral samples used for histological analyses were collected during 2021 and 2022, and each specimen was assigned a unique identification number. If necessary, samples were decalcified, using acid-based protocols, routinely embedded in paraplast blocks, sectioned into 12 µm slices using a rotary microtome, and subsequently stained with standard histological dyes.

3.6.1. Fixation and embedding

To preserve the tissue's morphology, the coral tissue samples were fixed with Zinc formalin fixative (Sigma Aldrich) diluted at a ratio of 1:4 (fixative:sea water) for 24 hours at room temperature. Following the fixation, all stony coral fragments were decalcified by immersion for 24 hours in RDO Rapid Decalcifier solution (Apex Engineering Products Corporation). After 24 hours, the tissues were placed in 70% ethanol for at least two days. After fixation, the tissue was embedded in paraffin blocks. First, the samples were run through a series of increasing concentrations of ethanol alcohols (Histanol 70, 80, and 96, Biognost; Ethanol absolute anhydrous, Carlo Erba reagents) to progressively remove water (Table A- 1) (Mescher, 2013). Following the dehydration, the tissues were cleared of alcohol by immersion in chloroform (Carlo Erba reagents) overnight to facilitate the impregnation of paraffin. Samples were then embedded in paraplast by gradually replacing the chloroform with molten paraplast through a series of three steps. Paper containers were used as moulds for tissue embedding. Each sample was carefully positioned at the centre of the mould using a needle and tweezers, with the surface intended for sectioning oriented downward. To prevent cooling and solidification of the paraplast, all steps were conducted in a 60 °C oven (Shel Lab). This temperature also

accelerates chloroform evaporation, thereby enhancing paraplast infiltration throughout the tissue (Mescher, 2013). Tissues were first immersed in a 1:1 chloroform–paraplast mixture at 60 °C for 60 minutes, followed by two successive immersions in pure paraplast at 60 °C for 60 minutes (Table A- 1). Finally, tissues were embedded in clean paraplast by pouring molten paraplast from the dispenser onto the sample, after which the blocks were allowed to harden at room temperature.

After gradual cooling to room temperature, blocks were sliced using a rotary microtome (Shadon Finesse 325, Thermo Fisher Scientific). The paraplast blocks were sliced to a thickness of 12 microns, and were then transferred with a brush to a water bath (GFL 1052) containing distilled water heated to 40°C for levelling over about 10 minutes. A drop of glycerine egg white, serving as an adhesive agent, was applied to the glass slide (VitroGnost, Biognost), and allowed to dry slightly. Subsequently, the section was collected from the water tank and positioned onto the glycerine egg white-coated glass slide. Each slide was pre-assigned its protocol number. Several hours later, the sections were positioned vertically on a drying rack at room temperature for drying and then placed in histological containers.

3.6.2. Staining procedures

Following a minimum of three days of drying at room temperature, the coral samples were stained with the following histochemical techniques: Hematoxylin and Eosin (HE), Masson Trichromatic, Grocott methenamine silver stain for fungal detection, and Gramme staining (all Biognost kits). For each histochemical staining protocol, two slides were prepared from each embedded sample, each containing three cross-sections. After triple deparaffinization in xylene (Bioclear, Biognost) and rehydrating the sample with increasing concentrations of alcohol (Histanol 95 and 100, Biognost) and distilled water (Table A- 2), the samples were stained using specific protocols (Table A- 3; Table A- 4; Table A- 5; Table A- 6).

Tissue sections stained with a mixture of the basic dye hematoxylin and the acidic dye eosin can distinguish nuclei from cytoplasmic structures. Hematoxylin selectively binds to acidic cellular components, staining nuclei and other basophilic structures violet-blue, while eosin stains cytoplasmic components, and connective tissue in varying shades of pink to red.

The Grocott kit is used in histology to visualize fungi, certain pathogenic organisms, basement membranes and general histological argentophilic structures. This technique results in the staining of basement membranes, glycogen, bacteria, and fungi in brown to black, while the background appears green, enhancing contrast for microscopic analysis.

The Masson Trichrome set is utilised to visualise negative staining muscles, collagen fibres, connective tissue, gametes, nuclei, neurofibrils, neuroglia, collagen, keratin intracellular fibrils, and the Golgi apparatus. This technique employs three dyes, with aniline blue selectively binding to muscle and collagen fibres. In addition, it is used to visualise pathological collagen accumulation, distinguishing fibrotic scar tissue from functional tissue, as well as differentiating collagen from smooth muscle fiber.

Gram staining is a differential method used to distinguish between Gram-positive and Gram-negative bacteria based on structural differences in their cell walls and their ability to retain dye. Gram-positive bacteria possess a thicker peptidoglycan layer, allowing them to retain the primary stain following iodine treatment, which forms an insoluble dye-iodine complex. In contrast, Gram-negative bacteria have a thinner cell wall that is unable to retain the primary stain, resulting in its decolorization and subsequent counterstaining with a secondary dye, enabling differentiation between the two bacterial groups.

Following the staining, all histological coral samples were dehydrated through a graded series of ethanol concentrations (Histanol 95 and 100, Biognost), cleared in xylene (Bioclear, Biognost), and mounted in Canadian balsam (BioMount C, Biognost) to create permanent slides. The prepared histological slides were then air-dried at room temperature for at least two days before microscopic examination.

To analyse histopathological lesions qualitatively and quantitatively, I microscopically screened a minimum of 10 randomly selected histological slides at various magnifications (20x, 40x, 100x, 1000x). Each sample was then assigned a general state code, which was the average value of the analysed histological slides per sample. A general state code followed the classification of Zodrow et al. (2004): 0 – healthy, no histopathology in sample; 1 - light

histopathology, present in <25% of the slides; 2 - moderate histopathology, present in 25%–75% of the slides; and 3 -heavy histopathology, present in >75% of the slides.

The prepared histological slides were analysed using a light microscope (Nikon Eclipse E600) in the ZEN2 program, generally used for imaging and morphometry. Depending on the species examined, distinct protocols were established for gorgonians and stony corals to accommodate their specific anatomical characteristics. The degree of diverse tissue damage and necrosis, as well as the potential invasion of foreign organisms into the coral body, were identified and quantified, following observations from similar studies (Gobbato et al., 2024; Hawthorn et al., 2023; Work, 2004; and Work & Aeby, 2006). Histopathological lesions were qualitatively classified through the presence of necrotic cells (cytoplasmic changes, cariorexia, karyolysis, pycnosis), degradation of cellular layers and inflammatory signs in mesoglea, morphological changes of symbiotic dinoflagellate cells, and changes in axis.

3.7.Statistical methods

The detection and classification of MHWs were performed using the open-source R package (R Core Team, 2021) developed by the authors of the reference study, incorporating key metrics such as duration, intensity, and cumulative thermal exposure. The implementation of this framework facilitated an objective assessment of temperature anomalies and their temporal evolution. Furthermore, Mann-Kendall trend analyses were employed to statistically evaluate long-term changes in sea temperature, thereby quantifying the significance of observed warming trends. This methodological rigour allows for a robust assessment of the relationship between increasing sea temperatures and biological stress responses, particularly in terms of species mortality.

The results of the morphological analysis were processed using Statistica (version 14.1.0.8., Cloud Software Group, Inc.). For each species, the normality of data distribution was first assessed using the Shapiro–Wilk test. When data followed a normal distribution, a one-way ANOVA was applied; otherwise, the non-parametric Kruskal–Wallis test was used, both at a

significance level of $\alpha = 0.05$. Where the Kruskal–Wallis test indicated significant differences, pairwise comparisons were performed using the Dunn post-hoc test ($p < 0.05$).

Statistical analyses of the microbiome were performed in the R programming language, version 4.0.4 (R Core Team, 2021). The resulting ASV tables were converted into a phyloseq object using the phyloseq package v.1.34.0 (McMurdie & Holmes, 2013). From the bacterial community dataset, unclassified ASVs, ASVs classified as Eukaryota, Mitochondria, and Chloroplast, as well as singleton ASVs (i.e., ASVs represented by a single sequence across the entire dataset), were excluded. Alpha diversity metrics were calculated using the vegan package (Oksanen et al., 2020). All graphical visualizations were generated using the ggplot2 package v.3.3.3 (Wickham, 2016).

4. RESULTS

4.1. Marine environmental parameters and marine heat waves (MHW)

To assess seasonal and spatial variations in hydrographic parameters and nutrient concentrations, field measurements were conducted at the following six stations across five locations: Ronek, the Slovenian coast; Ljubačka vrata; Veli Garmenjak (Nature Park Telašćica); Mana (National Park Kornati) and Rt Lenga and Veliko Jezero (National Park Mljet). Sampling was performed twice annually, in July and October, over the period from 2020 to 2022. The study aimed to evaluate fluctuations in salinity, dissolved oxygen, pH, and essential nutrients (nitrate, nitrite, phosphate, and ammonium) across different depths.

Five locations were used to measure the sea temperature continuously for four years: the Slovenian coast (Ronek), Nature Park Telašćica (station Veli Garmenjak), National Park Kornati (station Mana), and National Park Mljet (stations Veliko jezero and Lenga).

Unfortunately, due to adverse weather and meteorological conditions at the sea, some data loggers with recorded temperatures were never recovered. The following data are missing: complete data for the Ronek station at depths of 5 and 15 metres for 2020 and partially for 2021, the partial data for the Mana temperature station at a depth of 40m in 2020; the partial data for the Veli Garmenjak station at a depth of 5 m in 2020; and on the same station, the incomplete data are at a depth of 30m for both 2020 and 2021. During the 2020 and 2021 seasons, there was also a lack of data for the Veliko Jezero location of Mljet National Park at a depth of 5 m. In addition, for the Lenga station in Mljet National Park, the temperature data are incomplete at depths of 5, 10, and 20 metres for both 2020 and 2021 and completely missing at a depth of 40 metres in 2023. Due to missing temperature data, the mean values and Marine Heatwave (MHW) analysis for the specified time intervals are not included in the following analyses, as a minimum of three years of continuous data is required to establish the climatology and threshold for MHW detection.

The highest sea water temperature during the entire four-year period along eastern Adriatic coast was documented at Veli Garmenjak station in Telašćica Nature Park at a depth of 10

metres in 2020, reaching a value of 30.26°C. Conversely, the lowest sea temperature was observed at the Ronek station on the Slovenian coast in 2021 at a depth of 5 metres, measuring 9.00°C. It is predictable that the Slovenian coast, with its geographical and geological features, would experience the most extreme sea temperature values, as well as a different value distribution than other open-sea stations. Additionally, the highest oscillation of sea temperature for the four-year period under investigation was recorded at Veliko Jezero station at a depth of 15 metres in 2020 (19.30°C).

Particularly high extremes were also observed at Lenga station, Mljet National Park (the open column of seawater) at 5 and 10 metres depth in 2023 with temperatures of 29.95°C. Conversely, the lowest recorded values of 12.40°C were observed in 2021 at Veli Garmenjak station, Telašćica Nature Park at a depth of 30 metres and in 2022 at the Mana station, Kornati National Park, at a depth of 40 metres. When looking at the annual average sea temperature by depth at Veliko jezero station, Mljet National Park, the highest average temperature at a depth of 5 metres was 20.98°C in 2021, while at a depth of 10 metres it was 18.73°C in 2020, and at a depth of 15 metres it was 18.12°C in 2022.

A comparative analysis of the mean annual temperature values at the open sea stations (Telašćica, Mana, Lenga) reveals that the Veli Garmenjak station registered the highest value of 19.55°C for a depth of 5 metres in 2023. Moreover, across all open sea locations where data were collected, the mean annual sea temperature at a depth of 10 metres varied between 16.58°C (Veli Garmenjak in 2021) and 19.53°C (the same station in 2023). When comparing extremes in mean yearly temperatures at 20 metres depth, the difference between the Lenga and Mana stations in 2023 is a maximum of 1.36 degrees Celsius. The Mana station recorded the highest mean annual value of seawater temperature at 30 metres throughout the research period in 2020, with a value of 17.51°C. The other two stations at the same depth, Veli Garmenjak and Lenga, recorded their mean maximums in 2021 with a value of 17.75°C, and in 2020 with a value of 17.15°C, respectively. Except for Lenga station in 2022, where the annual mean temperature was recorded at 15.29°C, the mean annual sea temperature predicted by the deepest depth measurement at 40 metres corresponds to approximately 16°C.

4.1.1. Slovenian coast, Ronek

Ronek exhibited slightly higher salinity values compared to other stations, reaching 38.5‰ at 5 metres and 38.2‰ at 15 metres. Oxygen concentrations declined from 7.22 mg/L at 5 metres to 7.14 mg/L at 15 metres, while pH values remained relatively stable at 8.21–8.19 (Table A- 8, Table A- 10, Table A- 12). Nitrate levels in October 2020 ranged from 0.54 µmol/L at 15 metres to 0.61 µmol/L at 5 metres, indicating decreasing nitrogen availability with depth. Nitrite concentrations were highest at 5 metres (0.031 µmol/L) and lowest at 15 metres (0.026 µmol/L). Phosphate concentrations were generally low, with values ranging from 0.008 µmol/L at 15 metres to 0.021 µmol/L at 5 metres. Ammonium concentrations were highest at 5 metres (0.08 µmol/L) and lowest at 15 metres (0.06 µmol/L) (Figure A- 7, Table A- 9, Table A- 11).

Temperature data from the Ronek site revealed consistent vertical stratification accompanied by pronounced interannual variability. At 5 m depth, seasonal temperature oscillations remained relatively stable throughout the study period, with maximum temperatures consistently approaching 28°C each year (Table 3; Figure A- 1). Mean annual temperature increased slightly between 2021 and 2023, indicating a modest warming trend in the shallow layer.

At 15 m depth, minimum temperatures remained comparatively stable, whereas maximum and mean temperatures increased progressively over time (Table 3). The warming signal was particularly pronounced in the deeper layer, where maximum temperatures increased from 21.33°C in 2021 to 24.67°C in 2023, suggesting enhanced thermal penetration into the water column in recent years. Median temperatures followed a similar pattern, reflecting gradual warming at mid-depth.

Overall, both depths exhibited a clear interannual increase in mean and maximum temperatures, with a more pronounced warming signal at 15 m, implying progressive deepening of thermal anomalies and reduced vertical thermal gradients over the study period (Figure A- 2).

Table 3. Minimum, maximum, mean and median recorded sea temperature values (in °C) on station Ronek, Slovenian coast depending on the depth and observed year

Ronek 5m			
	2021	**2022**	**2023**
min	9.00	9.20	9.76
max	28.09	27.84	27.95
mean	17.67	17.95	18.11
median	16.16	18.69	17.82
Ronek 15m			
	2021	**2022**	**2023**
min	9.36	9.34	9.87
max	21.33	23.44	24.67
mean	14.52	16.27	16.56
median	13.48	16.66	15.98

4.1.1. Ljubačka vrata

Salinity at station Ljubačka vrata was relatively stable, with values ranging from 38.1‰ at 15 metres to 38.3‰ at 5 metres. Oxygen concentrations varied from 7.33 mg/L at 10 metres to 7.22 mg/L at 15 metres, with minor seasonal fluctuations. pH values ranged from 8.12 at 5 metres to 8.09 at 15 metres (Table A- 8, Table A- 10, Table A- 12).

Nitrate concentrations varied between 1.07 µmol/L at 5 metres and 1.29 µmol/L at 15 metres, indicating higher nitrogen levels at greater depths. Nitrite concentrations ranged from 0.031 µmol/L at 10 metres to 0.038 µmol/L at 5 metres. Phosphate levels were highest at 10 metres (0.021 µmol/L) and lowest at 15 metres (0.018 µmol/L). Ammonium concentrations exhibited depth-dependent variation, with values ranging from 0.12 µmol/L at 5 metres to 0.19 µmol/L at 15 metres (Table A- 7, Table A- 9, Table A- 11).

4.1.2. Nature Park Telašćica, Veliki Garmenjak

Throughout the years 2020, 2021, and 2022, the salinity at Veli Garmenjak remained relatively stable across different depths. In 2020, values ranged from 37.9‰ at 10 metres to 38.4‰ at 40 metres, with a similar pattern in subsequent years, when salinity reached 38.4‰ at 40 metres in 2021 and 2022. Oxygen concentrations demonstrated a gradual decline with depth, from 8.22 mg/L at 10 metres to 8.12 mg/L at 40 metres in 2020. A similar trend was observed in 2021 and 2022, with slight interannual variations. The pH values exhibited minimal fluctuations, ranging from 8.12 at 10 metres to 8.10 at 40 metres in 2020, with consistent stability across subsequent years (Table A- 8, Table A- 10, Table A- 12).

Nitrate (NO_3^-) concentrations at Veli Garmenjak in 2020 ranged from 0.31 µmol/L at 20 metres to 0.35 µmol/L at 10 metres in October. In 2021 and 2022, seasonal variability was more pronounced, with nitrate levels peaking at 1.05 µmol/L at 10 metres in October 2021. Nitrite (NO_2^-) concentrations followed a similar trend, with values ranging from 0.064 µmol/L at 40 metres to 0.086 µmol/L at 30 metres in 2020, and increased seasonal fluctuations in 2021 and 2022. Phosphate (PO_4^{3-}) concentrations were characteristic of oligotrophic conditions, with values fluctuating between 0.037 µmol/L at 40 metres and 0.042 µmol/L at 10 metres in 2020, and slightly increased concentrations in 2021 and 2022. Ammonium (NH_4^+) concentrations varied slightly with depth, with values ranging from 0.031 µmol/L at 40 metres to 0.039 µmol/L at 20 metres, showing a pattern indicative of organic matter remineralization (Table A- 8, Table A- 9, Table A- 11). In parallel with these relatively stabile physicochemical conditions, marked interannual variability was observed in the thermal regime at the site.

At the Veli Garmenjak station, shallow layers (5–10 m) exhibited pronounced seasonal and interannual variability throughout the four-year monitoring period. Temperatures above 20°C persisted from late May to early November in all analysed years, indicating extended summer stratification in the upper water column (Figure A- 3, Figure A- 4). The most pronounced warming was observed in 2023, when the highest temperatures were recorded at both depths, while an anomalous temperature peak of 30.26°C was documented at 10 m in June 2020 (Table 4). In contrast, summer temperatures during 2020 and 2021 remained comparatively lower,

particularly at 10 m depth, where values generally fluctuated between 16°C and 19°C from June to October.

At 20 m depth, thermal conditions were considerably more stable between October and May, with limited interannual variability in mean annual temperature (Table 4). Nevertheless, pronounced warming episodes occurred between June and September in all investigated years, with particularly prolonged high-temperature periods recorded in 2023, when temperatures exceeded 26°C for extended intervals (Figure A- 5).

Deeper layers (30–40 m) displayed a more gradual seasonal thermal regime characterised by progressive cooling from November to March and steady warming from April onwards (Figure A- 6, Figure A- 7). Despite the generally attenuated variability at depth, positive thermal anomalies were also recorded in the deeper water column. Most notably, at 40 m depth, temperatures exceeding 22°C persisted for an extended period during 2020, including a short-term maximum approaching 28°C (Figure A- 7).

Table 4. Minimum, maximum, mean and median recorded sea temperature values (in °C) on station Veli Garmenjak, Nature Park Telašćica, depending on the depth and observed year

Veli Garmenjak 5m				
	2020	**2021**	**2022**	**2023**
min	15.86	13.37	12.50	13.85
max	27.17	28.46	26.78	28.56
mean	21.50	18.88	18.90	19.55
median	21.38	18.43	18.90	17.86
Veli Garmenjak 10m				
	2020	**2021**	**2022**	**2023**
min	13.85	13.08	12.50	13.85
max	30.26	23.00	26.78	28.66
mean	17.30	16.58	18.90	19.53
median	17.28	17.00	19.00	17.86
Veli Garmenjak 20m				
	2020	**2021**	**2022**	**2023**
min	13.37	13.27	12.50	13.75
max	29.35	26.39	25.51	27.96
mean	17.76	17.54	17.41	17.95
median	17.86	18.05	17.86	17.28
Veli Garmenjak 30m				
	2020	**2021**	**2022**	**2023**
min	13.46	15.66	12.40	13.94
max	19.47	19.76	25.03	27.17
mean	15.37	17.75	16.62	17.04
median	14.71	17.95	16.81	17.19
Veli Garmenjak 40m				
	2020	**2021**	**2022**	**2023**
min	13.46	13.17	12.50	13.85
max	28.75	22.53	22.53	24.35
mean	16.59	16.18	16.24	16.21
median	16.43	16.14	16.24	16.62

A total of 53 marine heat wave (MHW) events were recorded in the Nature Park Telašćica, distributed across five depth levels. The highest number of events was observed at 5m (13 events) and 10m (11 events), while slightly fewer occurrences were recorded at 20m (10 events), 30m (9 events), and 40m (10 events) (Figure 11). These results indicate that MHWs were present at all monitored depths, with shallow waters (5m and 10m) experiencing the most frequent thermal anomalies. The observed distribution suggests a potential susceptibility

of surface and near-surface waters to temperature extremes, likely influenced by atmospheric conditions and seasonal variability.

The three longest MHW events varied in duration, depth, and timing, with the most prolonged events occurring in 2023 and 2020. The longest event lasted 21 days at 20m depth, occurring from September 22 to October 12, 2023. The second-longest event lasted 19 days at 10m depth, observed between July 20 and August 7, 2023. The third-longest event persisted for 15 days at 30m depth, recorded from June 4 to June 18, 2020. These extended MHWs primarily occurred during summer and early autumn, suggesting a seasonal trend in the persistence of warm anomalies. The presence of prolonged events at greater depths highlights the potential for subsurface heat retention, which may contribute to prolonged thermal stress in marine ecosystems.

The frequency of MHWs varied significantly across years and depths, with a notable increase in recent years. In 2020, MHWs were relatively infrequent, with only two events recorded at 5m, one at 10m, two at 20m, two at 30m, and four at 40m. In contrast, by 2023, MHW frequency increased markedly, with nine events at 5m, five at 10m, four at 20m, six at 30m, and four at 40m (Figure 12).

Notably, the shallowest depth (5m) experienced the most significant rise in MHWs, increasing from two events in 2020 to nine in 2023. Similarly, at 10m, events were nearly absent before 2022, but five occurrences were recorded in both 2022 and 2023. At 20m, 30m, and 40m, fluctuations were observed, but the general trend points toward increasing frequency, particularly in 2023. These findings suggest that MHWs have become more frequent and widespread in recent years, particularly in the upper layers of the water column (Figure 12).

The classification of MHW events by intensity revealed that most events fell within the moderate and strong categories, with one event classified as severe (Category III). The only severe MHW occurred in 2020 at 20m depth, lasting 6 days, with a maximum recorded intensity of 3.39°C above baseline conditions. In addition, several MHWs were categorized as strong (Category II), distributed across different years and depths. In 2020, three strong events were recorded, lasting between 6 and 15 days at 30m and 40m depths. In 2021, a single strong

MHW occurred at 5m depth, lasting 5 days. By 2022, three strong events were observed, with durations of 7 to 8 days at 5m, 30m, and 40m depths. In 2023, five strong MHWs were identified, lasting 5 to 11 days, occurring at 5m, 20m, 30m, and 40m depths. These findings indicate that while severe MHWs were rare, strong events were relatively frequent and have increased in occurrence over recent years. The clustering of strong MHWs in 2023 suggests a potential intensification of thermal anomalies in the region, highlighting the need for further investigation into long-term oceanographic and climatic drivers influencing MHW trends.

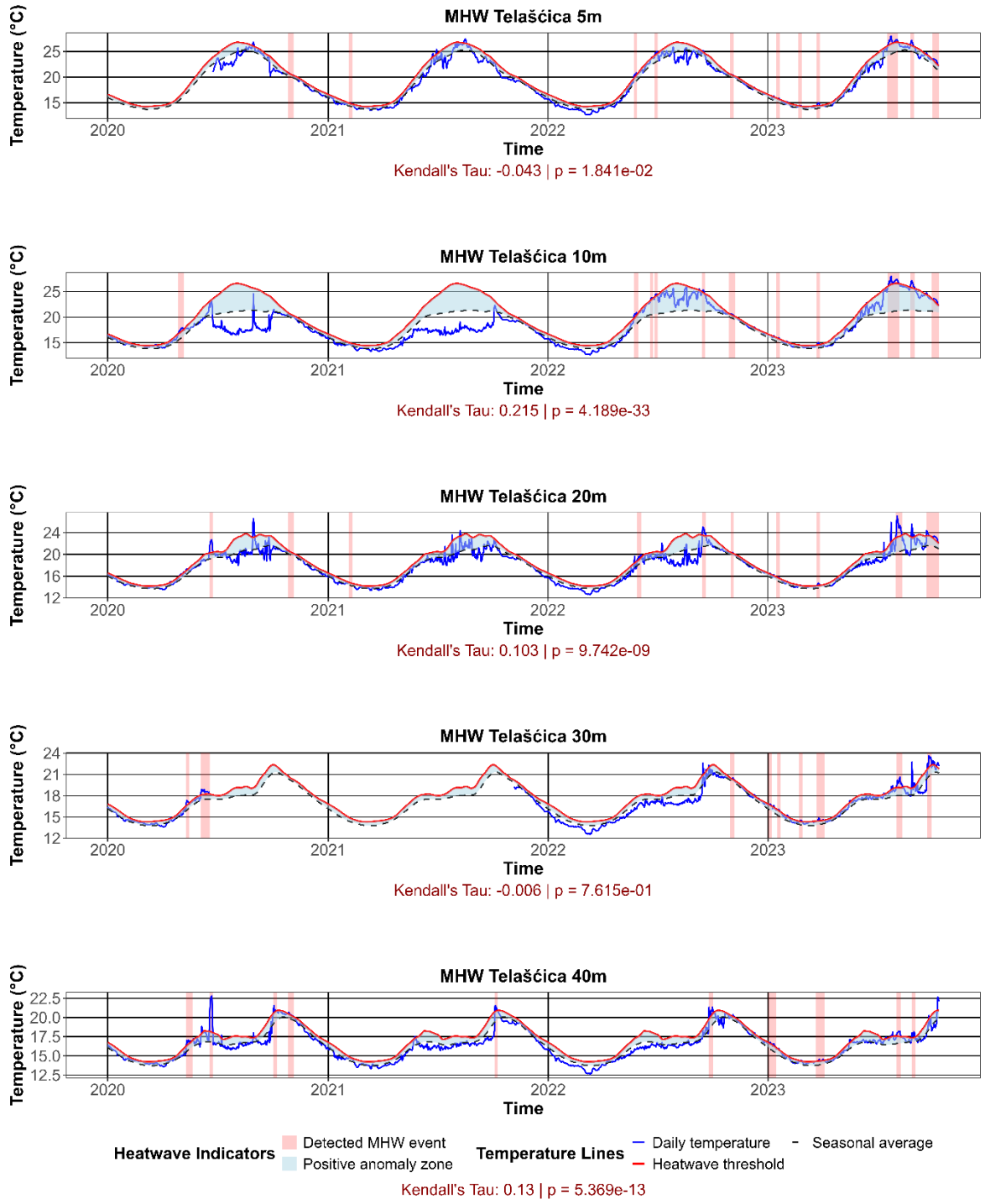

Figure 11. Visualisation of marine heatwaves across all depths (5, 10, 20, 30, and 40 m) at station Veli Garmenjak, Telašćica Nature Park, during the period 2020–2023. The plots display daily sea temperature (blue), the seasonal climatological mean (black dashed), and the marine heatwave (MHW) threshold (red). The light blue shaded area indicates the positive anomaly zone—temperatures exceeding the seasonal average but remaining below the MHW threshold. Red background areas highlight periods classified as marine heatwaves, defined as five or more consecutive days with temperatures above the 90th percentile threshold (Hobday et al., 2016). Each panel

includes Mann–Kendall trend statistics (Kendall's Tau and p-value) to assess monotonic trends in daily temperature.

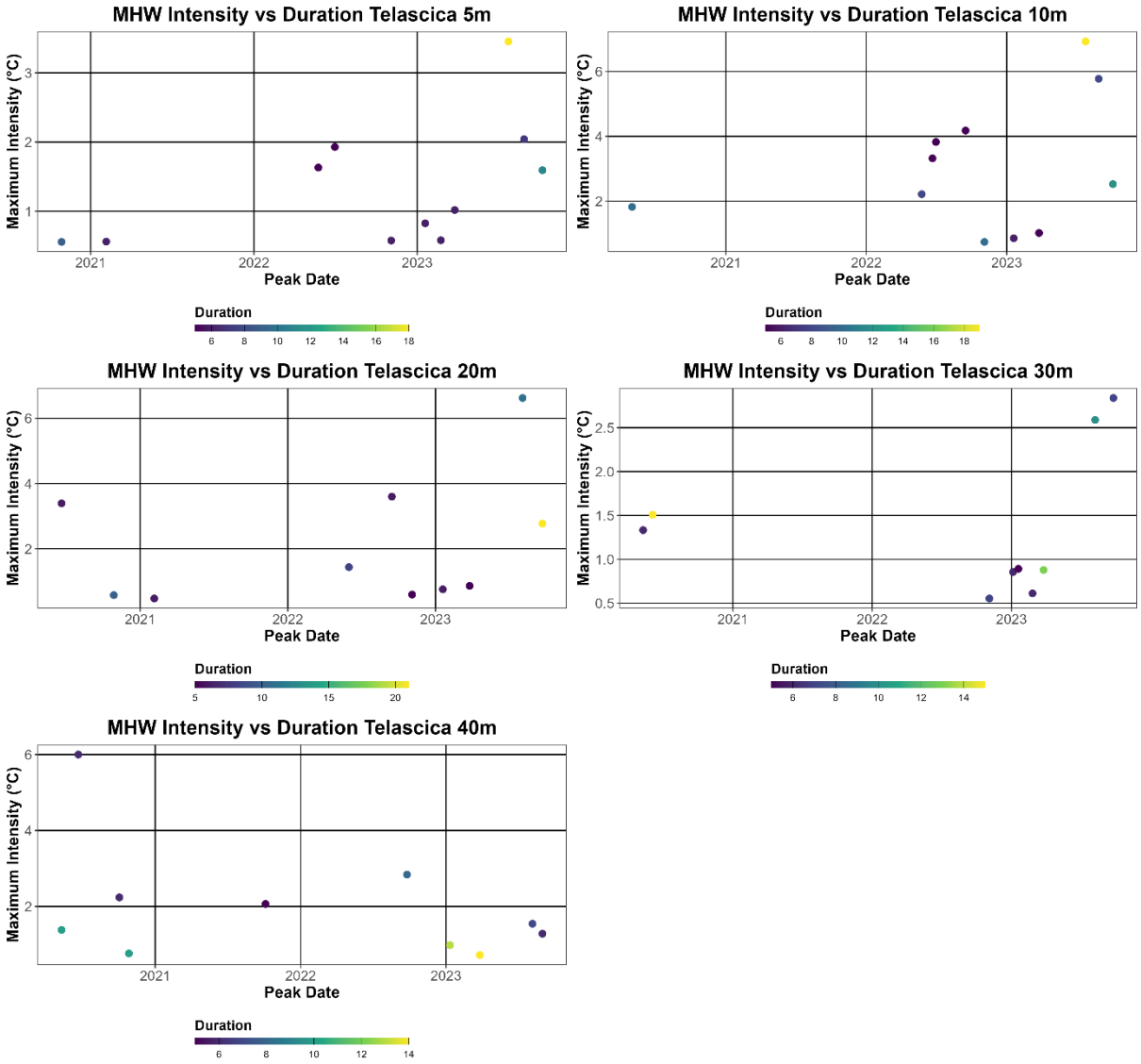

Figure 12. Visualisation of marine heatwave (MHW) intensity versus peak date across all depths (5, 10, 20, 30, and 40 m) at station Veli Garmenjak, Telašćica Nature Park, during the period 2020–2023. Each point on the scatter plots represents a detected MHW event, positioned by its peak date (x-axis) and maximum intensity in °C above the climatological mean (y-axis). The color gradient indicates the duration of each event, with warmer tones corresponding to longer-lasting MHWs.

4.1.3. Nacional Park Kornati, Mana

Salinity at Mana displayed stability throught the investigated period, with values ranging from 38.2‰ to 38.6‰, slightly increasing with depth. Oxygen concentrations decreased with depth, from 8.29 mg/L at 10 metres to 8.19 mg/L at 40 metres in 2020, with similar patterns in subsequent years. pH values ranged from 8.14 at 10 metres to 8.06 at 40 metres, indicating minor acidification at greater depths (Table A- 8, Table A- 10, Table A- 12).

Nitrate concentrations in October 2020 ranged from 0.36 µmol/L at 40 metres to 0.43 µmol/L at 20 metres, suggesting an accumulation of NO_3^- at intermediate depths. In 2021, nitrate concentrations exhibited greater variability, with peak values reaching 1.04 µmol/L at 10 metres. Nitrite values were highest at 30 metres (0.086 µmol/L) and lowest at 40 metres (0.076 µmol/L). Phosphate concentrations exhibited minor fluctuations, with values ranging from 0.037 µmol/L at 40 metres to 0.043 µmol/L at 20 metres. Ammonium concentrations were highest at 10 metres (0.036 µmol/L) and lowest at 40 metres (0.031 µmol/L), suggesting active nitrogen recycling processes at shallower depths (Table A- 7, Table A- 9, Table A- 11). Alongside these relatively stable nutrient conditions, pronounced variability was observed in the thermal regime at the Mana station.

Temperature records from the Mana station revealed substantial interannual and depth-related variability. The highest recorded temperature was 28.56°C at 10m depth in 2023, while the lowest recorded temperature was 12.40°C at 40m depth in 2022 (Table 5). At 10 metres deep, mean annual temperatures increased slightly throughout the study period, while seasonal minima remained relatively stable at approximately 12°C - 13°C during winter months. Summer maxima consistently exceeded 26°C, reflecting intense seasonal warming in the upper water column (Table 5, Figure A- 8).

At 20 m depth, thermal variability was slightly attenuated, although pronounced summer warming was still evident. Mean annual temperatures remained relatively stable, whereas maximum temperatures reached up to 28.16°C in 2023 (Table 5). The seasonal progression of

warming, particularly during August and September, indicated downward propagation of warm surface waters into deeper layers (Figure A- 9).

During the winter months, temperatures at the Mana station fluctuate between 12°C and 13°C at depths of 30 and 40 metres. The gradual warming of the lowest layers of the water mass is clearly observable, beginning in April-May and continuing until December during all analysed times. During the summer months (June-September), crucial temperature increases of up to 6 degrees or more are noticeable on the graphs, as seen in 2020, 2022, and 2023 at 30 metres (Figure A- 10) and 2021, 2022, and 2023 at 40 metres of depth (Figure A- 11).

Table 5. Minimum, maximum, mean and median recorded sea temperature values (in °C) on station Mana, National Park Kornati, depending on the depth and observed year

Mana 10m				
	2020	**2021**	**2022**	**2023**
min	13.27	12.98	12.59	13.85
max	27.08	27.47	26.00	28.56
mean	18.41	18.45	18.74	19.46
median	17.95	18.33	18.90	17.86
Mana 20m				
	2020	**2021**	**2022**	**2023**
min	13.46	13.08	12.50	13.85
max	27.17	27.08	25.61	28.16
mean	17.80	17.57	17.39	18.13
median	17.86	18.05	17.95	17.57
Mana 30m				
	2020	**2021**	**2022**	**2023**
min	13.85	13.08	12.50	13.75
max	26.29	22.81	24.93	27.17
mean	17.51	16.65	16.63	16.87
median	17.48	17.00	16.81	17.09
Mana 40m				
	2020	**2021**	**2022**	**2023**
min	15.38	12.98	12.40	13.85
max	22.24	22.24	22.33	25.61
mean	17.74	16.21	16.25	16.36
median	17.00	16.14	16.24	16.81

A total of 45 marine heat wave (MHW) events were recorded at different depths at the Mana station, NP Kornati. The distribution across depths was as follows: 10 events at 10m, 12 at 20m, 10 at 30m, and 13 at 40m (Figure 13). These findings indicate that MHWs occurred across all monitored depths, with a slightly higher prevalence at 40m and 20m.

The longest MHW event lasted 21 days at 20m depth, occurring between September 22 and October 12, 2023. The second-longest event persisted for 12 days at 10m depth, recorded from July 27 to August 7, 2023. The third-longest event lasted 11 days at 30m depth, occurring from June 24 to July 4, 2020. These results suggest that prolonged thermal anomalies were particularly evident in late summer and early autumn, with the most persistent events recorded at deeper depths.

The distribution of MHW events across years and depths revealed a significant increase in occurrence over the investigated period. In 2020, only one event was recorded at 10m, while in 2023, seven events were observed at this depth. A similar pattern was evident at 20m, where the number of events increased from two in 2020 to seven in 2023. At 30m depth, MHWs were infrequent in the early years, with only two events in 2020 and one in 2021, followed by a sharp rise to seven events in 2023. The most substantial increase was observed at 40m, where two events were recorded in 2020, one in 2021 and 2022, and nine in 2023. These results indicate a pronounced MHW frequency in 2023, which exhibited the highest number of events across all depths (Figure 14).

The classification of MHW events based on intensity revealed that most events fell within the moderate and strong categories, with only one event classified as severe (Category III). This severe MHW occurred in 2020 at 20m depth, lasting 9 days, with a maximum recorded intensity of 3.58°C above baseline conditions. In addition, 11 MHW events were classified as strong (Category II), distributed across different years and depths. One strong MHW occurred in 2020 at 30m depth, lasting 11 days. In 2021, two strong events were recorded, lasting 6 and 5 days at 30m and 40m depths, respectively. In 2022, two strong MHWs were observed, both lasting 8 days at 20m and 40m depths. The highest number of Category II events was recorded in 2023, with six occurrences. These events had durations ranging from 6 to 10 days and were distributed across all measured depths. While most MHWs were classified as moderate, the occurrence of several strong events in recent years indicates an upward shift in event intensity. In 2023, strong MHWs were clustered across multiple depth layers, marking the year as the period with the most pronounced thermal anomalies within the study.

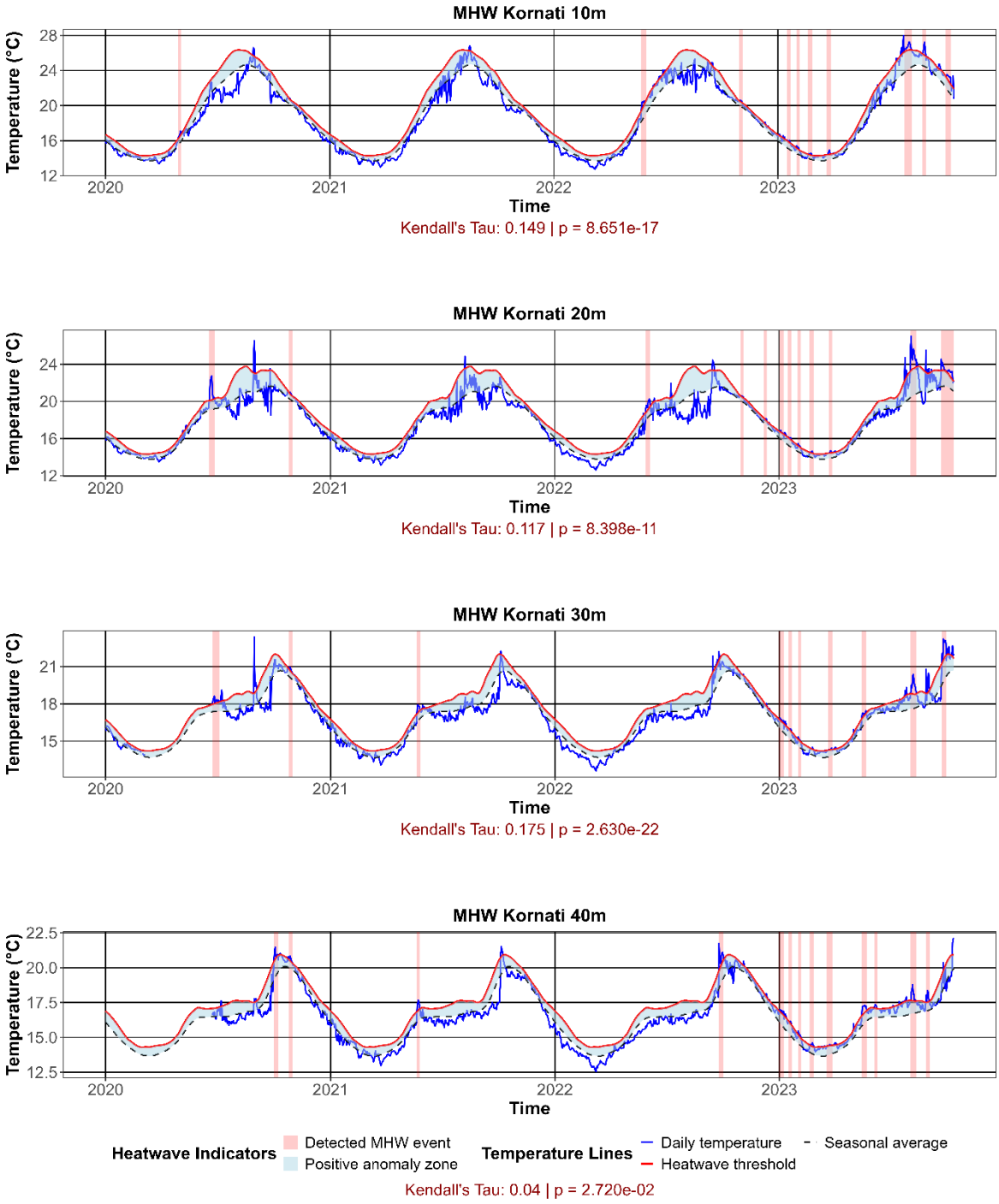

Figure 13. Visualisation of marine heatwaves across all depths (10, 20, 30, and 40 m) at station Mana, Kornati National Park, during the period 2020–2023. The plots display daily sea temperature (blue), the seasonal climatological mean (black dashed), and the marine heatwave (MHW) threshold (red). The light blue shaded area indicates the positive anomaly zone—temperatures exceeding the seasonal average but remaining below the MHW threshold. Red background areas highlight periods classified as marine heatwaves, defined as five or more consecutive days with temperatures above the 90th percentile threshold (Hobday et al., 2016). Each panel

includes Mann–Kendall trend statistics (Kendall's Tau and p-value) to assess monotonic trends in daily temperature.

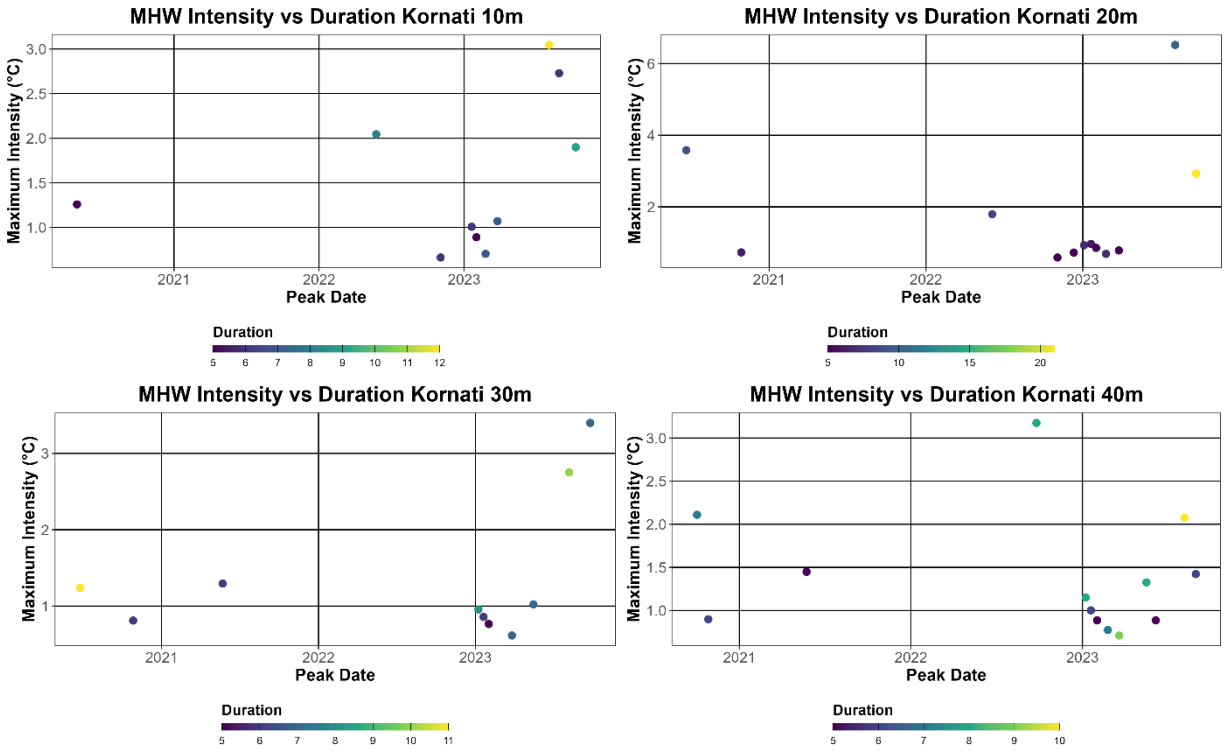

Figure 14. Visualisation of marine heatwave (MHW) intensity versus peak date across all depths (10, 20, 30, and 40 m) at station Mana, Kornati National Park, during the period 2020–2023. Each point on the scatter plots represents a detected MHW event, positioned by its peak date (x-axis) and maximum intensity in °C above the climatological mean (y-axis). The colour gradient indicates the duration of each event, with warmer tones corresponding to longer-lasting MHWs.

4.1.4. National Park Mljet, Veliko jezero

Veliko Jezero, located in the Mljet National Park, exhibited slightly lower salinity comparing to other stations, ranging from 37.7‰ at 15 metres to 38.1‰ at 5 metres. Oxygen levels declined with depth, from 7.41 mg/L at 5 metres to 7.27 mg/L at 15 metres. The pH values were lower than at other stations, ranging from 7.93 at 5 metres to 7.89 at 15 metres (Table A- 8, Table A- 10, Table A- 12).

Nitrate concentrations were highest at 5 metres (2.17 µmol/L) and lowest at 15 metres (2.03 µmol/L). Nitrite levels followed a similar trend, with values ranging from 0.049 µmol/L at 5 metres to 0.040 µmol/L at 15 metres. Phosphate values were highest at 15 metres (0.024 µmol/L) and lowest at 5 metres (0.011 µmol/L). Ammonium concentrations ranged from 0.36 µmol/L at 5 metres to 0.48 µmol/L at 15 metres, indicating localized nitrogen remineralization processes (Table A- 7, Table A- 9, Table A- 11).

The largest annual fluctuations in temperatures were recorded at this station. This is not surprising, considering that it is a submerged lagoon (closed basin). Annually, the water mass cooled more rapidly from September to February (when the lowest temperatures were recorded) and warmed more rapidly from the end of March to August (with peaks in July and August) at all three depths examined over the four-year period (Figure A- 12, Figure A- 13, Figure A- 14). Minimum annual temperatures at this location range from 18.12°C at 15 metres in 2020 to a maximum of 20.98°C at 5 metres in 2021 (Table 6).

Table 6. Minimum, maximum, mean and median recorded sea temperature values (in °C) on station Veliko jezero, National Park Mljet, depending on the depth and observed year

Veliko jezero 5m				
	2020	**2021**	**2022**	**2023**
min	11.53	13.17	10.65	11.43
max	29.45	28.46	29.15	29.45
mean	17.13	20.98	18.91	18.27
median	15.28	19.66	19.00	15.28
Veliko jezero 10m				
	2020	**2021**	**2022**	**2023**
min	11.53	11.04	10.46	11.43
max	29.45	28.06	28.36	28.95

mean	18.73	18.64	18.60	17.75
median	18.71	18.24	18.81	15.28
Veliko jezero 15m				
	2020	**2021**	**2022**	**2023**
min	11.53	11.04	10.65	11.24
max	29.45	27.86	29.95	22.33
mean	18.12	17.55	17.38	15.31
median	18.05	16.62	16.71	15.09

The analysis of marine heat waves (MHWs) in Veliko jezero reveals a total of 27 events recorded across three depth levels: 5m, 10m, and 15m. The distribution of events varied across depths, with 10 events observed at 5m, 7 events at 10m, and 10 events at 15m (Figure 15). This distribution suggests that MHWs were prevalent throughout the water column, with similar frequencies at the surface and deeper layers.

The duration of MHW events ranged from 5 to 18 days, with the longest event occurring at 5m depth from July 19 to August 5, 2023, lasting 18 days. The second-longest event, also at 5m, persisted for 15 days from August 15 to August 29, 2021. At 10m depth, the longest event lasted 16 days from July 21 to August 5, 2023 (Figure 16). These findings indicate that prolonged MHWs were more common in the upper layers of the water column, particularly during summer months.

Intensity analysis revealed that the majority of MHWs were classified as Category I (Moderate), with one exception. The most intense event, categorized as Category II (Strong), occurred at 15m depth from July 28 to August 5, 2020, with a maximum intensity of 4.72°C above the climatological mean. This event stood out as the only strong MHW in the dataset, suggesting that moderate events were common, while extreme thermal anomalies were rare.

Temporal trends in MHW occurrence showed an increase in frequency over the study period. In 2020, only three events were recorded across all depths. However, by 2023, the number of events increased significantly, with 10 MHWs observed across the three depth levels. This trend was particularly pronounced at 5m depth, where no events were recorded in 2020, but five events occurred in 2023 (Figure 15).

The seasonality of MHWs was evident, with a higher frequency of events during summer and early autumn months. July and August consistently experienced MHWs across multiple years and depths, indicating a seasonal vulnerability to thermal extremes. However, winter MHWs were also observed, particularly in January 2023, suggesting that thermal anomalies can occur year-round.

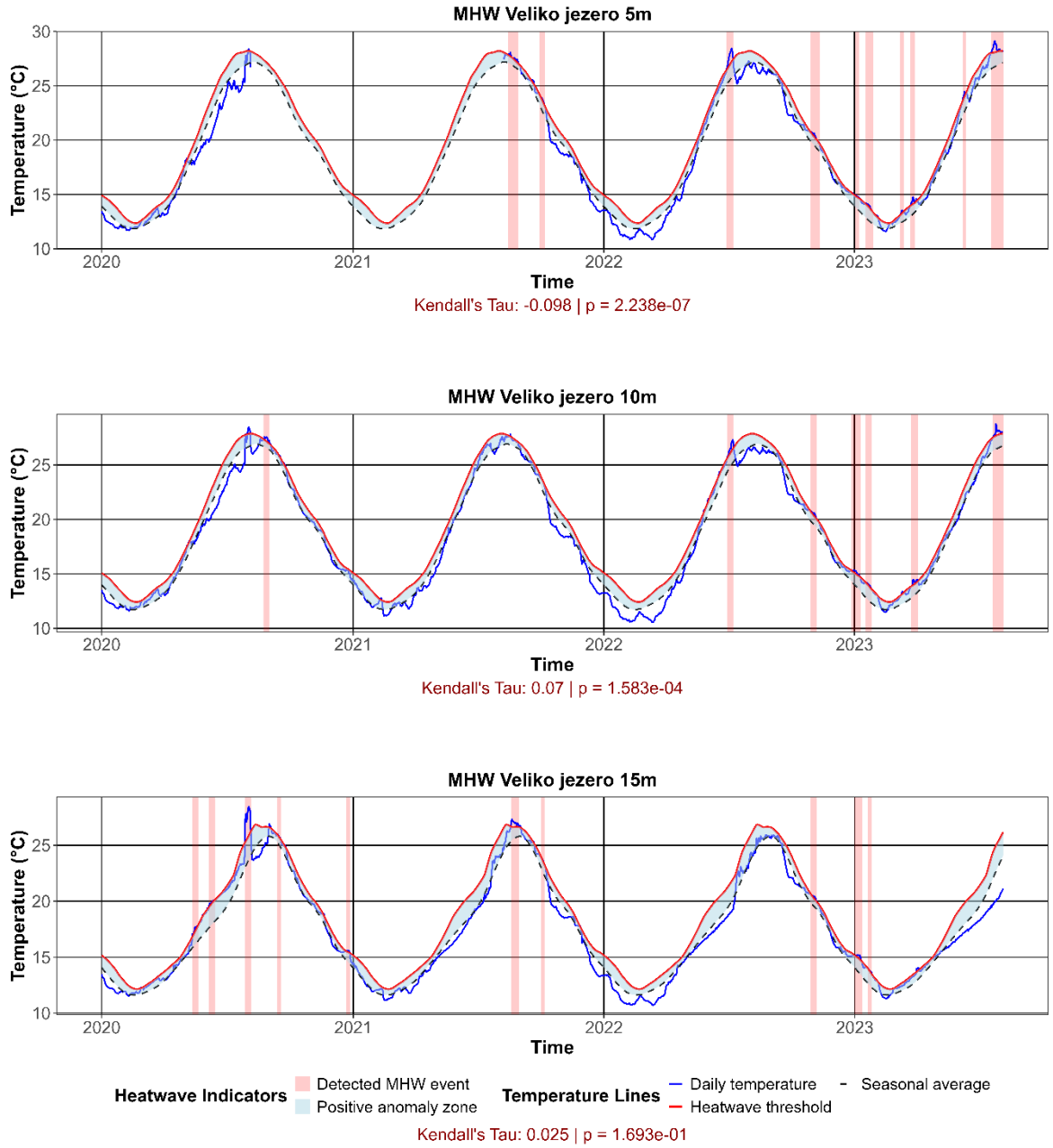

Figure 15. Visualisation of marine heatwaves across all depths (5, 10 and 15 m) at station Veliko jezero, Mljet National Park, during the period 2020–2023. The plots display daily sea temperature (blue), the seasonal climatological mean (black dashed), and the marine heatwave (MHW) threshold (red). The light blue shaded area indicates the positive anomaly zone—temperatures exceeding the seasonal average but remaining below the MHW threshold. Red background areas highlight periods classified as marine heatwaves, defined as five or more consecutive days with temperatures above the 90th percentile threshold (Hobday et al., 2016). Each panel includes Mann–Kendall trend statistics (Kendall's Tau and p-value) to assess monotonic trends in daily temperature.

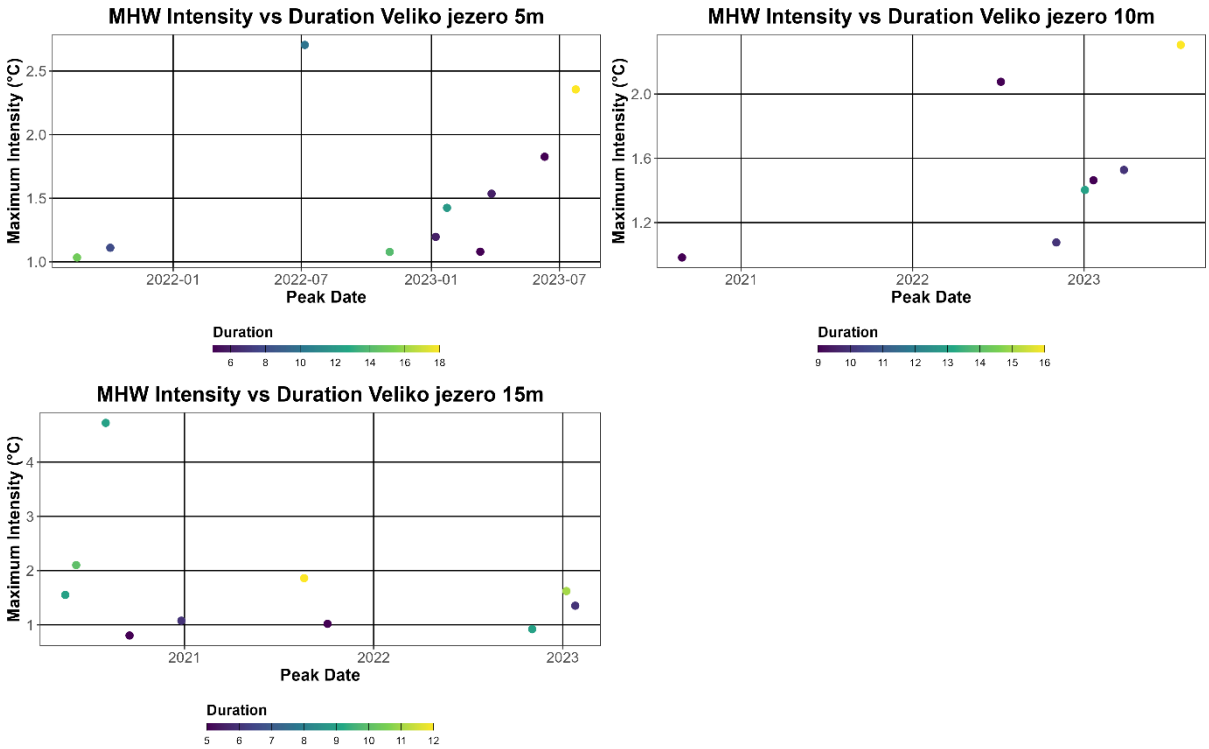

Figure 16. Visualisation of marine heatwave (MHW) intensity versus peak date across all depths (5, 10 and 15 m) at station Veliko jezero, Mljet Nature Park, during the period 2020–2023. Each point on the scatter plots represents a detected MHW event, positioned by its peak date (x-axis) and maximum intensity in °C above the climatological mean (y-axis). The color gradient indicates the duration of each event, with warmer tones corresponding to longer-lasting MHWs.

4.1.5. National park Mljet, Lenga

Salinity at Rt Lenga varied between 37.3‰ and 38.4‰, with slightly lower values compared to the other investigated stations. Oxygen concentrations ranged from 8.07 mg/L at 10 metres to 8.01 mg/L at 40 metres, indicating a gradual oxygen decline with depth. pH values showed slight variations, with values ranging from 7.90 at 10 metres to 7.86 at 40 metres (Table A- 8, Table A- 10, Table A- 12).

Nitrate levels at Rt Lenga ranged from 0.27 µmol/L at 40 metres to 0.33 µmol/L at 30 metres, indicating relatively low nitrogen availability. Nitrite concentrations were highest at 30 metres (0.024 µmol/L) and lowest at 40 metres (0.023 µmol/L). Phosphate values were within an oligotrophic range, with a maximum of 0.022 µmol/L at 40 metres. Ammonium concentrations varied between 0.025 µmol/L at 40 metres and 0.033 µmol/L at 10 metres, indicating potential surface-driven nitrogen cycling (Table A- 7, Table A- 9, Table A- 11).

At the Lenga station, the annual temperature oscillations at 5 and 10 meters depths show a similar pattern throughout a four-year period (Figure A- 15, Figure A- 16). The minimum temperatures remained relatively stable, generally ranging between 13°C and 16°C, whereas maximum temperatures increased substantially during summer months, reaching 29.95°C in 2023 at both depths (Table 7). Mean annual temperatures were consistently higher at 5 m and 10 m during 2021 and 2022, reflecting intensified warming in the upper water column. At 10 m depth, temperatures above 28°C occurred briefly during August 2022, while in 2023 temperatures exceeding 26°C persisted for more than one month (Figure A- 16).

The average sea temperature at a depth of 20 metres ranged from 16.77°C to 17.75°C (Table 7). Seasonal warming was nevertheless evident during summer months, particularly between June and August, followed by downward propagation of warmer surface waters into deeper layers during September and October (Figure A- 17). Maximum temperatures at this depth reached 27.96°C in 2023.

The seasonal dynamics observed at 30 m and 40 m depths reflected autumnal vertical mixing of the open-sea water column (Figure A- 18, Figure A- 19). Winter temperatures generally remained around 13°C and gradually increased from April onwards. During summer and early

autumn, periodic warming events were recorded, with particularly pronounced anomalies observed in 2020. At both depths, seawater temperature increased substantially towards the end of September, reaching peak values in mid-October, including a maximum of 24.55°C at 30 m depth in 2020 (Table 7). Temperatures remained above 18°C until early December before declining during winter months.

Table 7. Minimum, maximum, mean and median recorded sea temperature values (in °C) on station Lenga, National Park Mljet, depending on the depth and observed year

Lenga 5m				
	2020	**2021**	**2022**	**2023**
min	13.75	15.86	13.85	13.65
max	24.16	28.36	28.36	29.95
mean	17.17	21.52	19.23	18.27
median	16.05	20.90	19.85	16.52
Lenga 10m				
	2020	**2021**	**2022**	**2023**
min	13.65	15.76	13.75	13.85
max	22.53	28.56	27.37	29.95
mean	16.85	21.33	18.89	17.96
median	15.76	20.90	19.38	16.71
Lenga 20m				
	2020	**2021**	**2022**	**2023**
min	13.56	15.76	13.85	13.75
max	21.09	27.86	25.22	27.96
mean	16.33	20.05	17.75	16.77
median	15.57	20.23	17.67	16.52
Lenga 30m				
	2020	**2021**	**2022**	**2023**
min	13.75	13.65	13.75	13.75
max	24.55	23.00	23.00	18.62
mean	17.15	16.87	16.79	16.18
median	16.90	16.33	16.24	16.24
Lenga 40m				
	2020	**2021**	**2022**	**2023**
min	13.85	13.65	13.85	
max	24.16	22.91	17.86	
mean	16.97	16.77	15.29	
median	16.43	16.14	15.38	

A total of 29 marine heat wave (MHW) events were recorded at the Lenga station, distributed across four depth levels: 5m, 10m, 20m, and 30m. The highest number of events was observed at the depths of 5m and 10m (8 events each), followed by 20m (7 events), and 30m (5 events) (Figure 17). This distribution suggests that MHWs were more frequent in the upper layers of the water column, potentially due to their closer proximity to atmospheric influences and surface heating.

The duration of MHW events varied considerably, ranging from 5 to 19 days. The longest event persisted for 19 days at 30m depth, occurring from September 27 to October 15, 2020. Other notable long-duration events included an 18-day event at 10m (May 26 to June 12, 2022) and a 16-day event at both 5m (August 14-29, 2021) and 30m (June 5-20, 2020). These extended MHWs predominantly occurred during late spring, summer, and early autumn, indicating a seasonal pattern in the persistence of warm anomalies.

Temporal analysis revealed an increasing trend in MHW frequency over the study period. In 2020, only four events were recorded across all depths. However, by 2023, the number of events increased significantly, with 11 MHWs observed across four depth levels. This trend was particularly evident at 5m and 10m depths, where the number of events in 2023 (4 and 3 events, respectively) surpassed those of previous years (Figure 18).

The intensity of MHWs varied across depths and events. The most intense event occurred at 10m depth from July 19 to July 27, 2023, with a maximum intensity of 6.91°C above the climatological mean. Other high-intensity events were observed at 5m depth, with maximum intensities of 5.97°C (July 20 to August 1, 2023) and 4.65°C (June 28 to July 3, 2022) (Figure 18). These findings suggest that the most extreme thermal anomalies tended to occur in the upper water column during summer months.

Classification of MHW events by intensity revealed that the majority fell within Category I (Moderate), with several events classified as Category II (Strong) and one event reaching Category III (Severe). The sole severe MHW occurred at 20m depth from July 24 to August 1, 2023, with a maximum intensity of 4.29°C above baseline conditions. Strong (Category II) MHWs were observed across all depths, with a total of 8 events. These strong events were

more prevalent in recent years, with 5 out of 8 occurring in 2022 and 2023. The 5m depth experienced the highest number of strong MHWs (4 events), followed by 10m (2 events), 20m (1 event), and 30m (1 event). This distribution suggests that the upper layers of the water column are more susceptible to intense thermal anomalies.

Seasonality analysis indicated that MHWs were most frequent during summer months, particularly July and August. However, winter MHWs were also observed, especially in January 2023, suggesting that thermal anomalies can occur year-round in this region. The analysis of MHWs at the Lenga station demonstrates an increasing frequency and intensity of thermal anomalies, particularly in recent years and in the upper water column. The occurrence of a severe MHW and multiple strong events underscores the potential for significant thermal stress in the marine ecosystem.

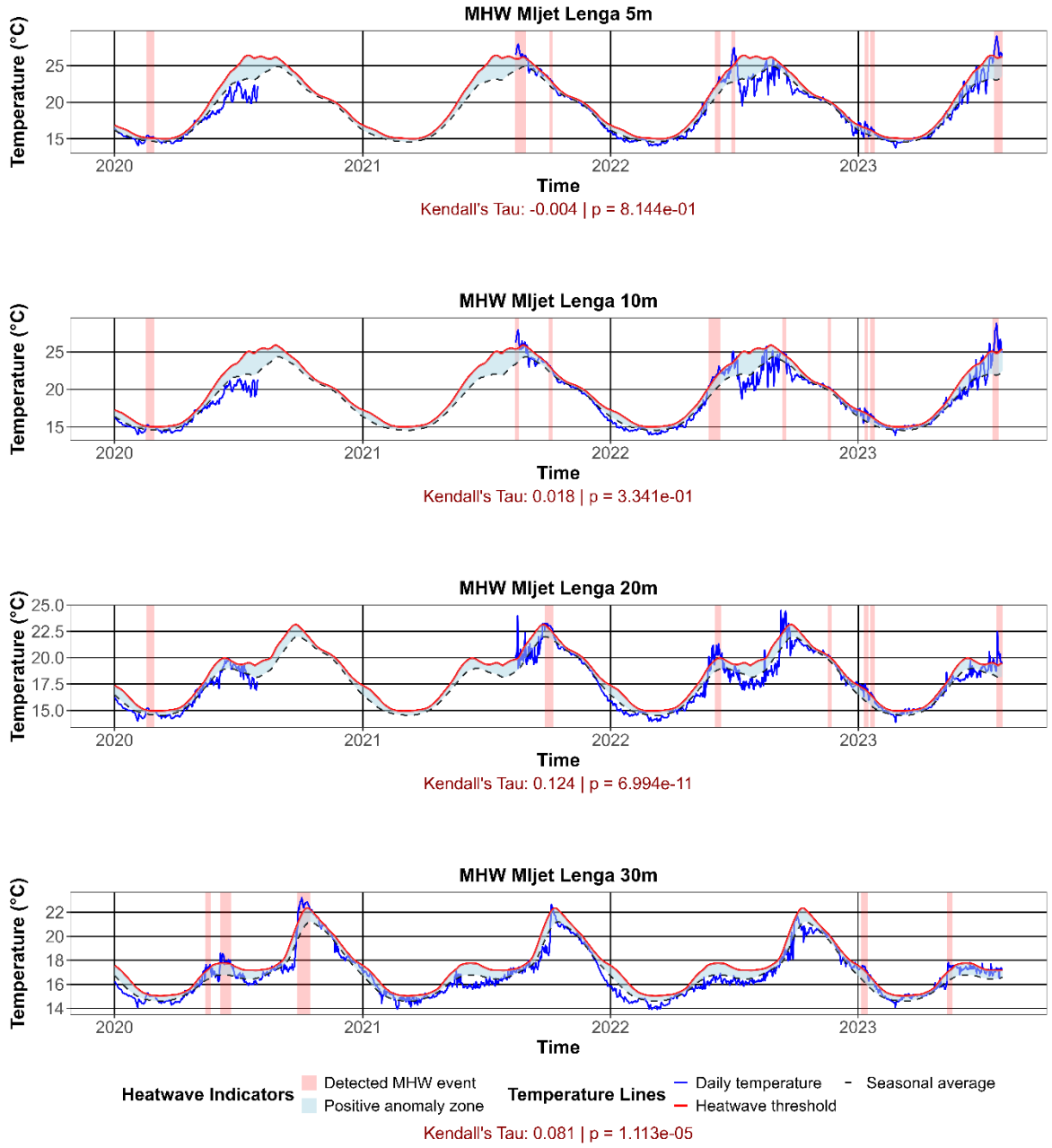

Figure 17. Visualisation of marine heatwaves across all depths (5, 10, 20 and 30 m) at station Lenga, Mljet National Park, during the period 2020–2023. The plots display daily sea temperature (blue), the seasonal climatological mean (black dashed), and the marine heatwave (MHW) threshold (red). The light blue shaded area indicates the positive anomaly zone—temperatures exceeding the seasonal average but remaining below the MHW threshold. Red background areas highlight periods classified as marine heatwaves, defined as five or more consecutive days with temperatures above the 90th percentile threshold (Hobday et al., 2016). Each panel includes Mann–Kendall trend statistics (Kendall's Tau and p-value) to assess monotonic trends in daily temperature.

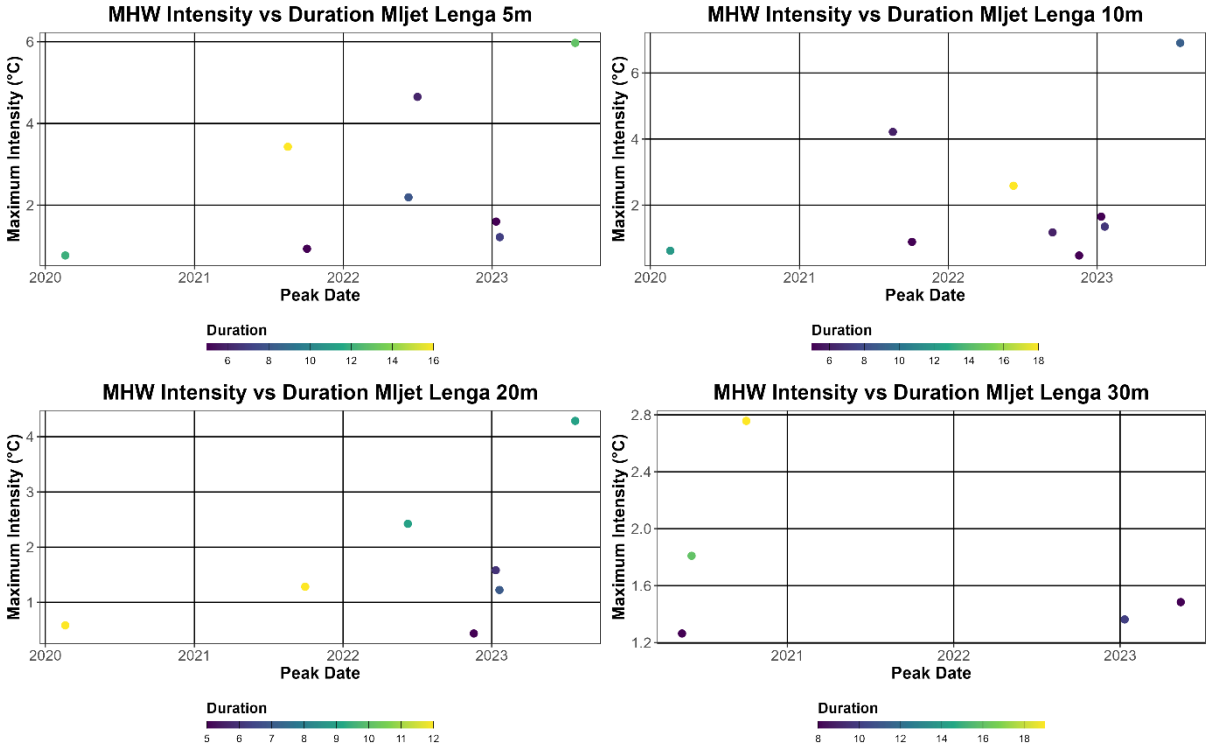

Figure 18. Visualisation of marine heatwave (MHW) intensity versus peak date across all depths (5, 10, 20 and 30 m) at station Lenga, Mljet Nature Park, during the period 2020–2023. Each point on the scatter plots represents a detected MHW event, positioned by its peak date (x-axis) and maximum intensity in °C above the climatological mean (y-axis). The color gradient indicates the duration of each event, with warmer tones corresponding to longer-lasting MHWs.

4.2. Molecular characterisation of the microbiome

To assess the diversity of coral-associated bacterial communities and their surrounding seawater, we conducted research on stations within the Mljet and Kornati National Parks, as well as Nature Park Telašćica.

4.2.1. Bacterial community composition in seawater samples

Seawater samples were collected during a two-year sampling period from multiple locations within Kornati National Park, Telašćica Nature Park and Mljet National Park to characterise bacterial community composition throughout the water column. Sampling was conducted at Obručan and Mana (Kornati), Mala Sestrica (Telašćica), and Veliko jezero, Štit and Lenga (Mljet), covering depth profiles between 2 and 40 m depending on the station (Figure 19).

Across all investigated locations and depths, bacterial assemblages exhibited broadly similar phylum-level composition. Proteobacteria consistently dominated the communities, representing the largest proportion of the assemblage in all samples (Figure 19). Bacteroidota, Cyanobacteria and Verrucomicrobiota constituted the principal secondary phyla, while Planctomycetota, Marinimicrobia (SAR406 clade), Actinobacteriota, Dadabacteria, Chloroflexi and SAR324 clade (Marine group B) occurred at comparatively low relative abundances.

At the open-sea and outer coastal stations (Obručan, Mana, Mala Sestrica, Štit and Lenga), bacterial community composition remained relatively uniform throughout the water column, with only minor depth-related variability in the relative abundances of secondary and low-abundance phyla. Slight increases in Planctomycetota, Marinimicrobia and Actinobacteriota were occasionally observed in deeper samples, particularly at 20–40 m, although these differences remained limited overall.

In contrast, Veliko jezero exhibited the most distinct vertical structuring of bacterial assemblages among all investigated sites. Compared to the other locations, the 20 m sample showed higher relative abundances of Cyanobacteria, Actinobacteriota and Verrucomicrobiota, whereas the 15 m sample displayed an increased contribution of Marinimicrobia (SAR406 clade). Bdellovibrionota were consistently detected across all

sampled depths at Veliko jezero, while remaining absent or negligible at most other locations. Overall, the bacterial community in Veliko jezero showed greater heterogeneity across depths compared to the relatively homogeneous assemblages observed at the remaining stations.

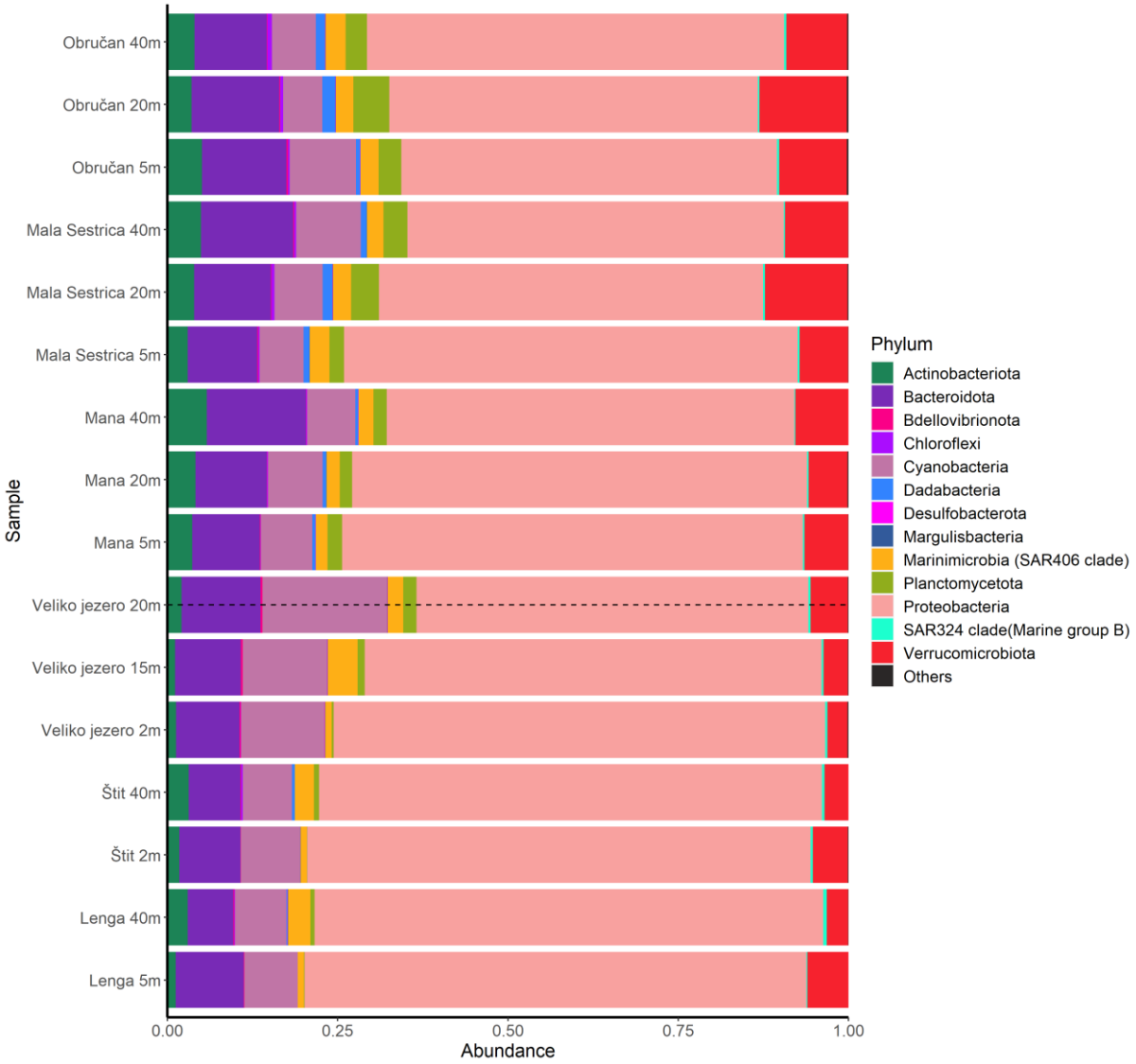

Figure 19. Relative abundance of bacterial community taxa in seawater samples, grouped by sampling site and depth, and colour-coded by phylum

4.2.2. Bacterial community composition in coral samples

A total of 26 coral samples were collected during a two-year sampling period from Kornati National Park and Mljet National Park, representing six coral taxa and two health states

(healthy, N; necrotic, NEC). Successful bacterial community profiles were obtained for 19 coral-associated microbiome samples originating from the Kornati (Obručan, Mana) and Mljet (Veliko jezero, Štit, Lenga) regions (Figure 20). Across the dataset, Proteobacteria represented the dominant bacterial phylum in most samples, although several coral microbiomes were characterised by strong enrichment of alternative phyla, particularly Bacteroidota and Acidobacteriota.

The microbiome of *Paramuricea clavata* was characterised by mixed Proteobacteria–Planctomycetota assemblages in both healthy and necrotic colonies. At Mana, microbiome composition remained relatively similar between health states, whereas at Obručan the NEC sample exhibited increased contributions of Planctomycetota, Bacteroidota and Cyanobacteria compared to the healthy colony.

Samples of *Eunicella cavolini*, collected exclusively at Mana, were dominated by Proteobacteria in both health states. However, the NEC sample displayed relatively higher contributions of Planctomycetota and Actinobacteriota, together with a reduced Bacteroidota fraction compared to the healthy colony.

The microbiome of *Balanophyllia europaea* exhibited pronounced variability between locations and health states. Healthy colonies from Obručan and Mana were strongly enriched in Bacteroidota, whereas the NEC sample from Mana showed a more heterogeneous composition with increased contributions of Actinobacteriota, Cyanobacteria and several low-abundance phyla. In contrast, both healthy and necrotic Balanophyllia colonies from Veliko jezero remained dominated by Proteobacteria, although the healthy sample displayed a comparatively larger “Others” fraction.

Among all investigated taxa, *Leptopsammia pruvoti* exhibited the highest compositional variability. The NEC samples from Obručan were strongly dominated by Bacteroidota, whereas the NEC sample from Štit showed a Proteobacteria-dominated profile with substantial Planctomycetota contribution. At Lenga, the NEC sample was characterised by exceptionally high relative abundance of Acidobacteriota. The healthy colony from Mana also showed strong Acidobacteriota dominance, while the NEC sample from the same locality exhibited a markedly

more heterogeneous community comprising Bacteroidota, Proteobacteria, Planctomycetota, Chloroflexi and several minor phyla.

Cladocora caespitosa, sampled exclusively at Veliko jezero, was dominated by Proteobacteria in both health states. Nevertheless, the NEC sample exhibited a more compositionally heterogeneous microbiome, with increased relative abundances of Bacteroidota, Chloroflexi and several low-abundance phyla compared to the healthy colony.

The microbiome of *Madracis pharensis*, represented by a single healthy sample from Lenga, exhibited a mixed community profile dominated by Proteobacteria, with substantial contributions of Chloroflexi, Acidobacteriota and Dadabacteria.

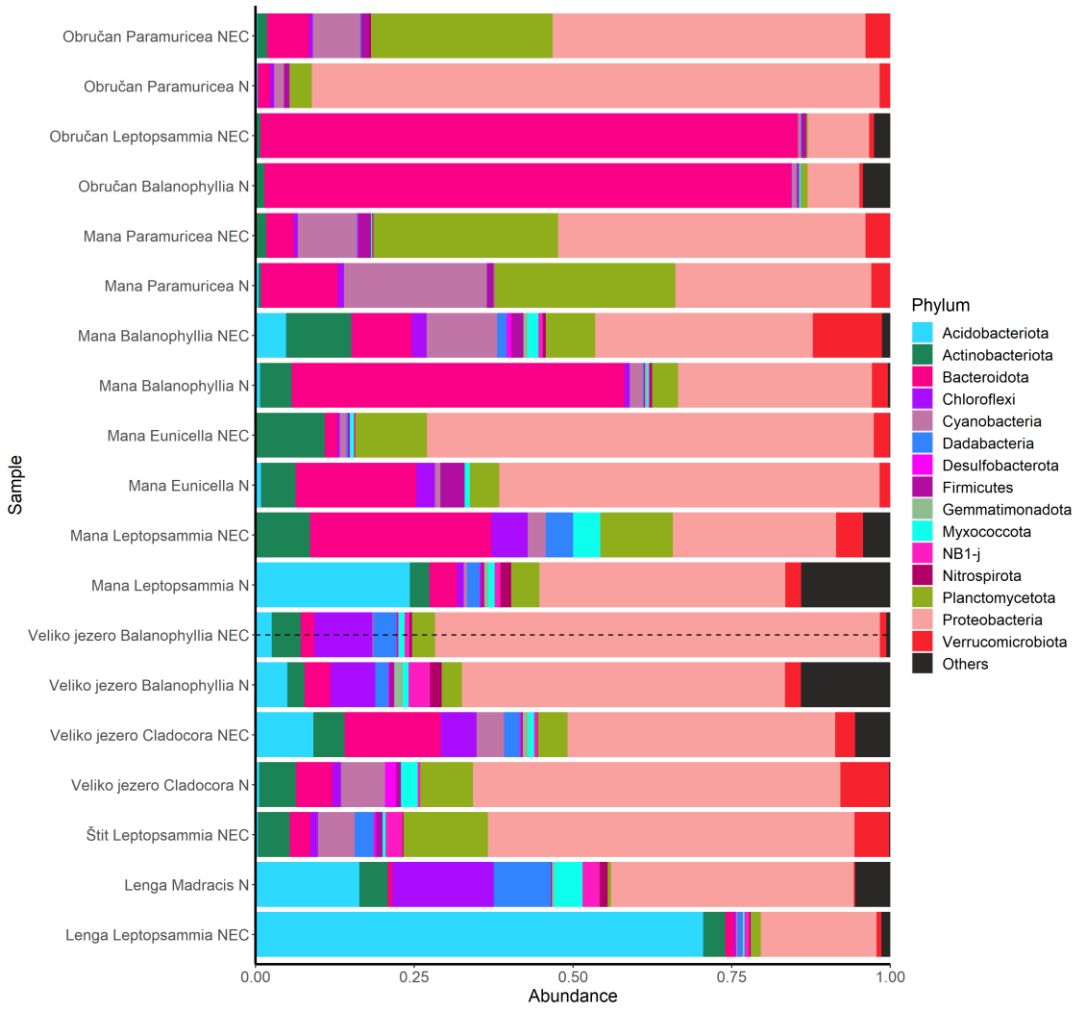

Figure 20. Relative abundance of bacterial community taxa in coral tissue samples, grouped by species and tissue condition (healthy – N; necrotic – NEC), and colour-coded by phylum. Each bar represents one sample. Coral

species were collected from the Mljet and Kornati National Parks, and include Cladocora caespitosa, Madracis pharensis, Balanophyllia europaea, Leptopsammia pruvoti, Eunicella cavolini, and Paramuricea clavata. ASV, amplicon sequence variant.

4.2.3. Alpha diversity of microbial communities

Alpha diversity indices were calculated to evaluate within-sample diversity. According to the Chao1 richness estimator, the necrotic *Balanophyllia europaea* sample from Veliko jezero exhibited the highest species richness, while coral samples in general displayed higher bacterial richness compared to seawater. The Shannon index, accounting for both richness and evenness, was highest in the necrotic *B. europaea* sample from Mana. The inverse Simpson index confirmed this pattern, as did Pielou's evenness, further supporting elevated diversity in necrotic coral tissues. In contrast, the lowest diversity and richness values were recorded in healthy coral samples of *B. europaea* and *Paramuricea clavata* from Obručan.

Additionally, the highest Shannon diversity indices were recorded in seawater samples collected from Kornati National Park (Figure 21). In general, seawater samples exhibited greater evenness and overall Shannon diversity compared to coral-associated microbiomes, suggesting a more balanced and taxonomically distributed microbial community in the water column.

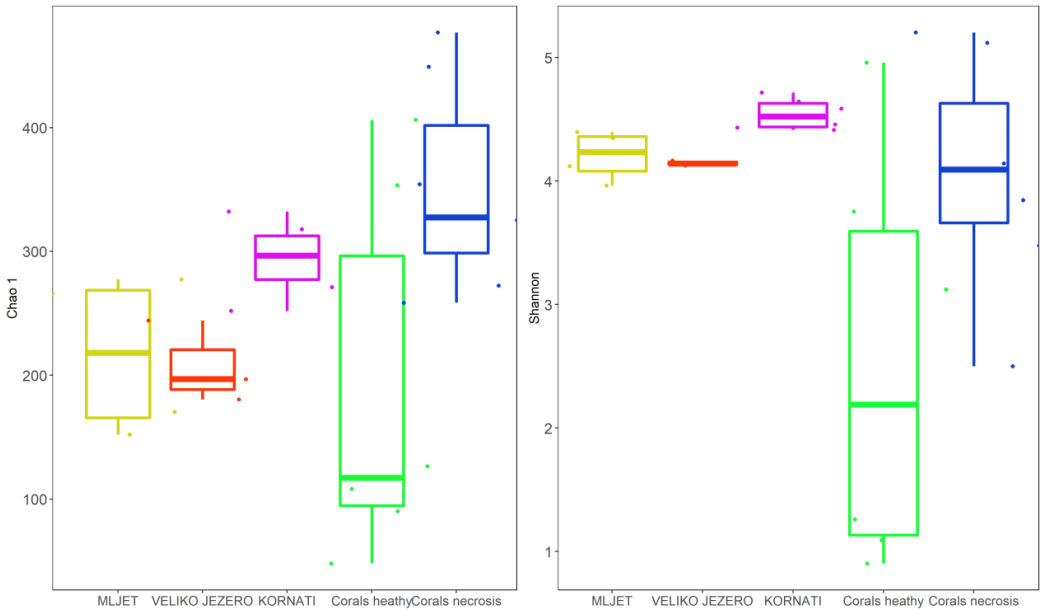

Figure 21. Alpha diversity metrics of bacterial communities associated with seawater and coral microbiomes from Kornati and Mljet regions. Boxplots represent Chao1 richness (left) and Shannon diversity index (right) calculated for seawater samples from Mljet, Veliko jezero and Kornati, as well as for healthy and necrotic coral-associated microbiomes.

4.2.4. Beta diversity and community structure

Principal coordinate analysis (PCoA) based on Bray–Curtis dissimilarity was performed to explore differences in bacterial community composition between seawater and coral samples at the level of amplicon sequence variants (ASVs). The analysis revealed a clear separation between seawater and coral microbiomes, with all seawater samples clustering closely together, indicating high similarity among water-derived bacterial communities, regardless of park location. In contrast, coral samples were more dispersed and exhibited grouping based on geographic origin. Coral microbiomes from Mljet and Kornati National Parks formed distinct clusters, suggesting island-specific structuring of microbial communities, potentially driven by local environmental conditions or host-specific factors. These observed differences were statistically supported by PERMANOVA analysis (R^2 = 0.35347, p = 0.001), confirming that microbial community composition significantly differed between sample types and across locations (Figure 22).

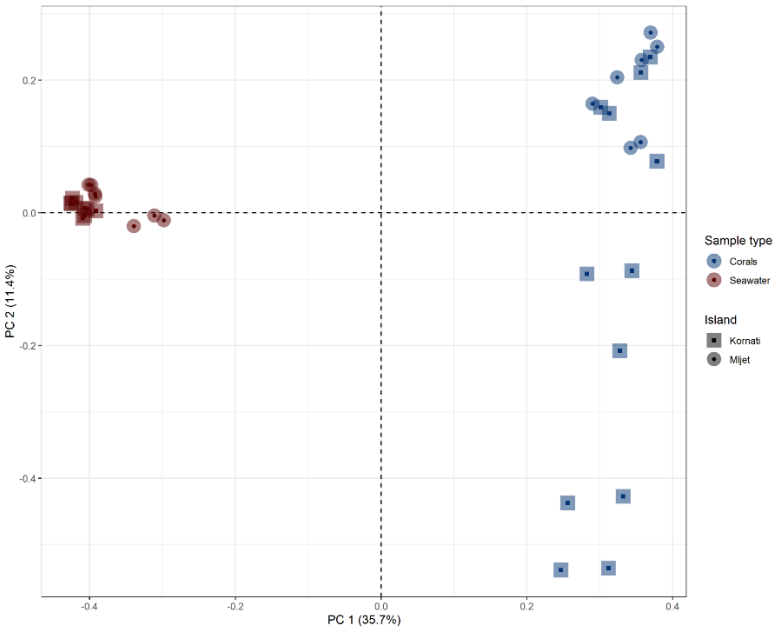

Figure 22. Principal coordinate analysis (PCoA) of bacterial communities in seawater and coral samples based on Bray–Curtis distances at the ASV level. Samples are colour-coded by type (seawater or coral) and shaped by origin (Mljet or Kornati National Park)

Principal coordinate analysis (PCoA) based on Bray–Curtis dissimilarity was conducted to investigate the patterns in bacterial community composition among coral samples. The analysis revealed that coral-associated microbiomes from Mljet National Park clustered more tightly, indicating a higher degree of similarity among those samples, despite differences in host species and tissue condition. In contrast, coral samples collected from Kornati National Park showed greater dispersion and lacked a clear grouping pattern, suggesting higher variability in microbial community composition within this region. This may reflect the broader range of coral species sampled at Kornati, as well as environmental heterogeneity across the sites. These observations were statistically supported by PERMANOVA analysis ($R^2 = 0.13981$, $p = 0.001$), confirming that geographic origin significantly influenced coral microbiome composition (Figure 23).

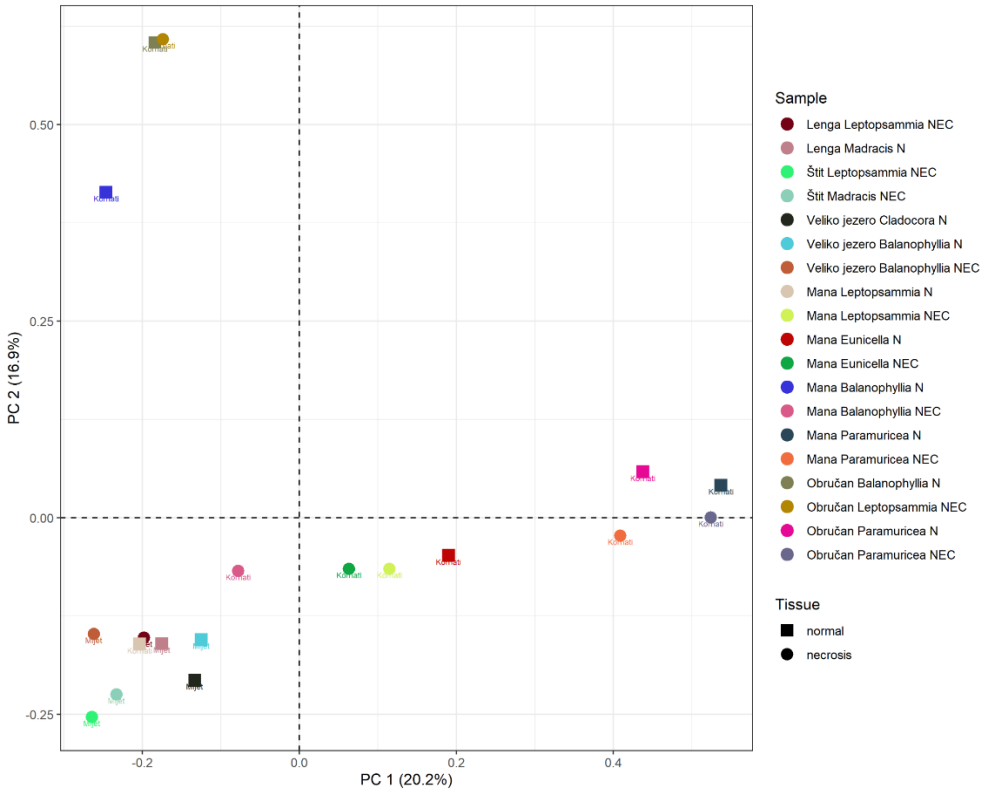

Figure 23. Principal coordinate analysis (PCoA) of bacterial communities associated with coral tissue samples based on Bray–Curtis distances at the ASV level. Samples are colour-coded by coral species and shaped by tissue condition (normal or necrotic). Islands of origin (Mljet or Kornati) are indicated in the sample labels.

Principal coordinate analysis (PCoA) based on Bray–Curtis dissimilarity was performed to investigate spatial structuring of bacterial communities in seawater samples across different sites and depths. The analysis revealed distinct clustering patterns according to geographic location, with samples from Mljet and Kornati National Parks forming separate groups. Notably, samples from Veliko jezero (Mljet) were clearly separated from those collected at Štit and Lenga, suggesting a unique microbial signature within the semi-enclosed lagoon system. Furthermore, samples collected at different depths (surface vs. deep water) within the same site showed relatively consistent community composition, as evidenced by their close clustering in the ordination space. This indicates that geographic factors, rather than depth, were the primary drivers of beta diversity in this dataset. These differences were statistically supported by PERMANOVA analysis ($R^2 = 0.37316$, $p = 0.001$), confirming a significant effect of location on microbial community composition (Figure 24). In addition, environmental

parameters were found to significantly influence microbial community structure. Temperature (R^2 = 0.93686, p = 0.002), pH (R^2 = 0.88312, p = 0.001), and salinity (R^2 = 0.96201, p = 0.001) all contributed significantly to the observed variation, underscoring the importance of local abiotic conditions in shaping seawater microbiomes.

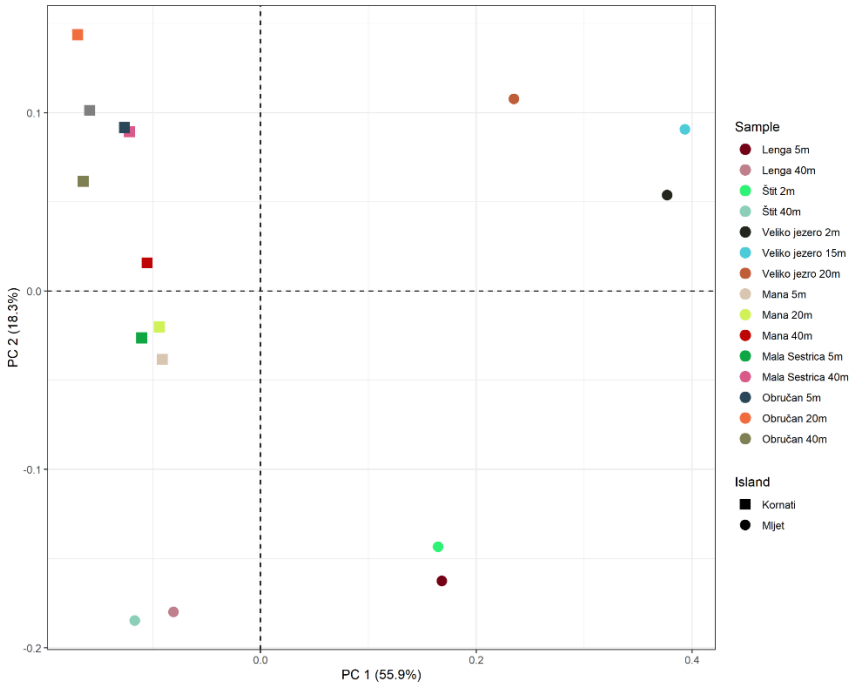

Figure 24. Principal coordinate analysis (PCoA) of bacterial communities in seawater samples based on Bray–Curtis distances at the ASV level. Points are coloured by sampling site and shaped by island of origin (Mljet or Kornati). The separation of Veliko jezero samples from Štit and Lenga indicates strong geographic structuring. Environmental factors (temperature, salinity, and pH) significantly contributed to variation in community composition, as confirmed by PERMANOVA.

Principal coordinate analysis (PCoA) based on Bray–Curtis dissimilarity was used to compare bacterial community composition between seawater and coral samples collected within Kornati National Park. The ordination revealed a clear separation between seawater and coral-associated microbiomes, with all seawater samples forming a tight cluster distinct from coral samples. This pattern is consistent with previous analyses and highlights the strong influence of substrate type on microbial community structure. Despite including multiple coral species and tissue conditions (healthy and necrotic), coral samples remained clearly distinct from the more uniform seawater microbiomes. This suggests a host- or tissue-specific microbial

signature in coral samples, compared to more environmentally structured communities in the surrounding water column. Statistical analysis using PERMANOVA confirmed the significance of this separation (R^2 = 0.41049, p = 0.001), indicating that sample type (seawater vs. coral) accounts for over 40% of the observed variance in microbial community composition within Kornati NP (Figure 25).

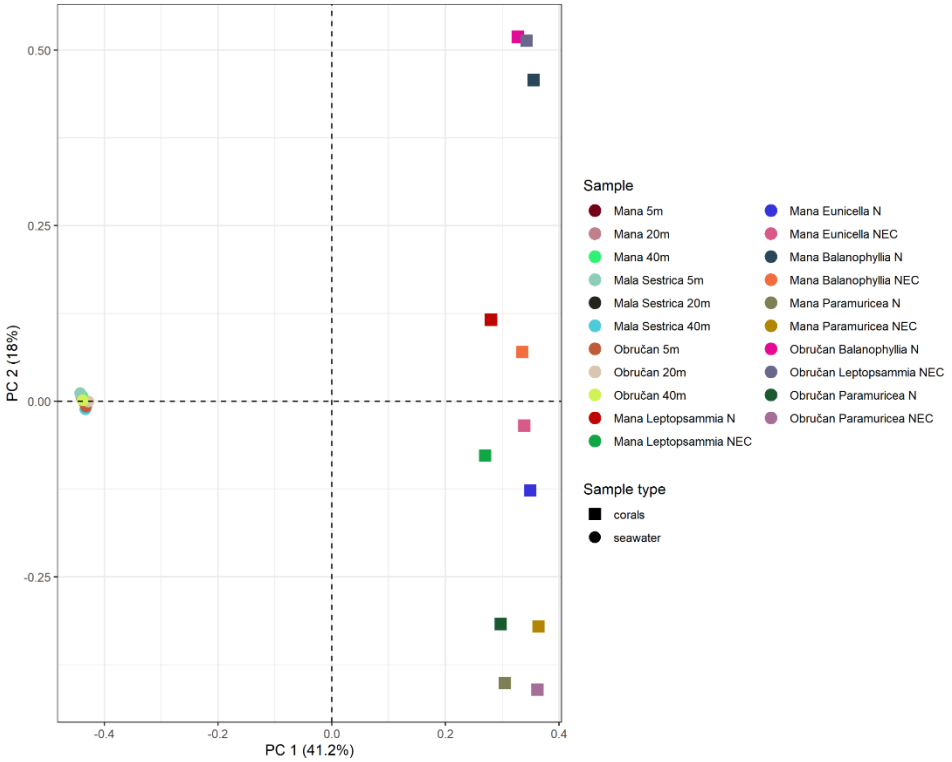

Figure 25. Principal coordinate analysis (PCoA) of bacterial communities in seawater and coral samples from Kornati National Park, based on Bray–Curtis distances at the ASV level. Samples are colour-coded by site and labelled by sample type (seawater or coral). Seawater and coral microbiomes show a clear separation in ordination space, supported by PERMANOVA.

Principal coordinate analysis (PCoA) based on Bray–Curtis dissimilarity was used to explore differences in bacterial community composition between seawater and coral samples collected at various sites within Mljet National Park. The analysis revealed a clear separation between seawater and coral-associated microbiomes. All seawater samples clustered tightly together and were distinctly separated from coral samples in ordination space. This result indicates minimal overlap between the microbial communities of the water column and coral

tissues, suggesting that coral-associated bacterial communities are host-specific and not directly influenced by the surrounding seawater microbiota at the time of sampling. Statistical validation via PERMANOVA confirmed a significant effect of sample type on microbial composition ($R^2 = 0.45864$, $p = 0.002$), with nearly half of the observed variance explained by whether the sample originated from water or coral tissue (Figure 26).

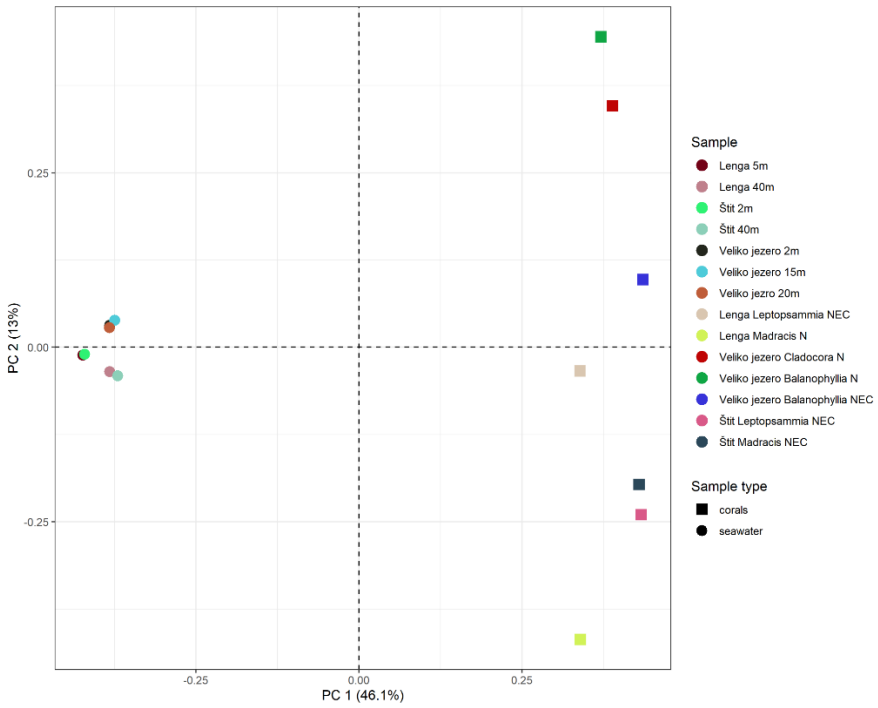

Figure 26. Principal coordinate analysis (PCoA) of bacterial communities in seawater and coral samples from Mljet National Park, based on Bray–Curtis distances at the ASV level. Samples are colour-coded by location and shaped by sample type (seawater or coral). Coral and seawater communities show clear separation, indicating distinct microbial assemblages.

4.3. Population status of *Cladocora caespitosa*

4.3.1. External appearance and gross lesions

Field surveys conducted along the Slovenian coast, at Ljubačka vrata, and at Veliko jezero (NP Mljet) revealed notable variation in the colonial morphology of *Cladocora caespitosa*. At Ljubačka vrata and at Veliko jezero, colonies predominantly exhibit cushion-shaped forms that frequently aggregate into extensive beds or banks covering several square metres, whereas colonies along the Slovenian coast are generally smaller, forming isolated ball-shaped or compact cushion-shaped structures. Macroscopically, healthy colonies present densely packed, tubular, pale yellowish-brown colour corallites, typically ranging from 3 to 6 mm in diameter, growing parallel to one another and forming robust, calcareous branches that give rise to a hemispherical, bush-like architecture (Figure 27). Each corallite features well-developed septa and calyces with relatively uniform radial symmetry and is interconnected by coenosteum. At the apical part of each corallite, a distinct crown of translucent brownish tentacles is visible, with the coloration derived from the presence of symbiotic algae. The coral surface is covered by a continuous layer of golden-brown tissue harbouring endosymbiotic dinoflagellates (Symbiodiniaceae), which substantially contribute to the host's energetic requirements via photosynthetic activity. All visible tissue appears turgid, uniformly pigmented, and devoid of any signs of necrosis, bleaching, or sediment accumulation, reflecting optimal physiological status and sustained metabolic function.

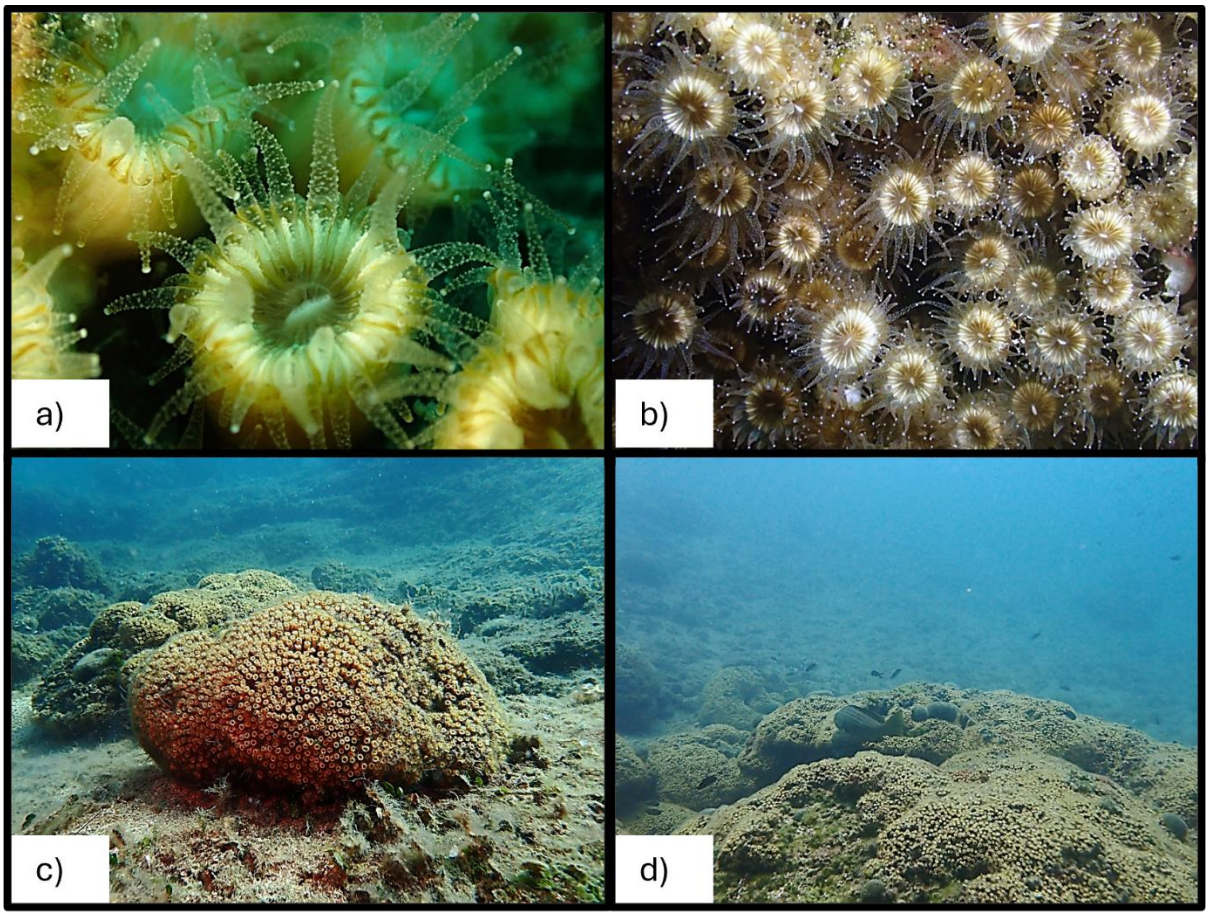

Figure 27. Macroscopic appearance of healthy polys (a-b) and colonies (c-d) of *Cladocora caespitosa* at 10m depth (Mljet National Park). (a-b) Close-up views of intact, golden-brown polyps, exhibiting full tissue coverage, uniform pigmentation and no visible signs of necrosis. (c–d) Overview of structurally intact colonies displaying cushion-shaped morphology with no evidence of polyp degradation or biofouling.

Necrotic and bleached colonies of *Cladocora caespitosa* exhibit a spectrum of macroscopic and morphological alterations, ranging from subtle tissue degradation to extensive structural damage. Macroscopically, tissue changes can vary in severity—from localized alterations affecting only a portion of a single polyp to extensive and noticeable damage involving the majority or all polyps within a colony. Early signs of stress typically include slight retraction of polyp tentacles (in one or more polyps within the colony), changes in tentacle colouration, and subtle disruptions to the integrity of the corallite margin or its overall architecture (Figure 28). Necrotic tissue changes often present as partial degradation of the tentacular crown, frequently accompanied by dark discoloration in affected areas and reduced polyp size. In contrast, bleaching is manifested by a complete loss of pigmentation in polyp tissue, rendering

it translucent or stark white due to the loss of symbiotic dinoflagellates (Symbiodiniaceae), thus severely impairing the coral's autotrophic capacity. Bleached polyps progressively undergo tissue degradation as a result of diminished energy input from both autotrophic and heterotrophic pathways, ultimately leading to their death and the exposure of the underlying white skeleton. As tissue degradation advances throughout the colony, driven by necrotic and/or bleaching processes, large portions of the skeleton are left exposed, creating substrates conducive to sedimentation and subsequent colonization by various epibiotic organisms. Recently exposed skeletal areas appeared clean and white, with little to no overgrowth. In contrast, older lesions exhibited visible colonization by calcareous algae, bryozoans, hydrozoans, and other encrusting epibionts. Some colonies showed signs of advanced and extensive tissue loss, characterized by substantial biofouling, including thick mucilaginous algal layers, filamentous cyanobacteria, sponges, and larger sessile invertebrates. These observations indicate a temporal progression from acute tissue loss to long-term degradation, with biofouling communities gradually establishing in necrotic zones.

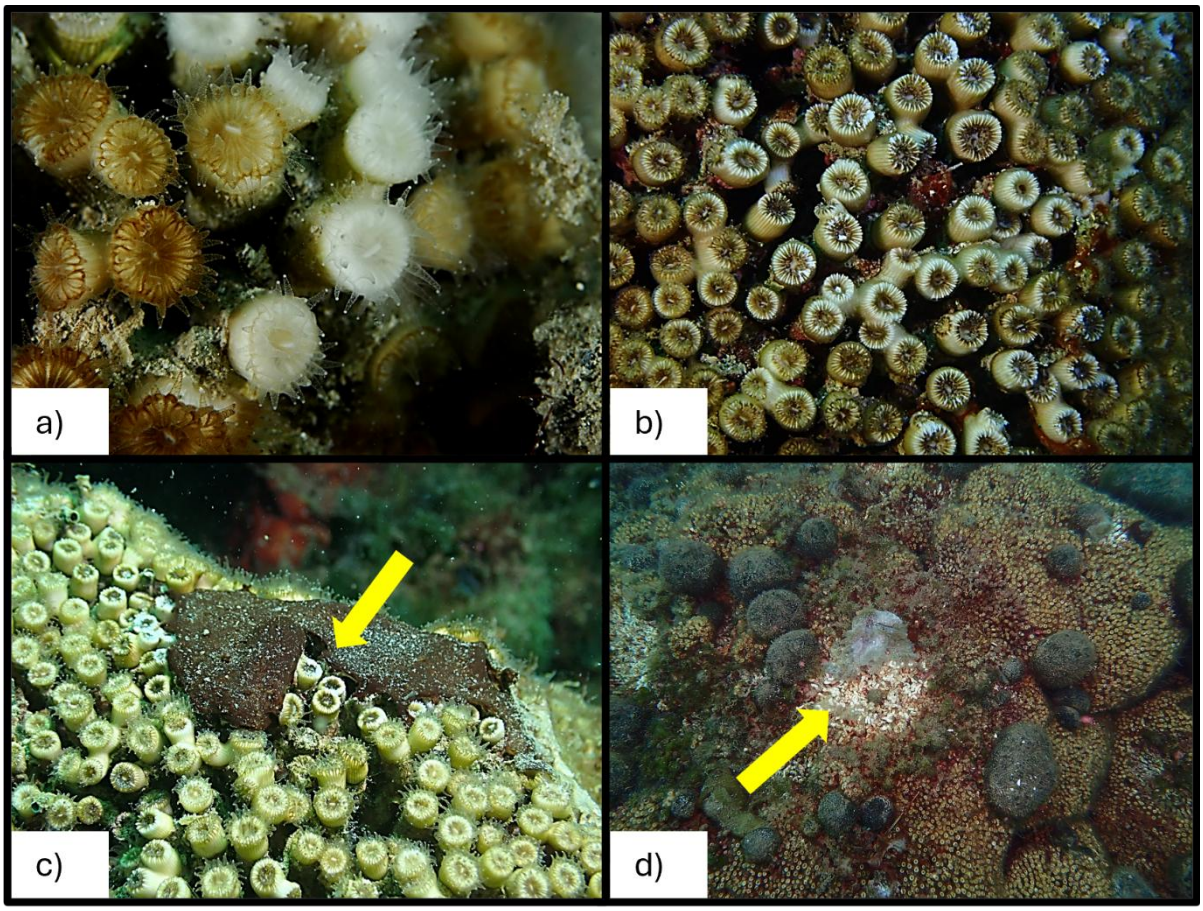

Figure 28. Macroscopic appearance of degraded *Cladocora caespitosa* colonies at 10 m depth (Mljet National Park) (a–d). (a) Close-up view of bleached polyps showing loss of pigmentation but retained tissue integrity. (b) Polyps exhibiting advanced-stage tissue necrosis with visible skeletal exposure. (c) Localized epibiotic overgrowth covering portions of the colony, beneath which necrotic polyps are discernible. (d) Reef partially overgrown by Codium bursa, with exposed dead polyps visible on colony areas previously covered by the alga.

4.3.2. Polyp density and mortality rate assesment

The highest recorded polyp density of *C. caespitosa* was observed at Veliko jezero in 2023, reaching 1110.54 ± 213.08 polyps/m², while the lowest density was recorded at Rt Madona in 2022, with 139.58 ± 17.85 polyps/m² (Figure 29). The highest mortality rate was recorded at Ljubačka vrata in 2023 (25.65 ± 6.85% polyps/m²), while the lowest mortality was observed at Ronek in 2021 (2.40 ± 2.29% polyps/m²) (Figure 30). Bleaching rates were most pronounced at Ronek in 2022 (38.00 ± 31.49%), while the lowest rates occurred at the same site in 2021 (0.57 ± 1.51%) (Figure 31). The Shapiro-Wilk test indicated that polyp density and mortality rate followed a normal distribution in most cases ($p > 0.05$), while bleaching rate exhibited significant deviations from normality ($p < 0.05$). Accordingly, ANOVA was employed for

normally distributed datasets, while Kruskal-Wallis was used where normality was violated. Statistical analysis confirmed significant ($p < = 0,05$) interannual variability in polyp density at Veliko jezero (Kruskal-Wallis: $H (3;99) = 13.896$, $p = 0.003$), mortality rate at Ljubačka vrata (ANOVA: $F (3;49) = 8.448$, $p = 0.0001$) and Veliko jezero (ANOVA: $F (3;98) = 30.326$, $p < 0.0001$), as well as bleaching rate across all stations (Ljubačka vrata ($H (3;68) = 47.92$, $p < 0.0001$), Ronek ($H (2;35) = 17.50$, $p = 0.0002$), Rt Madona ($H (2;51) = 23.69$, $p < 0.0001$), and Veliko jezero ($H (3;96) = 28.71$, $p < 0.0001$).

At Ronek (Slovenia), polyp density remained relatively stable over the years, fluctuating from 202.14 ± 88.10 polyps/m² in 2020 to 231.73 ± 46.71 polyps/m² in 2022 (Figure 29). Mortality rate exhibited slight decrease from 4.28 ± 8.30% in 2020 to 2.85 ± 0.99% in 2022 (Figure 30). Bleaching rate showed variability starting at 12.64 ± 26.57% in 2020, decreasing to 0.57 ± 1.51% in 2021 and increasing to 38.00 ± 31.49%. Although mortality rates at Ronek are not statistically significant, bleaching rates are statistically significant (Kruskal-Wallis: $H (2;35) = 17.50$, $p = 0.0002$) (Figure 31).

At Rt Madona (Slovenia), polyp density showed a consistent pattern, averaging 140.56 ± 20.56 polyps/m² in 2020 to 139.58 ± 17.85 polyps/m² in 2022 (Figure 29). Mortality rate varied across years indicating a slow increase (from 16.52 ± 8.37% to 24.19 ± 37.87%) but did not display a significant trend (Figure 30). Bleaching rate at rt Madona station fluctuated from 24.21 ± 17.62% in 2020, to 6.65 ±6.79% in 2021 and rose again to 21.36± 8.61% in 2022, indicating a statistically significant difference (Kruskal-Wallis: $H (2;51) = 23.69$, $p < 0.0001$) (Figure 31).

At Ljubačka vrata, polyp density remained stable, with values increasing from 427.0 ± 92.42 polyps/m² in 2020 to 518.62 ± 124.56 polyps/m² in 2023 (Figure 29). However, the mortality rate exhibited a statistically significant increase, rising from 15.11 ± 5.78% in 2020 to 26.65 ± 6.85% in 2023 (ANOVA: $F (3;49) = 8.448$, $p = 0.0001$) (Figure 30). Similarly, bleaching rate showed a marked increase, progressing from 2.36 ± 3.77% in 2020 to 19.50 ± 6.38% in 2023, with statistically significant differences detected (Kruskal-Wallis: $H (3;68) = 47.92$, $p < 0.0001$) (Figure 31).

At Veliko jezero, polyp density remained stable, with values fluctuating across years between 918.72 ± 162.95 polyps/m² in 2022 and 1110.54 ± 213.08 polyps/m² in 2023 (Figure 29). Mortality rate initially declined from 11.25 ± 5.11% in 2020 to 3.91 ± 1.63% in 2021, before increasing to 7.11 ± 2.82% in 2023, showing statistically significant differences (ANOVA: $F(3;98) = 30.326$, $p < 0.0001$) (Figure 30). Bleaching rates first decreased from 2020 (25.16 ± 17.89%) to 2021 (11.31 ± 9.95%) and later increase, reaching 23.24 ± 7.40% in 2023 with statistically significant differences detected (Kruskal-Wallis: $H(3;96) = 28.71$, $p = 0.0001$) (Figure 31).

Overall, these results highlight notable temporal and spatial variability in polyp density, mortality rate, and bleaching rate across the analysed stations for *Cladocora caespitosa*.

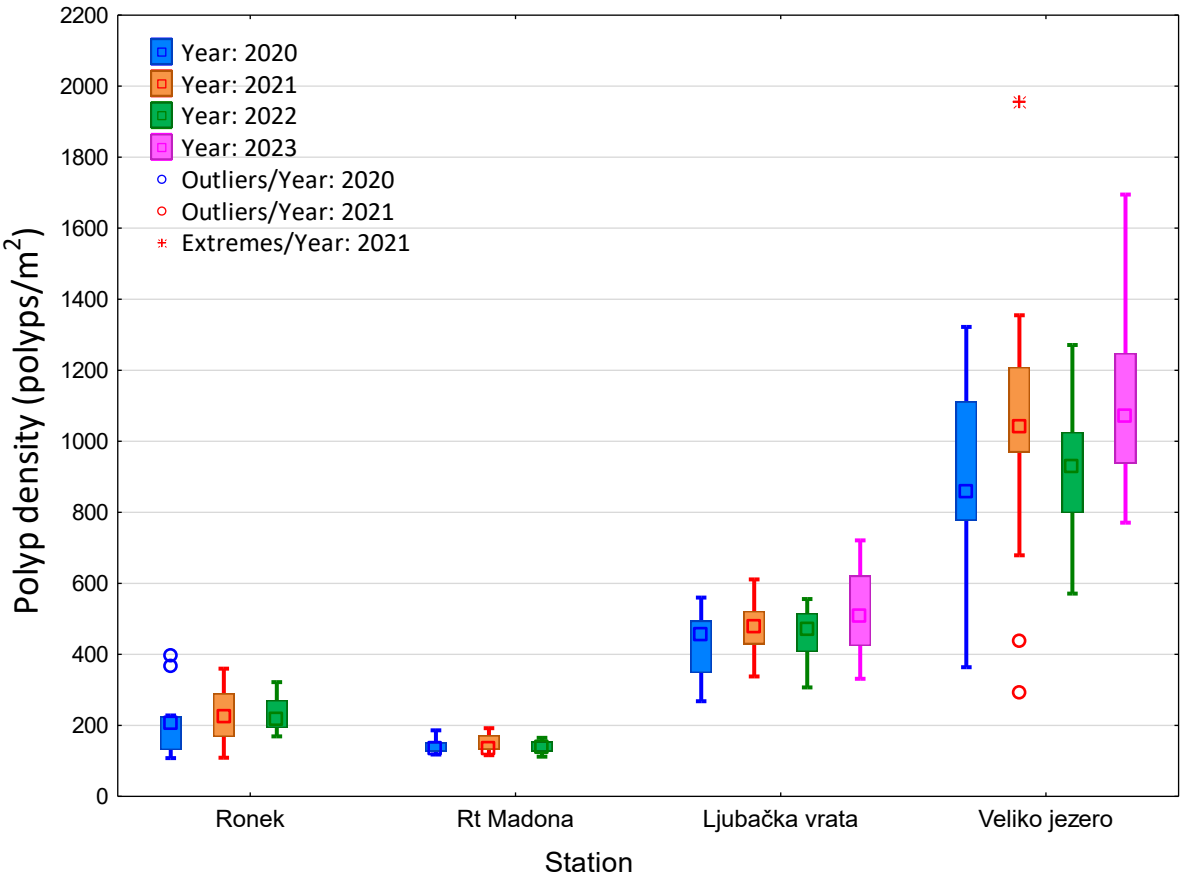

Figure 29. Polyp density of *Cladocora caespitosa* on stations: Ronek [KW-H(2;52) = 2.1983; p = 0.3332], rt Madona [F(2;25) = 0.367; p = 0.696], Ljubačka vrata [F(3;45) = 2.1205; p = 0.1109] and Veliko jezero [KW-H(3;99) = 13.8968; **p = 0.0030**] across period 2020 – 2023. Values in bold indicate statistically significant differences ($p < 0.05$).

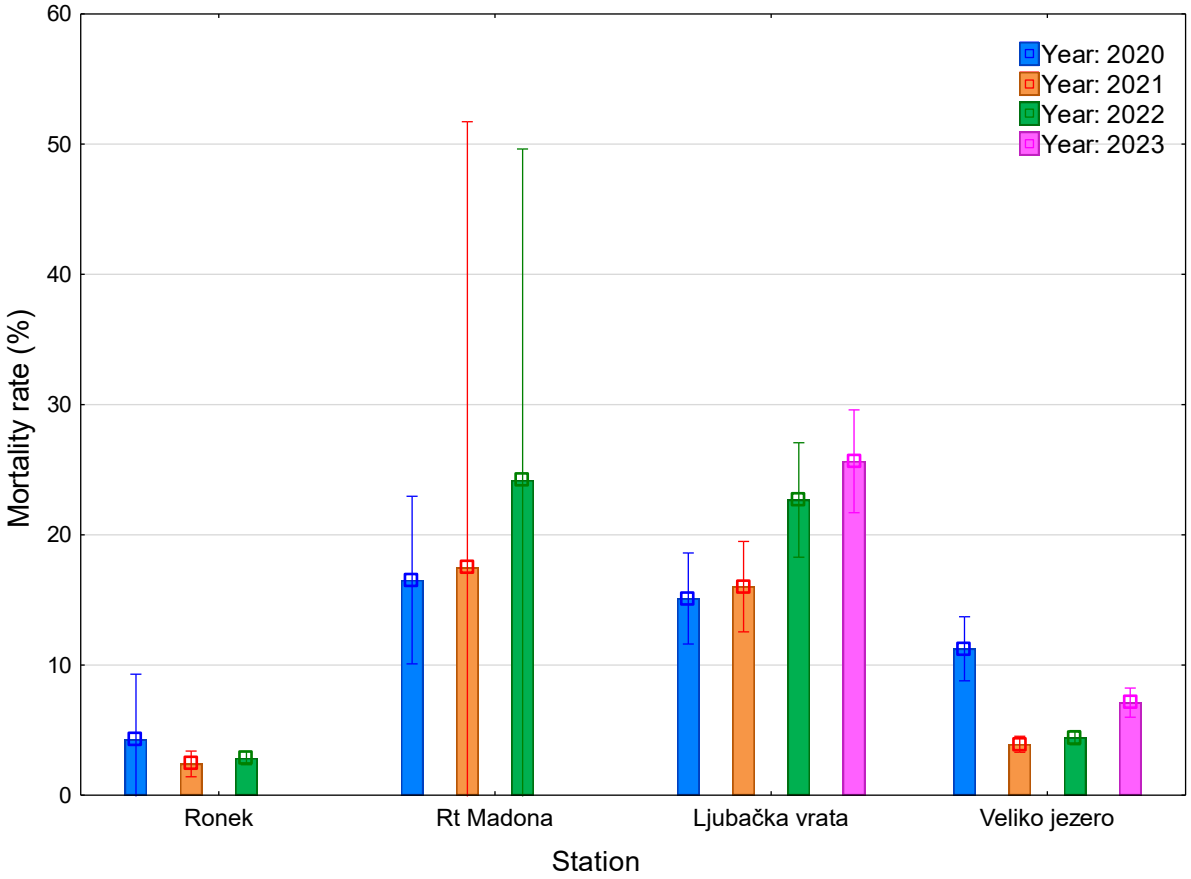

Figure 30. Mortality rate of *Cladocora caespitosa* on stations Ronek [KW-H(2;53) = 2.1725; p = 0.3375], rt Madona [KW-H(2;27) = 3.6335; p = 0.1626], Ljubačka vrata [F(3;49) = 8.4479; **p = 0.0001**] and Veliko jezero [F(3;98) = 30.3257; **p < 0.0001**] across period 2020 - 2023. Values in bold indicate statistically significant differences (p < 0.05).

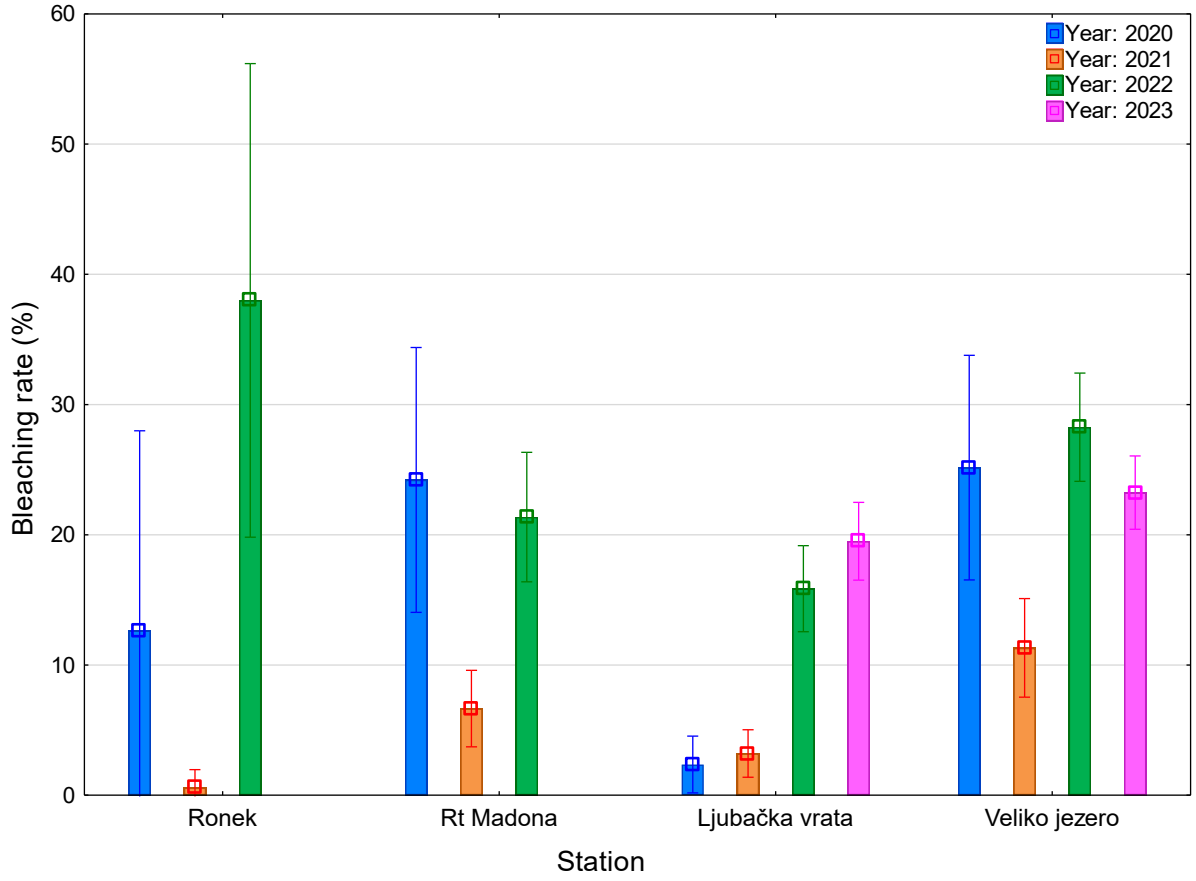

Figure 31. Bleaching rate of *Cladocora caespitosa* on stations: Ronek [KW-H(2;35) = 17.4974; **p = 0.0002**], rt Madona [KW-H(2;51) = 23.6868; **p < 0.0001**], Ljubačka vrata [KW-H(3;68) = 47.9249; **p < 0.0001**], and Veliko jezero [KW-H(3;96) = 28.7116; **p < 0.0001**] across period 2020 – 2023. Values in bold indicate statistically significant differences ($p < 0.05$).

4.3.3. Histological and histopathological description

Macroscopically, of 32 samples collected at stations Ronek and rt Madona (Slovenian coast) and at Veliko Jezero in NP Mljet, 13 were considered healthy, 10 necrotic and 9 bleached samples. All collected samples were examined microscopically and 8 samples were confirmed as healthy tissue, while remaining 24 were reclassified as necrotic: 5 samples were categorised as light histopathology (general state code 1; <25% of tissues contained lesions), 14 samples were categorised as moderate histopathology (general state code 2; 25-75% of tissues contained lesions) while heavy histopathology was confirmed in 5 samples (general state code 3; >75% of tissues contained lesions).

The histological architecture of a healthy *Cladocora caespitosa* polyp exhibited a well-preserved microanatomical structure with no evidence of pathological changes (Figure 32). Each polyp consisted of two primary epithelial layers: the outer epidermis (ectoderm) and the inner gastrodermis (endoderm), separated by a thin, gelatinous, acellular mesoglea. The epidermis was clearly distinguishable as a specialized, monolayer epithelium composed of cylindrical epithelial cells, interspersed with individual mucocyte cells and cnidocytes containing nematocysts. The mesoglea appeared homogeneous in texture and was tightly adhered to the surrounding epithelial layers, providing structural support, cohesion and flexibility. The gastrodermis, enriched with ciliated and glandular cells, enclosed a central gastrovascular cavity containing a limited number of mesenteries. These mesenteries, derived from endodermal folds extending into the cavity, were functionally involved in intracellular digestion, nutrient absorption, gametogenesis, and broader physiological regulation within the polyp. Within the gastrodermis, symbiotic dinoflagellates were visible as round cells with well-defined internal structures, occasionally exhibiting discernible chromatin. In the basal wall, all tissue layers were intact, continuous, and firmly interconnected. Gram staining revealed a moderate presence of bacteria localized within both the basal and superficial regions of the epidermal layer. Of the 13 samples macroscopically identified as healthy, 16% of polyps exhibited tissue affected by some form of pathological alteration. Among these, 47% of the samples showed moderate pathological changes affecting between 25% and 75% of the polyp tissue, while 16% of the samples showed light pathological changes affecting less than 25% of the tissue.

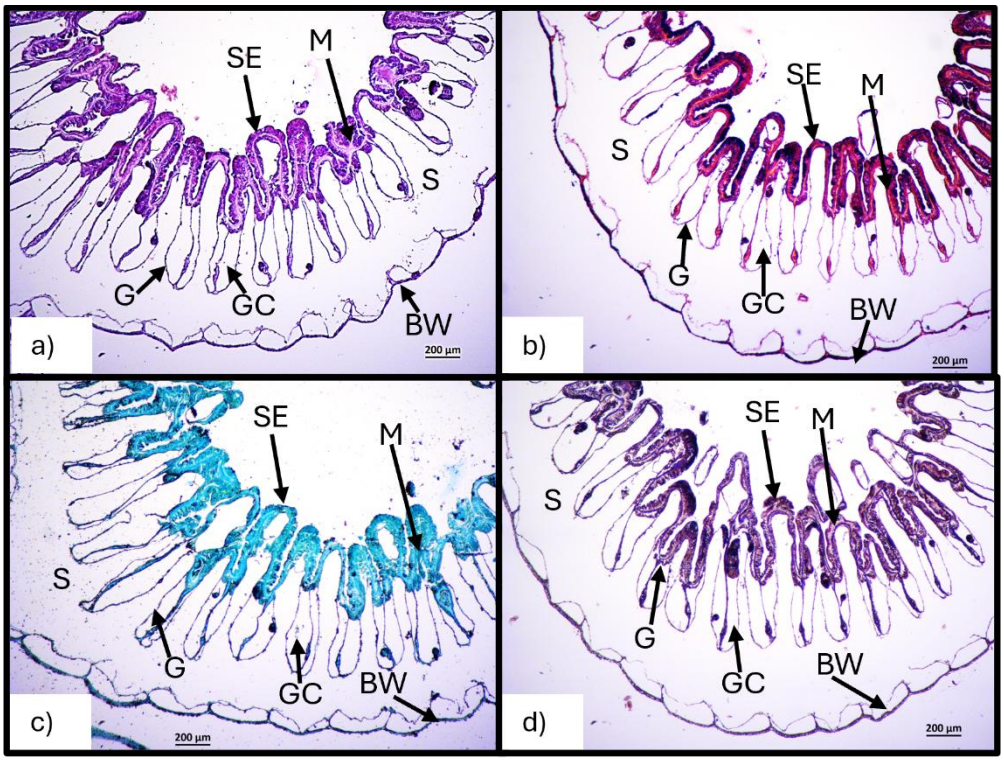

Figure 32. Histological cross-sections of a healthy polyp of *Cladocora caespitosa*, stained with (a) hematoxylin and eosin, (b) Gram, (c) Grocott's methenamine silver, and (d) Masson's trichrome stain. The normal architecture and characteristic cellular organisation of the polyp (P) are visible, including the gastrodermis (G), gastrovascular cavity (GC), mesoglea (M), surface epithelium (SE), basal body wall (BW), and skeletal space (S).

Table 8. Specific histopathological lesions and patogens of *Cladocora caespitosa* and their frequency

Specific histopathological lesions	**Light lesion (state 1)**	**Freq (%)**	**Heavy lesion (state 2)**	**Freq (%)**
Bassal body wall epidermis - loss of integrity	7	21.9	3	9.4
Bassal body wall epidermis - reduction	3	9.4	1	3.1
Surface body wall epidermis - loss of integrity	14	43.8	3	9.4
Surface body wall epidermis - increase in mucocytes	18	56.3	6	18.8
Surface body wall epidermis - hyperthrophy	16	50.0	6	18.8
Surface body wall epidermis - reduction	2	6.3	3	9.4
Mesoglea - swelling	17	53.1	4	12.5
Mesoglea - nude	9	28.1	2	6.3
Mesoglea - reduction	4	12.5	5	15.6
Gastrodermal disruption, desintegration, loss of integrity	13	40.6	12	37.5
Gastrodermal necrotic zones	18	56.3	7	21.9
Gastrodermis reduction	10	31.3	5	15.6
Endosymbionts dark and shrunken	17	53.1	1	3.1
Endosymbionts reduction in number	9	28.1	6	18.8
Reduction of mesenterial filaments	8	25.0	5	15.6
Patogens	**Light lesion (state 1)**	**Freq (%)**	**Heavy lesion (state 2)**	**Freq (%)**
Presence of Alghae	0	0.0	0	0.0
Presence of Crustacea	0	0.0	0	0.0
Presence of Funghi	1	3.1	0	0.0
Bacteria quantity bassal wall epidermis	9	28.1	2	6.3
Bacteria quantity surface wall epidermis	18	56.3	7	21.9
Bacteria quantity gastrodermis	9	28.1	3	9.4

I observed several distinct histopathological changes in the surface body wall epidermis of both bleached and necrotic coral polyps, indicative of stress and tissue degeneration. The most frequent lesion across all samples was a marked increase in mucocytes, recorded in 56% of polyps with mild lesions and 19% of those with severe damage (Table 8). Mucocyte proliferation was especially pronounced in bleached specimens, likely representing a protective mucus-mediated response to environmental stress. Epidermal hypertrophy, often accompanying mucocyte proliferation, was present in 50% of lightly affected polyps and 19%

of heavily affected ones. This cellular enlargement was typically associated with an expansion of cylindrical epithelial cells and suggested a compensatory regenerative response in early-stage lesions. A loss of epidermal integrity, characterised by partial disintegration of the surface epithelium and detachment from the mesoglea, was observed in 44% of polyps with mild lesions and in 9% of those with severe necrosis. In these cases, epidermal cells appeared dissociated and often separated from the basal membrane, leading to exposure of the underlying mesoglea (Figure 33). This lesion was particularly prominent in necrotic polyps and often accompanied by widespread epithelial collapse. In contrast, epidermal reduction, defined as thinning or atrophy of the epithelial layer, was the least frequent alteration, recorded in 6% of mild cases and 9% of severely affected polyps (Table 8). This lesion likely reflects a breakdown in regenerative capacity and advanced tissue degradation.

The mesoglea in necrotic samples exhibited three main types of alterations. The most prevalent change was mesogleal thickening observed in 53% of polyps with light lesions and 13% of those with heavy lesions (Table 8). This swelling often resulted in partial detachment from adjacent epithelial layers and was more pronounced when compared to the atrophied gastrodermis. A nude mesoglea, interpreted as a separation of adjacent layers (epidermis and/or gastrodermis), was recorded in 28% of light lesion polyps and 6% of heavily affected ones. Lastly, mesogleal reduction was identified in 13% of polyps with light lesions and more frequently (16%) in those with severe tissue damage (Figure 34).

In a subset of necrotic samples, extensive necrotic zones within the gastrodermis were detected in 56% of polyps with mild lesions and 22% of those with heavy lesions, leading to structural disintegration and localized tissue loss (Table 8). Gastrodermal disruption, disintegration, and loss of integrity were observed in 41% of mild and 38% of heavily affected polyps. Additionally, gastrodermal reduction was recorded in 31% of mild and 16% of severe cases. Symbiotic dinoflagellates in the gastrodermis were frequently darkened and shrunken in 53% of polyps with mild lesions, while only 3% of heavily affected polyps retained such altered symbionts. A reduction in the number of symbionts was found in 28% of mild and 19% of severe lesions, indicating both quantitative and morphological degradation (Figure 33). Polyps affected by necrosis also displayed a mesenterial filaments reduction in 25% of mild

and 16% of heavy lesions (Table 8). Gametes were absent in all examined necrotic samples, regardless of lesion severity. Similarly, bleached polyps showed a reduced abundance of symbiotic dinoflagellates, with variable morphological features; in some cases (notably 19%), symbionts appeared degraded, reduced in volume, and exhibited distinct structural and pigmentary alterations (Figure 34).

The basal body wall in necrotic samples also showed signs of tissue damage, primarily within the epidermis and, to a lesser extent, the gastrodermis, while the mesoglea generally retained its structural integrity. In bleached samples, more extensive histological changes were consistently observed in the surface body wall compared to the basal region. Gram staining of necrotic polyps revealed an elevated bacterial presence, particularly within the epidermis of both examined regions, with occasional bacterial infiltration of the gastrodermis. In bleached polyps, Gram staining indicated a moderate presence of bacteria in both the basal and superficial epithelial layers.

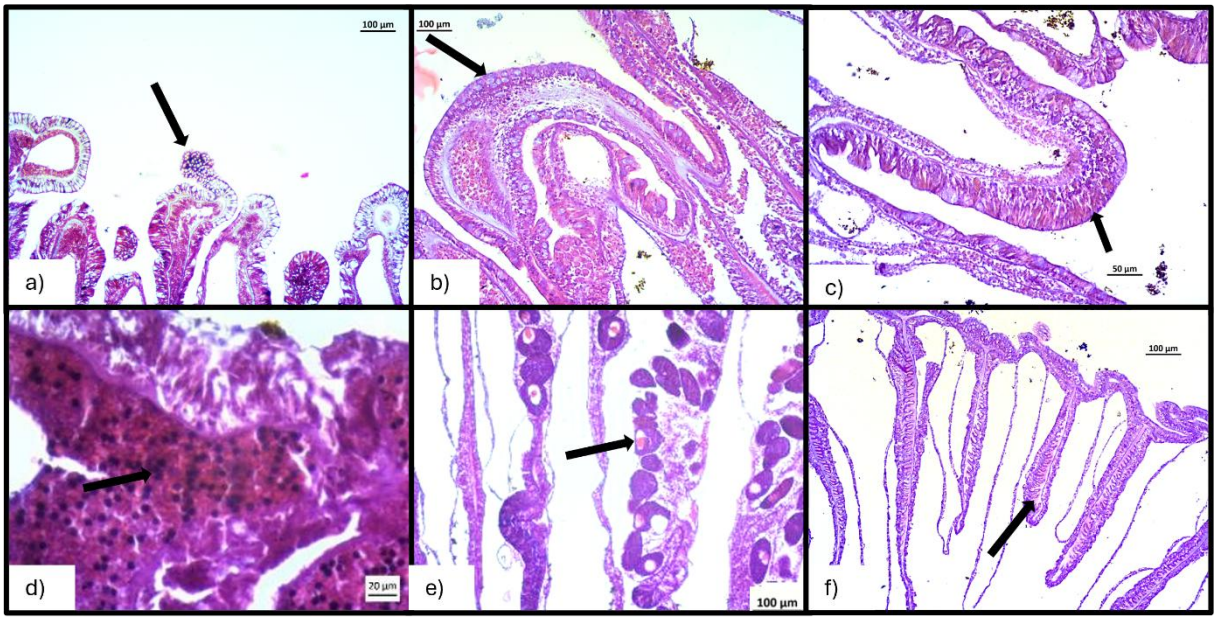

Figure 33. Histological cross (a, c-d, f) and longitudinal (b, e) sections of *Cladocora caespitosa* samples showing light microscopic lesions (a-f). Observed changes include (a) structural alterations in the surface epithelium, (b) mucocyte proliferation, (c) epidermal hypertrophy with reduced mesogleal thickness, (d) dark and shrunken endosymbionts within the gastrodermis accompanied by structural disintegration, (e) atretic oocytes and loss of gastrodermal tissue in the mesenterial filaments, and (f) mesogleal swelling. HE stain.

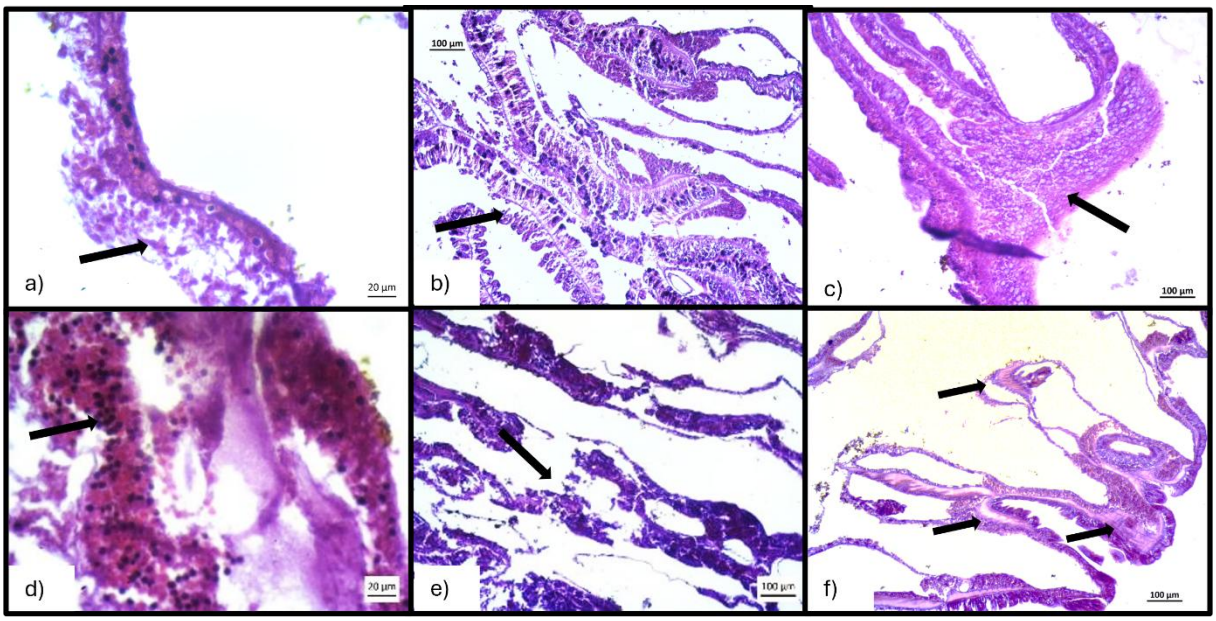

Figure 34. Histological cross (a, c-d, f) and longitudinal (b, e) sections of *Cladocora caespitosa* samples with heavy microscopic lesions (a-f) show (a, b) complete loss of integrity and peeling of the epithelium, (c) massive necrotic lesion and mucocyte proliferation, (d) dark and shrunken endosymbionts in the gastrodermis with extensive lytic lesions, (e) disintegration of gastrodermal tissue and reduction of mesenterial filaments, and (f) necrotic gastrodermal tissue with exposed (nude) mesoglea. HE stain.

4.4. Population status of *Balanophyllia europaea*

4.4.1. External appearance and gross lesions

At all surveyed stations, the solitary scleractinian coral *Balanophyllia europaea* was commonly observed inhabiting shallow waters up to 15 metres in depth, firmly attached to hard substrates such as rocks or shells. Morphologically, the healthy polyps were characterized by a robust, cylindrical to cup-shaped calice, measuring up to 10–15 mm in diameter and up to 20 mm in height (Figure 35). Specimens exhibited well-defined radial septa arranged in hexamerous symmetry, often accompanied by a prominent columella. The external skeleton appeared either smooth or with subtle longitudinal ridges, while the polyps displayed a fleshy, translucent appearance with yellowish to brown pigmentation. At the apical part of each corallite, numerous translucent brownish tentacles were visible, particularly evident during nocturnal polyp expansion. The coral surface was enveloped by a continuous layer of golden-brown tissue harbouring endosymbiotic dinoflagellates.

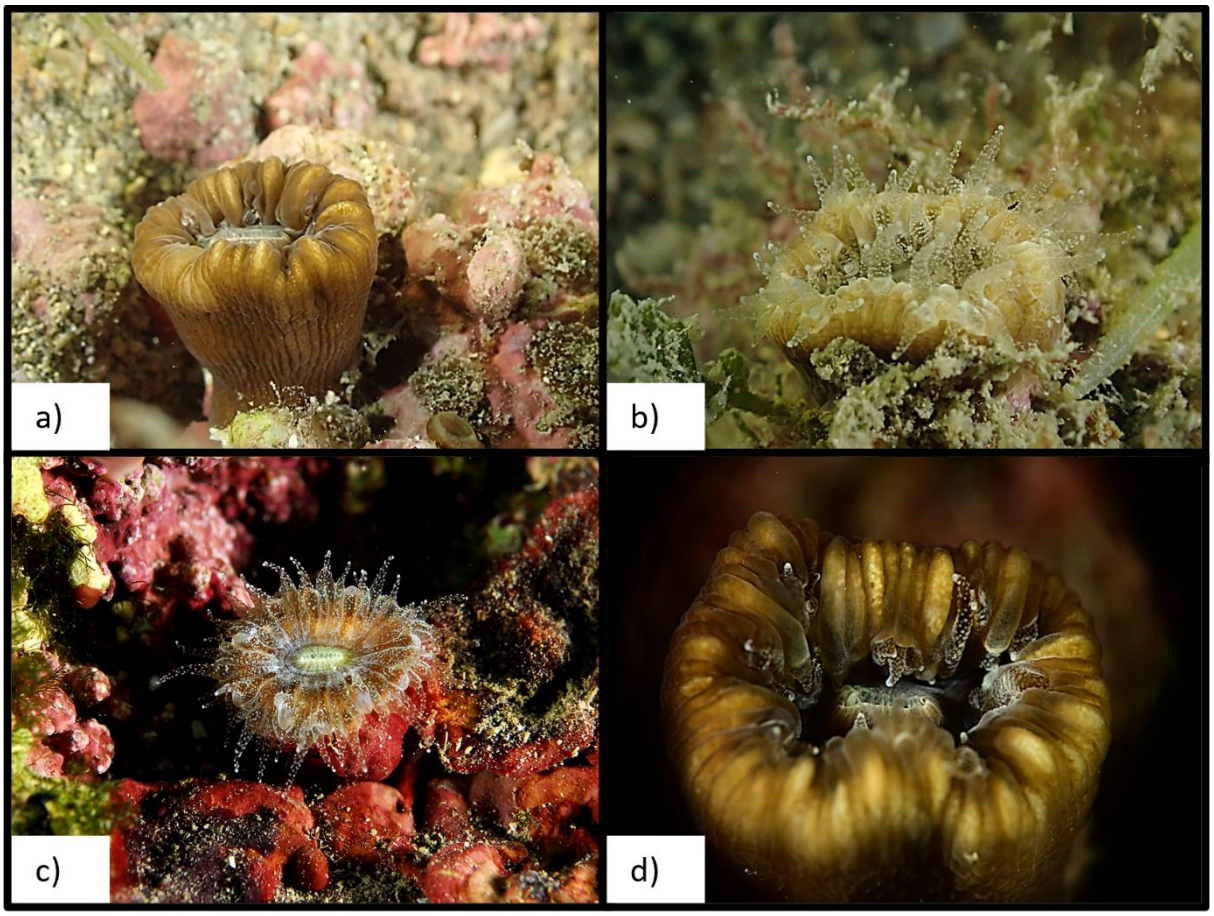

Figure 35. Macroscopic appearance of a healthy *Balanophyllia europaea* polyp at 10 m depth (Kornati National Park) (a–d). Close-up views of polyps with structurally intact corallites exhibiting full tissue coverage, uniform coloration, and no visible signs of necrosis or biofouling, with tentacles extended in (b, c) and retracted in (a, d).

Necrotic individuals of *B. europaea* exhibited a broad range of macroscopic and morphological alterations, ranging from localized tissue degradation to extensive skeletal damage. These changes manifested at varying intensities, beginning with minor lesions confined to a portion of the polyp and potentially progressing to partial tissue loss and structural compromise (Figure 36). Early manifestations of stress typically included partial retraction of the polyp, fading of tentacle pigmentation, and subtle architectural irregularities along the calice margin or within the corallite structure. Necrosis was characterized by localized tissue disintegration, often manifesting as greyish or whitish lesions, accompanied by progressive thinning or partial loss of polyp tissue, which led to the exposure of the underlying white aragonitic skeleton in affected areas. As necrosis progressed, the calice often appeared eroded or fragmented, with disrupted septal organization and reduced integrity of the thecal wall. In contrast, some

individuals retained intact tissue structure, but the tissue appeared pale, translucent, or completely depigmented due to the loss of endosymbiotic dinoflagellates (family Symbiodiniaceae), resulting in the absence of the characteristic yellow to brown coloration. Advanced necrotic zones were characterized by sloughing tissue, sediment accumulation, and dense colonization by biofilms and epibiotic organisms. These opportunistic colonizers were consistently associated with extensive tissue loss and were observed in areas where polyp mortality had already occurred. In such cases, only the empty corallite remained, often secondarily colonized by a variety of epibiotic taxa.

Figure 36. Macroscopic appearance of necrotic (a–c) and discolored (d) polyps of *Balanophyllia europaea* at 10 m depth (Kornati National Park) (a–d). (a–c) Close-up views of polyps showing: (a) localized tissue loss, (b) necrotic lesions of coenenchymal tissue, and (c) near-complete tissue loss with exposure of the underlying skeleton. (d) Advanced-stage discoloration of an entire polyp.

4.4.2. Polyp density and mortality rate assesment

Polyp density of *Ballanophylia europea* varied across stations and years, exhibiting both increasing and decreasing trends. The highest recorded polyp density was observed at Lenga in 2020, reaching 9.1 ± 2.85 polyps/m², while the lowest was recorded at Ronek in 2022 at 2.9 ± 1.20 polyps/m² (Figure 37). The Shapiro-Wilk test indicated that polyp density data followed a normal distribution in most cases ($p > 0.05$), while in cases where normality was not met, the Kruskal-Wallis test was applied. Consequently, ANOVA was used for normally distributed datasets, and Kruskal-Wallis was applied where normality was violated. Statistical analysis confirmed significant interannual variability in polyp density at Balun (ANOVA: $F(3;36) = 4.996$, $p = 0.005$), Mana (ANOVA: $F(3;36) = 3.104$, $p = 0.039$), and Rt Lenga (ANOVA: $F(3;36) = 2.929$, $p = 0.047$).

At Ronek and Rt Madona, polyp density remained relatively stable over the years, with minor fluctuations observed. At Ronek, values ranged from 3.5 ±1.08 polyps/m² in 2020 to 2.9 ± 1.20 polyps/m² in 2023. At Rt Madona, polyp density exhibited a slight decline from 4.7 ± 1.64 polyps/m² to 4.0 ± 1.15 polyps/m², though no statistically significant differences were detected (Figure 37).

At Ljubačka vrata, polyp density remained stable throughout the study period, with values fluctuating between 5.0 ± 1.33 polyps/m² in 2020 and 4.6 ± 1.90 polyps/m² in 2023, with the lowest population density in 2022 of 3.9 ± 1.45 polyps/m² (Figure 37). Statistical tests did not reveal significant interannual differences.

At Nature Park Telašćica, on stations Vela Sestrica and Veli Garmenjak, a gradual decline in polyp density was observed. At Vela Sestrica, density decreased from 6.3 ± 2.26 polyps/m² in 2020 to 5.4 ± 1.71 polyps/m² in 2023, while at Veli Garmenjak, values declined from 7.3 ± 2.62 polyps/m² to 5.9 ± 1.52 polyps/m² over the same period (Figure 37).

Within National Park Kornati, polyp density at Balun exhibited a declining trend, dropping from 6.4 ± 2.17 polyps/m² in 2020 to 3.7 ± 1.34 polyps/m² in 2023, a statistically significant decrease (ANOVA: $F(3;36) = 4.996$, $p = 0.005$). Similarly, at Mali Obručan, density decreased from 7.9 ± 2.02 polyps/m² to 5.4 ± 1.96 polyps/m². At Mana, density exhibited a significant decline from

8 ± 2.49 polyp/m² in 2020 to 5.3 ± 1.49 polyps/m² in 2023 (ANOVA: F (3;36) = 3.104, p = 0.039) (Figure 37).

At National Park Mljet, contrasting trends were observed among stations. At Rt Lenga, polyp density exhibited a decline, decreasing from 9.1 ± 2.5 polyps/m² in 2020 to 6.1 ± 1.79 polyps/m² in 2023, a statistically significant decrease (ANOVA: F (3;36) = 2.929, p = 0.047). At Veliko jezero, density fluctuated from 4.4 ± 1.51 polyps/m² in 2020 to 3.5 ± 1.51 polyps/m² in 2023. At Štit, a similar pattern was observed, with density declining from 7.3 ±1.83 polyps/m² to 5.6 ± 1.90 polyps/m² (Figure 37).

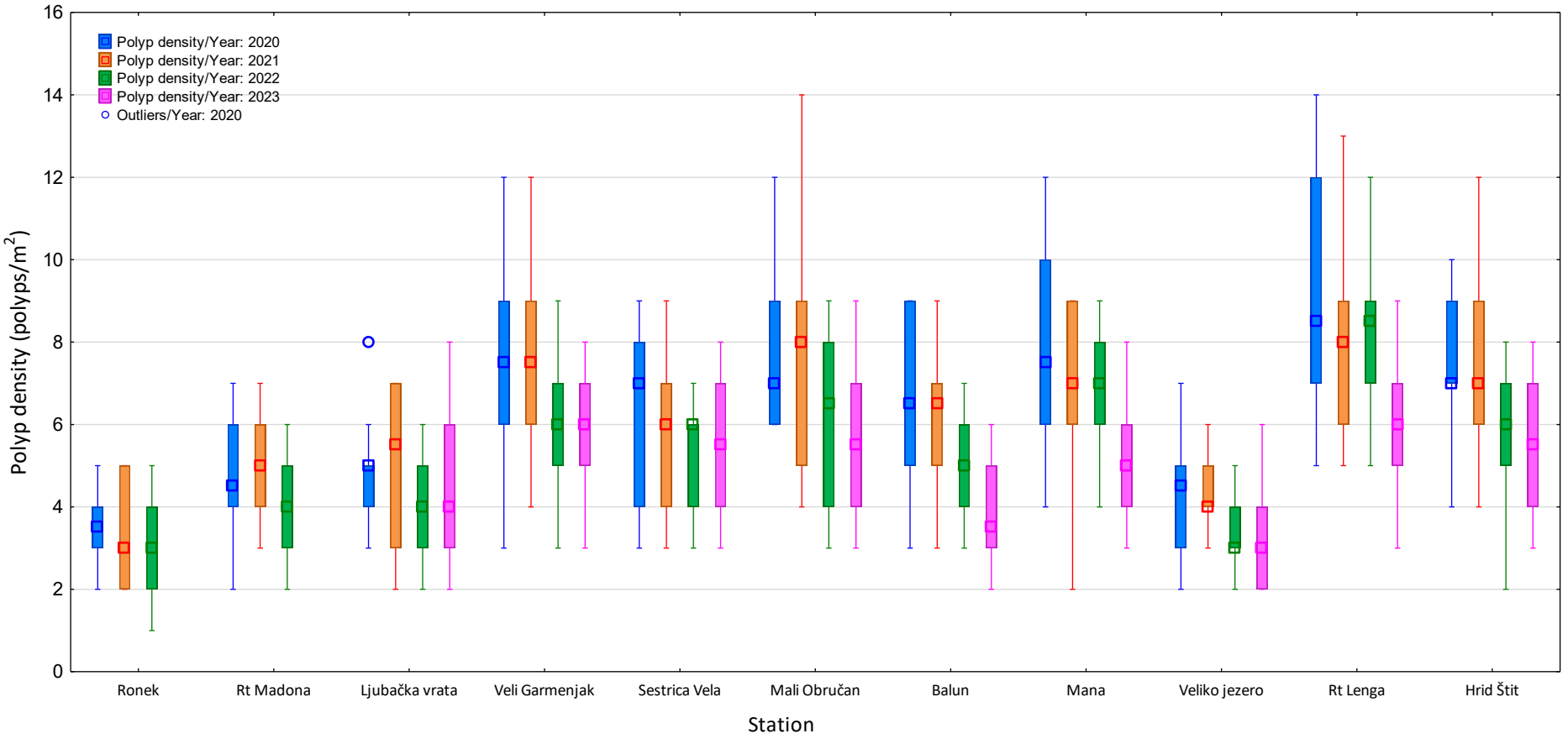

Figure 37. Polyp density of *Ballanophylia europea* on stations: Ronek [KW-H(2;30) = 1.3569; p = 0.5074], rt Madona [F(2;27) = 1.2238; p = 0.3099], Ljubačka vrata [F(3;36) = 1.045; p = 0.3844], Veli Garmenjak [F(3;36) = 1.6864; p = 0.1872], Sestrica Vela [F(3;36) = 0.6294; p = 0.6008], Mali Obručan [F(3;36) = 2.8459; p = 0.0511], Balun [F(3;36) = 4.9964; p = 0.0053], Mana [F(3;36) = 3.104; p = 0.0385], Veliko jezero [F(3;36) = 1.765; p = 0.1713], Lenga [F(3;36) = 2.9294; p = 0.0467], Štit [F(3;36) = 2.3046; p = 0.0933] across period 2020 – 2023

The mortality rate of *Ballanophylia europea* showed statistically significant increases across five stations (Figure 38). The highest recorded mortality rate was at Rt Lenga in 2023 at 53.8 ± 22.57%, whereas the lowest was at Ljubačka vrata in 2020 at 4.0 ± 8.76%. The Shapiro-Wilk test confirmed that mortality rate data were normally distributed in most cases ($p > 0.05$). ANOVA was used for normally distributed datasets, and in instances where normality was not met, the Kruskal-Wallis test was applied. Statistically significant changes were confirmed at Ljubačka vrata (Kruskal-Wallis: $H(3;40) = 13.723$, $p = 0.003$), Veli Garmenjak (Kruskal-Wallis: $H(3;40) = 8.723$, $p = 0.033$), Mali Obručan (Kruskal-Wallis: $H(3;40) = 16.469$, $p = 0.001$), Veliko jezero (ANOVA: $F(3;36) = 3.898$, $p = 0.016$), and Rt Lenga (ANOVA: $F(3;36) = 4.311$, $p = 0.011$).

At Ronek and rt Madona, mortality rates exhibited only minor changes; at station Ronek mortality rate slightly increased from 13.5 ± 11.69% in 2020 to 24.1 ± 27.88% in 2022, while at station rt Madona mortality rate increased from 12.1 ± 11.41 in 2020 to 28.6 ± 25.05% in 2022 (Figure 38). No significant differences were detected.

Mortality rates exhibited an increasing trend at Ljubačka vrata, rising from 4 ± 8.76% in 2020 to 24.8 ± 9.76% in 2023, demonstrating a statistically significant increase (Kruskal-Wallis: $H(3;40) = 13.723$, $p = 0.003$) (Figure 38).

Mortality rates in Nature Park Telašćica exhibited a pronounced increase, particularly at Veli Garmenjak, where values tripled from 15.2 ± 16.44% in 2020 to 44.4 ± 28.81% in 2023, with statistically significant differences (Kruskal-Wallis: $H(3;40) = 8.723$, $p = 0.033$). At Vela Sestrica, mortality rates also increased over time, rising from 14.2 ± 17.72% in 2020 to 31.1 ± 15.22% in 2023 (Figure 38).

Mortality rates showed a clear increasing trend at stations within the National Park Kornati. At Mali Obručan, mortality rates rose from 16.9 ± 12.53% in 2020 to 28.5 ± 12.65% in 2023, with statistically significant interannual differences (Kruskal-Wallis: $H(3;40) = 16.469$, $p = 0.001$). At Balun, mortality also increased significantly from 13.8 ± 17.51% in 2020 to 29.2 ± 23.59% in 2023 (Kruskal-Wallis: $H(3;40) = 7.749$, $p = 0.051$). Finally, although Mana had a high mean mortality rate over the examined years (35.07 ± 18.68 %, values annually increased from 32.9 ± 17.93% in 2020 to 48.2 ± 19.06% in 2022 and decreased to 26.0 ± 17.27 % in 2023) they remained statistically insignificant (Figure 38).

Mortality rates at National Park Mljet were among the highest recorded. At Rt Lenga, mortality rose from 45.6 ± 18.06% in 2020 to 71.2 ± 24.27% in 2023, with significant interannual variation (ANOVA: $F(3;36) = 4.311$, $p = 0.011$). At Veliko jezero, mortality also increased from 12.5 ± 12.35% in 2020, reaching 36.5 ± 32.15% in 2023 (ANOVA: $F(3;36) = 3.898$, $p = 0.016$). At Štit, mortality rates increased from 36.8 ± 16.4% in 2020 to 47.8 ± 34.64% in 2023, reflecting a gradual worsening trend (Figure 38).

These findings indicate a general decline in polyp density across multiple stations, coupled with a significant increase in mortality rates. The observed trends, particularly in National Parks Kornati and Mljet, suggest increasing environmental pressures on *Ballanophylia europea* populations.

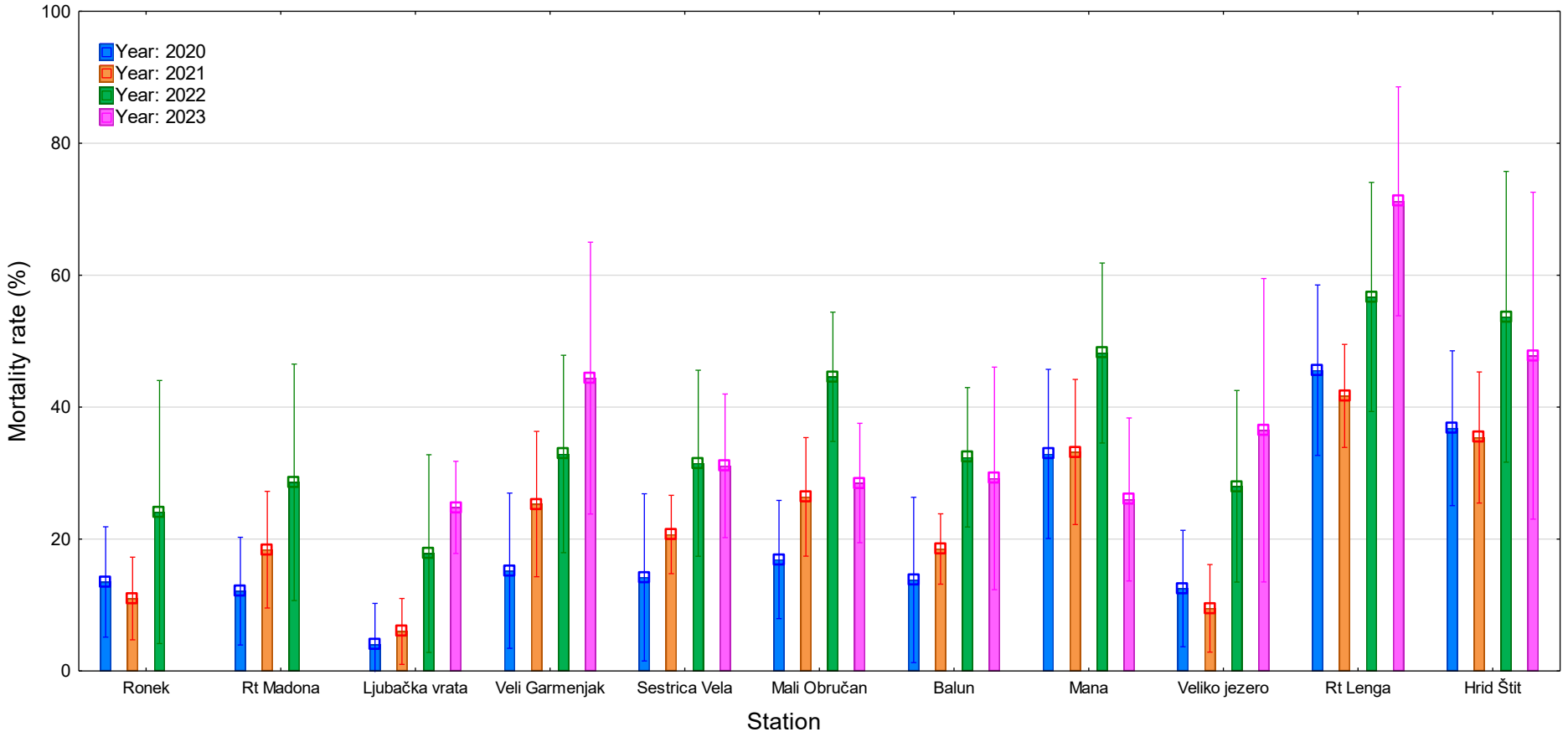

Figure 38. Mortality rate of *Ballanophylia europea* on stations: Ronek [KW-H(2;30) = 0.4822; p = 0.7858], Rt Madona [KW-H(2;30) = 3.4775; p = 0.1757], Ljubačka vrata [KW-H(3;40) = 13.7227; **p = 0.0033**], Veli Garmenjak [KW-H(3;40) = 8.7231; **p = 0.0332**], Sestrica Vela [KW-H(3;40) = 7.0464; p = 0.0704], Mali Obručan [KW-H(3;40) = 16.4699; **p = 0.0009**], Balun [KW-H(3;40) = 7.7492; p = 0.0515], Mana [KW-H(3;40) = 6.3248; p = 0.0968], Veliko jezero [F(3;36) = 3.8981; **p = 0.0165**], Lenga [F(3;36) = 4.3106; **p = 0.0107**], Štit [KW-H(3;40) = 2.2031; p = 0.5313] across period 2020 – 2023. Values in bold indicate statistically significant differences (p < 0.05).

4.4.3. Histological and histopathological description

Macroscopically, from 32 samples collected across all stations, 18 were considered healthy and 14 were necrotic samples. All collected samples were examined microscopically and 8 samples were confirmed as healthy tissue, while remaining 24 were reclassified as necrotic: 15 samples were categorised as light histopathology (general state code 1; <25% of tissues contained lesions), 7 samples were categorised as moderate histopathology (general state code 2; 25-75% of tissues contained lesions) while heavy histopathology were confirmed in 2 samples (general state code 3; >75% of tissues contained lesions).

Histological analysis of healthy *Balanophyllia europaea* polyps revealed a clearly organized and intact microanatomical structure, with no detectable signs of pathology (Figure 39). The polyp body consisted of two distinct epithelial layers—the external epidermis and the internal gastrodermis—separated by a thin, gelatinous, and acellular mesoglea. The epidermis was composed of a monolayer of cylindrical epithelial cells, interspersed with mucocytes and cnidocytes containing nematocysts, forming a well-defined and specialized epithelial barrier. The mesoglea was uniform in appearance and closely adhered to the adjacent epithelial layers, contributing to structural integrity and mechanical flexibility. The gastrodermal layer, rich in ciliated and glandular cells, enclosed a central gastrovascular cavity containing a limited number of mesenteries. Symbiotic dinoflagellates (family Symbiodiniaceae) were observed within the gastrodermis as rounded pinky red cells with visible internal organization, including occasional chromatin structures. All tissue layers within the basal region were continuous, morphologically preserved, and tightly interconnected. Gram staining indicated a moderate density of bacterial cells located within the surface epidermis. Of the 18 samples that were macroscopically identified as healthy, 61% of polyps exhibited tissue affected by some form of pathological alteration. Among these, 36% of the samples showed moderate pathological changes involving between 25% and 75% of the polyp tissue, 9% of the samples showed severe pathological changes, while 55% of the samples showed light pathological changes affecting less than 25% of the tissue. All lesions recorded in analysed samples were chategorised as light and heavy, and their frequency is presented in Table 9.

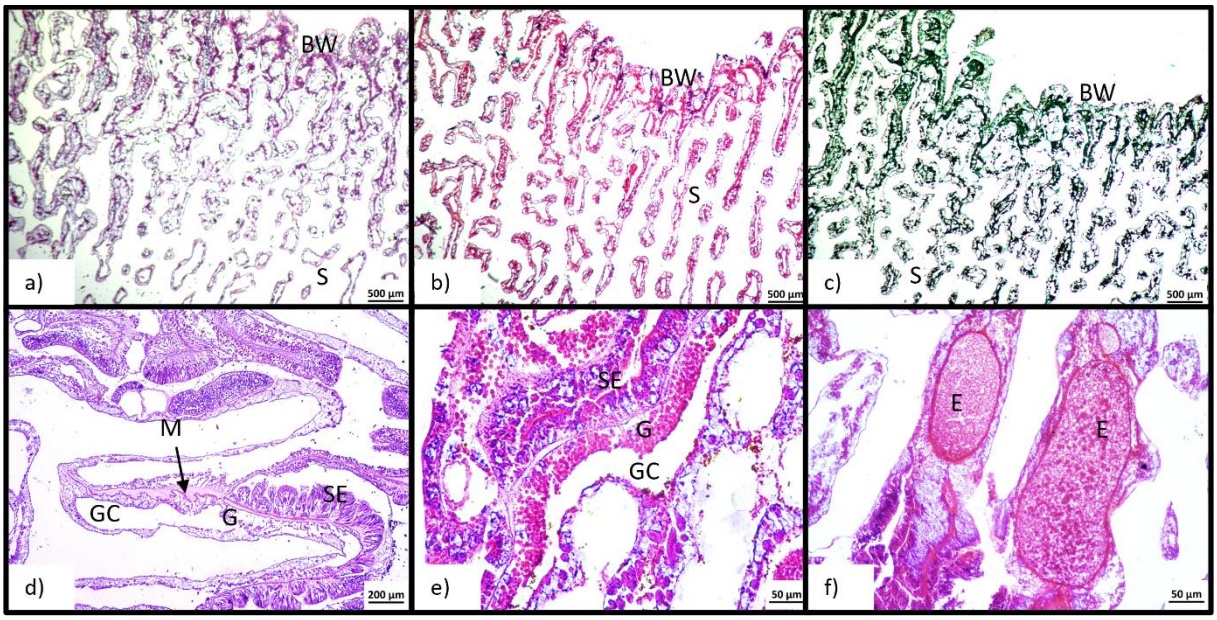

Figure 39. Histological longitudinal sections of healthy tissue of *Balanophyllia europaea* polyp, stained with (a, d–f) hematoxylin and eosin, (b) Gram stain for bacteria, and (c) Grocott's methenamine silver stain for fungi. (a–c) Longitudinal sections showing the aboral side of the polyp with the basal body wall (BW) and skeletal space (S). (d–f) Detailed views show (d) healthy surface epithelium (SE) and mesenterial filaments with mesoglea (M), gastrodermis (G), gastrovascular cavities (GC) and skeletal space (S), (e) gastrodermis (G) containing abundant endosymbiotic dinoflagellates (Symbiodiniaceae), and (f) mesenteries with large oocytes (E).

Table 9. Specific histopathological lesions and patogens of *Ballanophylia europeae* and their frequency

Specific histopathological lesions	**Light lesion (state 1)**	**Freq (%)**	**Heavy lesion (state 2)**	**Freq (%)**
Bassal body wall epidermis - loss of integrity	15	46.9	1	3.1
Bassal body wall epidermis - reduction	6	18.8	0	0.0
Surface body wall epidermis - loss of integrity	17	53.1	4	12.5
Surface body wall epidermis - mucocytes	7	21.9	2	6.3
Surface body wall epidermis - hyperthrophy	9	28.1	1	3.1
Surface body wall epidermis - reduction	5	15.6	1	3.1
Mesoglea - swelling	8	25.0	2	6.3
Mesoglea - nude	6	18.8	1	3.1
Mesoglea - reduction	7	21.9	4	12.5
Gastrodermal disruption, desintegration, loss of integrity	14	43.8	10	31.3
Gastrodermis necrotic zones	17	53.1	7	21.9
Gastrodermis reduction	9	28.1	4	12.5
Endosymbionts dark and shrunken	21	65.6	1	3.1
Endosymbionts reduction in number	7	21.9	2	6.3
Reduction of mesenterial filaments	15	46.9	0	0.0
Presence of ova/spermal cells	18	56.3	6	18.8
Presence of atretic eggs	7	21.9	1	3.1
Patogens	**Light lesion (state 1)**	**Freq (%)**	**Heavy lesion (state 2)**	**Freq (%)**
Presence of Alghae	6	18.8	3	9.4
Presence of Crustacea	2	6.3	0	0.0
Presence of helminthes	1	3.1	0	0.0
Presence of Funghi	6	18.8	0	0.0
Presence of Porifera	2	6.3	5	15.6
Bacteria quantity surface wall epidermis red	8	25.0	0	0.0
Bacteria quantity surface wall epidermis blue	26	81.3	4	12.5
Bacteria quantity gastrodermis	10	31.3	1	3.1

The most frequent and evident changes in structure (lesions) in solitary scleractinian coral *B. europaea* were recorded in gastrodermal layer in polyps. Changes in endosymbiont appearance in gastrodermis were the most frequent light lesion, occurring in 66% of samples. Necrotic endosymbionts showed nuclear fragmentation and brown cytoplasmic pigment

accumulation, visible as darker coloration. A reduced number of endosymbionts was recorded in some samples, where light lesions were present in 22% and heavy lesions in 6% of samples (Table 9). Other lesions in this layer included necrotic areas, disintegration and loss of structural organisation, and an evidently reduced amount of tissue (endosymbiont and gastrodermal cells) (Figure 40, Figure *41*). Smaller diffuse focal necrotic zones and disintegration of gastrodermis were categorised as light in 53% and 44% of examined samples, while heavier lesions in gastrodermis progressed to complete necrosis in 31% and loss of tissue cohesion in 22% of samples, when connection with mesoglea was lost and cell debris was present. Gastrodermal tissue loss was recorded as a light lesion in 28% of samples and as a heavy lesion in 13% of samples (Table 9). A reduced number of mesenterial filaments was observed in 47% of necrotic polyps, while atretic oocytes were recorded as a light lesion in 22% of analysed samples.

The mesogleal layer was structurally quite stabile, without accumulation of cells such as eosinophilic granular amoebocytes, which suggests a visible immune response. Mesogleal lesions in *B. europaea* included swelling stage, recorded as a light change in 25% of samples and as a heavy change in 6% of samples (Table 9). Furthermore, the opposite tissue reaction was manifested in reduced mesogleal layer, recorded in both light and heavy lesion types (22% and 13%, respectively) (Figure 40, Figure *41*). Reduced mesoglea and reduced tissue in gastrodermis did not follow the same pattern and were not always present in the same samples. When gastrodermis exhibited lytic necrosis characterised by dissociation of tissue and cellular detachment, nude mesoglea was also recorded.

The surface epithelium frequently showed changes in the structure and loss of integrity, with mild necrotic changes observed in 53% of samples and heavy necrosis present in 13% (Table 9). Severe cases were marked by disruption of the epidermal layer, as well as frequent exposure of the underlying mesoglea (Figure 41). Samples with light lesions in the surface epithelium included an increase in mucocyte and columnar epithelial cell height, recorded as a light lesions in 28% of samples and heavy lesions in 3% of samples (Figure 40). However, in 16% of samples, marked thinning and atrophy of the surface epidermal layer were observed (Table 9).

The basal body wall in necrotic polyps showed histopathological changes primarily within the epidermal layer, while the mesoglea largely maintained its structural continuity. Gram staining revealed an increased bacterial presence in necrotic samples, particularly within the surface epidermis, occasionally extending into the gastrodermis.

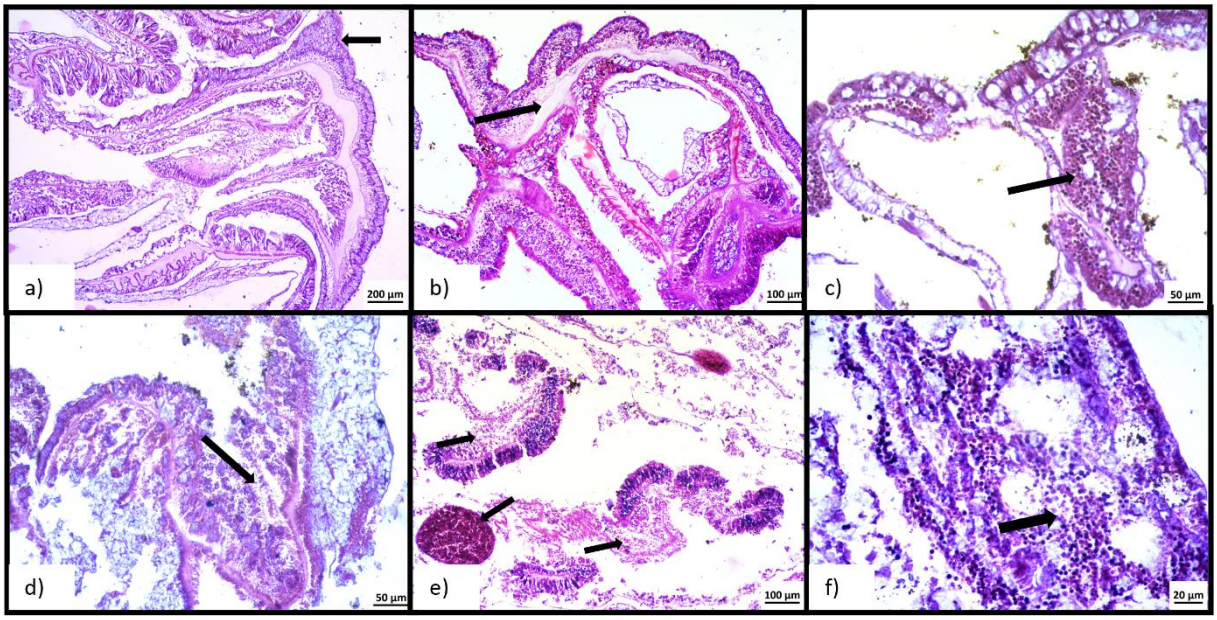

Figure 40. Histological longitudinal sections of *Balanophyllia europaea* samples with identified light microscopic lesions (a-c) show (a) structural changes in surface epithelium, (b) swelled mesoglea and (c) dark and shrunken endosymbionts in gastrodermis. Heavy microscopic lesions (d-f) show (d) complete loss of integrity and peeling of the surface epithelium, (e) loss of gastrodermal tissue, atretic eggs and filaments or (f) structural disintegration, necrotic gastrodermal tissue and dark and shrunken endosymbionts. HE stain.

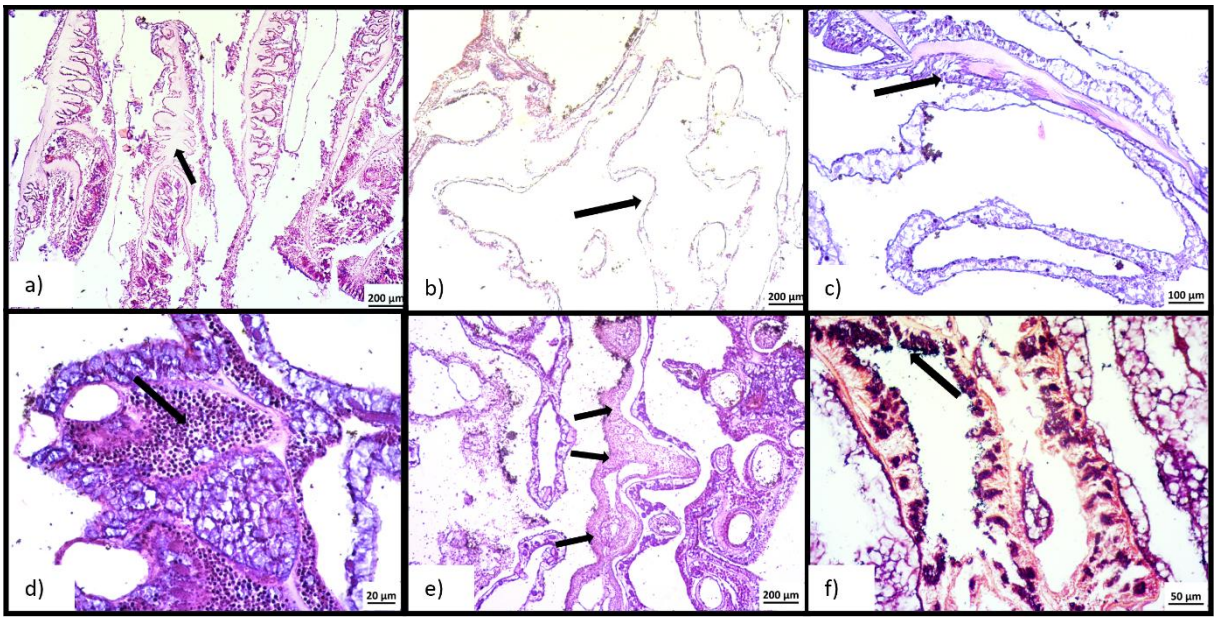

Figure 41. Histological longitudinal sections of *Balanophyllia europaea* showing details of frequent histopathological lesions in hematoxylin and eosin (a-e) and Gram (f) stained sections. Observed changes include (a) thickened and exposed (nude) mesoglea, (b) massive loss of gastrodermal tissue and severely reduced mesoglea, (c) loss of endosymbiotic dinoflagellates from the gastrodermis, (d) predominance of dark and shrunken endosymbionts, (e) ingrowth of foreign tissue (sponge) into coral tissue, and (f) increased abundance of bacteria in the surface epithelium associated with light lesions.

4.5. Population status of *Leptopsamia pruvoti*

4.5.1. External appearance and gross lesions

Leptopsammia pruvoti was recorded at Ljubačka vrata station, both stations within NP Telašćica, all stations within NP Kornati, and at Rt Lenga and Štit in NP Mljet, inhabiting poorly lighted coralligenous habitats between 20 and 40 metres in depth, typically encrusted on vertical rocky substrates or within shaded crevices. Morphologically, healthy individuals exhibited a compact, cup-shaped corallum reaching up to 10 mm in diameter and 10–15 mm in height (Figure 42). The skeleton was composed of aragonite with clearly defined radial septa arranged in hexamerous symmetry and a well-developed central columella. The external surface of the corallum was usually smooth or displayed faint costae. Polyps were fleshy and translucent, with an orange to yellow coloration, lacking endosymbiotic Symbiodiniaceae. Numerous short, translucent tentacles were arranged around the oral disc, becoming fully extended during nocturnal polyp expansion. The absence of tissue retraction and the presence of symmetrical skeletal structures, indicated a healthy physiological status.

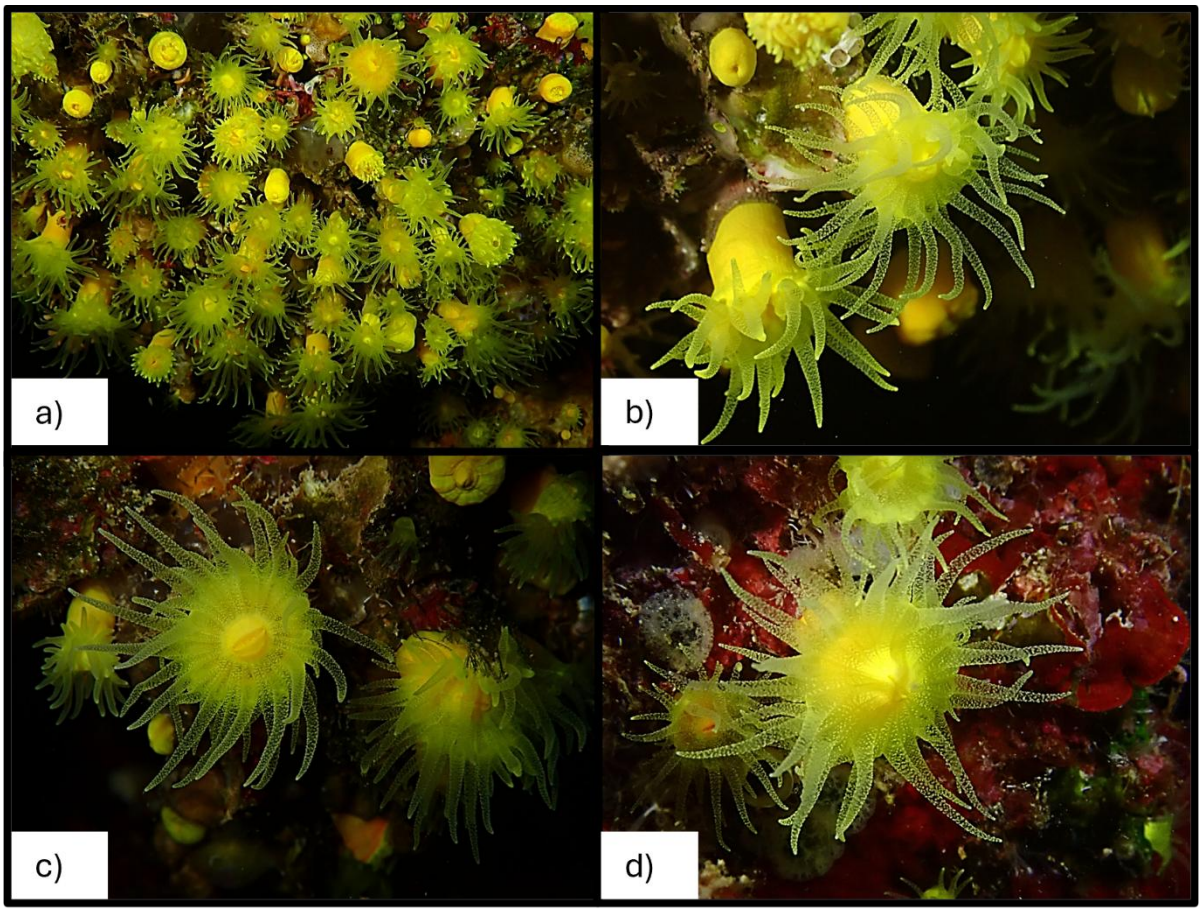

Figure 42. Macroscopic appearance of healthy polyps of *Leptopsammia pruvoti* (a–d). (a) Overview of a population of densely aggregated polyps attached to a hard substrate. (b–d) Close-up views of individual polyps exhibiting intact corallites, full tissue coverage, and vivid yellow-orange pigmentation, with no visible signs of necrosis, bleaching, or epibiotic overgrowth.

Necrotic individuals of *Leptopsammia pruvoti* exhibited a spectrum of macroscopic and morphological alterations indicative of advanced physiological stress. Initial signs of deterioration typically included partial polyp retraction, loss of the characteristic orange to yellow pigmentation, and the appearance of subtle irregularities along the calice rim (Figure 43). Localized tissue necrosis manifested as pale greyish or whitish lesions, progressively leading to tissue thinning and partial exposure of the underlying white aragonitic skeleton. In more advanced stages, polyp tissue disintegration resulted in extensive skeletal exposure, accompanied by erosion of the calice structure, disrupted septal architecture, and occasional fragmentation of the thecal wall. In some cases, although tissue remained structurally intact, it appeared markedly depigmented and translucent. Severely necrotic zones were often

characterized by sloughing of residual tissue, accumulation of fine sediments, and prolific colonization by microbial biofilms and epibiotic organisms. These opportunistic colonizers were frequently associated with areas of complete polyp mortality, where only the bare, degraded corallum remained, secondarily overgrown by diverse epibiotic taxa.

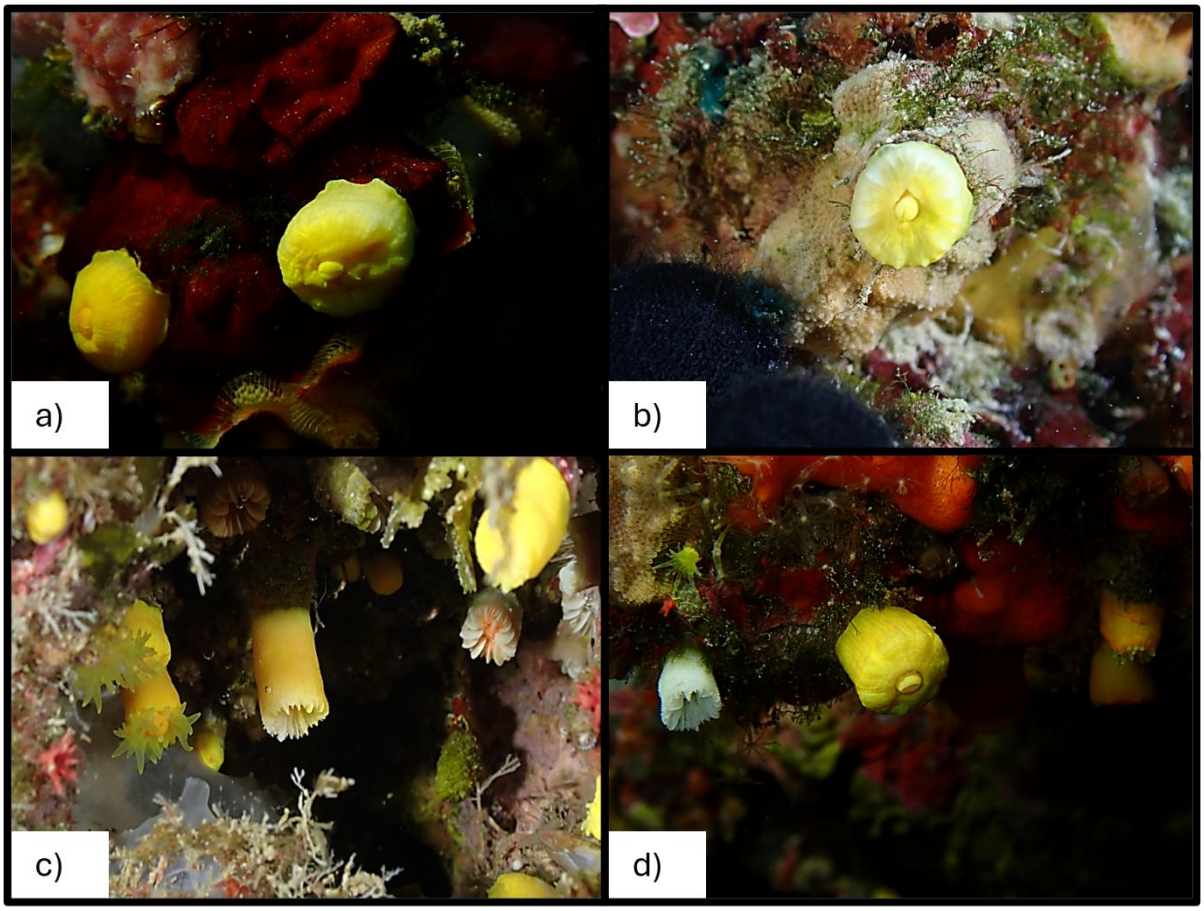

Figure 43. Macroscopic appearance of necrotic polyps of *Leptopsammia pruvoti* (a–d). (a–c) Close-up views of polyps exhibiting tissue degradation, partial necrosis, and loss of pigmentation, with exposed skeletal structures in some individuals. (d) Comparison between a dead specimen showing only the remaining corallite and a healthy polyp with retracted tentacles.

4.5.2. Polyp density and mortality rate assessment

Population density of *Leptopsamia pruvoti* showed variable trends across years and stations, though statistical analyses did not reveal significant interannual variability ($p > 0.05$) (Figure 44). The median polyp density remained relatively stable across the analysed period, with

slight fluctuations observed in certain stations. However, some stations, such as Mali Obručan, exhibited a continuous decline in density, while others, like Hrid Štit, experienced an overall increase. Shapiro-Wilk test confirmed that polyp density data followed a normal distribution across all stations and years ($p < 0.05$), except for station Mali Obručan in 2020, where a significant deviation from normality was detected ($p < 0.05$). Consequently, ANOVA was applied for normally distributed datasets, while the Kruskal-Wallis test was used for Mali Obručan in 2020 due to its non-normal distribution.

The highest recorded polyp density was observed at Mali Obručan in 2020, with a mean value of 336.0 ± 51.0 polyps/m², while this station also experienced the steepest decline throughout the study period. Conversely, the lowest polyp density was recorded at Ljubačka vrata in 2023, where the mean density reached 136.2 ± 24.7 polyps/m², reflecting overall stability at this site.

At Ljubačka vrata, the mean density remained relatively stable, ranging from 142.6 ± 14.6 polyps/m² in 2020 to 136.2 ± 24.7 polyps/m² in 2023 (Figure 44). The statistical test detected no significant differences over time, suggesting that this location maintains a stable polyp density despite minor fluctuations.

Within Nature Park Telašćica, polyp density showed slight declines over the years at both Sestrica Vela and Veli Garmenjak, two closely situated stations. At Sestrica Vela, density dropped from 326.2 ± 35.2 polyps/m² in 2020 to 298.2 ± 25.5 polyps/m² in 2023, while at Veli Garmenjak, values decreased from 276.8 ± 51.7 polyps/m² in 2020 to 274.2 ± 26.4 polyps/m² in 2023 (Figure 44). Statistical analyses detected no significant differences between years.

Within National Park Kornati, *Leptopsamia pruvoti* polyp density varied across stations. Mali Obručan station exhibited a notable decline, while station Balun experienced a slight increase over time. At station Mana, mean polyp density ranged from 273.4 ± 34.8 polyps/m² in 2020 to 264.1 ± 38.7 polyps/m² in 2023, while at Balun, values slightly increased from 286.0 ± 53.9 polyps/m² in 2020 to 303.9 ± 31.2 polyps/m² in 2023 (Figure 44). Despite minor interannual fluctuations, no significant differences between years were detected. At Mali Obručan, a clear downward trend was observed, with polyp density declining from 336.0 ± 51.0 polyps/m² in 2020 to 296.8 ± 31.3 polyps/m² in 2023, but the Kruskal-Wallis test ($H(3;32) = 0.771$, $p = 0.056$)

did not reveal statistically significant differences, suggesting that observed fluctuations were not ecologically meaningful.

At National Park Mljet, polyp density of *Leptopsamia pruvoti* varied significantly between stations, with Hrid Štit exhibiting an increasing trend, while Rt Lenga showed a slight decrease. At Rt Lenga, mean density ranged from 261.1 ± 50.8 polyps/m² in 2020 to 254.8 ± 40.1 polyps/m² in 2023, whereas at hrid Štit, values increased from 270.6 ± 23.9 polyps/m² in 2020 to 308.1 ± 36.6 polyps/m² in 2023 (Figure 44). Statistical analyses revealed no significant differences over time, further supporting the stability of polyp density within this marine reserve.

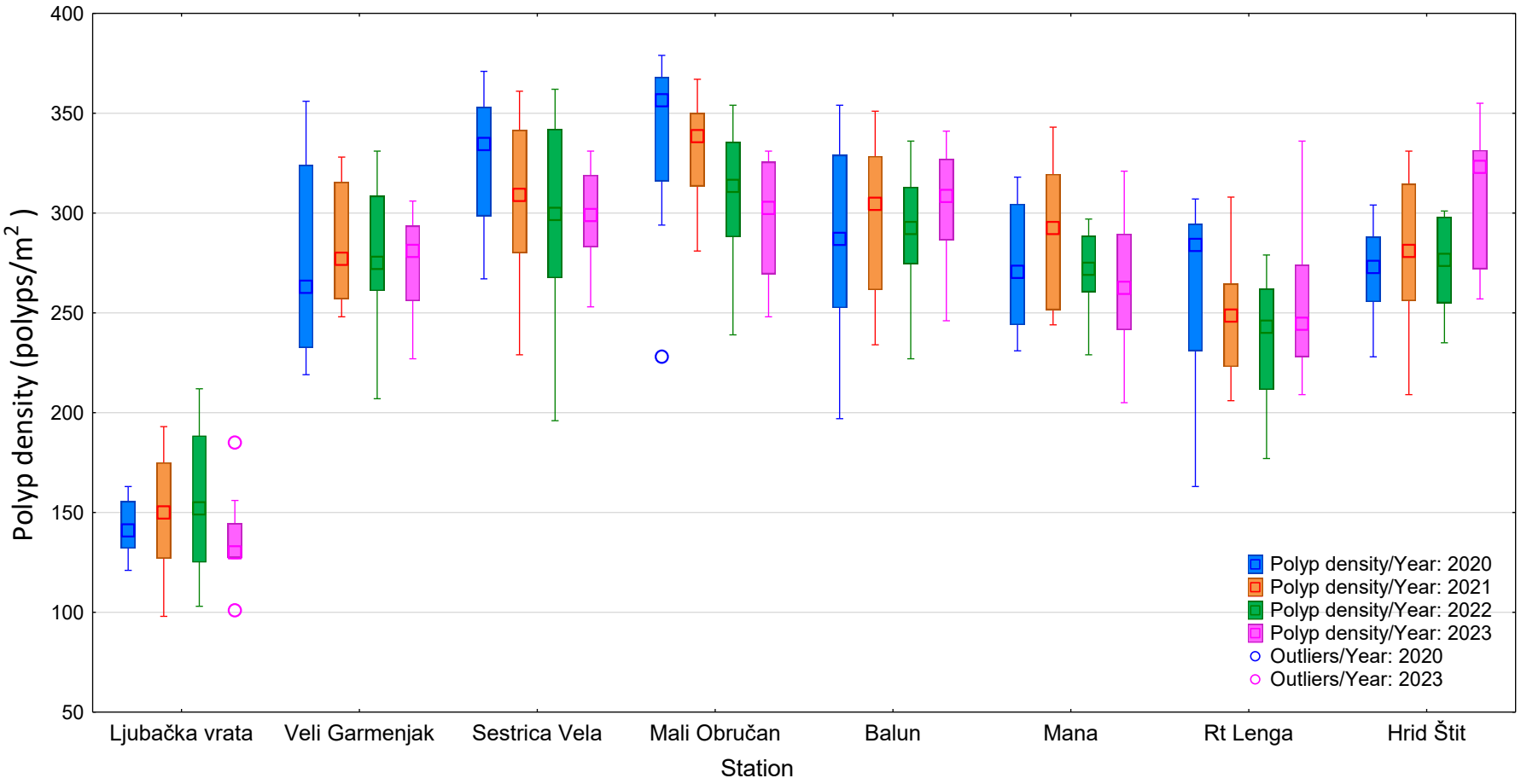

Figure 44. *Leptopsamia pruvoti* polyp density on stations Ljubačka vrata [F(3;28) = 0.6869; p = 0.5676], Veli Garmenjak [F(3;28) = 0.1; p = 0.9593], Sestrica Vela [F(3;28) = 0.8529; p = 0.4769], Mali Obručan [KW-H(3;32) = 7.5801; p = 0.0555], Balun [F(3;28) = 0.2872; p = 0.8342], Mana [F(3;28) = 0.7714; p = 0.5198;], Lenga [F(3;28) = 0.5583; p = 0.6470], Štit [F(3;28) = 2.1614; p = 0.1149] across period 2020 – 2023

The mortality rate of *Leptopsamia pruvoti* exhibited statistically significant changes across all monitored stations ($p < 0.05$), with the highest rates recorded in National Park Mljet and Kornati (Figure 45). Rt Lenga had the highest mean mortality rate over the entire study period (26.3 ± 4.8%), while the lowest was recorded at station Ljubačka vrata (9.3 ± 3.3%). The greatest single-year mortality rate was found at station Rt Lenga in 2023 (29.5 ± 3.0%), whereas the lowest was observed at Veli Garmenjak station in 2020 (6.0 ± 2.4%). The Shapiro-Wilk test confirmed that mortality rate data were normally distributed in most cases ($p > 0.05$). ANOVA was used for normally distributed datasets, and in instances where normality was not met, the Kruskal-Wallis test was applied.

At Ljubačka vrata, mortality rates of *Leptopsamia pruvoti* gradually increased, from 7.5 ± 2.7% in 2020 to 12.2 ± 2.1% in 2023 (Figure 45). Since the data at this site did not follow a normal distribution, a Kruskal-Wallis test was performed, which detected a significant variation over time ($H (3;32) = 12.861$, $p = 0.005$).

Within Nature Park Telašćica, mortality rates of *Leptopsamia pruvoti* rose sharply. At Sestrica Vela, values tripled, from 6.8 ± 2.3% in 2020 to 21.4 ± 3.7% in 2023, while at Veli Garmenjak, mortality more than doubled, increasing from 6.0 ± 2.4% to 15.9 ± 2.0% (Figure 45). ANOVA confirmed significant differences ($F (3;28) = 22.597$, $p = 0.000$ for Sestrica Vela; $F (3;28) = 16.308$, $p = 0.000$ for Veli Garmenjak).

At National Park Kornati, mortality rates of *Leptopsamia pruvoti* showed a clear increasing trend across all monitored stations. At Mana, mortality increased from 13.5 ± 4.8% in 2020 to 23.1 ± 2.4% in 2023, while at Balun, values more than doubled, from 11.2 ± 2.8% to 24.9 ± 2.4%. Meanwhile, at Mali Obručan, mortality rates also increased, from 9.5 ± 3.2% to 14.6 ± 3.2% (Figure 45). ANOVA ($F (3;28) = 13.309$, $p = 0.000$ for Mana; $F (3;28) = 21.754$, $p = 0.000$ for Balun; $F (3;28) = 4.911$, $p = 0.007$ for Mali Obručan) confirmed significant differences between years.

At National Park Mljet, mortality rates of *Leptopsamia pruvoti* were among the highest recorded. At Rt Lenga, values increased steadily, from 20.0 ± 4.5% in 2020 to 29.5 ± 3.0% in 2023, while at hrid Štit, mortality rose from 19.8 ± 5.2% to 28.8 ± 1.8% (Figure 45). ANOVA

confirmed significant interannual variability ($F(3;28) = 13.921$, $p = 0.000$ for Lenga; $F(3;28) = 6.328$, $p = 0.002$ for hrid Štit).

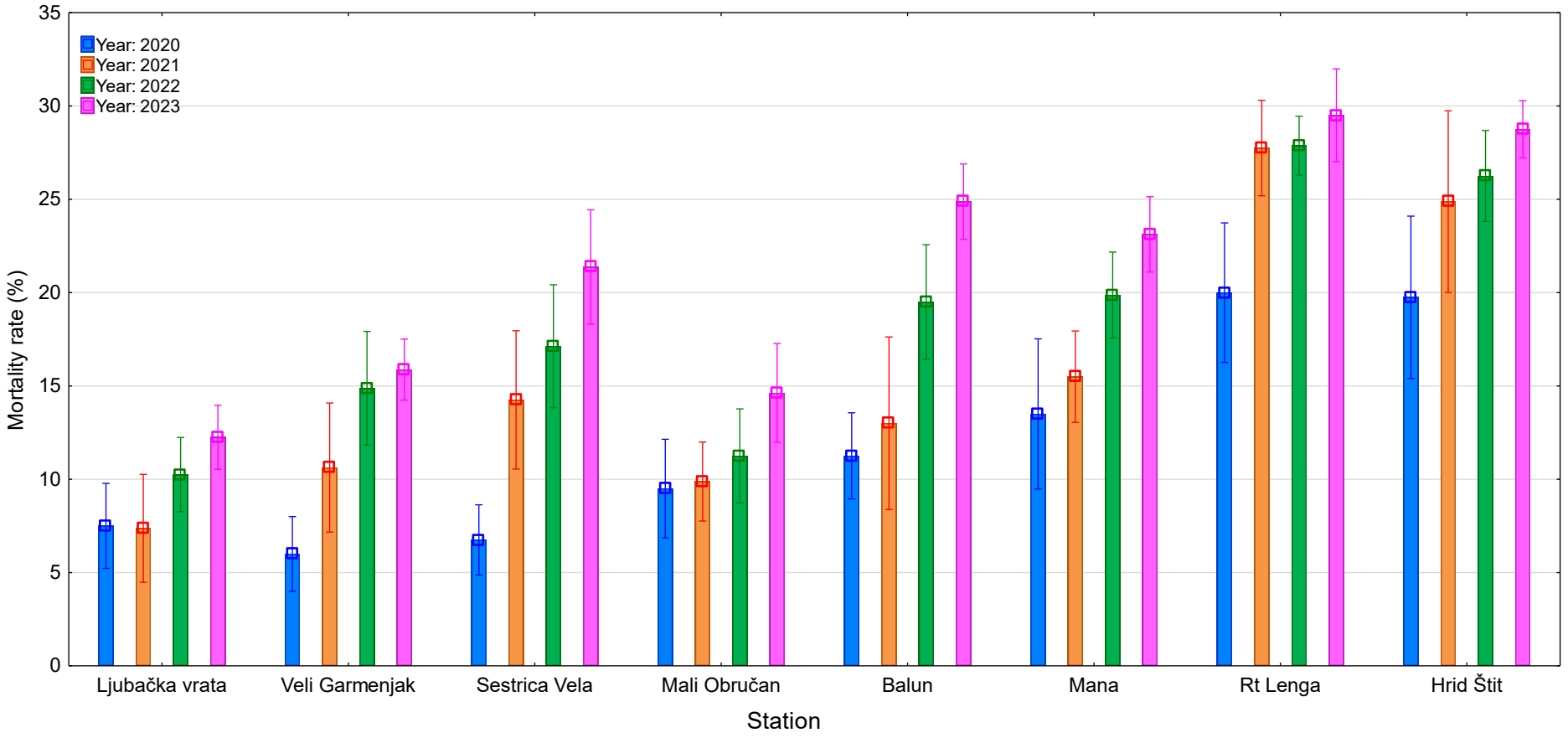

Figure 45. *Leptopsamia pruvoti* mortality rate on stations Ljubačka vrata [KW-H(3;32) = 12.8614; **p = 0.0049**], Veli Garmenjak [F(3;28) = 16.3083; **p < 0.0001**], Sestrica Vela [F(3;28) = 22.5975; **p < 0.0001**], Mali Obručan [F(3;28) = 4.911; **p = 0.0073**], Balun [F(3;28) = 21.7539; **p < 0.0001**], Mana [F(3;28) = 13.3091; **p = 0.00001**], Lenga [F(3;28) = 13.9212; **p = 0.00001**], Štit [F(3;28) = 6.3278; **p = 0.0021**] across period 2020 – 2023. Values in bold indicate statistically significant differences (p < 0.05).

4.5.3. Histological and histopathological description

Macroscopically, from 29 samples collected across stations from NP telašćica, NP Kornati and NP Mljet, 13 were considered healthy, while 16 were necrotic samples. All collected samples were examined microscopically and while 5 samples were confirmed as healthy tissue, the remaining 24 were reclassified as necrotic: 7 samples were categorised as light histopathology (general state code 1; <25% of tissues contained lesions), 7 samples were categorised as moderate histopathology (general state code 2; 25-75% of tissues contained lesions) while heavy histopathology were confirmed in 10 samples (general state code 3; >75% of tissues contained lesions).

The histological architecture of a healthy *Leptopsammia pruvoti* polyp exhibited a compact and well-organized tissue architecture, characteristic of a non symbiont scleractinian coral, with no evidence of pathological changes (Figure 46). Each polyp was composed of two principal epithelial layers: an outer epidermis and an inner gastrodermis, separated by a distinctly thicker and more robust mesoglea. Epidermal tissue displayed a uniform layer of columnar epithelial cells, accompanied by sporadically distributed mucocytes and rich cnidocytes. The mesoglea presented as a dense, homogeneous, acellular matrix, contributing to the polyp's increased rigidity and volume. In contrast to *Cladocora caespitosa* and *Ballanophylia europeae*, no endosymbiotic dinoflagellates were observed within the gastrodermis. The gastrodermal layer, although similar in basic cellular composition (with ciliated and glandular cells), appeared more compact and enclosed a relatively spacious gastrovascular cavity. Several well-defined mesenteries extended from the gastrodermis into the cavity, containing cells associated with digestion, nutrient processing, gametogenesis, and general physiological regulation. Along the septal margins, distinct connective tissue elements were evident and selectively stained with hematoxylin, providing structural reinforcement between the mesoglea and skeletal septa. All tissue layers remained continuous and morphologically intact, with no signs of necrosis or degeneration. Gram staining revealed a mild to moderate bacterial presence, primarily localized within the basal portions of the epidermis, but without any associated tissue disruption or inflammatory response. Histological analysis of *Leptopsammia pruvoti* polyps revealed extensive variability in tissue condition, encompassing a broad spectrum of structural and cellular alterations. Of the 13 samples that

were macroscopically identified as healthy, 54% of polyps exhibited tissue affected by some form of pathological alteration. Among these, 86% showed moderate pathological changes involving between 25% and 75% of the polyp tissue, while 14% of the samples showed light pathological changes affecting less than 25% of the tissue.

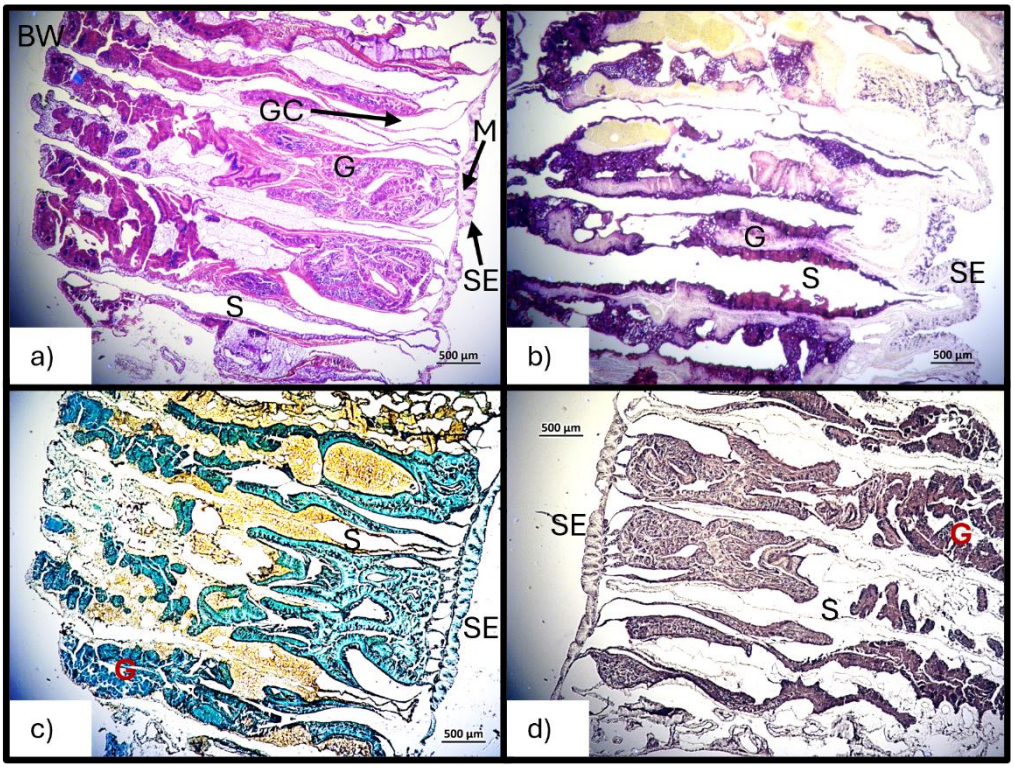

Figure 46. Histological longitudinal sections of a healthy polyp of *Leptopsammia pruvoti*, stained with (a) hematoxylin and eosin (H&E), (b) Gram, (c) Grocott's methenamine silver, and (d) Masson's trichrome. Sections show normal tissue architecture and clear organization of polyp, including the gastrodermis (G), gastrovascular cavity (GC), mesoglea (M), surface epithelium (SE), basal body wall (BW) and skeletal space (S).

Table 10. Specific histopathological lesions and patogens of *Leptopsamia pruvoti* and their frequency

Specific histopathological lesions	Light lesion (state 1)	Freq (%)	Heavy lesion (state 2)	Freq (%)
Bassal body wall epidermis - loss of integrity	11	55.0	7	35.0
Bassal body wall epidermis - reduction	9	45.0	2	10.0
Surface body wall epidermis - loss of integrity	11	37.9	12	41.4
Surface body wall epidermis - increase in mucocytes	9	31.0	9	31.0
Surface body wall epidermis - hyperthrophy	21	72.4	3	10.3
Surface body wall epidermis - reduction	3	10.3	10	34.5
Mesoglea - swelling	7	24.1	5	17.2
Mesoglea - nude	12	41.4	4	13.8
Mesoglea - reduction	7	24.1	10	34.5
Gastrodermal disruption, desintegration, loss of integrity	8	27.6	13	44.8
Gastrodermis necrotic zones	15	51.7	11	37.9
Gastrodermis reduction	2	6.9	7	24.1
Calicoderm decreased	2	6.9	10	34.5
Calicoderm increased	2	6.9	0	0.0
Reduction of mesenterial filaments	4	13.8	8	27.6
Presence of ova/spermal cells	3	10.3	14	48.3
Patogens	**Light lesion (state 1)**	**Freq (%)**	**Heavy lesion (state 2)**	**Freq (%)**
Presence of Algae	3	10.3	2	6.9
Presence of Crustacea	1	3.4	1	3.4
Presence of Funghi	1	3.4	0	0.0
Presence of Porifera	5	17.2	1	3.4
Bacteria quantity basal wall epidermis	12	57.1	5	23.8
Bacteria quantity surface wall epidermis	22	75.9	2	6.9
Bacteria quantity gastrodermis	20	69.0	4	13.8

Lesions were most pronounced in the gastrodermal layer, where necrotic zones were identified in 52% of polyps as light lesions and in 38% as heavy lesions (Table 10). These necrotic changes manifested as localized tissue disintegration, loss of cellular cohesion, and degradation of gastrodermal structure (Figure 47, Figure 48). Disruption and complete disintegration of the gastrodermis were present in 28% of mild and 45% of severe cases. Gastrodermal reduction, characterized by thinning of the layer and reduced cellular density, was noted in 7% of light and 24% of heavy lesions. In many cases, degradation progressed to lytic necrosis, exposing

the underlying mesoglea and resulting in a denuded mesogleal surface, recorded in 41% of polyps with mild lesions and 14% of heavily affected polyps (Table 10).

The basal body wall epidermis also displayed structural damage, with loss of integrity observed in over half of the mildly affected polyps and in more than a third of those with advanced lesions. Epidermal reduction in this region was noted in 45% of the mildly damaged samples, but was considerably less frequent in severely affected tissue, where it occurred in only 10% of cases (Table 10).

The surface body wall epidermis frequently showed hypertrophic responses, with 72% of mildly affected samples presenting increased epithelial cell volume, and 10% of severely affected samples exhibiting the same lesion. Increased mucocyte density was present in 31% of polyps across both mild and severe cases. Loss of epidermal integrity was identified in 38% of mild and 41% of severe lesions, while epidermal thinning or atrophy occurred in 10% of mildly and 35% of severely affected specimens (Table 10). These epithelial changes were often accompanied by mucocyte proliferation and changes in columnar cell morphology, suggesting a chronic or adaptive epithelial response to prolonged stress (Figure 47, Figure 48).

The mesogleal layer largely retained its structural continuity. Nonetheless, swelling was observed in 24% of mildly affected samples and 17% of those with severe lesions (Table 10). Mesogleal reduction occurred at a similar frequency in mildly affected specimens but was more pronounced in severe cases, where it was recorded in 35% of samples.

Reproductive structures were recorded in 59% of samples, with 48% classified as heavy and 10% as light presence of ova or spermatozoa, indicating that gametogenic activity persisted in a portion of the population despite visible tissue degeneration. Reduction in mesenterial filaments was detected in 14% of mild and 28% of severe affected polyps (Table 10), potentially reflecting chronic degeneration of internal gastrovascular structures.

Opportunistic colonization was prevalent across necrotic polyps. Gram staining confirmed elevated bacterial presence in the surface body wall epidermis in 76% of samples, and in the gastrodermis in 69% of polyps, with basal epidermal colonization in 57% of cases. Additionally,

epibiotic organisms, including Porifera (in 17% of polyps), algae (10%), fungi (3%) and crustaceans (3%) were detected, mostly in areas of extensive tissue loss and skeletal exposure.

Overall, the histopathological profile of *L. pruvoti* is characterized by frequent gastrodermal necrosis, epithelial degradation, and microbial colonization, indicating a high prevalence of sublethal and potentially lethal stress responses across the surveyed population.

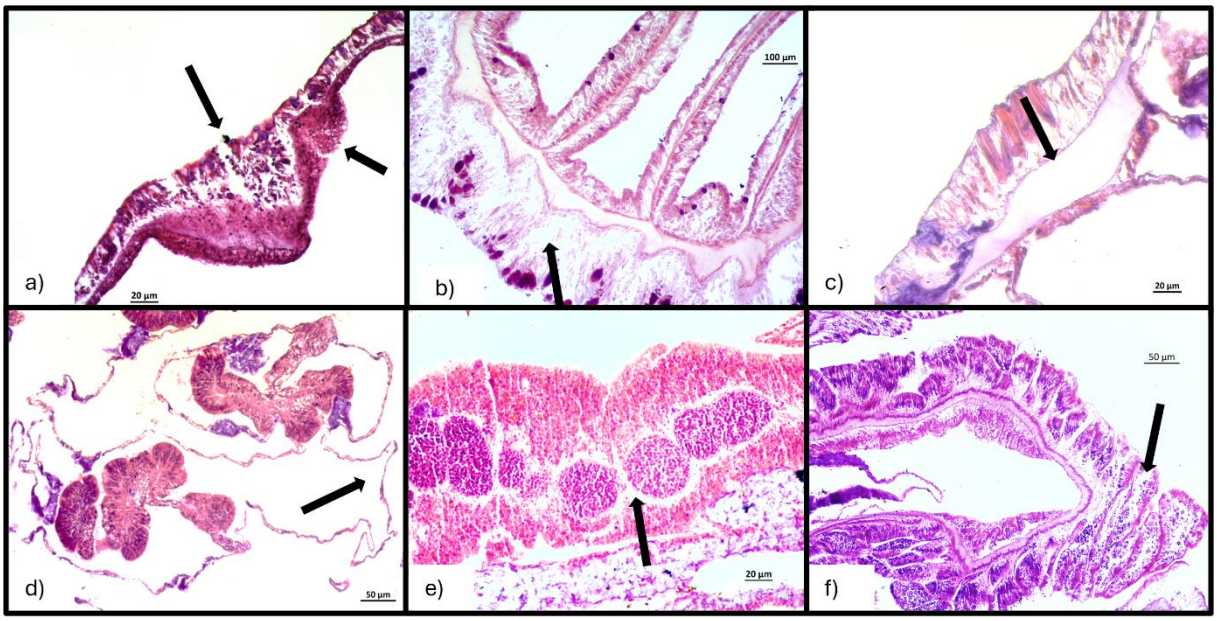

Figure 47. Histological longitudinal sections of *Leptopsamia pruvoti* samples with identified light microscopic lesions (a-f) show (a) necrotic proliferations in surface epithelium, (b) mucocyte proliferation in epithelium, (c) enlarged and swollen mesoglea, (d) reduction of gastodermic filaments, (e) increase in oocyte production and (f) structural disintegration in epithelium. HE stain.

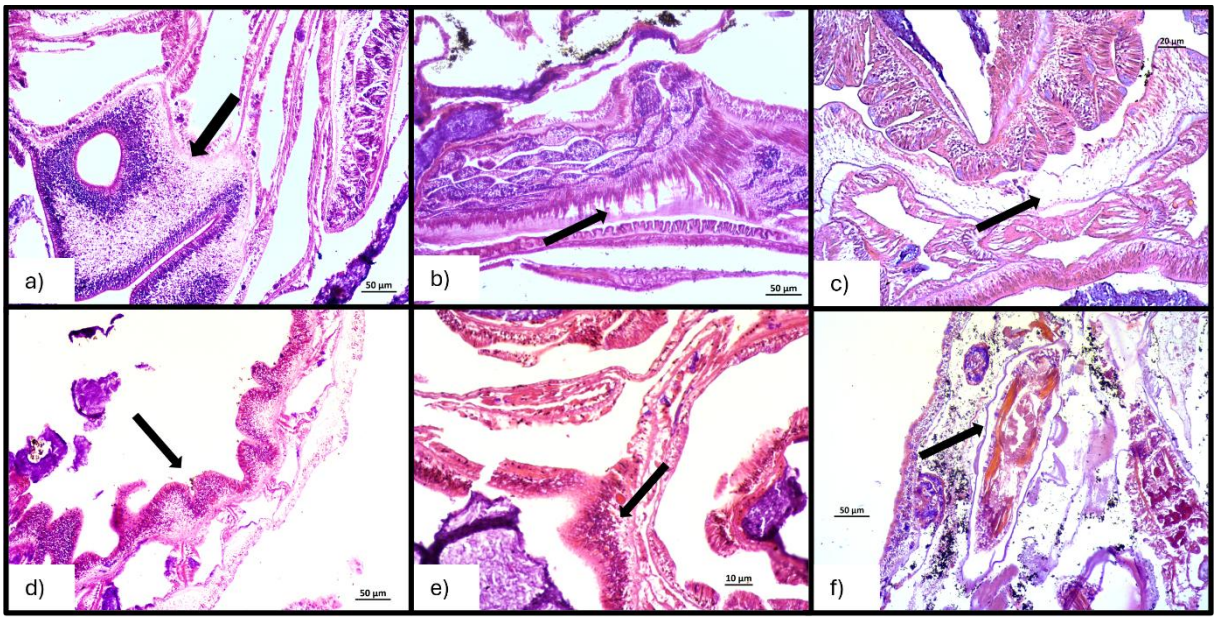

Figure 48. Histological longitudinal sections of *Leptopsamia pruvoti* samples with identified heavy microscopic lesions (a-f) show (a) notable proliferation of epidermis, (b) structural disintegration and denuded mesoglea, (c) mucocyte hypertrophy in epithelium, (d, e) necrotic zones with hyperthrophy and proliferation of gastrodermis and (e) incapsulate endoparasitic structure in the gastrodermal cavity. HE stain.

4.6. Population status of *Madracis pharensis*

4.6.1. External appearance and gross lesions

The colonial scleractinian coral *Madracis pharensis* was widespread across the stations Ljubačka vrata, Veli Garmenjak, Vela Sestrica, Mana, Mali Obručan, Balun, Rt Lenga, and Hrid Štit, where it typically occupied the upper zones of coralligenous habitats between 20 and 40 m depth, most often settling within shaded crevices. Healthy populations of *M. pharensis* exhibit a distinct macroscopic morphology, characterized by lobate, encrusting, or nodular growth forms (Figure 49). This species thrives in mesophotic reef environments and cryptic habitats, where it benefits from moderate water flow and stable temperature regimes. The species demonstrates high morphological plasticity, forming encrusting colonies in cryptic sites and nodular colonies in more exposed, light-rich environments. Colony coloration varies depending on habitat placement; colonies found in overhangs or at the edges of caves and crevices appear brownish due to the presence of endosymbiotic algae, whereas colonies inhabiting deeper sections of rock cavities appear white, as they exist in areas with reduced or minimal light exposure. The colonies typically have an irregular polygonal outline and a dense, compact calcareous skeleton, composed of numerous tightly packed corallites measuring 2 to 3 mm in diameter. Each corallite houses a single polyp with eight short, translucent tentacles, which extend at night for suspension feeding. The colony surface appears smooth to slightly undulating, with well-defined septa and costae visible in the skeletal structure. In healthy colonies, polyps are uniformly distributed across the surface, with fully extended tentacles and open antocodium, while the tissue remains intact and undamaged. Colony coloration is consistent with its light environment, as those in well-lit areas exhibit darker hues, whereas colonies in low-light habitats remain uniformly white, showing no variation in pigmentation over time.

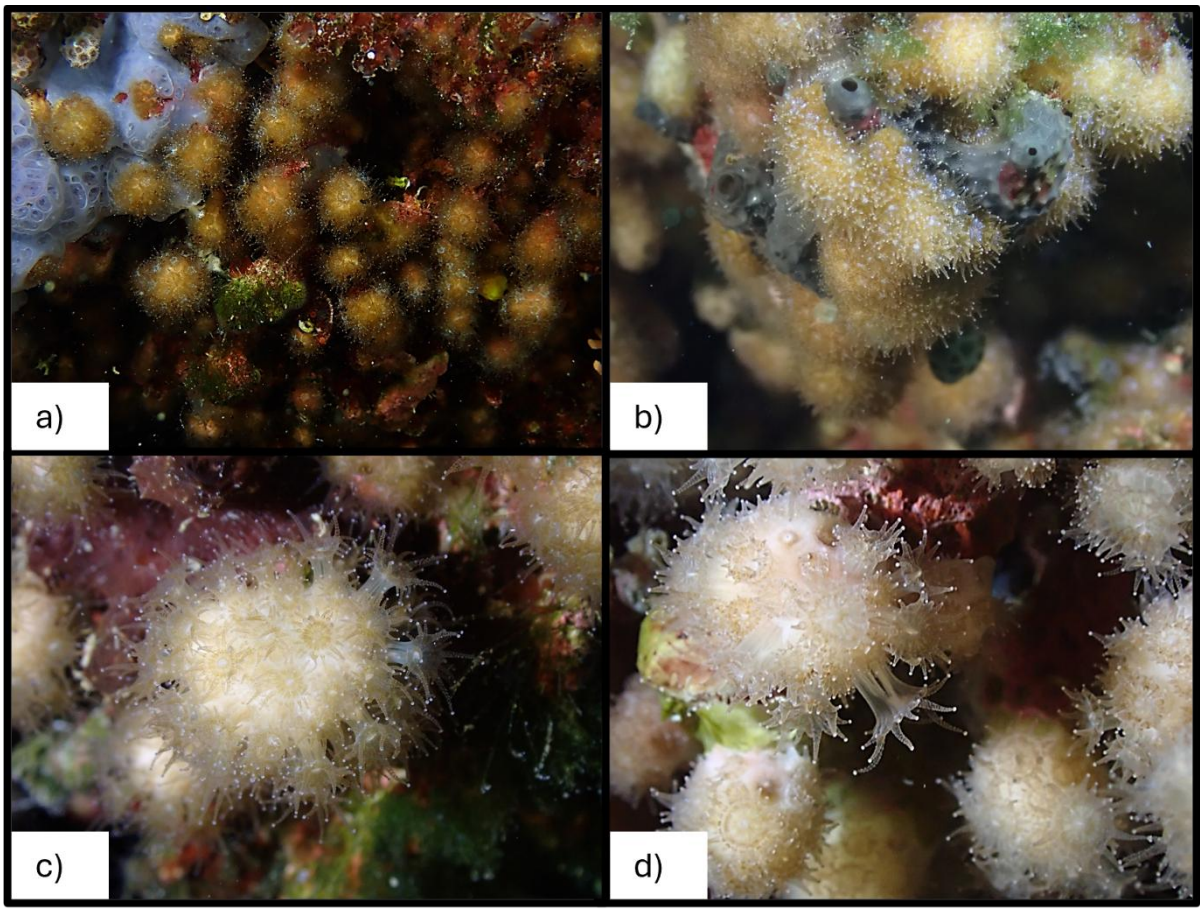

Figure 49. Macroscopic appearance of healthy colonies (a-d) of *Madracis pharensis* at 20m depth (Kornati National Park). (a-b) Overview of structurally intact colonies displaying nodular-shaped morphology with no evidence of polyp degradation or biofouling. (c–d) Close-up views of intact, brown polyps, exhibiting full tissue coverage, uniform pigmentation and no visible signs of necrosis.

Necrotic colonies of *Madracis pharensis* exhibit severe morphological and macroscopic alterations, characterized by progressive tissue degradation, skeletal exposure, and epibiont overgrowth (Figure 50). In early stages, affected areas display localized tissue discoloration, with colonies from well-lit environments developing whitish patches, while those from low-light habitats exhibit tissue deterioration without noticeable colour change, as they naturally lack pigmentation. Polyps in necrotic areas appear atrophied or absent, while surviving polyps at lesion margins exhibit irregular distribution and reduced extension. This degradation pattern suggests a gradual progression from acute tissue loss to long-term skeletal colonization. As necrosis advances, abrupt tissue loss exposes the underlying calcareous skeleton, which varies in colour from bright white to brownish, depending on the duration of

exposure and biofouling accumulation. Recently exposed skeletal areas remain clean and devoid of overgrowth, whereas older lesions are progressively colonized by encrusting organisms, including calcareous algae, bryozoans, and filamentous cyanobacteria. In advanced cases, extensive necrotic regions become densely overgrown with mucilaginous algal layers, sponges, and sessile invertebrates, further compromising the colony's structural integrity.

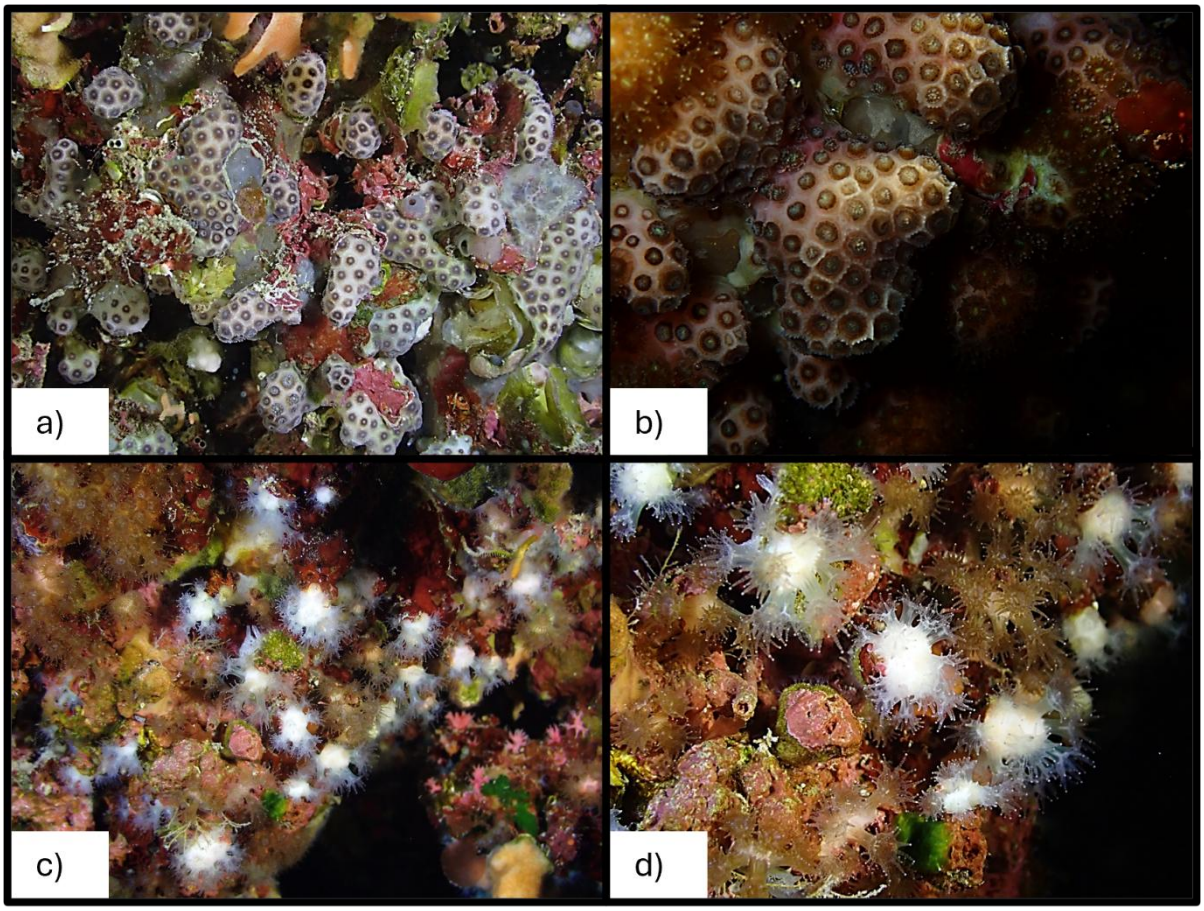

Figure 50. Macroscopic appearance of necrotic *Madracis pharensis* colonies at 20 m depth (Kornati National Park) (a–d). (a-b) Close-up view of necrotic polyps exhibiting advanced-stage tissue necrosis with visible skeletal exposure. (c-d) Bleached polyps showing loss of pigmentation but retained tissue integrity.

4.6.2. Polyp density and mortality rate assesment

The population density of *Madracis pharensis* exhibited interannual variability across observed stations, mostly showing decreasing trends (Figure 51). The highest recorded polyp density was observed at station Mali Obručan in 2020, with a mean value of 240.91 ± 33.71 colonies/m², while the lowest was recorded at Balun in 2023, where the mean density reached 114.69 ± 21.11 colonies/m². The station with the highest average polyp density across all years was Sestrica Vela, whereas Balun exhibited the lowest overall mean. Normality of data distribution was tested using the Shapiro-Wilk test, which confirmed that most datasets followed a normal distribution ($p > 0.05$). However, deviations were observed at Ljubačka vrata and Veli Garmenjak in 2021, requiring the use of the Kruskal-Wallis test. ANOVA was applied to normally distributed datasets to assess significant differences across years.

At Ljubačka vrata, polyp density remained relatively stable over the study period. The mean density in 2020 was 126.44 ± 32.86 colonies/m², with minor fluctuations in subsequent years, reaching 125.00 ± 34.91 colonies/m² in 2023 (Figure 51). No statistically significant differences between years ($p > 0.05$), indicating overall stability at this site.

Within Nature Park Telašćica, at Vela Sestrica station, population density slightly declined from 237.64 ± 38.36 colonies/m² in 2020 to 208.85 ± 47.02 colonies/m² in 2023, although no statistically significant differences were detected ($p > 0.05$) (Figure 51). The mean population density at Veli Garmenjak remained relatively stable, with values of 150.27 ± 55.37 colonies/m² in 2020 and 161.77 ± 35.97 colonies/m² in 2023, suggesting no significant interannual variability ($p > 0.05$).

In the Kornati National Park, the population density of *Madracis pharesis* declines across stations. At Balun, a declining trend was observed, with mean values decreasing from 136.82 ± 25.07 colonies/m² in 2020 to 114.69 ± 21.11 colonies/m² in 2023. Mana exhibited density fluctuating between 201.09 ± 48.08 colonies/m² in 2020 and 184.62 ± 38.35 colonies/m² in 2023. At Mali Obručan station, a decline was detected from 240.91 ± 33.71 colonies/m² in 2020 to 182.77 ± 40.31 colonies/m² in 2023 with no statistically significant differences (ANOVA: $F(3;46) = 4.720$, $p = 0.0059$) (Figure 51).

Within the National Park Mljet, density varied significantly between stations. At Hrid Štit, polyp density exhibited a stable trend, maintaining values around 219.91 ± 33.47 colonies/m² in 2020 and 211.31 ± 27.54 colonies/m² in 2023, with no statistically significant interannual variation ($p > 0.05$). At Lenga, density values fluctuated slightly from 177.09 ± 40.72 colonies/m² in 2020 to 155.23 ± 48.14 colonies/m² in 2023, but no significant differences were detected ($p > 0.05$) (Figure 51).

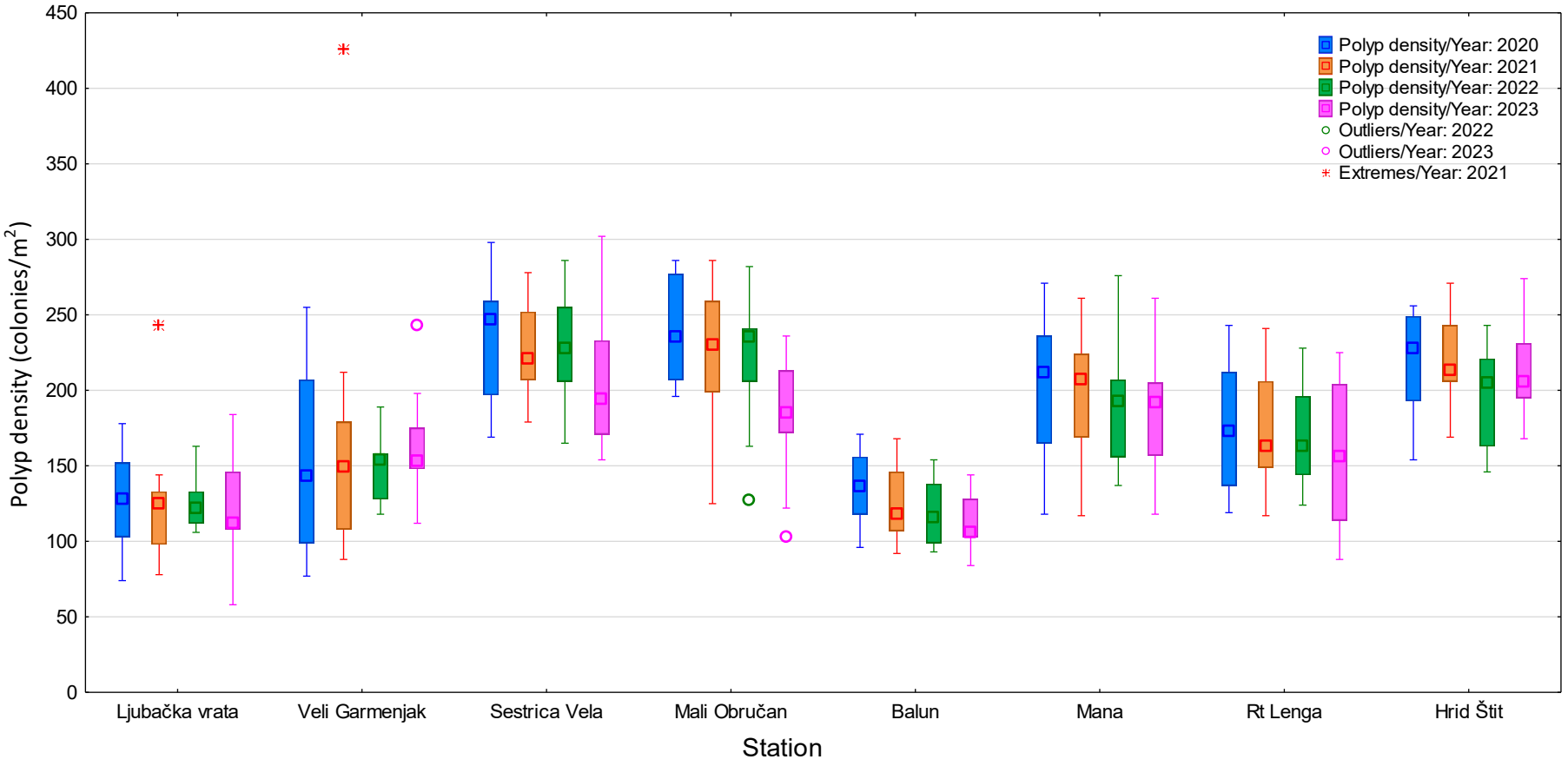

Figure 51. *Madracis pharensis* population density on stations Ljubačka vrata [KW-H(3;46) = 0.1641; p = 0.9832], Veli Garmenjak [KW-H(3;50) = 0.9662; p = 0.8094], Sestrica Vela [F(3;46) = 1.1835; p = 0.3264], Mali Obručan [F(3;46) = 4.7204; p = 0.0059], Balun [F(3;46) = 2.079; p = 0.1160], Mana [F(3;46) = 0.4902; p = 0.6908], Lenga [F(3;46) = 0.6964; p = 0.5590], Hrid [F(3;46) = 1.6875; p = 0.1828] across period 2020 – 2023.

Mortality rates of *Madracis pharensis* showed pronounced interannual variability across all observed stations between 2020 and 2023, with a consistent increasing trend throughout the study period (Figure 52). Across all sites, mortality rates were lowest in 2020 and reached their highest values in 2023. The lowest mortality during the study period was recorded at Paški most in 2020 (6%), while the highest was observed at Hrid Štit in 2023 (36%).

At Paški most, mortality remained low in 2020 (6%) and 2021 (6%) but increased markedly in subsequent years, reaching 12% in 2022 and 19% in 2023 (Figure 52). A similar pattern was observed at Veli Garmenjak, where mortality increased steadily from 9% in 2020 to 21% in 2023. At Sestrica Vela, mortality rose from 8% in 2020 to 26% in 2023, indicating a pronounced deterioration in colony survival over time.

Within Kornati National Park, mortality rates were consistently high and increased across all stations. At Mali Obručan, mortality rose from 12% in 2020 to 34% in 2023. Balun exhibited one of the steepest increases, from 15% in 2020 to 32% in 2023. At Mana, mortality increased from 10% in 2020 to 28% in 2023, reflecting substantial cumulative colony loss (Figure 52).

At the southern stations, elevated mortality rates were observed throughout the study period. At Rt Lenga, mortality increased from 14% in 2020 to 29% in 2023, while Hrid Štit exhibited the most severe mortality overall, rising from 18% in 2020 to 36% in 2023 (Figure 52).

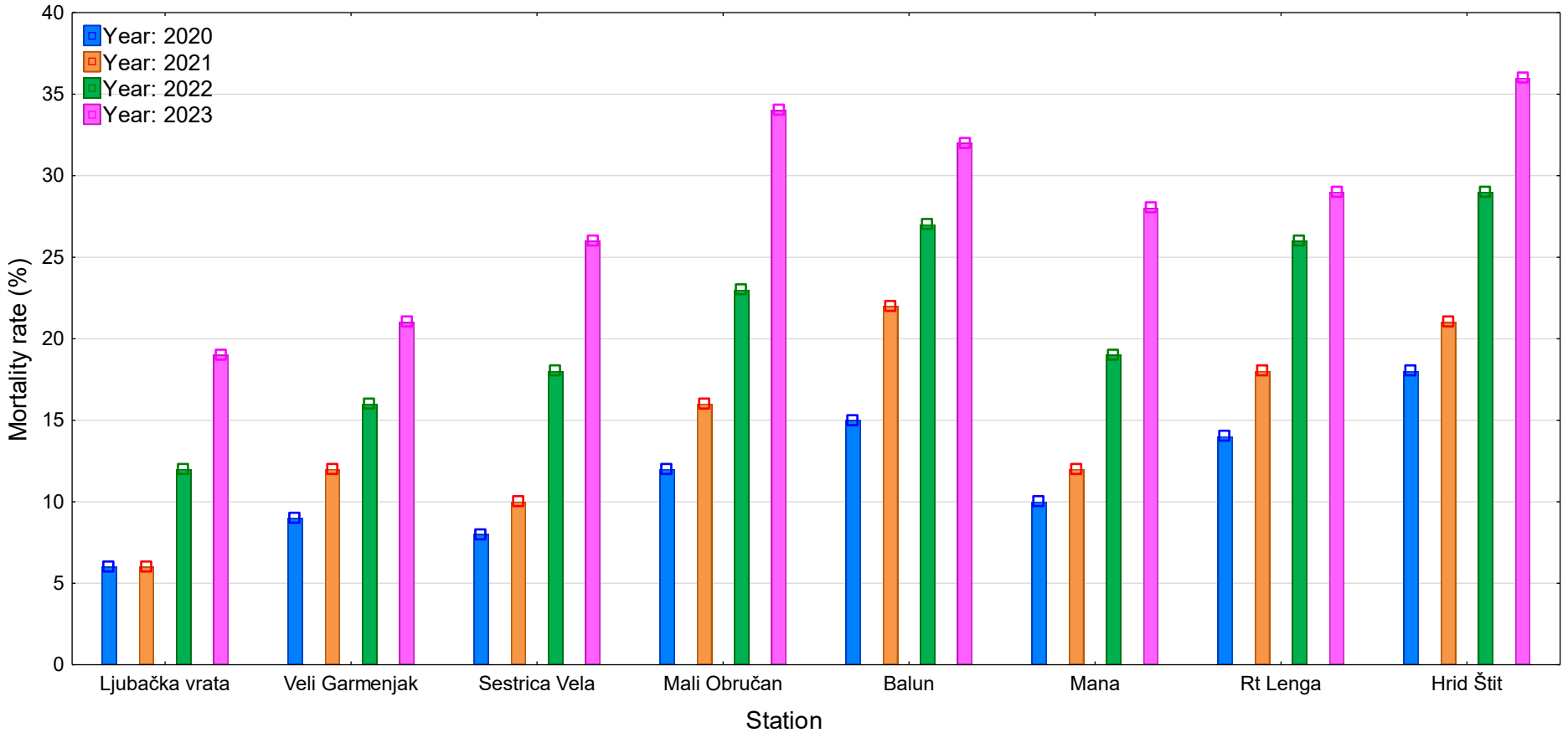

Figure 52. Mortality rate of *Madracis pharensis* on stations: Ljubačka vrata, Veli Garmenjak, Sestrica Vela, Mali Obručan, Balun, Mana, Lenga and Štit across period 2020 – 2023.

Bleaching rates also displayed marked interannual variability between 2020 and 2023, generally increasing over time with peak values recorded in the later years of the study period (Figure 53). Bleaching was lowest in 2020 at Paški most, where it remained absent (0%), while the highest bleaching rate was observed at Balun in 2023 (40%).

At Paški most, bleaching was absent in both 2020 and 2022 but increased slightly to 2% in 2021 and 7% in 2023. At Veli Garmenjak, bleaching increased from 16% in 2020 to 33% in 2023, with a steady rise over time. At Sestrica Vela, bleaching rose from 23% in 2020 to 33% in 2023, with remaining consistently high from 2021 onwards (Figure 53).

Within Kornati National Park, bleaching rates were elevated across all stations. At Mali Obručan, bleaching increased from 17% in 2020 to 37% in 2023. Balun showed a strong upward trend, from 26% in 2020 to 40% in 2023, representing the highest bleaching rate observed. At Mana, bleaching increased from 19% in 2020 to a peak of 29% in 2022, followed by a decrease to 19% in 2023 (Figure 53).

At the southern stations, bleaching rates remained high throughout the study period (Figure 53). At Rt Lenga, bleaching increased from 32% in 2020 to 31% in 2023, remaining consistently elevated despite interannual fluctuations. At Hrid Štit, bleaching peaked in 2021 (37%) and subsequently declined to 26% by 2023, indicating partial recovery following peak bleaching intensity.

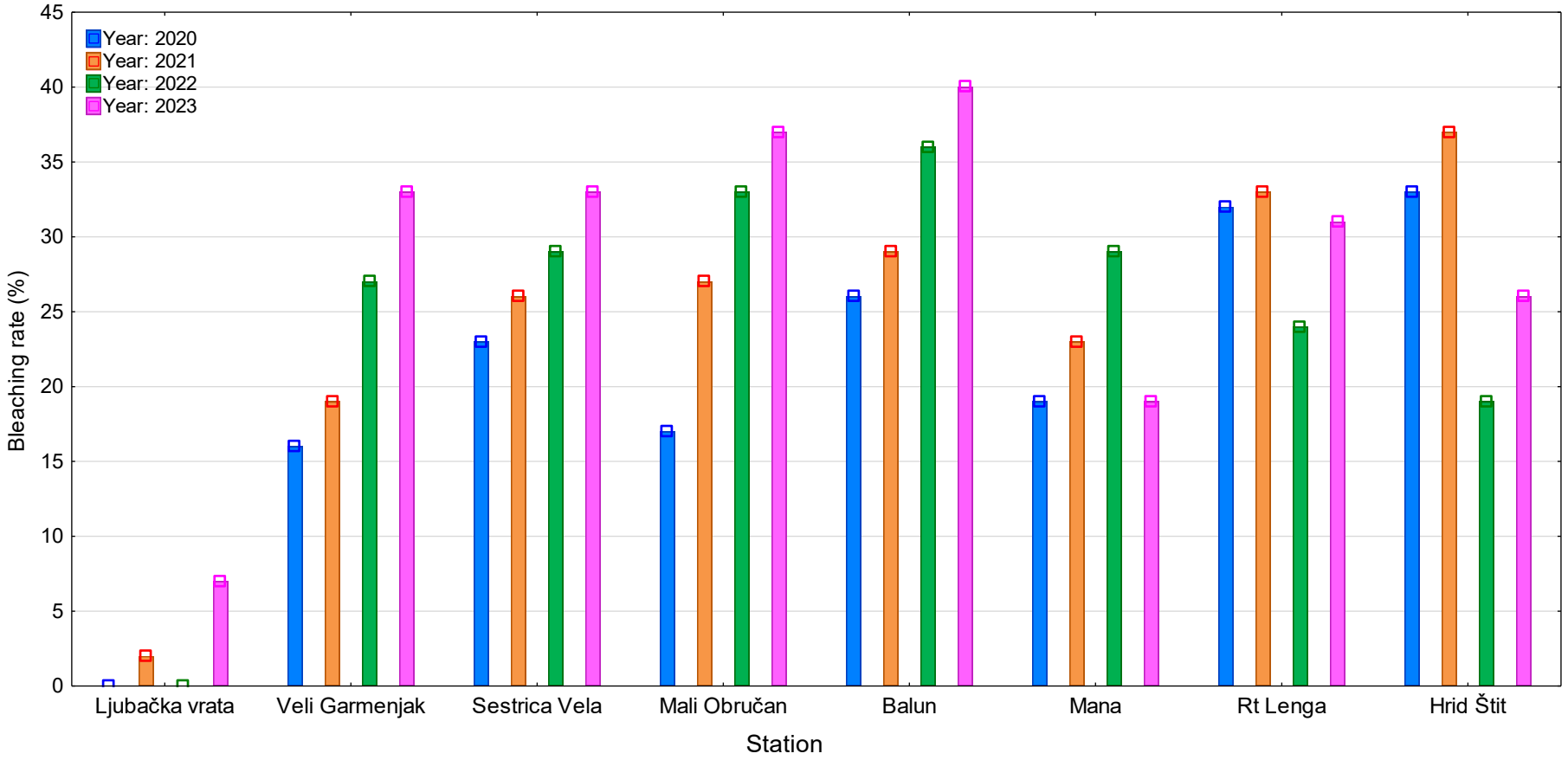

Figure 53. Bleaching rate of *Madracis pharensis* on stations: Ljubačka vrata, Veli Garmenjak, Sestrica Vela, Mali Obručan, Balun, Mana, Lenga and Štit across period 2020 – 2023.

4.6.3. Histological and histopathological description

Macroscopically, of 21 samples collected from NP Telašćica, NP Kornati and NP Mljet (Rt Lenga and Hrid Štit), 8 were considered healthy, 10 necrotic, and 3 were bleached samples. All collected samples were examined microscopically and 3 samples were confirmed as healthy tissue, while remaining 18 were reclassified as necrotic: 4 samples were categorised as light histopathology (general state code 1; <25% of tissues contained lesions), 11 samples as moderate histopathology (general state code 2; 25-75% of tissues contained lesions) while heavy histopathology were confirmed in 3 samples (general state code 3; >75% of tissues contained lesions).

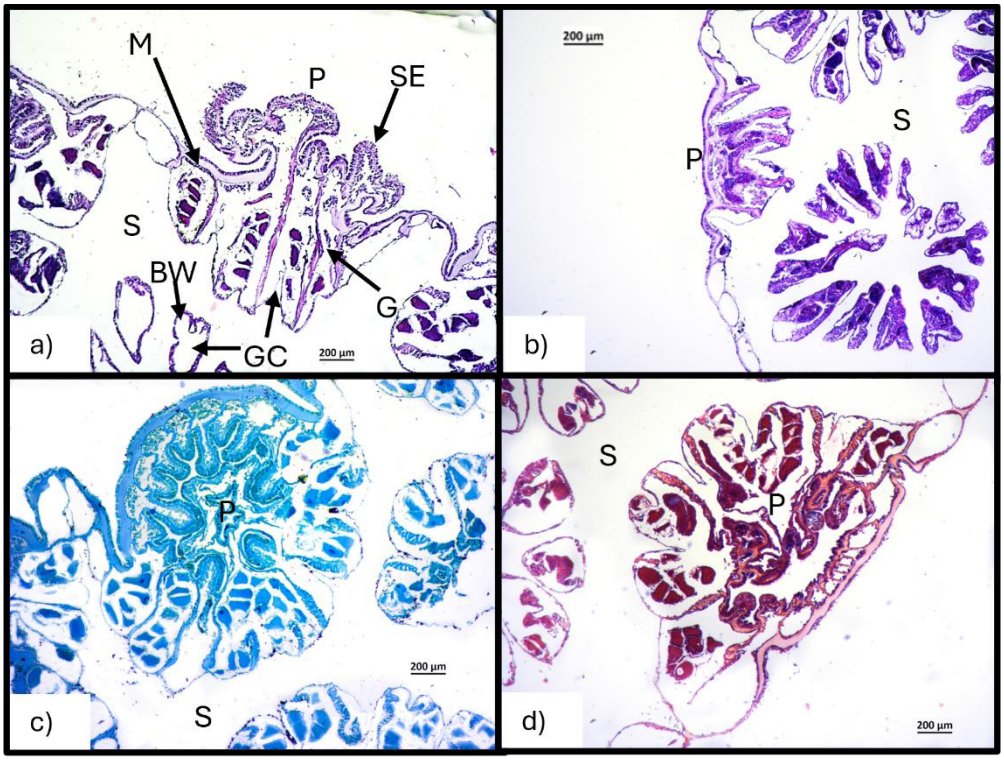

Figure 54. Histological sections of healthy extended (a) and retracted (b) polyps of *Madracis pharensis*, stained with (a–b) hematoxylin and eosin (H&E), (c) Grocott's methenamine silver stain, and (d) Gram stain. Sections reveal normal tissue organization and polyp (P) morphology, with visible structural elements including the surface epithelium (SE), mesoglea (M), gastrodermis (G), gastrovascular cavity (GC), basal body wall (BW), and skeletal space (S). Due to the spherical morphology of the colony, transverse sections provide cross-sectional views along multiple axes.

The histological architecture of a healthy *Madracis pharensis* polyp revealed a compact and highly organized microanatomy consistent with its colonial, small-polyp scleractinian structure (Figure 54). Each polyp was diminutive in size and structurally integrated into a dense coenosarc matrix, reflecting the species' obligatory colonial lifestyle. The polyp body comprised two principal epithelial layers: a thin outer epidermis and an inner gastrodermis, separated by a narrow, gelatinous mesoglea. The epidermis consisted of a monolayer of cuboidal to columnar epithelial cells interspersed with scattered mucocytes and cnidocytes harbouring small nematocysts. The mesoglea was homogeneous and acellular, closely associated with both epithelial layers, providing essential mechanical support and maintaining structural cohesion. The gastrodermis was densely populated with glandular and ciliated cells and housed symbiotic dinoflagellates (Symbiodiniaceae), visible as rounded cells with granular cytoplasm and occasionally prominent nuclei. Notably, each polyp contained ten distinct gastrovascular cavities, a defining anatomical trait of the species, corresponding to the decameric radial symmetry of the mesenteries. These endodermal mesenteries extended vertically into the central cavity and were involved in digestion, nutrient absorption, reproductive processes, and internal homeostasis. At the basal region, all tissue layers remained continuous and tightly interconnected, merging seamlessly into the coenosarc, which itself exhibited an organized arrangement of epithelial and connective components linking adjacent polyps. Gram staining demonstrated a sparse to moderate presence of bacteria, primarily localized to the superficial epidermal layer, with occasional colonization near the polyp-calyx interface.

Table 11. Specific histopathological lesions and patogens of *Madracis pharensis* and their frequency

Specific histopathological lesions	**Light lesion (state 1)**	**Freq (%)**	**Heavy lesion (state 2)**	**Freq (%)**
Bassal body wall epidermis - loss of integrity	11	34.4	3	9.4
Bassal body wall epidermis - hyperthropy	6	18.8	3	9.4
Surface epidermal coenenhyme - loss of integrity	7	21.9	6	18.8
Surface epidermal coenenhyme - increase in mucocytes	8	25.0	10	31.3
Surface epidermal coenenhyme - hyperthropy	4	12.5	10	31.3
Surface epidermis - loss of integrity	12	37.5	3	9.4
Surface epidermis - increase in mucocytes	11	34.4	7	21.9
Surfacel epidermis - hyperthropy	10	31.3	2	6.3
Surface epidermis - reduction	0	0.0	1	3.1
Mesoglea - swelling	5	15.6	11	34.4
Mesoglea - nude	11	34.4	6	18.8
Mesoglea - reduction	2	6.3	2	6.3
Gastrodermis necrotic zones	12	37.5	4	15.6
Gastrodermis reduction	4	12.5	5	15.6
Endosymbionts dark and shrunken	5	15.6	3	9.4
Endosymbionts reduction	2	6.3	9	28.1
Reduction of mesenterial filaments	0	0.0	1	3.1
Presence of ova/spermal cells	3	9.4	5	15.6
Patogens	**Light lesion (state 1)**	**Freq (%)**	**Heavy lesion (state 2)**	**Freq (%)**
Presence of Algae	0	0.0	0	0.0
Presence of Crustacea	0	0.0	0	0.0
Presence of Funghi	1	3.1	0	0.0
Presence of Porifera	2	6.3	0	0.0
Bacteria quantity bassal wall epidermis	0	0.0	0	0.0
Bacteria quantity surface wall epidermis	2	6.3	0	0.0
Bacteria quantity gastrodermis	0	0.0	0	0.0

Polyps of *Madracis pharensis* exhibiting macroscopically visible necrosis presented distinct histopathological lesions, predominantly affecting the surface body wall, while the basal tissue regions were less frequently and less severely involved. The surface body wall epidermis, which in *M. pharensis* forms a relatively thin but continuous layer over the dense skeletal surface, displayed several lesion types commonly associated with stress responses. The most prevalent alteration was an increase in mucocyte density, observed in 34% of polyps with mild lesions (Figure 55) and 22% of those with severe histopathology (Figure 56). This mucocyte

proliferation likely represents a defensive response, aiming to reinforce the mucus barrier under adverse conditions. Epidermal hypertrophy, interpreted as enlargement of individual epithelial cells, was recorded in 31% of mildly affected and 6% of severely affected polyps. Loss of surface epidermal integrity—characterized by epithelial disorganization, detachment from the mesoglea, and partial tissue collapse—was observed in 38% of mild and 9% of severe cases (Table 11). One case (3%) exhibited epidermal thinning, suggestive of advanced epithelial atrophy.

The coenenchymal epidermis, which envelops the intercorallite matrix and is morphologically less prominent than in other scleractinians due to the tightly packed corallite architecture in *Madracis*, exhibited frequent lesions. An increase in mucocytes and epithelial hypertrophy was observed in 25% and 13% of mildly affected polyps (Figure 55), respectively, while more pronounced changes were recorded in severely damaged tissues (31% in both lesion types) (Figure 56). Loss of integrity in this layer was detected in 22% of mild and 19% of severe lesions (Table 11).

The basal body wall epidermis—lining the lower polyp wall in contact with the calcareous skeleton—showed evidence of degeneration in multiple samples. Loss of basal epidermal integrity was recorded in 34% of mild and 9% of severe lesions, while hypertrophy was found in 19% and 9% of cases, respectively (Table 11). These changes likely reflect local stress exposure at the polyp-skeleton interface.

Mesogleal alterations were also prevalent and diverse. Swelling of the mesoglea, interpreted as expansion of the extracellular matrix and possible edematous change, was identified in 16% of mild (Figure 55) and 34% of severe lesions (Figure 56). Nude mesoglea—characterized by separation of the adjacent epithelial layers—was observed in 34% of mild and 19% of severe lesions (Table 11). Mesogleal reduction, likely indicating matrix degradation or collapse, was rare (6% in both mild and severe lesions).

Gastrodermal pathology was present in numerous specimens, particularly in the form of necrotic zones (38% of mild, 16% of severe cases), tissue reduction (13% mild, 16% severe), and endosymbiont abnormalities (Figure 55, Figure *56*). Symbiotic dinoflagellates appeared

darkened and shrunken in 16% of mild and 9% of severe lesions, while outright reduction in symbiont density was noted in 6% and 28% of mild and severe cases, respectively (Table 11). These findings are consistent with progressive loss of symbiotic function and photosynthetic capacity under stress.

Reduction of mesenterial filaments, although infrequent, was recorded in 3% of severely affected samples, suggesting possible functional impairment of the digestive system. Gametogenic activity was present in both mild (9%) and severe lesions (16%), indicating that reproductive structures may persist despite moderate to advanced tissue pathology.

Epibiotic organisms such as fungi and poriferans were occasionally observed in necrotic tissues (fungi in 3%, poriferans in 6% of mild lesions), likely representing secondary colonizers of exposed skeletal surfaces. Bacterial infiltration was limited; low bacterial loads were detected only in the surface epidermis (6% of mild cases), while the basal epidermis and gastrodermis appeared free of bacterial presence in all samples.

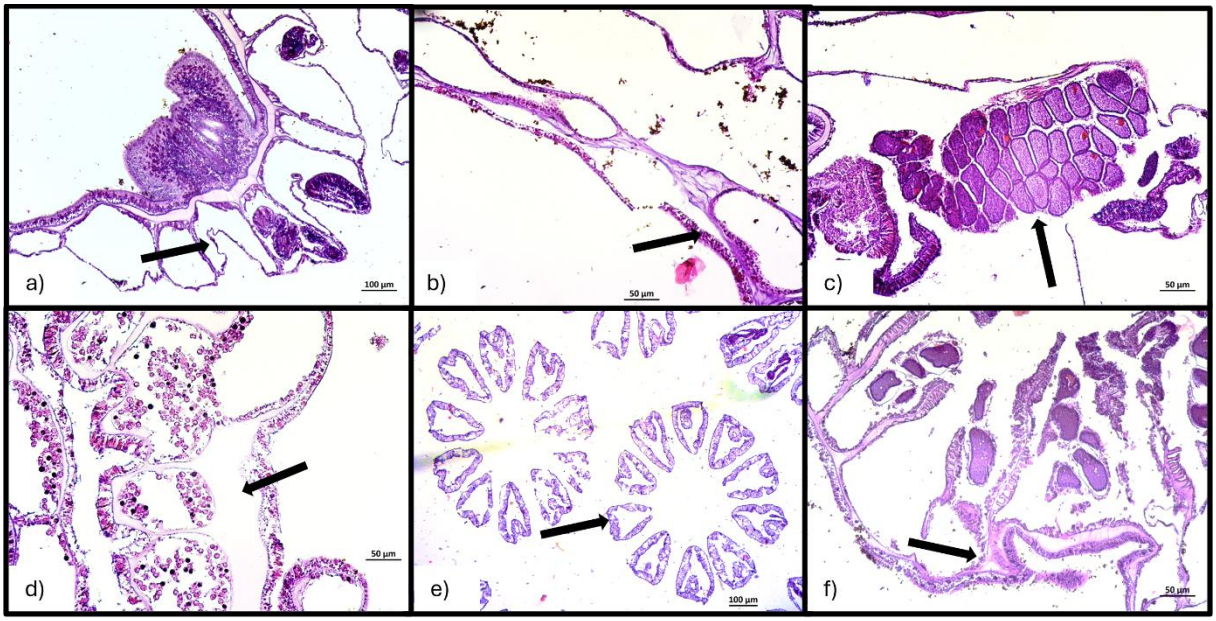

Figure 55. Histological cross sections of *Madracis pharensis* samples with identified light microscopic lesions (a-f) shows (a) loss of gastrodermal tissue and filaments, (b) nude mesoglea, (c) increase in oocyte production, (d) enlarged and swollen mesoglea, (e) reduction of gastodermic tissue in filaments, (f) structural disintegration and necrotic changes in gastrodermal and epithelial tissue. HE stain.

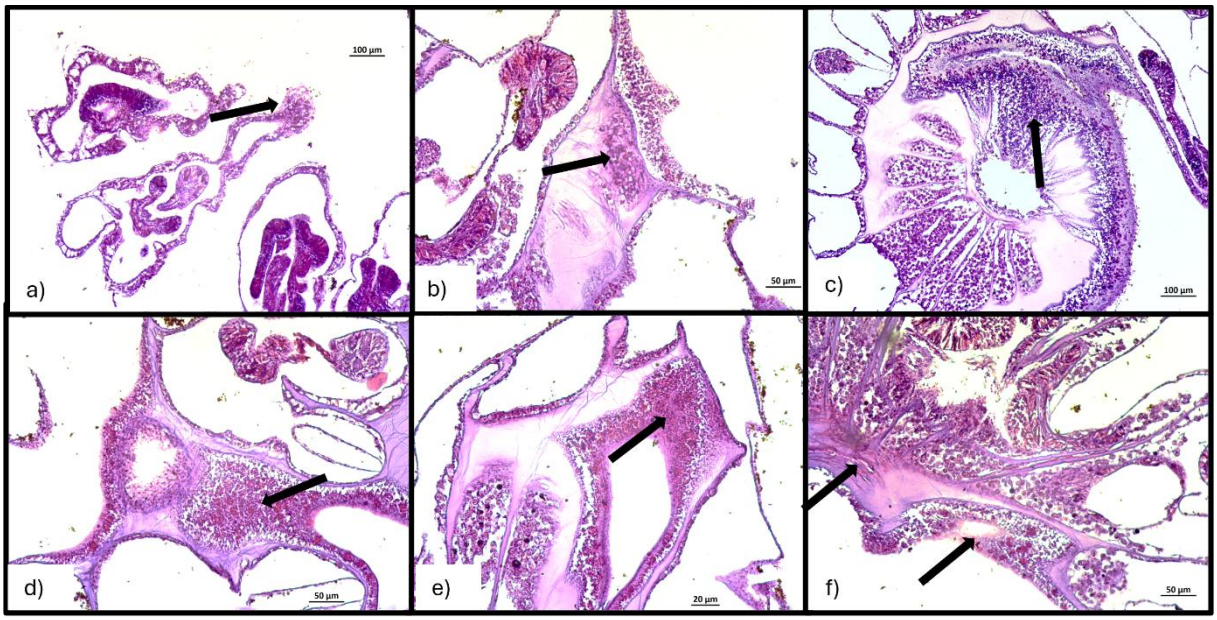

Figure 56. Histological cross sections of *Madracis pharensis* samples with identified heavy microscopic lesions (a-f) show (a) necrotic proliferations in basal epidermis, (b) swollen mesoglea with necrotic lesion, (c) mucocyte proliferation in surface epithelium and enlarged mesoglea, (d, e) distinct necrotic lesions in gastrodermis (f) and epidermis. HE stain.

4.7. Population status of *Eunicella cavolini*

4.7.1. External appearance and gross lesions

The colonial gorgonian coral *Eunicella cavolini* was recorded at depths between 20 and 40 m at Ljubačka vrata and at all stations within NP Telašćica and NP Kornati, inhabiting the lower infralittoral to the upper circalittoral zones. *E. cavolini* had a complex, fan-shaped morphology, characterized by a highly branched, planar or slightly three-dimensional structure. Its colonies typically reached heights of 10–50 cm, with axial branches displaying a sinuous growth pattern. All branches consisted of a central skeleton made of the protein gorgonin, covered by a coenenchyme that contained sclerites. The branches were cylindrical, with a diameter ranging from 1 to 3 mm. The transparent-coloured polyps, with fully expanded tentacles, were distributed along the branches in four rows, emerging from calyces that slightly protruded from the surface. The coloration of healthy *E. cavolini* varied from pale yellow to golden hues. The coral's base was enlarged, facilitating secure attachment to rocky substrates, and colonies often oriented their branches perpendicular to prevailing currents to optimize feeding efficiency and mitigate damage. Healthy colonies were characterized by intact branches, an absence of bleaching or discoloration, actively abundant, extended polyps regularly distributed across the colony surface, and no visible necrotic patches (Figure 57).

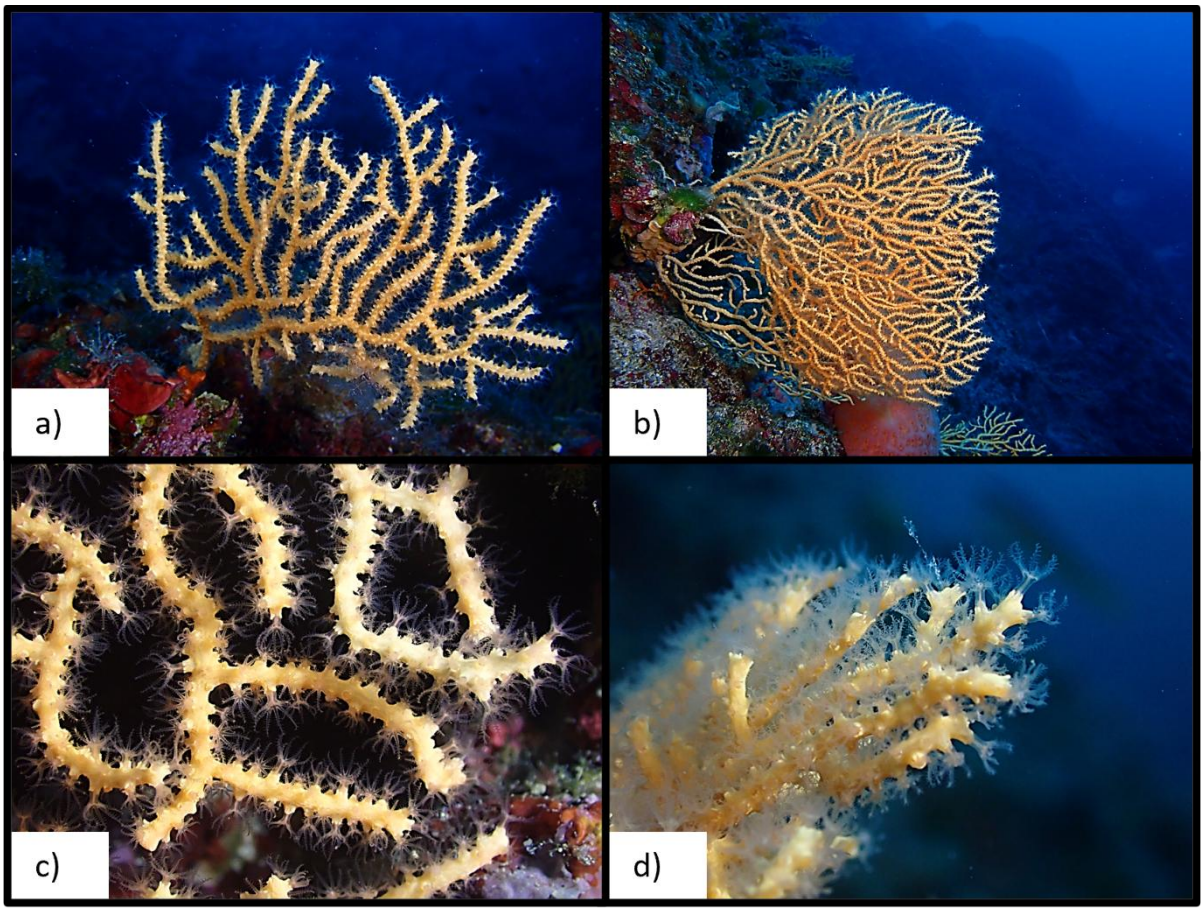

Figure 57. Macroscopic appearance of healthy *Eunicella cavolini* colonies at 30 m depth (Telašćica Nature Park) (a–d). (a–b) Overview of structurally intact colonies exhibiting full tissue coverage, uniform coloration, and no visible signs of necrosis or biofouling. (c–d) Close-up views of branch surfaces with expanded, evenly distributed polyps.

Field assessments revealed that *E. cavolini* exhibited distinct morphological and macroscopic alterations characterized by irregular, fragmented, or atrophic growth patterns (Figure 58). Initially, mild gross lesions of the coenenchyme began with discoloration ranging from localized paling to extensive darkening, primarily at the colony's periphery. The polyps appeared retracted or atrophied, significantly reducing the colony’s feeding capacity. As necrosis progressed, abrupt tissue loss of the coenenchyme and polyps predominantly occurred at the apical tips of branches, exposing the axial skeleton. In some cases, lesions also developed in the central median sections of the colony. The exposed skeleton varied in colour from bright white to brownish, and often appeared in circular to irregular patches with undulating margins, depending on the time elapsed since tissue degradation. In advanced stages, necrosis

manifested as progressive tissue sloughing, frequently accompanied by biofilm accumulation or opportunistic epibiont colonization. These lesions were often multifocally distributed, leading to a deterioration of the colony's structural integrity. The severity of tissue loss varied, with some colonies exhibiting only a few millimetres of affected tissue, while others experienced over 90% mortality. Even in colonies with extensive degradation, the surviving tissue often retained a macroscopically healthy appearance, preserving its characteristic yellow pigmentation and displaying fully extended polyps. The appearance of lesions varied over time, as recently exposed skeletal areas remained clean with minimal overgrowth, while older lesions became progressively colonized by various encrusting epibionts. In advanced cases, long-standing necrotic areas exhibited extensive biofouling, including mucilaginous algal layers, sponges, bryozoans, and filamentous cyanobacteria, indicating a transition from acute tissue loss to prolonged degradation. Our investigations during the collecting process revealed no indication of predators on the colonies or nearby areas that could account for this tissue loss.

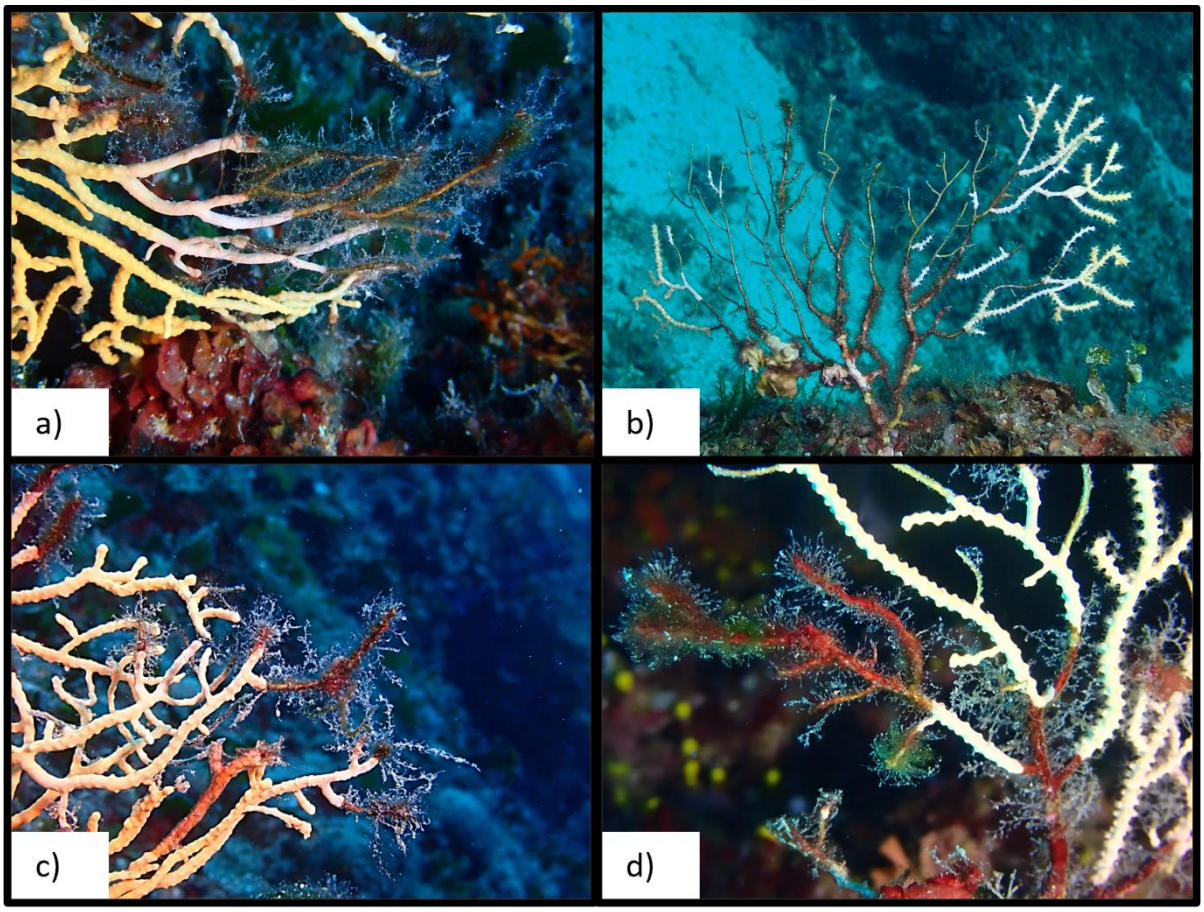

Figure 58. Macroscopic appearance of degraded *Eunicella cavolini* colonies at 30 m depth (Telašćica Nature Park) (a–d). (a) Colony exhibiting advanced-stage tissue loss with secondary colonization by epibiota. (b) Colony-wide view showing near-complete tissue loss and long-established epibiotic overgrowth in the basal region. (c) Discoloration of necrotic coenenchymal tissue, degraded polyps, and exposure of the underlying axial skeleton at the apical branches. (d) Localized tissue loss at the apical tip of a branch with evidence of recent colonization.

4.7.2. Polyp density and mortality rate assesment

Population density of *Eunicella cavolini* exhibited mostly decreasing trends across years and stations, though statistical analyses did not reveal significant interannual variability ($p > 0.05$). Shapiro-Wilk test confirmed that population density data followed a normal distribution across all stations and years ($p < 0.05$). Consequently, ANOVA was applied, but no significant differences were detected across time and stations ($p > 0.05$). The highest population density was observed at Veli Garmenjak in 2020, with a mean value of 4.08 ± 1.50 colony/m², while the lowest colony density was recorded at Mana in 2021, where the mean density reached 2.67 ± 1.07 colony/m² (Figure 59).

At Ljubačka vrata station, population density decreased from 3.62 ± 1.76 colony/m² in 2020 to 3.25 ± 1.42 colony/m² in 2021 (Figure 59).

Within Nature Park Telašćica, trends in population density varied across stations. At Veli Garmenjak station, population density decreased from 4.08 ± 1.50 colony/m² in 2020 to 3.17 ± 1.34 colony/m² in 2021. In contrast at Vela Sestrica station, population density increased from 2.92 ± 1.38 colony/m² in 2020 to 3.08 ± 1.00 colony/m² in 2021 (Figure 59).

Within National Park Kornati, trends in population density of *Eunicella cavolini* exhibited a notable decline across stations. At Mana, population density decreased from 3.00 ± 1.68 colony/m² in 2020 to 2.67 ± 1.07 colony/m² in 2021. At Balun, population density decreased from 3.92 ± 1.71 colony/m² in 2020 to 3.17 ± 1.64 colony/m² in 2021 over the same period. At Mali Obručan, population density decreased from 3.46 ± 1.51 colony/m² in 2020 to 3.08 ± 1.56 colony/m² in 2021 (Figure 59).

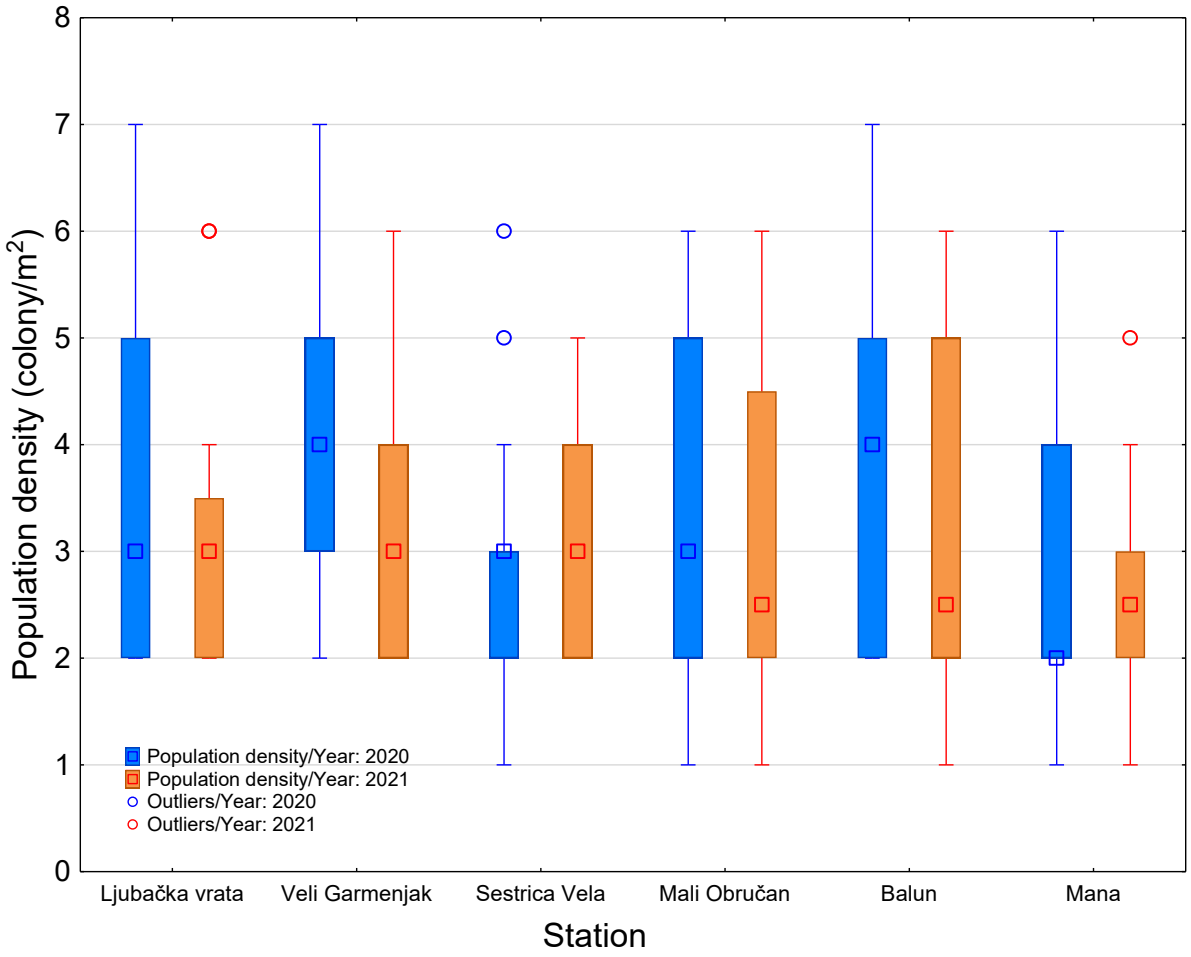

Figure 59. Population density of *Eunicella cavolini* on stations Ljubačka vrata ($F(1;23) = 0.323$; $p = 0.5753$), Veli Garmenjak ($F(1;23) = 2.5524$; $p = 0.1238$), Sestrica Vela ($F(1;23) = 0.1089$; $p = 0.7444$), Mali Obručan ($F(1;23) = 0.3791$; $p = 0.5441$), Balun ($F(1;23) = 1.2713$; $p = 0.2711$) and Mana ($F(1;23) = 0.3417$; $p = 0.5645$) across period 2020 – 2021

The mortality rate and colony degradation of *Eunicella cavolini* exhibited notable temporal variations across all monitored stations (Figure 60, Figure 61). The highest single-year mortality rate was recorded at Vela Sestrica station in 2022 (35.35 ± 5.33%), while the lowest was found at Veli Garmenjak station in 2020 (17.35 ± 3.82%). The maximum colony degradation percentage was documented at Veli Garmenjak station in 2023 (39.06 ± 12.36%), whereas the lowest was observed at Ljubačka vrata in 2020 (14.31 ± 3.22%). The mean mortality rate across the study locations was highest at Mali Obručan station (29.71 ± 6.65%), and lowest at Veli Garmenjak (21.13 ± 5.40%). Similarly, the mean colony degradation rate was highest at Veli Garmenjak (34.28 ± 10.08%), and lowest at Sestrica Vela (24.16 ± 7.61%). Normality tests

(Shapiro-Wilk test) confirmed that most datasets followed a normal distribution ($p > 0.05$), justifying the use of ANOVA for statistical comparisons. In cases where normality was not met, the Kruskal-Wallis test was applied.

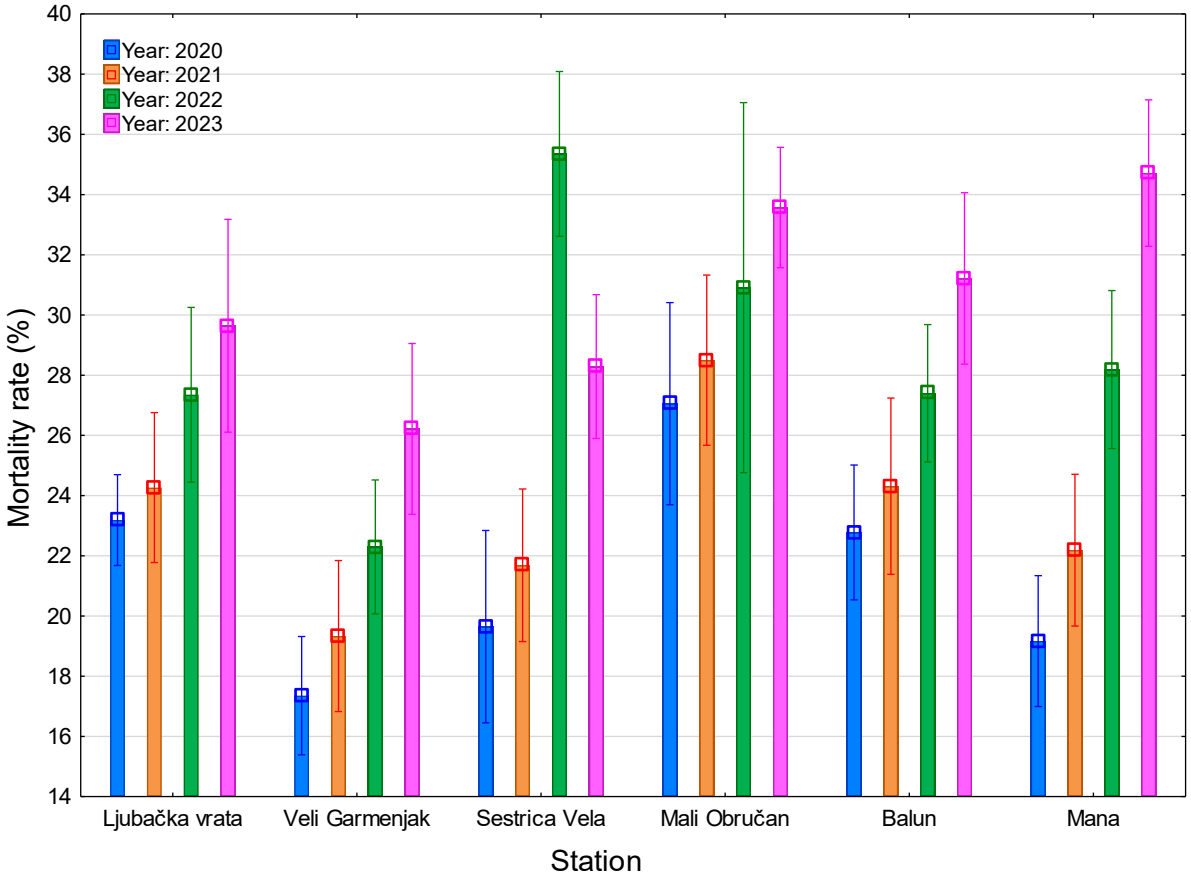

Figure 60. Mortality rate of *Eunicella cavolini* colonies on stations Ljubačka vrata [F(3;58) = 5.3617; **p = 0.0025**], Veli Garmenjak [F(3;59) = 11.7103; **p < 0.0001**], Sestrica Vela [KW-H(3;64) = 36.9348; **p < 0.0001**], Mali Obručan [F(3;55) = 3.1388; p = 0.0325], Balun [F(3;59) = 9.3238; **p = 0.00004**], Mana [F(3;60) = 35.0473; **p < 0.0001**] across period 2020 – 2023. Values in bold indicate statistically significant differences ($p < 0.05$).

At Ljubačka vrata station, mortality rates exhibited a minor increase, starting at 23.19 ± 2.83% in 2020 and rising to 29.64 ± 6.12% in 2023. The colony degradation rate increased from 14.31 ± 3.22% in 2020 to 36.19 ± 9.45% in 2023. The increase in both parameters was statistically significant (Mortality rate F (3;58) = 5.361, p = 0.002); Colony degradation rate F (3;55) = 25.854, p < 0.001).

In Nature Park Telašćica, distinct upward trends for mortality rates were recorded (Figure 60, Figure *61*). At Sestrica Vela station, mortality increased from 19.65 ± 6.21% in 2020 to 28.29 ± 4.14% in 2023, while colony degradation rate rose from 16.15 ± 4.04% in 2020 to 31.67 ± 6.61% in 2023. A statistically significant trend was observed in both parameters (Mortality rate KW – H (3;64) = 36.934, $p < 0.001$); Colony degradation rate $F(3;51) = 18.501$, $p < 0.001$). A similar trend was observed at Veli Garmenjak, where mortality rose from 17.35 ± 3.82% in 2020 to 26.21 ± 4.92%, also statistically significant ($F (3;59) = 11.710$, $p < 0.001$), while colony degradation rate nearly doubled, rising from 23.46 ± 6.13% in 2020 to 39.06 ± 12.36%, also confirming statistical significance ($F (3;56) = 9.754$, $p < 0.001$).

In Kornati National Park, mortality rates and colony degradation rates showed a consistent increase at all monitored stations (Figure 60, Figure *61*). At Mana, mortality rate values rose from 19.17 ± 4.37% in 2020 to 34.71 ± 4.21% in 2023, a statistically significant trend ($F (3;60) = 35.047$, $p < 0.001$). Similarly, Balun exhibited an increase in mortality rate from 22.78 ± 4.51% in 2020 to 31.21 ± 4.93% in 2023 ($F (3;59) = 9.324$, $p < 0.001$). At Mali Obručan, mortality increased from 27.06 ± 6.75% in 2020 to 33.57 ± 3.46% in 2023 ($F (3;55) = 3.139$, $p = 0.033$). At station Mana, the percentage of colony degradation rate climbed from 17.31 ± 5.12% in 2020 to 33.29 ± 7.62% in 2023, which was statistically significant ($F (3;56) = 14.927$, $p < 0.001$). The most dramatic change occurred at Balun, where colony degradation rate increased from 19.46 ± 4.48% in 2020 to 36.83 ± 10.61% in 2023, confirmed by ANOVA ($F (3;57) = 19.119$, $p < 0.001$). At Mali Obručan, colony degradation rate increased from 21.54 ± 5.81% in 2020 to 35.19 ± 8.04% in 2023, also reaching statistical significance ($F (3;55) = 7.026$, $p < 0.001$). Overall, these results indicate a general increase in both mortality and colony degradation rate of *Eunicella cavolini* across all stations, with confirmed statistical significance.

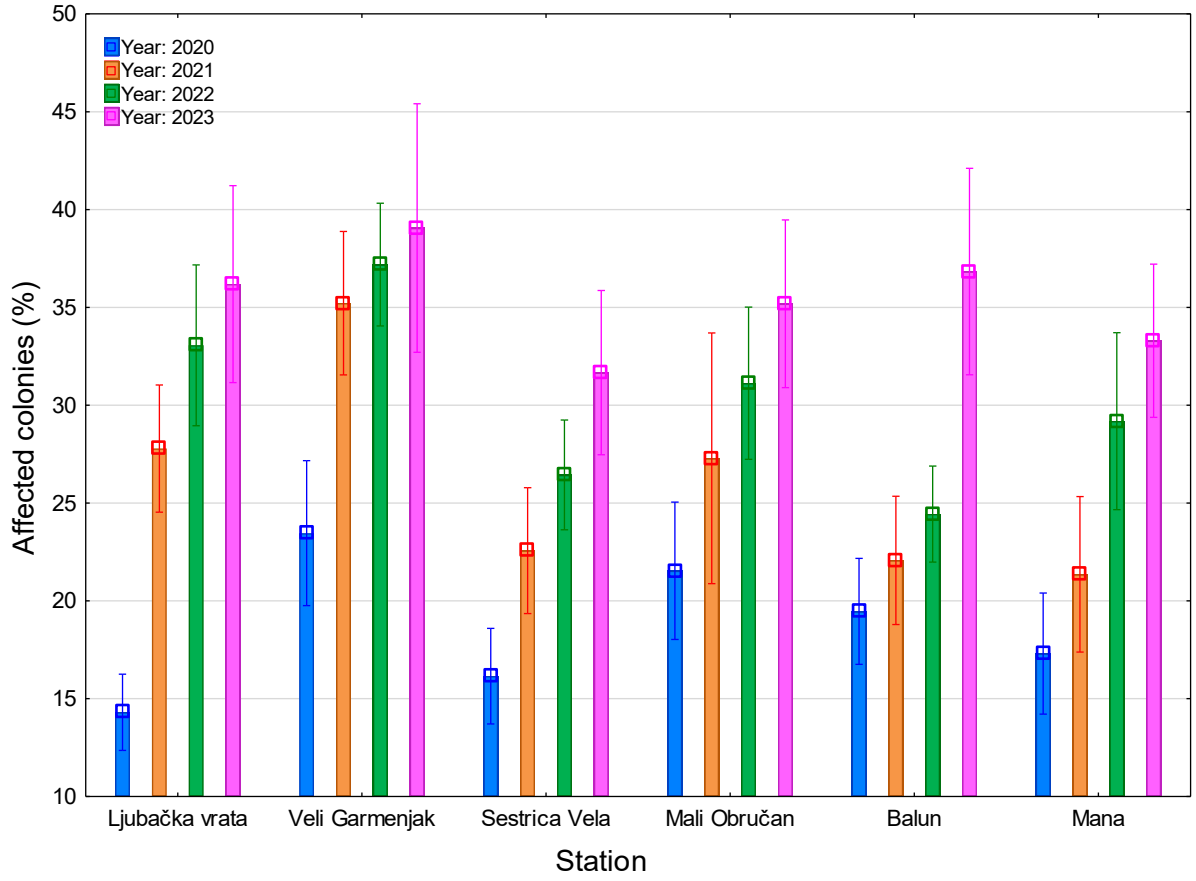

Figure 61. Colony degradation of *Eunicella cavolini* colonies on stations Ljubačka vrata [F(3;55) = 25.8541; **p < 0.0001**], Veli Garmenjak [F(3;56) = 9.7541; **p = 0.00003**], Sestrica Vela [F(3;51) = 18.5012; **p < 0.0001**], Mali Obručan [F(3;55) = 7.0264; **p = 0.0004**], Balun [F(3;57) = 19.1187; **p < 0.0001**], Mana [F(3;56) = 14.9266; **p < 0.0001**] across period 2020 – 2023. Values in bold indicate statistically significant differences (p < 0.05).

Moreover, colony damage in *Eunicella cavolini* was evaluated across all surveyed stations and categorised as minimal (<10%), moderate (10–90%), or severe (>90%).

At the Ljubačka vrata station, the percentage of colonies with less than 10% damage decreased from 38.4% in 2020 to 21.9% in 2023. Colonies with 10-99% damage showed an increasing trend, rising from 38.4% in 2020 to 48.4% in 2023. Significantly damaged colonies (more than 90%) recorded a slight increase from 23.2% in 2020 to 29.7% in 2023, indicating a gradual deterioration of colony conditions at this station (Figure 62).

The percentage of colonies with minimal damage (less than 10%) at the Garmenjak Veli station declined from 43.5% in 2020 to 28.3% in 2023. Moderately damaged colonies (10-99%)

increased from 39.1% to 45.5% over the same period. Significantly damaged colonies (more than 90%) showed a marked increase from 17.4% in 2020 to 26.2% in 2023, suggesting a significant worsening of colony conditions at the Garmenjak station (Figure 62).

At the Sestrica Vela station, we observed fluctuations in trends (Figure 62). The percentage of minimally damaged colonies varied, dropping from 53.0% in 2020 to 26.1% in 2022, then slightly increasing to 33.7% in 2023. Moderately damaged colonies show an increasing trend from 27.3% in 2020 to 38.0% in 2023. Significantly damaged colonies recorded a marked increase from 19.7% in 2020 to 35.4% in 2022, followed by a decrease to 28.3% in 2023.

At the Mali Obručan station, the percentage of minimally damaged colonies decreased from 50.1% in 2020 to 27.3% in 2023. Moderately damaged colonies recorded a significant increase from 22.8% in 2020 to 39.1% in 2023. Significantly damaged colonies showed a gradual increase from 27.1% in 2020 to 33.6% in 2023 (Figure 62). These data indicate a gradual deterioration of colony conditions at this station.

At the Balun station, the percentage of minimally damaged colonies decreased from 42.9% in 2020 to 23.4% in 2023. Moderately damaged colonies increased from 34.3% to 45.4% over the same period. Significantly damaged colonies showed a gradual increase from 22.8% in 2020 to 31.2% in 2023 (Figure 62), indicating a continuous deterioration of colony conditions at this station.

The Mana station shows the most pronounced deterioration trends (Figure 62). The percentage of minimally damaged colonies drastically decreased from 38.2% in 2020 to only 13.5% in 2023. Moderately damaged colonies recorded a significant increase from 42.6% to 51.8% over the same period. Significantly damaged colonies showed a marked increase from 19.2% in 2020 to 34.7% in 2023. These data indicate a dramatic worsening of colony conditions at the Mana station.

All observed stations show a trend of increasing coral colony damage over the four-year observation period, with the most pronounced deterioration at the Mana station.

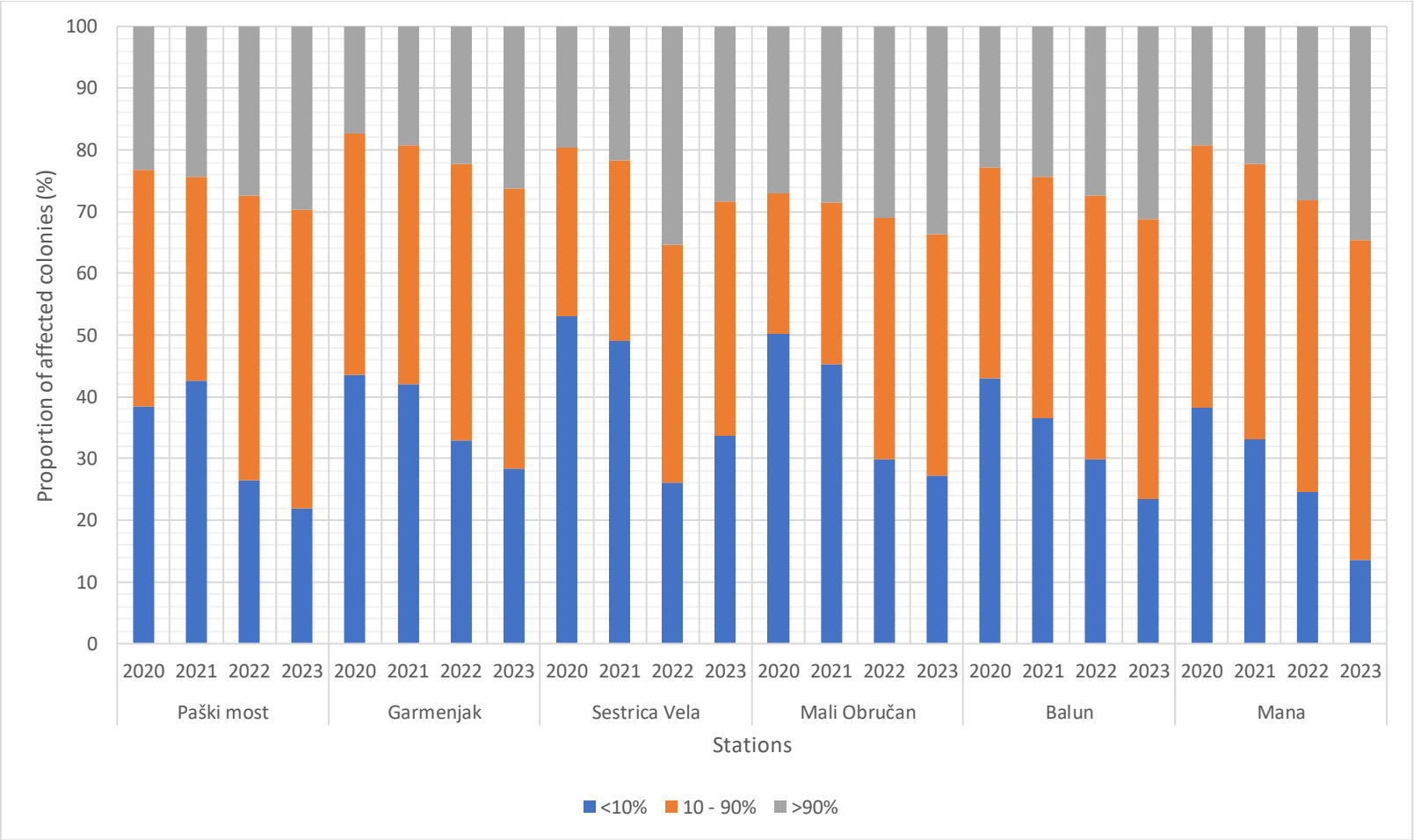

Figure 62. Proportion of affected *Eunicella cavolini* colonies during the period 2020 – 2023. Stacked bar charts show the proportion of affected colonies per year, with blue indicating <10% affected colonies (low impact), orange indicating 10–90% affected colonies (moderate impact), and grey indicating severe impact (>90% affected colonies).

4.7.3. Histological and histopathological description

Microscopic examination of healthy *E. cavolini* showed the presence of an intact axis (composed of gorgonin) and healthy polyps connected with the mesogleal matrix with solenia and empty lacunae without sclerites (as a result of the decalcification procedure) (Figure 63). The polyps are mainly cylindrical in shape, with the aboral part attached to the coenenchyme, and the oral disc with tentacles in contact with the marine environment. Tentacles are composed of an outer ectodermal layer, a gelatinous mesoglea layer, and an inner gastrodermal layer. Mesenteries within the polyp are lined with muscular epithelial cells, and gastrodermis and carry gonads. The gastrodermal layer forms the interior structures of the colony, and the epidermis appears on the external side of the colony, with the mesoglea located between the two cell layers.

When samples were visually macroscopically assessed from 14 collected samples, 8 were considered healthy and 6 were necrotic samples. After microscopic examination of histological slides from every sample, no completely healthy sample suitable as a control was found, hence all 14 were reclassified as necrotic. Within those 14 samples, 8 were categorised as light histopathology (general state code 1; <25% of tissues contained lesions), moderate histopathology (general state code 2; 25-75% of tissues contained lesions) was determined in 4 samples, while heavy histopathology (general state code 3; >75% of tissues contained lesions) was recorded in 2 analysed samples. Similarly to *P. clavata*, this is likely due to macroscopical field sampling bias, and avoiding sampling parts of the colonies which appeared dead/ without living tissue.

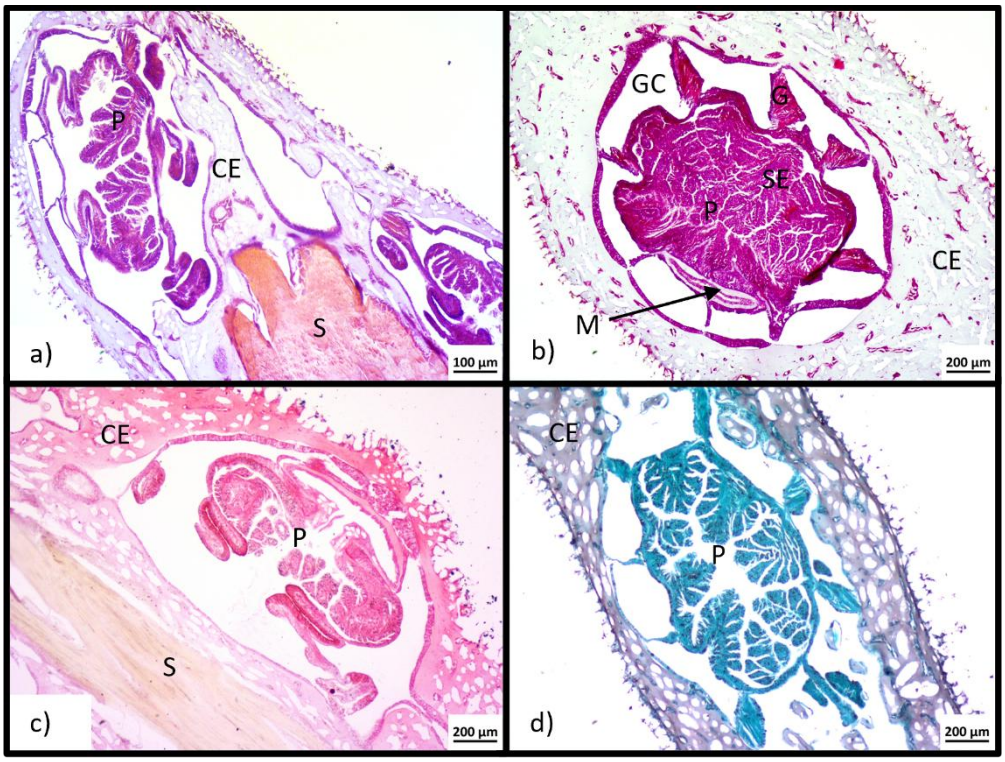

Figure 63. Histological sections of a healthy branch of *Eunicella cavolini*, stained with (a) Hematoxylin and eosin, (b-c) Gram and (c) Grocott's methenamine silver stain. Normal architecture of the coenenchyme (CE) is visible, along with the axial skeleton (S) and characteristic cellular organization of polyps (P), which appear in cross-section (b, d) due to their perpendicular orientation to the branch axis. Visible structures include the gastrodermis (G), gastrovascular cavity (GC), mesoglea (M), and surface epithelium (SE).

Table 12. Specific histopathological lesions of *Eunicella cavolini* and their frequency

Specific histopathological lesions	Light lesion (state 1)	Freq (%)	Heavy lesion (state 2)	Freq (%)
Coenenchyme epidermis necrosis	12	85.7	1	7.1
Polyp necrosis	7	50.0	5	35.7
Endosymbionts dark and shrunken	2	14.3	1	7.1
Tissue loss in mesoglea	8	57.1	6	42.9
Eosinophilic amoebocytosis in mesoglea	10	71.4	4	28.6
Gastrodermal disociation and /or hyperthrophy	5	35.7	9	64.3
Gastrodermis necrosis - foamy cells	10	71.4	4	28.6
Axis – changes in colour – violet cells	7	50.0	1	7.1
Melanin deposition in/near axis	8	57.1	4	28.6
Changes in axis stucture and rigidity	9	64.3	1	7.1
Eggs in polyps present	4	28.6	0	0.0
Red bacteria present	1	7.1	0	0.0
Blue bacteria present	0	0.0	1	7.1
Algae in the axis	3	21.4	0	0.0
Cyanobacteria in the axis	1	7.1	0	0.0
Diatoms along the axis	1	7.1	0	0.0

The most common lesions present in all samples were inflammatory lesions represented by the presence of granular amoebocytes in the mesoglea, significant gastrodermal necrosis and mesogleal tissue loss (Figure 64). Eosinophilic granular amoebocytes infiltrating the mesoglea were visible in mesogleal cell cords, with granules in the cytoplasm staining intensely and of different sizes. When heavy lesions were present, the number of amoebocytes increased (29% of samples). The gastrodermis of *E. cavolini* contained several cell types, including some cells with phagocytic vesicles and acidophilic cells with red granules in the cytoplasm. In light lesions, the gastrodermal layer showed loss of structure and dissociation (in 36% of samples), while in heavy lesions (64% of samples) gastrodermal cells were completely dissociated, changed their appearance into foamy cells, with a change in colour to yellow-light brown (Table 12). Unexplained tissue loss, with no evidence of predation or a clear cause, was evident in the coenenchyme mesoglea, the connective tissue between the polyps. While the light lesion,

present in 53% of samples, was visible as a small holes in mesoglea, in heavy lesions, mesoglea was seriously reduced, while gastrovascular canals and solenia expanded in size, in 47% of samples (Table 12). Coenenchyme epidermis necrosis was recorded in almost all samples (93%), showing discontinuity in epidermis and necrotic tissue fragments (Figure 64).

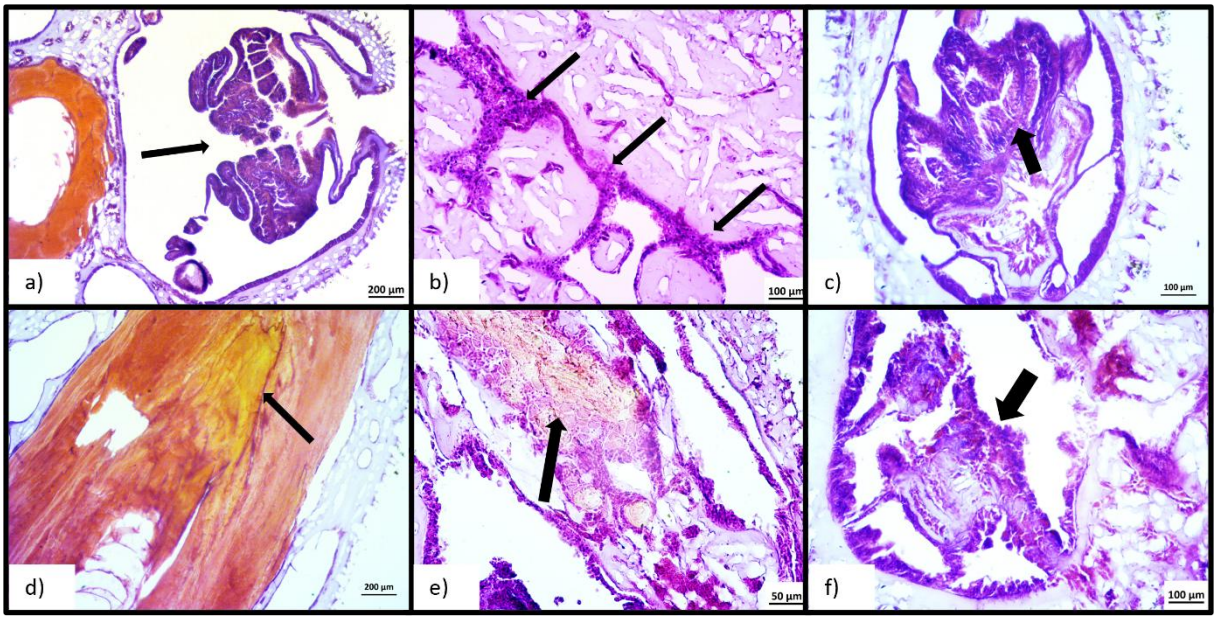

Figure 64. Histological longitudinal sections of *Eunicella cavolini* samples showing light (a–c) and heavy (d–f) microscopic lesions. Light lesions include (a) structural changes in the polyp, (b) increased numbers of granular amoebocytes within the mesoglea accompanied by an inflammatory response, and (c) necrotic changes in the gastrodermis. Heavy lesions include (d) melanin deposition between axial layers, (e) necrotic areas in the mesoglea of the coenenchyme filled with eosinophilic and basophilic granular cells, and (f) gastrodermal necrosis with structural disintegration of the polyp. Hematoxylin and eosin (H&E) stain.

Polyp tissues were also affected, with gastrodermal and epidermal cells in the tentacles and digestive system losing cohesion, often to the point that polyp structures such as the actinopharynx and tentacles could no longer be distinguished. In 3 samples, Symbiodiniaceae in the polyps appeared darker and shrunken.

The H&E stain identified melanin as a yellow band within or along the axis (Figure 65). Melanisation in the axis was a quite frequent immune response, recorded in 12 samples, with 57% of samples indicating light lesions and 29% heavy lesions (Table 12). In most cases, thick deposits of melanin were visible along areas of the axial skeleton, particulary in 3 samples

invaded by parasite. On the contrary, healthy segments of colonies did not contain melanin layers in the axes or mesoglea. Two other types of lesions visible in the axial skeleton were small multifocal changes in colour (from red to violet, in 8 samples) and changes in the structure which became loosely organised (in 10 samples) (Figure 65), which consequently led to fragility in one heavy lesion. Penetration of pathogen (arrowheads) was visible in four samples within the axial centre, possibly leading or enhancing axis necrosis. Algae were most frequently recorded, in 3 samples, while cyanobacteria and diatoms were only recorded once (Table 12). In the remaining 10 samples, no pathogens were noted on histological sections, suggesting that the disease was either caused by a non-infectious agent or that the infectious agent is not evident on light microscopy, while a higher resolution technique could possibly identify the pathogen.

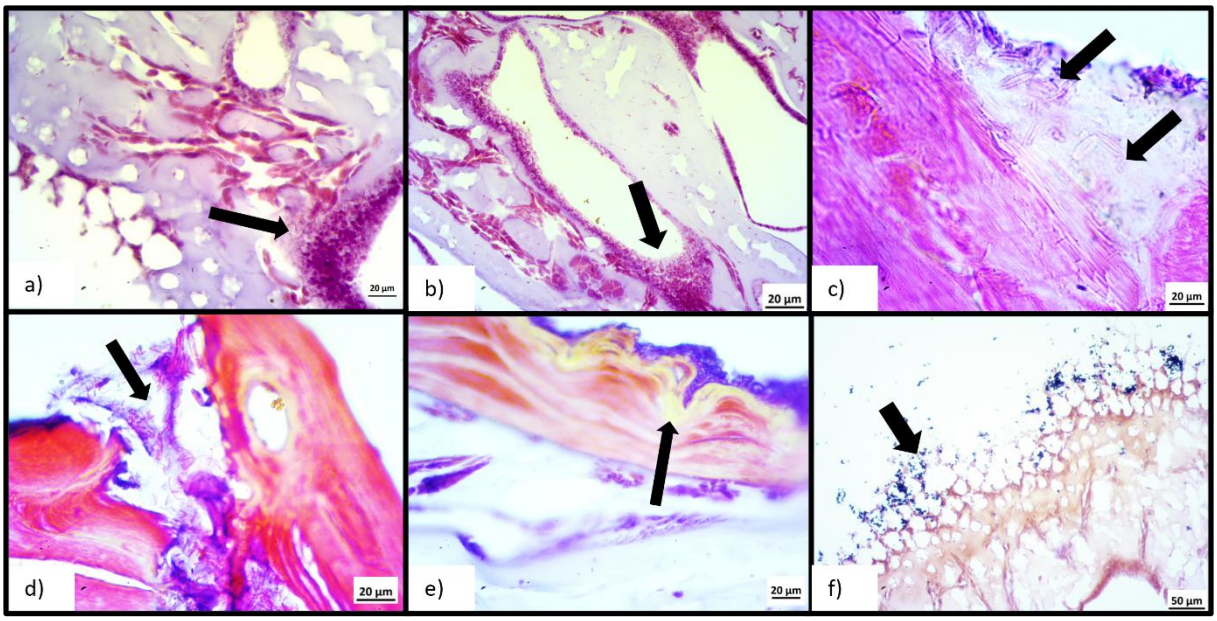

Figure 65. Histological sections of *Eunicella cavolini* samples showing frequent axis-associated histopathological lesions. Observed alterations include (a) increase of granular amoebocyte in the mesoglea with inflammatory response, (b) gastrodermal necrosis within the solenia, (c) presence of diatoms along the axial skeleton, (d) cyanobacteria located inside the skeletal axis, (e) algae delimited by melanization along the axis surface and (f) bacteria present on the surface of the coenenchyme. HE stain (a-e), Gram stain (f).

4.8. Population status of *Paramuricea clavata*

4.8.1. External appearance and gross lesions

Paramuricea clavata at all studied locations within NP Telašćica and NP Kornati was characterized by large, solid, densely branched colonies up to 1 m height, red or red-yellow in colour. It had a fan-shaped structure with numerous smaller, irregular branches that are arranged in a single plane. The central skeleton, made of the protein gorgonin, is located inside all branches, while the living, organic and shared tissue of the colony (coenenchyme) covers the skeleton and connects the polyps. The red polyps located on the branches consists of a calyx that supports eight tentacles, symmetrically arranged in a circular pattern around the central mouth. Healthy colonies exhibited well-developed, intact branched structures with uniform pigmentation, and their polyps were fully extended and regularly distributed across the colony surface, with no noticeable necrotic regions (Figure 66).

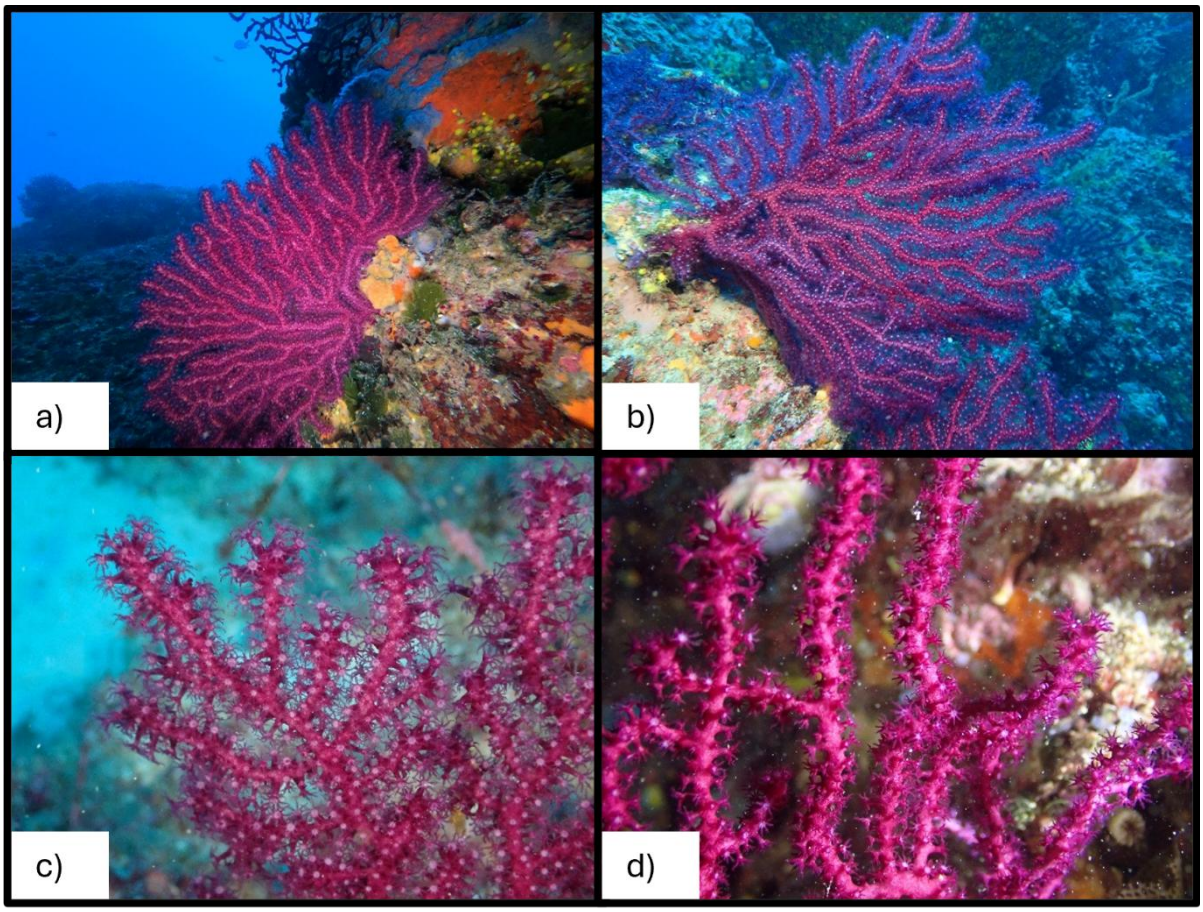

Figure 66. Macroscopic appearance of healthy *Paramuricea clavata* colonies at 40 m depth (Kornati National Park) (a–b) Overview of structurally intact colonies exhibiting full tissue coverage with no visible signs of discoloration and necrosis. (c–d) Close-up views of branch surfaces with fully expanded, regularly distributed polyps.

In contrast, affected colonies displayed a spectrum of gross lesions ranging from mild discoloration in localized areas of the coenenchyma to severe tissue loss affecting significant portions of the colony (Figure 67). Abrupt tissue loss of the coenenchyme and polyps predominantly occurred at the apical tips of branches, exposing the axial skeleton, though in some cases, lesions were also observed in the central median sections of the colony. The exposed skeleton varied in colour from bright white to brownish, depending on the time elapsed since tissue degradation. The extent of tissue loss ranged from a few millimetres of affected tissue to colonies experiencing over 90% tissue mortality. Notably, even in colonies with extensive tissue loss, the remaining living tissue often appeared macroscopically healthy, maintaining its characteristic deep red pigmentation and displaying extended polyps. The nature and degree of epibiont colonization on the denuded skeleton could provide insight into

the relative timing of tissue loss. Recently exposed skeletal areas appeared clean and white, with little to no overgrowth, sometimes colonized by hydrozoan species. In contrast, older lesions exhibited colonization by calcareous algae, bryozoans, and other encrusting epibionts. Some colonies displayed advanced, extensive tissue loss, characterized by substantial biofouling, including thick mucilaginous algal layers, sponges, larger sessile invertebrates, and filamentous cyanobacteria. These findings suggest a progression from acute tissue loss to long-term degradation, with biofouling communities establishing over time in necrotic areas. Our investigations during the collecting process revealed no indication of predators on the colonies or nearby areas that could account for this tissue loss.

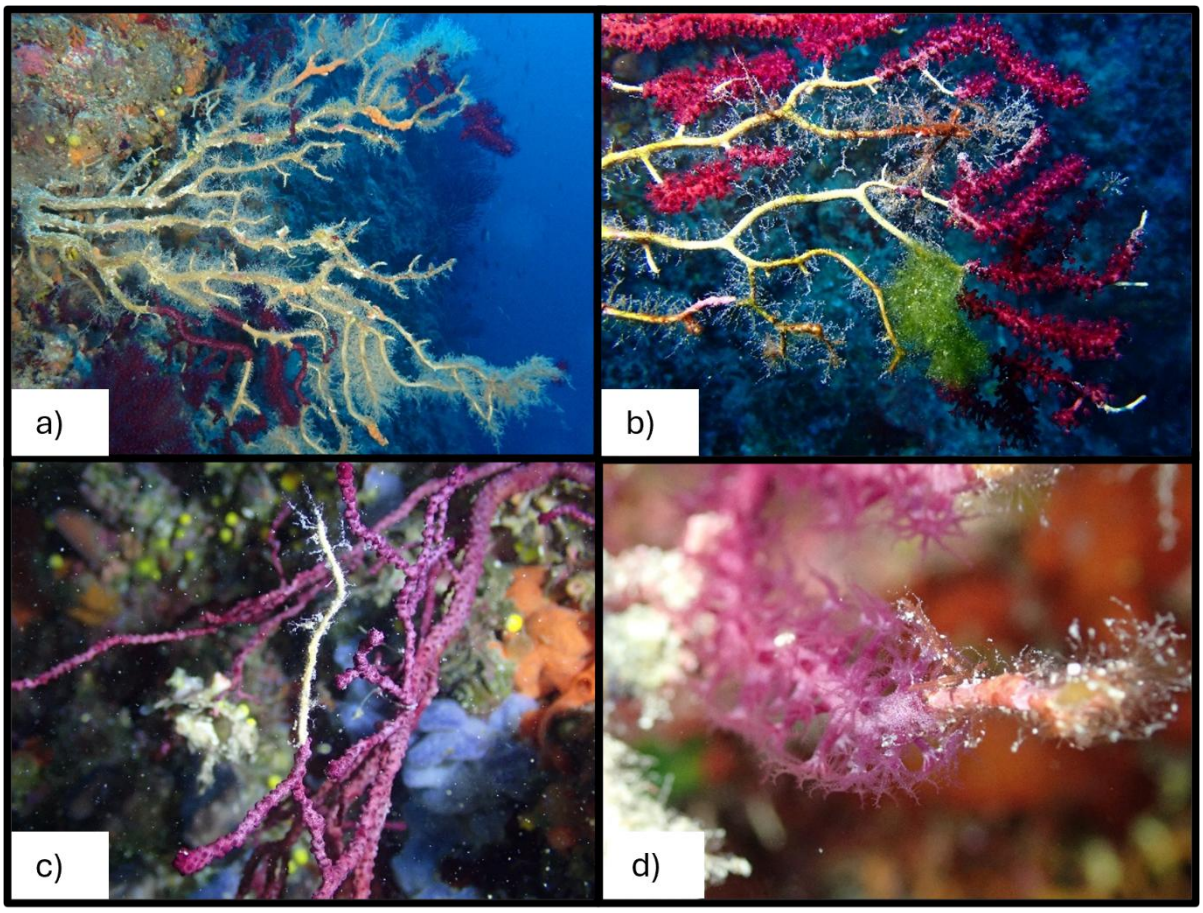

Figure 67. Macroscopic appearance of degraded *Paramuricea clavata* colonies at 40 m depth (Kornati National Park) (a–d). (a) Overview of a colony exhibiting near-complete tissue loss and long-established epibiotic overgrowth. (b) Section of the colony showing extensive tissue loss, with parts covered by mature epibiota and others still displaying limited recent colonization. (c–d) Close-up views of the apical branch tips with exposed axial skeleton, indicative of recent tissue detachment.

4.8.2. Polyp density and mortality rate assessment

Population density of *Paramuricea clavata* exhibited mostly decreasing trends across years and stations, though statistical analyses did not reveal significant interannual variability ($p > 0.05$). The highest population density was observed at Mana in 2020, with a mean value of 5.78 ± 1.92 colony/m², while the lowest colony density was recorded at Mali Obručan in 2020, where the mean density reached 2.78 ± 1.09 colony/m² (Figure 68). Shapiro-Wilk test confirmed that population density data followed a normal distribution across all stations and years ($p < 0.05$). Consequently, ANOVA was applied but detected no significant differences over time and stations ($p > 0.05$).

At Sestrica Vela station, Nature Park Telašćica, population density remained relatively stable, with 3.78 ± 1.64 colony/m² in 2020 and 3.75 ± 1.54 colony/m² in 2021 (Figure 68).

Within Kornati National Park, at Balun station, population density decreased from 5.33 ± 1.32 colony/m² in 2020 to 4.33 ± 1.37 colony/m² in 2021 (Figure 68). At Mali Obručan station, population density increased from 2.78 ± 1.09 colony/m² in 2020 to 3.00 ± 0.95 colony/m² in 2021. At Mana station, population density decreased from 5.78 ± 1.92 colony/m² in 2020 to 4.92 ± 1.38 colony/m² in 2021.

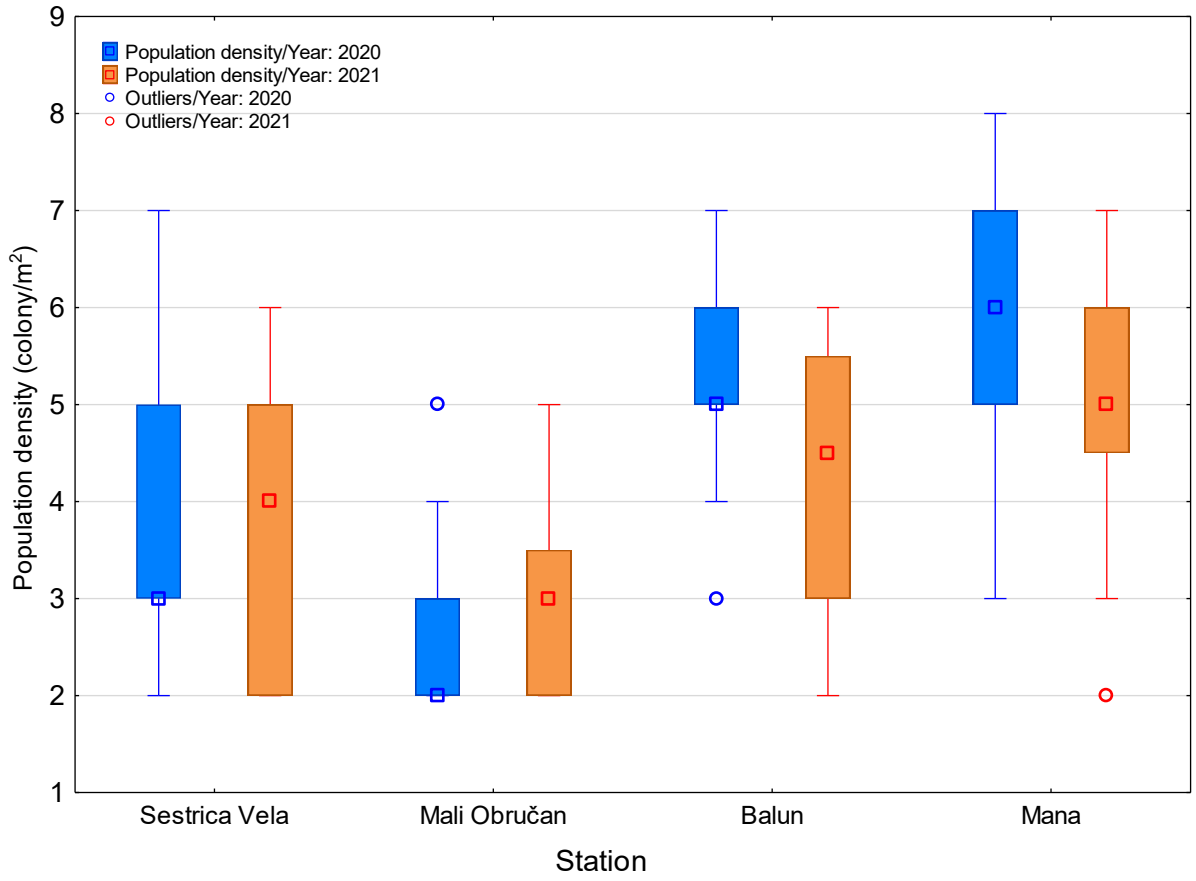

Figure 68. Population density of *Paramuricea clavata* on stations Sestrica Vela [F(1;19) = 0.0016; p = 0.9687], Mali Obručan [F(1;19) = 0.2468; p = 0.6251], Balun [F(1;19) = 2.8187; p = 0.1095] and Mana [F(1;19) = 1.4356; p = 0.2456] across period 2020 – 2021

The mortality rate and colony degradation of *Paramuricea clavata* exhibited a notable increase at all monitored stations (Figure 69, Figure 70). The highest and lowest recorded mortality rates were both observed at the Mali Obručan station, with a mean of 4.70 ± 1.64% in 2020, and a peak of 18.30 ± 36.67% in 2023. Similarly, the greatest colony degradation was recorded at Balun in 2023 with a mean value of 41.11 ±6.79%, while the lowest colony degradation occurred at Mana station in 2020 with a mean value of 22.10 ±4.63%. Considering station-wide averages, Mali Obručan station exhibited the highest mean mortality rate (12.73 ± 6.17%), while Sestrica Vela station had the lowest (9.05 ±3.80%). For colony degradation, Balun station recorded the highest mean (34.18 ±7.90%), and Mana the lowest (27.26 ±7.05%). Normality of the data distribution was assessed using the Shapiro-Wilk test, confirming that all datasets

followed a normal distribution ($p > 0.05$), and ensuring the appropriate selection of a parametric statistical method for further analysis.

In Nature Park Telašćica, at Sestrica Vela station, both the mortality rate and colony degradation rate exhibited a consistent and statistically significant increase over time (Figure 69, Figure *70*). The mortality rate rose from 5.20 ± 1.99% in 2020 to 12.40 ± 3.37% in 2023, while colony degradation increased from 23.10 ± 5.76% to 32.56 ± 4.22% over the same period. (Mortality rate $F(3;36) = 12.751$, $p = 0.000$; Colony degradation rate $F(3;35) = 3.128$, $p = 0.038$).

In Kornati National Park, mortality rates and colony degradation rates exhibited a consistent upward trend across all monitored stations (Figure 69, Figure *70*). At Mana, mortality rates increased from 7.10 ± 2.51% in 2020 to 14.60 ± 5.52% in 2023, representing a statistically significant trend ($F(3;36) = 7.501$, $p = 0.001$). Similarly, Balun showed an increase in mortality rate from 6.40 ± 2.22% in 2020 to 15.50 ± 5.78% in 2023 ($F(3;36) = 9.845$, $p < 0.001$). At Mali Obručan, mortality rates rose from 4.70 ± 1.64% in 2020 to 18.30 ± 4.11% in 2023 ($F(3;36) = 31.786$, $p < 0.001$). At Mana, the percentage of colony degradation increased from 22.10 ± 4.63% in 2020 to 32.67 ± 7.91% in 2023, demonstrating statistical significance ($F(3;35) = 4.839$, $p = 0.006$). The largest relative increase in colony degradation was observed at Balun, where values rose from 29.70 ± 4.19% in 2020 to 35.30 ± 6.29% in 2023, confirmed by ANOVA ($F(3;35) = 5.173$, $p = 0.005$). At Mali Obručan, colony degradation increased from 31.20 ± 5.25% in 2020 to 36.67 ± 8.19% in 2023.

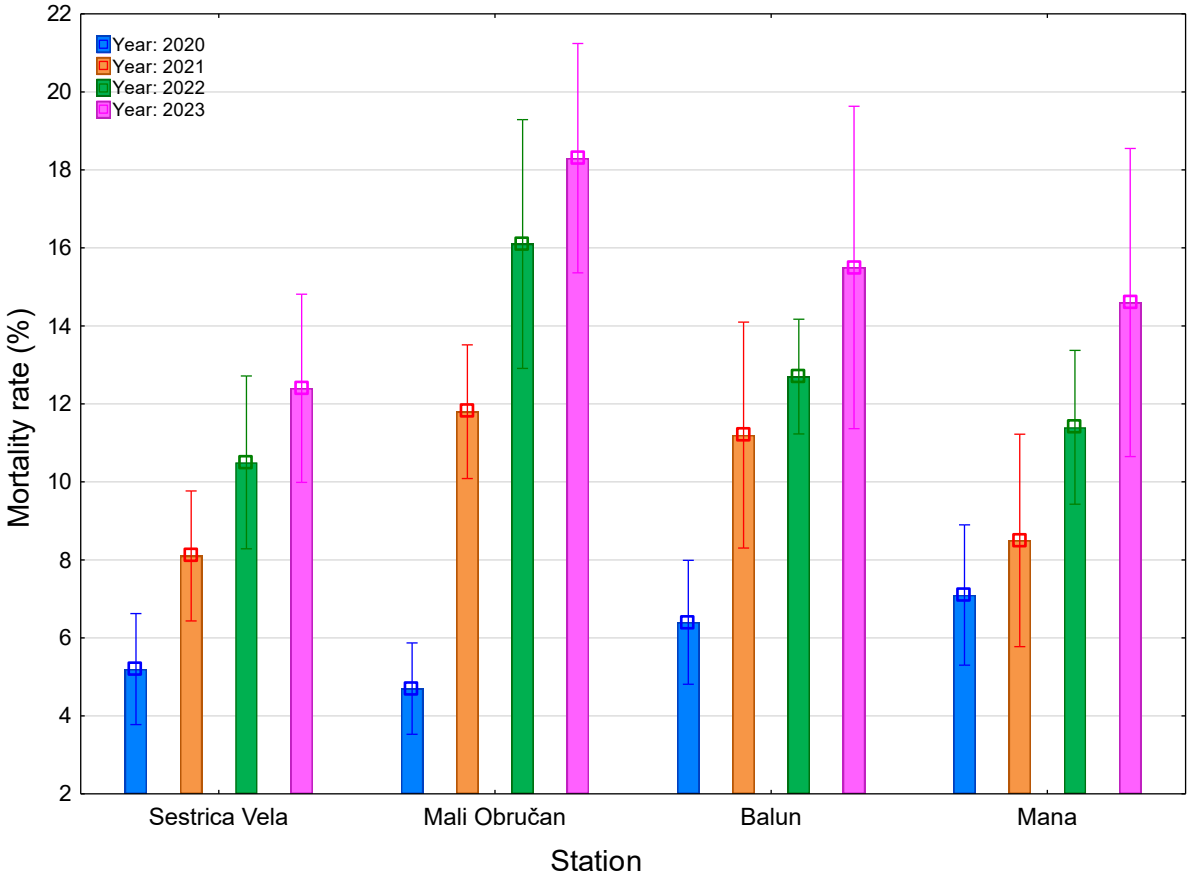

Figure 69. Mortality rate of *Paramuricea clavata* colonies on stations Sestrica Vela [F(3;36) = 12.7505; **p = 0.00001**], Mali Obručan [F(3;36) = 31.7858; **p < 0.0001**], Balun [F(3;36) = 9.8447; **p = 0.00007**], Mana [F(3;36) = 7.5006; **p = 0.0005**] across period 2020 – 2023. Values in bold indicate statistically significant differences (p < 0.05).

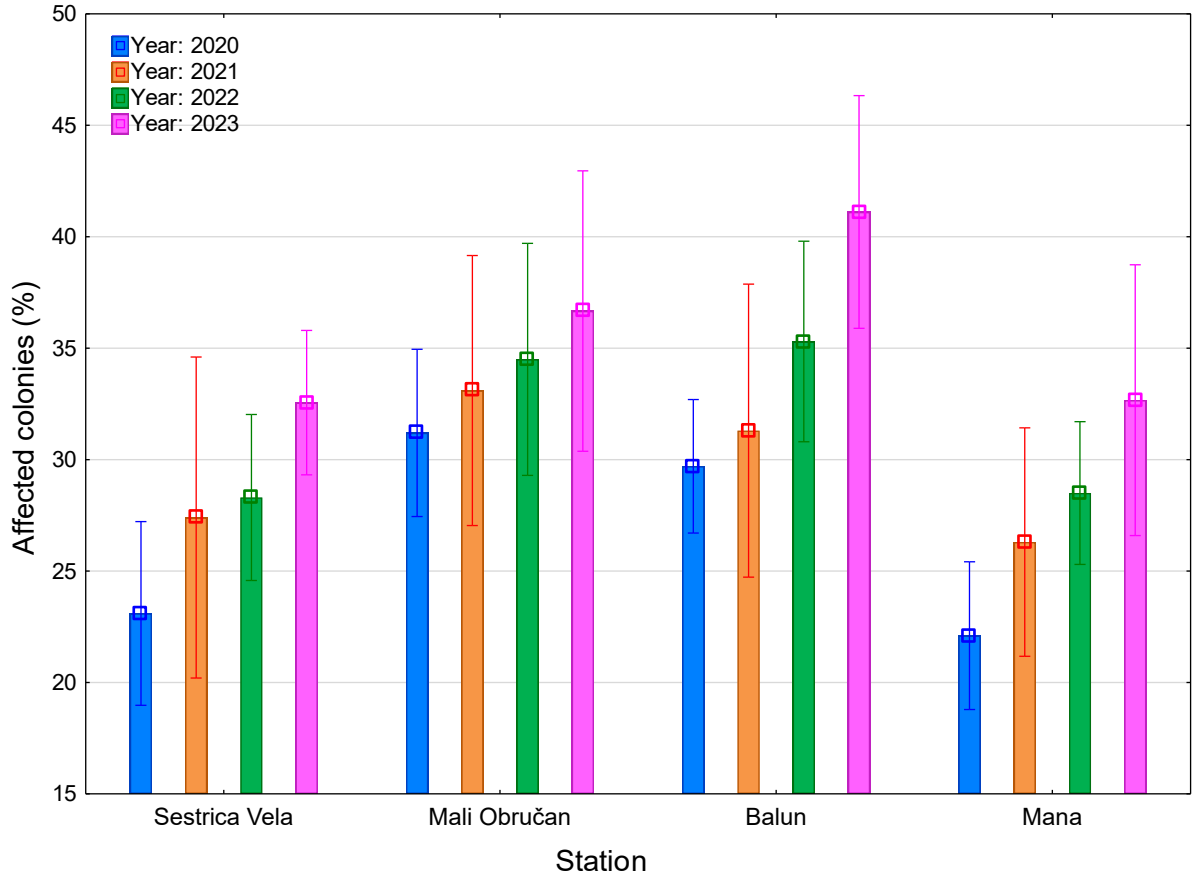

Figure 70. Colony degradation of *Paramuricea clavata* colonies on *stations*: Sestrica Vela [F(3;35) = 3.1275; p = 0.0380], Mali Obručan [F(3;35) = 0.927; p = 0.4379], Balun [F(3;35) = 5.1727; **p = 0.0046**], Mana [F(3;35) = 4.8391; **p = 0.0064**] across period 2020 – 2023. Values in bold indicate statistically significant differences (p < 0.05).

The extent of damage to coral colonies was assessed at four stations (Sestrica Vela, Mali Obručan, Balun, and Mana) and classified as minimal (<10%), moderate (10–90%), or severe (>90%). Across all stations, the general trend indicated increasing severity of damage over the four-year period (Figure 71). The percentage of minimally damaged colonies consistently decreased, while moderately and severely damaged colonies increased at all stations.

At Sestrica Vela, a consistent increase in severely damaged colonies was observed over the study period (Figure 71). The percentage of minimally damaged colonies decreased from 48.4% in 2020 to 33.4% in 2023, while moderately damaged colonies (10-90%) increased from 46.4% to 54.2%. Severely damaged colonies (>90%) showed a notable rise from 5.2% in 2020 to 12.4% in 2023.

Mali Obručan exhibited a similar trend of increasing damage (Figure 71). Minimally damaged colonies decreased sharply from 58.2% in 2020 to 33.5% in 2023. Moderately damaged colonies increased from 37.1% in 2020 to 48.2% in 2023, while severely damaged colonies rose significantly from 4.7% to 18.3% over the same four-year period.

At the Balun station, minimally damaged colonies decreased from 45.0% in 2020 to 30.7% in 2023. Moderately damaged colonies increased slightly from 48.6% in 2020 to 53.8% to 2023, and severely damaged colonies more than doubled from 6.4% in 2020 to 15.5% in 2023.

Mana station demonstrated the most pronounced increase in damage (Figure 71). Minimally damaged colonies decreased substantially from 36.3% in 2020 to 21.7% in 2023. Moderately damaged colonies increased from 56.6% in 2020 to 63.7% in 2023, while severely damaged colonies doubled from 7.1% to 14.6% in the same period.

Mali Obručan showed the most dramatic change in severely damaged colonies, with an increase from 4.7% to 18.3%. Mana station exhibited the most serious overall damage, with 78.3% of colonies showing moderate to severe damage by 2023. These results suggest a concerning trend of increasing coral damage across all studied locations, with variations in the rate and extent of deterioration among different stations.

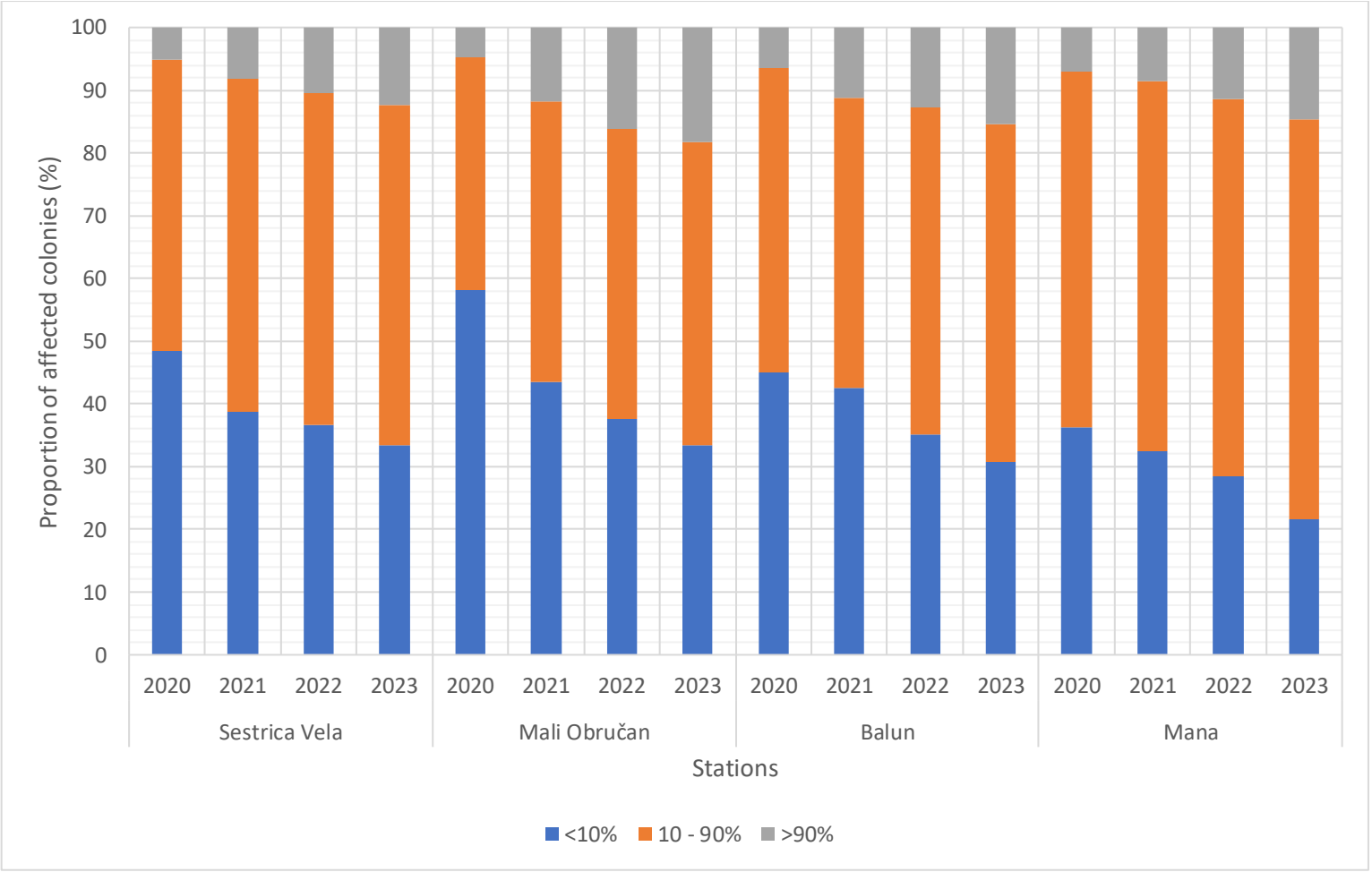

Figure 71. Proportion of affected *Paramuricea clavata* colonies on stations Sestrica Vela (NP Telašćica), Mali Obručan, Balun and Mana (NP Kornati) during the period 2020 – 2023. Stacked bar charts show the proportion of affected colonies per year, with blue indicating <10% affected colonies (low impact), orange indicating 10–90% affected colonies (moderate impact), and grey indicating severe impact (>90% affected colonies).

4.8.3. Histological and histopathological description

Macroscopically, from 21 samples collected at the Mana and Mali Obručan stations, 12 were considered healthy and 9 were necrotic samples. Of the 21 collected samples, 20 were examined and microscopically analysed while one (1) was excluded due to poor tissue condition. Surprisingly, only one (1) sample was confirmed as healthy upon microscopic examination, while the remaining 19 were reclassified as necrotic: 4 samples were categorised as light histopathology (general state code 1; <25% of tissues contained lesions), while moderate histopathology (general state code 2; 25-75% of tissues contained lesions) was determined in 15 samples (Table 13). Although heavy histopathology (general state code 3; >75% of tissues contained lesions) was not determined in the analysed samples, this is likely due to macroscopical field sampling bias and avoiding sampling parts of the colonies which appeared dead or lacked living tissue.

The internal axis is composed of concentric layers (resembling tree rings) of gorgonin, surrounded by an axial sheath and a gastrodermal (axis parallel) canal. The coenenchyme, which surrounds the gastrodermal canal and connects the polyps, is composed of mesogleal matrix with solenia and sclerites. Solenia are tubes lined by gastrodermis which connect the axis parallel canal and interconnect the gastrovascular cavities of the individual polyps. Sclerites are small calcite skeletal elements, important for taxonomic identification but not visible in histological slides due to decalcification, hence only empty lacunae without sclerites were present in decalcified histological slides.

The polyps of *P. clavata* are cylindrical in shape, the aboral part is attached to the coenenchyme, while the oral disc with tentacles is exposed to the external (marine) environment (Figure 72). Tentacles are built from an outer ectodermal layer, a thin acellular mesoglea and an inner gastrodermal layer. The mesenteries are located within the polyps and divide the gastrovascular cavity, lined with muscular epithelial cells and gastrodermis and carry gonads.

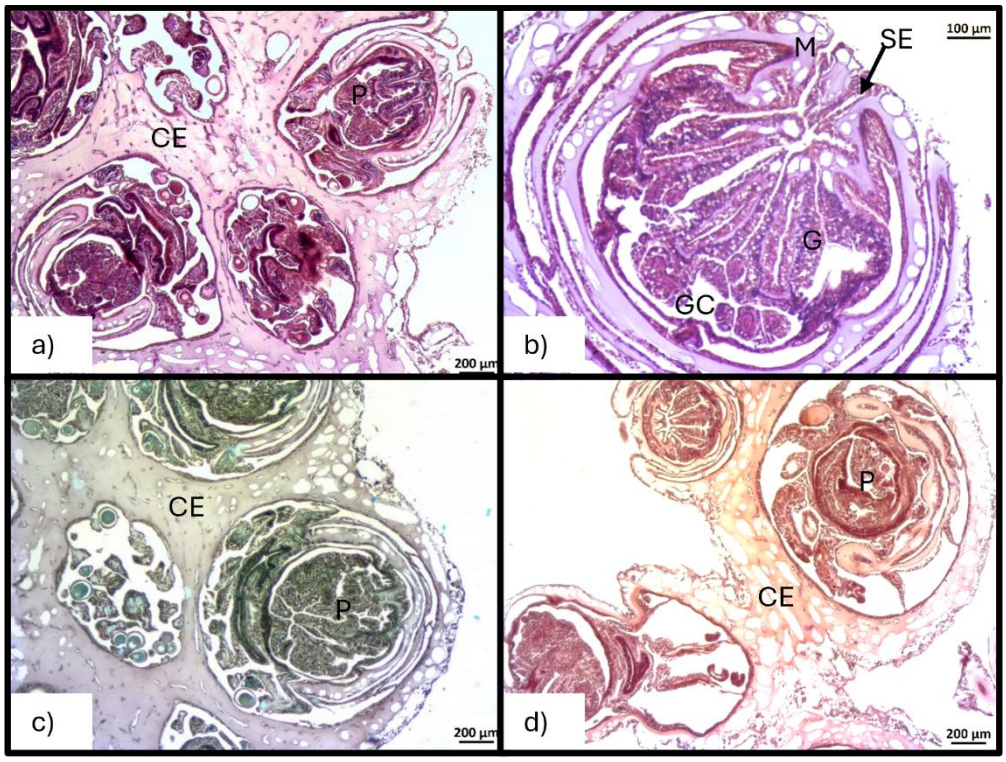

Figure 72. Histological longitudinal sections of a healthy branch of *Paramuricea clavata*, stained with (a–b) hematoxylin and eosin, (c) Grocott's methenamine silver, and (d) Gram stain. Normal architecture of the coenenchyme (CE) is visible, along with the characteristic cellular organization of polyps (P), which appear in cross-section due to their perpendicular orientation to the branch axis. Visible structures include the gastrodermis (G), gastrovascular cavity (GC), mesoglea (M), and surface epithelium (SE).

Table 13. Specific histopathological lesions and patogens of *Paramuricea clavata* and their frequency

Specific histopathological lesions	Light lesion (state 1)	Freq (%)	Heavy lesion (state 2)	Freq (%)
Surface epithelium (loss of integrity, necrosis)	9	47.4	10	52.6
Polyp necrosis	4	21.1	15	78.9
Basophilic cells in polyp	6	31.6	13	68.4
Infiltrates of basophilic granular cells in mesoglea	9	47.4	9	47.4
Infiltrates of eosinophilic granular cells (amoebocytosis) in mesoglea	6	31.6	12	63.2
Small blue fibrilar cells in mesoglea	10	52.6	3	15.8
Mesogleal tissue loss (large holes present)	10	52.6	5	26.3
Gastrodermall disassociated cells in solenia (necrosis)	13	68.4	5	26.3
Gastrodermis with foamy cells (light bubble cells)	8	42.1	6	31.6
Axis – black deposits	10	52.6	4	21.1
Axis – cavities of the axial skeleton, finely fibrillar material	18	94.7	0	0.0
Axis – red or violet deposits	6	31.6	1	5.3
Changes in the axis structure and rigidity	11	57.9	6	31.6
Melanin deposition in/near axis	8	42.1	0	0.0
Eggs (absence 0, few 1, many 2)	11	57.9	1	5.3
Patogens	**Light lesion (state 1)**	**Freq (%)**	**Heavy lesion (state 2)**	**Freq (%)**
Red bacteria	1	5.3	0	0.0
Blue bacteria	0	0.0	0	0.0

Surface epithelium showed signs of inflammatory response with lightly (47%) or highly necrotic histopathological lesions in 53% of necrotic samples (Table 13), with epidermal necrosis, loss of integrity and dissociation, and frequent exposure of underlying mesoglea (Figure 73).

In tissue with lesions, was recorded increase in the number of cells in mesoglea, mainly granular amoebocytes (in 95% of necrotic samples), which indicated a classic inflammatory response. This cellular host response was manifested by an increase in the number and size of eosinophilic granular cells, and occasionally the fragmentation with karyorrhexis and karyolysis (dissolution or swelling of cell nuclei). Additionally, a larger infiltration of basophilic cells in mesoglea (95%) and smaller fibrillar mesogleal cells (68% of samples) followed an inflammatory response (Table 13). In addition to the increase in cell number, a decrease of

mesogleal tissue (expanded solenia and loss of mesogleal tissue) has been recorded in 79% of necrotic samples (Figure 73). In two samples, melanisation in mesoglea, circumscribing the unknown pathogen was recorded.

The most frequent lesion was necrosis and dissociation of gastrodermis, present in all 19 necrotic samples (Figure 73). In light lesions, necrotic gastrodermis showed loss of integrity and sloughing into solenia, while severely necrotic gastrodermis, found in 42% of necrotic samples, included clusters of gastrodermal epithelial cells detached within gastrovascular canals, with loss of distinction of cell borders, scattered karyorrhexis (fragmentation of cell nuclei), or pyknosis (shrinkage of cell nuclei), cytoplasmic vacuolation and foamy light yellow-brownish cells. Light changes in polyp structure (mainly mesenterial filaments and gastrodermis) with an increased number of small black cells were recorded in 21% of necrotic samples, while heavy necrosis of the entire polyp was recorded in 79% of samples (Table 13).

Axial skeleton also exhibited several frequent histopathological lesions, visible as small black deposits within the axis in 74% of necrotic samples, melanin depositions (in 42% of necrotic samples) infiltrated between tissue coenenchyme and the surface of the axial skeleton or forming visible nodules, the rupture of the axis with possible gorgonin thickening (90% of necrotic samples) (Figure 74) and, in one case, amoebocyte infiltration within the axis (Table 13). In one sample, melanin layers were deposited between the pathogen (most likely algae) and the axial skeleton.

No foreign organisms (crustaceans, parasites, sponges) were recorded, except in one sample. Histochemical stains for fungi and bacteria did not indicate the possible pathogen identity. Oocytes of various stages were present in the majority of samples (63% of samples), and occasionally, when severe histopathological signs were present, some oocytes were undergoing resorption.

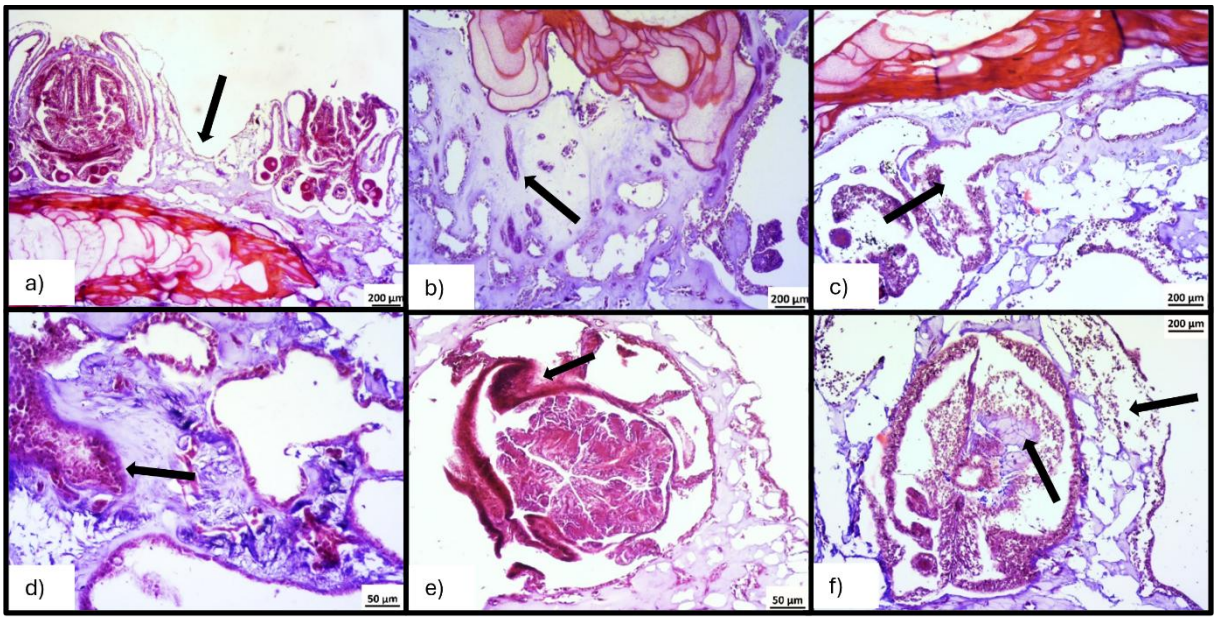

Figure 73. Histological longitudinal sections of *Paramuricea clavata* samples with identified light microscopic lesions (a–c) show (a) structural changes in surface apithelium, and (b-c) an increase of granular amoebocyte in mesoglea with inflammatory response in mesoglea. Heavy microscopic lesions (d–f) shows (d) a necrotic lesion in mesoglea of cenenhim filled with eosinophilic and basophilic granular cells, (e) necrotic gastrodermal tissue and (f) structural disintegration of polyp and cenenhim tissue. HE stain.

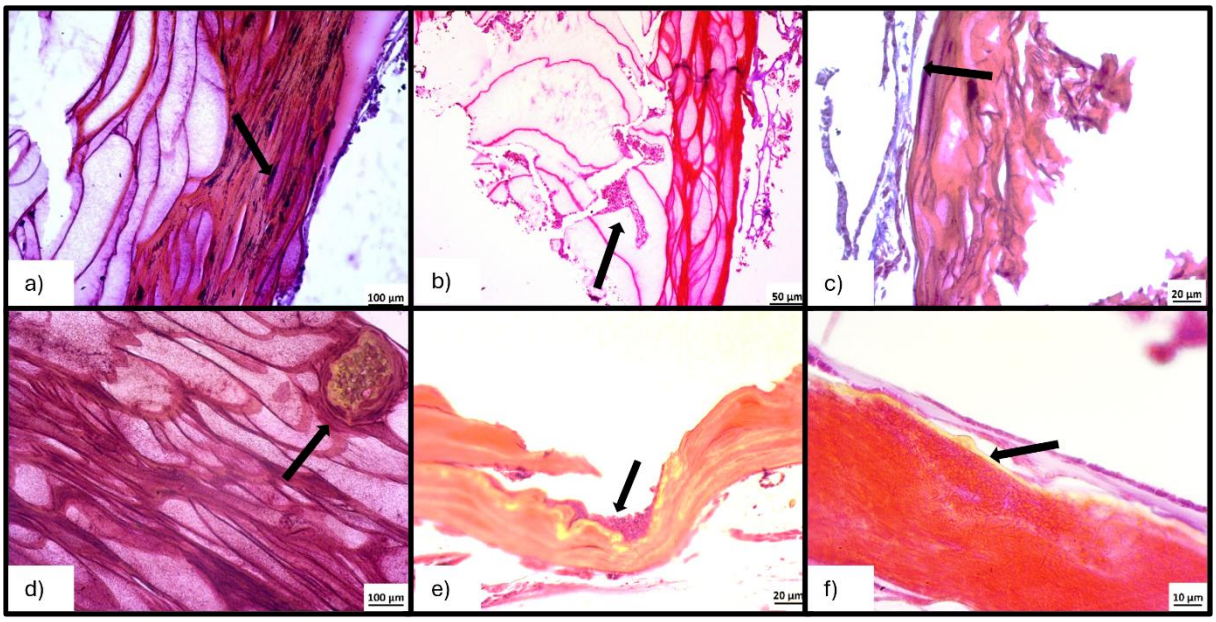

Figure 74. Histological longitudinal sections of *Paramuricea clavata* samples showing axis-associated histopathological lesions. Observed alterations include (a) necrotic zones visible as small black deposits, (b) amoebocyte infiltration within the axis, (c) disintegrated axis, (d) melanin depositions forming visible nodules, (e) algae ingrowth along areas of intense melanin depositions and (f) melanin deposits along the axis. HE stain.

5. DISCUSSION

5.1. Marine environmental parameters and marine heat waves

The marine enviromental parameters reveals a predominantly seasonal signal, with concentrations generally differing between summer (July) and autumn (October) sampling periods across all three years. October values tend to be higher than those recorded in July, suggesting a recurrent seasonal pattern rather than interannual variability. This pattern is consistent across most locations and depths, indicating that temporal changes within a year are more pronounced than differences among years. Such consistency points to stable background conditions, with seasonal processes exerting a stronger influence on nutrient availability than longer-term temporal changes. This interpretation is consistent with studies from Mediterranean coastal environments showing that nutrient availability is strongly influenced by seasonal hydrographic forcing, stratification, and mixing dynamics, which can generate recurrent annual nutrient cycles even in the absence of sustained directional change (Arin et al., 2013; DeCarlo et al., 2020).

Overall, the enviromental data describe a system in which seasonal variability and spatial differences are evident, while interannual conditions remain largely stable. The absence of a consistent temporal trend, together with persistent contrasts among locations and only minor depth-related variation, suggests that nutrient dynamics during the study period were mainly controlled by recurring physical and ecological processes. Importantly, there is no indication of sustained nutrient enrichment or depletion over time. Consequently, the observed nutrient regime represents a relatively stable environmental framework within which the effects of other stressors, including biological or climatic drivers, can be assessed without confounding influences from long-term nutrient change. At the same time, this does not imply that nutrients were ecologically unimportant, as nutrient availability and nutrient cycling are known to modulate coral physiology and interact with heat stress, particularly under conditions of chronic enrichment or nutrient imbalance (Donovan et al., 2020; Rädecker et al., 2021).

Marine heatwaves have emerged over the last decade as a key framework for quantifying extreme thermal events in the ocean and assessing their ecological relevance. The statistical definition proposed by Hobday et al. (2016) has become the standard among marine scientists and underpins the vast majority of recent regional and global MHW studies. This definition was adopted in the present study to identify MHWs as prolonged periods of anomalously warm water, occurring when temperature exceeds a seasonally varying threshold set at the 90th percentile of a local calendar-day climatology for at least five consecutive days, allowing brief interruptions of up to two days. Building on this definition, Hobday et al. (2018) further introduced an intensity-based categorisation, in which MHW severity is expressed as multiples of the local difference between the climatological mean and the threshold, enabling comparison of event severity across regions with contrasting thermal regimes.

This threshold-based approach has fundamentally shaped the way extreme sea warming is interpreted, shifting emphasis away from absolute temperature alone toward relative thermal anomalies and cumulative exposure (Rosselló et al., 2023). Subsequent studies have demonstrated that, under ongoing sea warming, MHW characteristics such as duration, cumulative intensity, and frequency have increased globally and across the Mediterranean Sea, often with stronger ecological consequences than suggested by mean temperature trends alone (Darmaraki et al., 2019; Garrabou et al., 2022). Importantly, recent analyses also stress that MHWs are not confined to the surface but can propagate vertically through the water column, with their subsurface expression strongly modulated by stratification, circulation, and local hydrographic conditions (Darmaraki et al., 2024).

Within the Mediterranean, the Adriatic Sea represents a particularly sensitive sub-basin due to its semi-enclosed geometry, pronounced seasonal stratification, and rapid response to atmospheric forcing. Analyses of marine climate indicators show that the Adriatic has experienced marked increases in ocean heat content, stratification strength, and the persistence of warm anomalies during the warm season (da Costa et al., 2024). At the same time, recent observations document unprecedented warming and salinisation of deep and near-bottom Adriatic waters, indicating that the thermal background state of the basin is changing not only at the surface but throughout the water column (Terzić et al., 2025).

Within this context, the present dataset provides a depth-resolved, event-based characterisation of MHWs across multiple Adriatic environments (Telaščica, Kornati, Mljet – Lenga, Mljet – Veliko jezero) and depths ranging from 5 to 40 m. By applying the Hobday et al. framework consistently across depths, the analysis captures not only when and where MHWs occur, but also how their relative intensity, cumulative anomaly load, duration, and onset dynamics vary vertically and spatially. This approach allows direct comparison of shallow and deeper thermal extremes within the same statistical framework and offers a physically grounded basis for interpreting how hydrographic processes shape thermal stress in the Adriatic Sea. The further discussion focuses on linking the observed depth-dependent MHW characteristics to known patterns of stratification, circulation, and heat retention, before considering their implications for sessile benthic organisms.

Across all depths and locations, the category distribution is strongly skewed toward Category I (Moderate) events (116 out of 152), followed by Category II (Strong) events (32), with only three Category III (Severe) and a single Category IV (Extreme) event. This distribution conforms to expectations under percentile-based MHW definitions, where moderate events dominate statistically (Rosselló et al., 2023).

However, the rarity of high-category events makes them disproportionately important for interpretation. The only Category IV (Extreme) MHW in the dataset occurred at 40 m depth in Telaščica between 18 and 23 June 2020. This event exhibits both the highest cumulative intensity relative to threshold (21.36) and the highest maximum (4.76) and mean (3.56) intensity relative to threshold across all 152 events, despite reaching a maximum absolute temperature of only 22.80°C. This result illustrates a fundamental aspect of MHW interpretation repeatedly emphasised in recent Mediterranean literature: severity is defined relative to local climatology rather than absolute temperature (Rosselló et al., 2023; Darmaraki et al., 2024). In environments characterised by cooler and less variable thermal regimes, such as deeper coastal layers, relatively modest absolute temperatures can nonetheless represent extreme departures from historical conditions. Comparable conclusions have been drawn in Mediterranean-wide assessments documenting subsurface MHWs capable of driving ecological impacts without exceptional surface warming (Darmaraki et al., 2019).

From a physical standpoint, the occurrence of an extreme-category MHW at 40 m in mid-June 2020 coincided with severe (Category III) MHWs recorded on the same date (18 June 2020) at 20 m depth in both Kornati and Telašćica, lasting nine and six days, respectively. This vertical coherence at intermediate and deeper layers, in the absence of concurrent MHWs at shallower depths (<20 m) at the same sites, could suggest that the observed thermal anomalies were not driven solely by surface heating. Instead, these patterns could be consistent with subsurface heat advection associated with Adriatic circulation, or with downward propagation and retention of heat within the water column, operating independently of shallow-layer temperature extremes. This interpretation aligns with recent evidence showing that warming signals and anomalous water masses increasingly penetrate deeper layers of the Adriatic water column, modifying the thermal baseline at depth (Terzić et al., 2025).

The comparison between seasonal event counts and cumulative thermal metrics indicates that event frequency alone does not adequately reflect thermal stress magnitude. Although the number of detected MHW events is identical in winter (December-January-February, DJF) and summer (June-July-August, JJA), with 42 events in each season, cumulative thermal exposure differs profoundly. The sum of cumulative intensity relative to the local threshold reaches 297.30 in JJA, compared to only 43.69 in DJF, representing a ~6.8-fold difference in thermal load. This pattern is consistent with Mediterranean-wide analyses showing that the ecological relevance of MHWs is primarily driven by warm-season events, when elevated background temperatures amplify both anomaly magnitude and persistence (Darmaraki et al., 2019; Garrabou et al., 2022). In the Adriatic, marine climate indicators further show that summer increases in water-column heat content and stratification enhance heat retention in upper and intermediate layers, favouring prolonged thermal exposure (da Costa et al., 2024).

The seasonal asymmetry observed here is reinforced by the absolute temperature context. Mean maximum absolute temperature during summer MHWs reaches 24.44°C, compared with 15.82°C in winter. Thus, although winter conditions may frequently exceed climatological thresholds, they do so with relatively small anomaly magnitudes and limited cumulative exposure. In contrast, summer events combine elevated background temperatures with sustained positive anomalies, concentrating the majority of the system's thermal stress into

the warm season. This distinction mirrors conclusions from basin-scale Mediterranean studies emphasising cumulative exposure rather than event counts as the primary driver of ecological impact (Garrabou et al., 2022).

When examined by depth, the dataset reveals a clear differentiation between intermediate depths (20 m) and deeper layers (40 m) in terms of dominant stress characteristics. Twenty metres depth emerges as the principal contributor to cumulative thermal stress under typical conditions, exhibiting the highest mean cumulative intensity relative to threshold (4.09). This depth also hosts some of the longest-lasting events in the dataset, most notably the 21-day MHWs recorded simultaneously at Telaščica and Kornati between 22 September and 12 October 2023. Although classified as Category I (Moderate), these events display substantial cumulative intensities (7.15 and 8.76, respectively), indicating prolonged anomaly exposure. In addition, the timing of these events is particularly informative. Their occurrence in early autumn suggests delayed seasonal cooling and prolonged heat retention at intermediate depths, consistent with enhanced stratification and reduced vertical mixing. Similar behaviour has been reported for the central and southern Adriatic, where marine climate indicators show increasing water-column stability at mid-depths during the warm season and into autumn (da Costa et al., 2024).

In contrast, 40 m depth is characterised less by long durations and more by extreme anomaly dynamics. The two highest onset rates in the entire dataset occur at 40 m on 25 September 2022, simultaneously in Kornati and Telaščica, reaching 3.73 and 3.31°C day^{-1}, respectively. Such rapid warming is unlikely to be driven by gradual atmospheric forcing alone and instead points to short-lived hydrographic processes such as advection or episodic mixing. Subsurface intensification driven by such mechanisms has been identified as an important component of Mediterranean MHW dynamics (Darmaraki et al., 2019; Darmaraki et al., 2024). The presence of rapid-onset MHWs at depth is particularly notable given recent observations of altered dense-water properties and circulation pathways in the Adriatic, which may facilitate the penetration of warm anomalies into deeper layers (Terzić et al., 2025).

A further key result is the pronounced distinction between absolute temperature maxima and threshold-relative severity across environments. The highest absolute temperatures in the

dataset occur in the Mljet system, particularly in Veliko jezero at 5 m, where a summer MHW between 19 July and 5 August 2023 reached 29.12°C. Despite this extreme absolute value, the event is classified as Category I (Moderate), with relatively modest relative intensities. Such behaviour is characteristic of warm, semi-enclosed systems with elevated baseline temperatures, where extreme absolute values do not necessarily translate into exceptional threshold-relative anomalies. Comparable contrasts between absolute exposure and relative severity have been highlighted in Mediterranean analyses comparing enclosed and open coastal systems (Darmaraki et al., 2024). Conversely, some of the most severe threshold-relative anomalies in the present dataset occur at deeper or more open sites with substantially lower absolute temperatures, most notably the Telaščica 40 m Category IV event. Situation on station Lenga further illustrates this complexity by combining high absolute exposure with strong threshold-relative anomalies. These site-specific contrasts reinforce the importance of interpreting MHW metrics within their local climatological and hydrographic context rather than relying on absolute temperature or category alone (Rosselló et al., 2023).

The dataset captures a clear example of regional-scale coherence in MHW onset during late July 2023, with multiple events initiating between 19 and 21 July across different locations and depths, including at Telaščica (5 and 10 m), Mljet – Veliko jezero (5 and 10 m), and Mljet – Lenga (5 and 10 m). This synchrony strongly suggests a basin-scale atmospheric forcing phase affecting the wider Adriatic region, consistent with Mediterranean-wide analyses of recent extreme summers (Darmaraki et al., 2024). Despite this shared onset, the expression of the events diverges substantially among sites and depths, with durations ranging from 9 to 19 days and categories from I to II. This divergence reflects strong modulation by local hydrography and site-specific thermal regimes, a pattern repeatedly emphasised in Adriatic climate indicator studies (da Costa et al., 2024). The July 2023 sequence, therefore exemplifies how regional forcing interacts with local physical conditions to shape realised thermal stress.

These results indicate that depth does not uniformly modulate thermal exposure during MHWs. Such depth-dependent patterns are directly relevant for sessile benthic organisms when interpreting thermal stress across habitats. The occurrence of the most extreme threshold-relative event at 40 m, combined with repeated observations of rapid deep

warming, indicates that deeper habitats can experience abrupt and highly anomalous thermal exposure. This conclusion is consistent with recent ecological studies documenting that extreme MHWs can erode the buffering capacity of deeper habitats and threaten climatic refugia during particularly intense events (Rovira et al., 2024). At the same time, the prominence of long-lasting events at intermediate depths highlights these layers as zones of prolonged sublethal stress, potentially compressing recovery windows between events. Such mechanisms have been implicated in Mediterranean-wide mass mortality patterns associated with cumulative thermal exposure (Garrabou et al., 2022).

5.2. Microbiome

The coral microbiome represents a fundamental component of the holobiont concept, encompassing complex microbial assemblages that inhabit the surface mucus layer, epidermis, gastrodermis, and skeletal compartments of corals. These communities comprise bacteria, archaea, viruses, fungi, and protists, which play integral roles in host nutrition, immune defence, and resistance to environmental stressors (Rosenberg et al., 2007; Bourne et al., 2016; van Oppen & Blackall, 2019).

Increasing evidence indicates that coral-associated microbial communities are not passive assemblages, but are actively regulated by the host through a combination of immune responses, antimicrobial compounds, and niche structuring, resulting in relatively stable and host-specific microbiomes under non-stressful conditions (Brown & Bythell, 2005; Hunt et al., 2012; van de Water et al., 2018). Disruption of this regulation under environmental stress, particularly thermal anomalies and marine heatwaves (MHWs), has been repeatedly associated with microbial dysbiosis, increased community heterogeneity, and disease development in both tropical and temperate corals (Harvell et al., 2007; Boilard et al., 2020; Corinaldesi et al., 2022).

In this study, although the microbiome was not the primary focus of the analytical framework, bacterial community structure was examined as a complementary component at locations exhibiting pronounced signs of thermal stress on all investigated coral species. Sampling was

conducted in 2022 and 2023 at locations exhibiting pronounced signs of thermal stress. Amplicon sequencing of the 16S rRNA gene revealed distinct, site- and species-specific microbial profiles, highlighting measurable shifts in bacterial community composition associated with coral health status and environmental context. While the resolution of the present dataset is limited to the phylum level, these patterns provide a valuable first-order insight into microbial responses to coral tissue condition and local environmental variability, particularly in temperate and semi-enclosed Adriatic systems that remain underrepresented in coral microbiome research.

The phylum-level composition of seawater bacterial communities across Kornati, Telašćica and Mljet National Parks revealed a highly consistent dominance of Proteobacteria, irrespective of location, station or depth. This pattern reflects the presence of a broadly conserved pelagic bacterial assemblage characteristic of marine water columns and has been widely documented in both coastal and open-ocean systems (Giovannoni & Stingl, 2005; van Oppen & Blackall, 2019). The ecological success of Proteobacteria in marine environments is commonly attributed to their metabolic versatility and capacity to exploit diverse organic substrates, allowing them to persist across strong environmental gradients and varying nutrient regimes.

Across all locations, Bacteroidota and Cyanobacteria represented the most abundant secondary phyla, although their relative contributions varied subtly among stations and depths. In Kornati and Telašćica, these phyla exhibited relatively stable proportions throughout the vertical profile, suggesting weak depth-related structuring at the phylum level. The occurrence of additional low-abundance phyla, including Actinobacteriota, Dadabacteria, Marinimicrobia (SAR406 clade), and Planctomycetota, suggests subtle differences in seawater bacterial community composition between the central Adriatic sites and the southern Adriatic stations at Mljet National Park. Such regional differentiation is consistent with previous observations that semi-enclosed or hydrographically distinct systems may support locally variant microbial assemblages superimposed on a conserved core community (Glasl et al., 2017; van de Water et al., 2017).

In contrast, the semi-enclosed system of Mljet National Park, and particularly Veliko jezero, exhibited more pronounced depth-related differences among low-abundance phyla. At Veliko jezero, the 20 m sample showed elevated relative contributions of Cyanobacteria and Verrucomicrobiota compared to shallower depths, while the 15 m layer was characterised by a visibly higher proportion of Marinimicrobia (SAR406 clade). Although these shifts did not alter the overall dominance structure of the community, they point to subtle vertical heterogeneity within the water column that is less evident at the more open stations. Such patterns are consistent with the unique hydrodynamic and biogeochemical properties of semi-enclosed lagoons, where restricted water exchange and longer residence times can enhance vertical stratification and promote the persistence of locally adapted microbial assemblages (Meron et al., 2012; Corinaldesi et al., 2022).

Depth-related differentiation was also apparent, though less pronounced, at Štit and Lenga. At both stations, Planctomycetota were confined to deeper samples, while Marinimicrobia exhibited slightly higher relative abundance at greater depth. The appearance of additional low-abundance SAR324 clade (Marine group B) exclusively or more clearly in deeper samples at Lenga, further indicates that deeper water layers harbour a more taxonomically complex assemblage, even if such differences remain minor at the phylum level.

Overall, the results indicate limited vertical structuring of bacterial communities when assessed at the phylum level, with depth-related differences primarily reflected in changes among low-abundance taxa rather than shifts in dominant groups. Spatial differences among locations and stations—particularly between open coastal sites and semi-enclosed systems—appear to exert a stronger influence on community composition than depth alone. This relative homogeneity at higher taxonomic levels suggests that environmental gradients within the sampled depth range may be insufficient to drive major taxonomic turnover, while finer-scale ecological differentiation is likely to be expressed at lower taxonomic or functional levels. Consequently, analyses targeting genus-level composition or metabolic potential may provide deeper insight into microbial responses to local environmental conditions within these Adriatic marine systems.

Comparisons between healthy (N) and necrotic (NEC) colonies within the same coral species revealed consistent changes in bacterial community structure, although the magnitude and direction of these shifts were species and site-specific. In several taxa, necrotic tissues were characterised by increased compositional heterogeneity and a relative enrichment of bacterial phyla typically present at low abundance in healthy colonies. This pattern was particularly evident in *Balanophyllia europaea*, *Cladocora caespitosa*, *Eunicella cavolini*, and *Leptopsammia pruvoti*, where NEC samples showed broader phylum-level representation and reduced dominance of a single taxonomic group. Such increases in microbial heterogeneity associated with tissue degradation are consistent with the concept of coral microbial dysbiosis, whereby stress-induced disruption of host–microbe regulation allows the proliferation of opportunistic or environmentally derived bacteria (Harvell et al., 2007; Boilard et al., 2020; Morrow et al., 2018).

In contrast, healthy colonies were more frequently characterised by a simpler community structure dominated by one or two phyla, most commonly Proteobacteria or, in some cases, Bacteroidota or Acidobacteriota. Such patterns are consistent with the concept of a relatively stable host-associated microbiome in healthy corals, where microbial community structure is maintained through host-mediated regulation and competitive exclusion. Similar patterns of reduced microbial variability and dominance of a limited number of bacterial taxa in healthy corals have been reported across a range of coral species, including Mediterranean gorgonians and scleractinians, suggesting that microbiome stability represents a common feature of coral health rather than a species-specific phenomenon (Hunt et al., 2012; van de Water et al., 2017; van de Water et al., 2018).

When comparing the same coral species and health state across different locations, bacterial community composition was broadly conserved at the phylum level, but with notable site-specific differences. This was particularly apparent for species sampled across both Kornati and Mljet National Parks. For example, *Balanophyllia europaea* colonies from Mana (Kornati NP) and Veliko jezero (Mljet NP) were consistently dominated by Proteobacteria in both healthy and necrotic states, but differed in their representation of additional phyla, with greater representation of minor groups and “Others” in samples from Veliko jezero.

Comparable spatial modulation of coral-associated microbiomes has been documented in Mediterranean corals, where locally variable environmental conditions overlay a conserved, host-specific core community (La Rivière et al., 2013; van de Water et al., 2017).

Similarly, *Leptopsammia pruvoti* NEC samples from Obručan, Mana, Štit and Lenga displayed marked variability in dominant and secondary phyla, ranging from Bacteroidota-dominated profiles in Kornati to Acidobacteriota dominance at Lenga. These differences suggest that, while host identity and health state exert strong control over microbial assemblages, local environmental conditions could further modulate community composition, particularly among secondary and low-abundance phyla.

Veliko jezero emerged as a site where coral-associated bacterial communities exhibited particularly high compositional complexity, especially in necrotic colonies. Both *Cladocora caespitosa* and *Balanophyllia europaea* necrotic samples from Veliko jezero showed a relative reduction in Proteobacteria dominance, accompanied by increased representation of multiple additional phyla, including Bacteroidota, Chloroflexi and other low-abundance groups. This pattern contrasts with the more open-water sites in Kornati, where coral-associated bacterial assemblages were typically dominated by one or two major phyla. The enhanced heterogeneity observed in Veliko jezero is consistent with previous studies linking semi-enclosed systems and prolonged water residence times to increased microbial diversity and altered host–microbe interactions (Meron et al., 2012; Corinaldesi et al., 2022).

The consistent detection of Bdellovibrionota in coral-associated samples from Veliko jezero, but not from other Mljet sites, further suggests site-specific microbial dynamics within this semi-enclosed lagoon. Bdellovibrionota are known bacterial predators and have been proposed to influence microbial community structure through top-down control, particularly in environments characterised by high microbial turnover. Although their functional role within coral holobionts remains poorly resolved, the presence of predatory bacteria has been hypothesised to reflect intensified microbial interactions under stress conditions, potentially contributing to the restructuring of microbial communities during dysbiosis (Morrow et al., 2018; van Oppen & Blackall, 2019).

Although direct comparisons among different coral species are constrained by their distinct ecological niches, limited comparisons between closely related or functionally similar taxa provide additional insight into host–microbiome relationships. The two scleractinian corals *Cladocora caespitosa* and *Balanophyllia europaea*, both inhabiting relatively shallow environments, exhibited broadly similar health-related trends, with necrotic samples showing increased bacterial heterogeneity and reduced dominance of a single phylum. Likewise, the octocorals *Eunicella cavolini* and *Paramuricea clavata*, sampled at greater depths, displayed more subtle differences between healthy and necrotic states, suggesting a comparatively stable phylum-level structure even under tissue degradation. Such patterns are consistent with previous observations that gorgonian corals often harbour highly conserved, host-specific microbial assemblages that may be less prone to rapid restructuring than those associated with scleractinian corals (Hunt et al., 2012; van de Water et al., 2017; van de Water et al., 2018).

When coral-associated bacterial communities are considered in the context of the surrounding seawater microbiome, clear parallels emerge between host depth distribution and microbial composition. Species inhabiting shallow waters (*Cladocora caespitosa*, *Balanophyllia europaea*) were associated with bacterial assemblages containing higher relative contributions of Cyanobacteria and Bacteroidota, mirroring the composition of seawater communities at corresponding depths. In contrast, deeper-dwelling species (*Leptopsammia pruvoti*, *Madracis pharensis*, *Eunicella cavolini*, *Paramuricea clavata*) frequently hosted bacterial communities enriched in Planctomycetota, Chloroflexi, Acidobacteriota and Marinimicrobia, taxa that were also more prominent in deeper seawater samples. These patterns suggest that coral-associated microbiomes are shaped not only by host identity and health status, but also by the microbial composition of the surrounding water mass at the depth inhabited by each species (Glasl et al., 2017; Rubio-Portillo et al., 2016).

In semi-enclosed systems such as Veliko jezero, the coupling between seawater microbial communities and coral-associated microbiomes may be particularly strong. Restricted water exchange and prolonged residence times can enhance the persistence of locally adapted microbial assemblages, increasing the likelihood of microbial exchange between the water

column and stressed coral tissues. Under such conditions, the breakdown of host-mediated microbial regulation during thermal stress or tissue necrosis may facilitate the incorporation of environmentally derived bacteria into the coral holobiont, resulting in the increased heterogeneity observed in necrotic colonies. Similar processes have been proposed for both tropical and temperate corals exposed to thermal anomalies, where microbial community restructuring precedes or accompanies visible signs of tissue degradation (Harvell et al., 2007; Corinaldesi et al., 2022; van Oppen & Blackall, 2019).

Overall, the results indicate that coral health status is a key driver of bacterial community structure within species, while spatial context and depth-related environmental conditions modulate the expression of these changes. The observed shifts in necrotic colonies towards more heterogeneous and environmentally influenced bacterial assemblages support the view that coral tissue degradation is associated with a breakdown of host-mediated microbial regulation. At the same time, the persistence of host-specific patterns across locations highlights the resilience of coral–microbe associations under moderate stress, particularly in gorgonian corals. Future studies targeting finer taxonomic resolution and functional potential should be essential to disentangle opportunistic colonisation from active microbial processes underlying coral health decline in Adriatic marine ecosystems.

5.3. Comparative analyses of scleractinian corals

Mortality was recorded in all four analysed scleractinian species across sites and years, whereas bleaching occurred exclusively in *Cladocora caespitosa* and *Madracis pharensis*, since bleaching is a species-specific morphological response. Clear interspecific differences were evident in both the magnitude and temporal dynamics of mortality.

Balanophyllia europaea exhibited the highest and most variable mortality rates, frequently exceeding 40% and locally reaching extreme values above 60–70%, indicative of severe and episodic population-level impacts. *Leptopsammia pruvoti* showed intermediate but highly consistent mortality, with a gradual, near-linear increase through time, suggesting progressive cumulative loss rather than abrupt mortality events. *Madracis pharensis* displayed moderate

mortality levels, higher than those of *Cladocora caespitosa* but consistently lower than those observed in *Balanophyllia europaea*, with a clear temporal increase across most stations. The lowest overall mortality occurred in *Cladocora caespitosa*, where values generally remained below 25%, despite pronounced spatial and temporal variability.

Bleaching patterns revealed contrasting trajectories between the two bleaching-capable species. *Cladocora caespitosa* exhibited frequent and pronounced bleaching that consistently exceeded mortality, particularly in later years, indicating a predominantly sublethal morphological response. In contrast, bleaching in *Madracis pharensis* was more closely related to mortality in both magnitude and temporal progression, indicating a reduced buffering ability between pigment loss and tissue death. These patterns demonstrate that bleaching cannot be interpreted as a direct proxy for mortality across species.

Growth form further modulated these responses. Colonial species exhibited greater spatial heterogeneity and lower mortality relative to bleaching, consistent with partial tissue loss and persistence of unaffected areas, whereas solitary species showed a more direct translation of tissue damage into whole-organism mortality. This interpretation is consistent with the broader view that coral morphology is functionally important and influences how corals interact with their environment (Zawada, Dornelas and Madin, 2019). Among solitary taxa, *Balanophyllia europaea* was characterised by extreme, episodic mortality, while *Leptopsammia pruvoti* showed slower but persistent population decline.

Across all analysed scleractinian species, microscopically intact tissue was rare, even in colonies classified as macroscopically healthy, indicating that sublethal tissue stress is widespread and often not detectable at the colony scale. Histopathological alterations consistently targeted the surface body wall epidermis and the gastrodermis, while the mesoglea generally retained structural integrity until advanced stages of tissue degradation. This pattern suggests that tissues directly involved in environmental interaction and metabolic function represent the primary targets of stress, whereas the mesoglea acts as a comparatively resilient compartment. Microbial accumulation, particularly within the epidermis, was consistently associated with necrotic tissue, although its extent varied among species. These observations are in line with coral pathology frameworks showing that gross appearance may

substantially underestimate tissue-level damage and that microscopic lesions commonly involve the epidermis, gastrodermis, and host–microbe interface before total structural collapse becomes macroscopically evident (Work and Aeby, 2006; Galloway et al., 2007; Hawthorn et al., 2023).

Clear interspecific differences emerged in overall histological condition. *Balanophyllia europaea* and *Madracis pharensis* showed relatively better tissue preservation, with a predominance of light lesions, low frequencies of severe pathology, and persistence of reproductive structures even in necrotic specimens. *Cladocora caespitosa* exhibited an intermediate profile, characterised by frequent moderate histopathology, a marked mismatch between macroscopic and microscopic health status, and progression from epithelial stress responses to gastrodermal necrosis, accompanied by complete loss of gametes in necrotic tissues. The most severe histological deterioration was observed in *Leptopsammia pruvoti*, which showed extensive gastrodermal necrosis, frequent epithelial collapse, and intense microbial and epibiotic colonisation, despite retaining gametogenic activity in a substantial proportion of degraded tissues.

Lesion severity followed a consistent trajectory across species, with light alterations dominated by epithelial hypertrophy and mucocyte proliferation, moderate lesions involving partial epithelial disintegration and gastrodermal degradation, and heavy pathology characterised by widespread gastrodermal necrosis, epithelial collapse, mesogleal denudation and skeletal exposure. This progression is consistent with histopathological descriptions of coral stress responses in which epithelial remodelling and mucus-related responses represent early protective reactions, while advanced lesions reflect loss of barrier integrity, tissue lysis, and systemic failure of host tissue organisation (Brown et al., 1995; Galloway et al., 2007; Hawthorn et al., 2023). Growth form further modulated these responses: colonial species displayed spatially heterogeneous lesions and partial tissue persistence, whereas solitary corals lacked intra-colony buffering capacity, resulting in rapid progression from localised damage to whole-polyp involvement. Together, these patterns indicate that histological vulnerability in scleractinian corals is governed by tissue function, growth form and species-specific life-history traits, rather than by symbiotic status alone.

5.4. *Cladocora caespitosa*

Cladocora caespitosa, the endemic coral of the Mediterranean, is distributed predominantly between 5 and 15 m depth, where it is highly exposed to thermal stress. In the present study, bleaching and partial tissue mortality were recorded in colonies during late summer months (August–September), coinciding with sea temperatures exceeding 28°C. This is consistent with long-term observations from Mljet National Park, where temperatures between 28–29°C have previously been identified as the threshold for bleaching onset in this species (Kružić et al., 2014).

Morphometric analyses revealed that *Cladocora caespitosa* exhibited spatially heterogeneous and parameter-specific responses during the 2020–2023 period, indicating that different aspects of colony condition respond at different temporal scales to environmental stress. Polyp density remained relatively stable at most stations, with a statistically significant interannual variation detected only at Veliko jezero. This limited response of polyp density contrasts with more dynamic patterns observed in bleaching and mortality and is consistent with previous observations that structural metrics in *C. caespitosa* change slowly and often only after prolonged or repeated stress (Kružić & Požar-Domac, 2003; Kersting et al., 2013; Zunino et al., 2018). In semi-enclosed systems such as Veliko jezero, however, reductions in polyp density have been reported following sustained thermal stress and progressive tissue loss (Kružić & Benković, 2008; Kružić et al., 2014; Kružić et al., 2025), supporting the interpretation that the significant variability observed at this site reflects cumulative rather than acute impacts. Long-term monitoring at Veliko jezero shows that reductions in polyp density can occur despite the persistence of relatively high colony density at the bank scale, indicating that structural population metrics may remain apparently stable while living tissue is progressively lost through repeated bleaching and necrosis (Kružić et al., 2025). This supports the interpretation that the significant interannual variability detected at this site reflects cumulative sublethal impacts rather than abrupt population decline (Kružić et al., 2012; Kružić et al., 2014; Kružić et al., 2025).

In contrast, the mortality rate exhibited statistically significant interannual increases at Ljubačka vrata and Veliko jezero, while remaining unchanged at the northern Adriatic stations. This spatial pattern is consistent with the species' characteristic response to thermal stress, in which tissue necrosis and partial colony mortality are more prominent than abrupt whole-colony loss (Rodolfo-Metalpa et al., 2005; Jiménez et al., 2016). At Veliko jezero, mortality is predominantly expressed as partial colony mortality driven by tissue necrosis following repeated thermal stress, with complete colony mortality exceeding 10% during extreme warm years such as 2003 and 2009 (Kružić et al., 2012; Kružić et al., 2014). The absence of recovery of necrosed areas indicates that the significant mortality signal reflects the accumulation of irreversible tissue loss across successive warming events rather than episodic whole-colony death (Kružić et al., 2025). Elevated seawater temperatures have repeatedly been identified as a primary driver of mortality in *C. caespitosa* and other sessile Mediterranean invertebrates, both during discrete warming events and under sustained anomalously warm conditions (Rodolfo-Metalpa et al., 2000, 2005, 2006; Garrabou et al., 2009; Jiménez et al., 2013, 2014; Kersting et al., 2013a, 2014a; Kružić et al., 2016). Similar site-dependent mortality responses have been documented during previous Mediterranean warming events, where local hydrodynamics, depth distribution, and cumulative heat exposure modulated biological outcomes (Kružić & Benković, 2008; Kersting et al., 2013; Kružić et al., 2014; Kružić et al., 2025).

Bleaching rate showed the strongest and most consistent interannual signal, with statistically significant differences detected at all stations. This confirms bleaching as the most sensitive morphometric indicator of thermal stress in *Cladocora caespitosa*, in agreement with earlier studies reporting rapid bleaching responses during anomalously warm summers in both the Adriatic and the eastern Mediterranean (Rodolfo-Metalpa et al., 2006; Kersting et al., 2013). In Veliko jezero, bleaching of *C. caespitosa* polyps has been documented since the late 1990s and represents the earliest recorded coral bleaching event in the Mediterranean (Kružić et al., 2014; Kružić et al.,2025). Bleaching is typically initiated during summer months, when seawater temperatures exceed approximately 27°C and thermal anomalies penetrate to depths of up to 15 m, underscoring the sensitivity of this semi-enclosed system to positive temperature anomalies (Kružić et al., 2014). Extreme bleaching events have been reported during particularly warm summers, such as in 2003, when prolonged exposure to

temperatures around 29°C resulted in extensive partial bleaching and complete colony mortality, particularly at 10 m depth (Kružić et al., 2014). Variability in bleaching severity among colonies within the coral bank has been attributed to local-scale factors, including bank morphology and hydrodynamic conditions, which may modulate thermal exposure and stress intensity (Kružić et al., 2025). Importantly, elevated bleaching did not always translate into immediate mortality, supporting the view that bleaching in this species often represents an early or intermediate stress response rather than a direct predictor of colony death (Jiménez et al., 2016).

Histological analyses revealed extensive tissue-level pathology across samples, including those classified as healthy based on macroscopic appearance. Only a subset of macroscopically healthy samples were confirmed as histologically intact, demonstrating that visual assessments alone substantially underestimate tissue impairment. This discrepancy is well documented in coral health studies and reflects the high sensitivity of histopathological methods for detecting early or sublethal stress (Work & Aeby, 2006; Galloway et al., 2007).

The most frequent epidermal alteration was an increase in mucocytes, often accompanied by epidermal hypertrophy. Such changes are widely interpreted as early protective responses to environmental stress, associated with enhanced mucus production and epithelial remodelling (Brown et al., 1995; Oakley & Davy, 2018). Similar mucocyte proliferation has been described in *C. caespitosa* and other temperate corals exposed to elevated temperatures and is considered indicative of acute stress that may still be reversible (Rodolfo-Metalpa et al., 2005; Jiménez et al., 2016).

More advanced lesions, including loss of epidermal integrity, mesogleal disruption, and extensive gastrodermal necrotic zones, indicate a transition towards irreversible tissue damage. The frequent observation of degraded and reduced symbiotic dinoflagellates within the gastrodermis aligns with cellular-scale models of bleaching that emphasise oxidative stress, symbiont dysfunction, and host-mediated breakdown of the symbiosis (Nielsen et al., 2018; Oakley & Davy, 2018). Elevated bacterial presence, particularly within necrotic tissues, further suggests the development of dysbiosis and opportunistic microbial proliferation, a

pattern increasingly recognised as a secondary but important component of coral stress responses (Galloway et al., 2007; Smith et al., 2023).

The complete absence of gametes in necrotic samples indicates that thermal stress and tissue degradation are accompanied by a suppression of reproductive investment. Reduced gametogenesis following warming events has previously been reported for *C. caespitosa* and may have long-term consequences for population resilience and recovery (Rodolfo-Metalpa et al., 2008; Kersting et al., 2017).

Because *C. caespitosa* inhabits depths between 5 and 15 m, marine heatwave (MHW) exposure was interpreted exclusively using temperature records from these depths. Moreover, all biological sampling was conducted in autumn, after the summer thermal maximum, meaning that the observed morphometric and histological conditions reflect the integrated effects of preceding warm-season MHWs, including both acute bleaching responses and delayed outcomes such as necrosis and microbial dysbiosis.

At Slovenian and middle Adriatic stations, where site-specific MHW data were unavailable, increased bleaching in 2022–2023 likely reflects regionally warm summers rather than discrete local events. The absence of a uniform mortality signal at these sites highlights the importance of local environmental modulation and supports the view that background warming can predispose populations to stress while not necessarily triggering immediate tissue loss (Kersting et al., 2017; Smith et al., 2023).

At Veliko jezero, MHW exposure intensified progressively between 2020 and 2023, both in frequency and cumulative duration, with a clear shift from predominantly deep to shallow and vertically extensive warming. In 2020, MHW activity was limited and mainly confined to depth, with a single short event at 10 m (9 days) and multiple events at 15 m (five events; 39 days cumulative), while no MHWs were recorded at 5 m. In 2021, MHWs expanded into shallower water, with two events at 5 m (23 days) and a reduced signal at 15 m (two events; 17 days). A pronounced escalation occurred in 2022, when MHWs affected the entire depth range occupied by *Cladocora caespitosa*, with events recorded at 5 m (2 events; 24 days), 10 m (3 events; 32 days), and 15 m (1 event; 9 days). This pattern intensified further in 2023,

particularly in shallow water, where six MHW events at 5 m lasted a total of 52 days, accompanied by substantial exposure at 10 m (3 events; 35 days) and continued, though weaker, exposure at 15 m (2 events; 17 days). Importantly, several MHWs in both 2022 and 2023 occurred synchronously at 5 and 10 m, indicating coherent warming of the upper water column rather than isolated surface heating.

The biological responses observed at Veliko jezero are consistent with this progressive intensification of MHW exposure. Elevated bleaching rates in 2022 and 2023 coincide with prolonged shallow-water MHWs, while increased mortality and severe histological damage reflect cumulative stress following repeated exposure. Similar lagged progressions from bleaching to necrosis have been documented during previous warming events affecting *C. caespitosa* in the Mediterranean (Rodolfo-Metalpa et al., 2005; Kersting et al., 2013; Kružić et al., 2014; Jiménez et al., 2016; Kružić et al., 2025) and are increasingly recognised as characteristic of temperate corals exposed to recurrent heatwaves (Smith et al., 2023).

Histological evidence provides a mechanistic explanation for this progression. Early responses such as mucocyte proliferation and epidermal hypertrophy correspond to short-term protective mechanisms, while widespread loss of tissue integrity, gastrodermal necrosis, symbiont degradation, and elevated bacterial loads indicate a shift towards systemic tissue failure. Experimental and observational studies have shown that repeated or prolonged thermal stress can overwhelm compensatory responses, leading to irreversible damage even when peak temperatures are only moderately elevated (Rodolfo-Metalpa et al., 2008; Sahin et al., 2023). The temporal offset between peak summer MHWs and autumn sampling is critical for interpreting these patterns. Rather than capturing acute bleaching alone, the dataset reflects a post-MHW damage window, in which delayed necrosis, microbial proliferation, and partial colony mortality become apparent. This lagged response explains why bleaching and mortality do not always peak simultaneously and underscores the importance of histological analyses for detecting cumulative and sublethal effects that remain largely undetectable at the colony scale.

Across the full study period, bleaching emerged as the most sensitive and immediate morphometric indicator of thermal stress, while mortality was spatially constrained and

primarily evident at sites exposed to repeated and prolonged marine heatwave events. Polyp density remained comparatively stable, even under conditions of pronounced histological pathology, indicating that structural metrics alone may underestimate the extent of physiological impairment. Collectively, the integration of morphometric, histological, and marine heatwave data supports a model in which *Cladocora caespitosa* can withstand episodic thermal stress through short-term protective responses, but where repeated, shallow-water marine heatwaves of increasing duration substantially elevate the probability of transition from sublethal stress to tissue necrosis, microbial dysbiosis, and partial or whole-colony mortality.

5.5. Balanophyllia europaea

Balanophyllia europaea is a solitary, zooxanthellate coral endemic to the Mediterranean Sea, predominantly inhabiting shallow infralittoral zones (up to 15 m depth). Its wide distribution, ecological plasticity, and sensitivity to thermal fluctuations make it a valuable model species for studying the impacts of climate change on temperate coral communities (Goffredo et al., 2009). As a non-reef-building scleractinian, *B. europaea* maintains a symbiotic relationship with dinoflagellates from the family Symbiodiniaceae, which are critical to its nutrition and thermal resilience.

Morphometric analyses indicated that *Balanophyllia europaea* exhibited a spatially heterogeneous and parameter-specific response during the 2020–2023 period, reflecting differences in local environmental conditions and cumulative stress exposure. Polyp density remained relatively stable at most stations across the study period, with statistically significant interannual variation detected only at Balun, Mana, and Rt Lenga. The overall stability of polyp density, despite evident tissue-level impairment and elevated mortality at several sites, suggests that this structural parameter responds slowly to environmental stress and likely reflects long-term population processes rather than short-term disturbances. Similar inertia of population density has been reported for *B. europaea*, where growth and recruitment

dynamics buffer immediate numerical declines even under unfavourable thermal conditions (Goffredo et al., 2004; Goffredo et al., 2008; Caroselli et al., 2011).

In contrast, the mortality rate exhibited clearer interannual variability and site-specific responses. Statistically significant differences were detected at Ljubačka vrata, Veli Garmenjak, Mali Obručan, Veliko jezero, and Rt Lenga, while other stations showed increasing but non-significant trends. This spatial pattern indicates that mortality in *B. europaea* is mostly modulated by local environmental context rather than regional background warming alone. Previous observations from the Adriatic Sea have shown that *B. europaea* experiences partial or total polyp mortality during anomalously warm summers, particularly in semi-enclosed or weakly flushed environments, where heat accumulation is more pronounced (Kružić & Popijač, 2015; Garrabou et al., 2009). The lack of a consistent mortality signal across all stations further supports the notion that mortality represents a later-stage response, emerging only where cumulative stress exceeds the species' compensatory capacity.

Histological analyses revealed extensive tissue-level pathology, including in samples that were macroscopically classified as healthy. Only a small subset of visually healthy polyps retained a fully intact microanatomical organisation, confirming that macroscopic assessment alone substantially underestimates sublethal stress in *B. europaea*. This discrepancy is well documented in coral health studies and reflects the high sensitivity of histopathological approaches in detecting early or cryptic lesions (Work & Aeby, 2006; Galloway et al., 2007; Hawthorn et al., 2023).

The most frequent lesions were recorded in the gastrodermis and involved the symbiotic dinoflagellates. Alterations in endosymbiont morphology, including darkened and shrunken cells, were the most prevalent light lesions, affecting more than 65% of analysed samples. Reductions in endosymbiont abundance and extensive gastrodermal necrosis were also common, particularly in samples categorised as moderate to severe histopathology. These findings align with established cellular models of thermal stress in symbiotic cnidarians, where elevated temperatures disrupt photosynthetic function, promote oxidative stress, and ultimately lead to host-mediated degradation or loss of symbionts (Brown et al., 1995; Dunn et al., 2004; Helgoe et al., 2024).

The epidermal layer also showed frequent pathological changes, including loss of integrity, hypertrophy, and increased mucocyte abundance. Such epidermal remodelling is widely interpreted as an early protective response, associated with enhanced mucus production and barrier function under stress conditions (Palmer et al., 2008; Banin et al., 2001). However, severe cases characterised by epidermal disruption and exposure of the mesoglea indicate a transition towards irreversible tissue damage. Mesogleal alterations were comparatively less frequent, but both swelling and reduction were recorded, often in association with extensive gastrodermal lysis, resulting in areas of nude mesoglea. Increased bacterial presence, particularly within the surface epidermis and necrotic gastrodermal zones, further suggests the development of dysbiosis and opportunistic microbial proliferation, a pattern increasingly recognised as a secondary consequence of thermal stress rather than a primary cause (Galloway et al., 2007; Palladino et al., 2022).

Reproductive structures were present in a substantial proportion of samples; however, atretic oocytes were recorded in 22% of analysed polyps, and severe histopathology was associated with reduced mesenterial filaments. These observations suggest that thermal stress and tissue degradation may compromise reproductive investment in *B. europaea*, consistent with previous findings indicating that gametogenesis and brooding can be impaired under unfavourable thermal conditions (Goffredo et al., 2002; Kružić & Popijač, 2015).

Because *B. europaea* inhabits shallow infralittoral depths, interpretation of biological responses was restricted to marine heatwave (MHW) exposure recorded at 5, 10, and 15 m. All biological sampling was conducted in autumn, after the summer thermal maximum, meaning that the observed morphometric and histological conditions reflect integrated post-MHW responses rather than immediate thermal effects.

Analysis of temperature records revealed an increase in both the frequency and duration of MHWs between 2020 and 2023, with several intense and prolonged events affecting the shallow water column. Notably, multiple MHWs were recorded simultaneously at Kornati National Park and Veliko jezero (Mljet National Park), particularly during 2022 and 2023, indicating coherent regional warming rather than isolated local anomalies. These synchronous events affected the full depth range occupied by *B. europaea* (5–15 m), increasing the

likelihood of sustained thermal exposure. Such vertically extensive MHWs have been identified as particularly detrimental, as they limit the availability of thermal refugia in shallow-water habitats (Hobday et al., 2016; Darmaraki et al., 2024; Garrabou et al., 2022).

The biological patterns observed are consistent with a cumulative stress model. Repeated exposure to MHWs across consecutive years likely predisposed polyps to progressive tissue impairment, first detectable at the cellular level as symbiont degradation and gastrodermal necrosis, and later expressed macroscopically as increased mortality. The lack of a consistent response in polyp density supports the interpretation that population-level structural change lags behind physiological deterioration and individual loss. Similar delayed progressions from sublethal stress to necrosis and mortality have been documented for *B. europaea* and other Mediterranean corals following recurrent warming events (Garrabou et al., 2009; Kružić & Popijač, 2015; Carbonne et al., 2024).

Histological evidence provides a mechanistic framework linking MHW exposure with morphometric outcomes. Early tissue responses, such as epidermal hypertrophy and mucocyte proliferation, likely represent short-term protective mechanisms following thermal stress. However, repeated or prolonged MHWs appear to overwhelm these compensatory responses, leading to systemic tissue failure, disruption of host–symbiont associations, microbial proliferation, and suppression of reproductive processes. Experimental and field studies have shown that even moderate but sustained thermal anomalies can induce irreversible damage when exposure is recurrent, particularly in temperate corals adapted to strong seasonal variability (Rodolfo-Metalpa et al., 2005; Sahin et al., 2023).

The temporal offset between peak summer MHWs and autumn sampling is therefore critical for interpreting these results. Rather than capturing acute bleaching alone, the dataset reflects a post-MHW damage window, in which delayed necrosis, microbial dysbiosis, and reproductive impairment become evident. This explains why mortality and severe histopathological damage were observed even when changes in polyp density remained limited. Collectively, the integration of morphometric, histological, and marine heatwave data indicates that *Balanophyllia europaea* can tolerate episodic thermal stress through short-term protective responses, but repeated shallow-water marine heatwaves of increasing frequency and

duration substantially elevate the risk of transition from sublethal stress to tissue necrosis, population-level decline, and reduced reproductive capacity.

5.6. *Leptopsammia pruvoti*

Leptopsammia pruvoti is a solitary, azooxanthellate scleractinian coral distributed in shaded vertical cliffs and overhangs, typically between 15 and 40 m depth in the Mediterranean Sea. Unlike shallow-water zooxanthellate corals, *L. pruvoti* does not engage in symbiosis with dinoflagellates, which may provide certain advantages under thermal stress conditions. Nevertheless, it remains vulnerable to prolonged heat exposure, particularly in the absence of refugia or in poorly ventilated microhabitats (Goffredo et al., 2008; Caroselli et al., 2021).

Across all analysed stations and throughout the study period (2020–2023), polyp density of *Leptopsammia pruvoti* remained remarkably stable, with no statistically significant interannual differences detected. This pattern was consistent across protected and unprotected sites, as well as across regions characterised by contrasting thermal regimes. Such stability in standing density is in line with previous demographic studies on *L. pruvoti*, which have shown that population density in this species is weakly coupled to temperature variability and does not exhibit a direct relationship with sea surface temperature (Goffredo et al., 2008; Goffredo et al., 2010; Caroselli et al., 2012). Moreover, the solitary growth form of *L. pruvoti* and its occupation of shaded coralligenous microhabitats likely present a degree of demographic inertia, buffering short-term losses and delaying detectable changes in population density.

In contrast to polyp density, mortality rate exhibited a strong and consistent temporal signal, with statistically significant differences among years at all stations ($p < 0.05$). Mortality increased progressively towards 2022 and peaked in 2023, a pattern observed across regions and depths. The highest mortality rates were recorded at Mljet (Rt Lenga and Štit), followed by Kornati and Telašćica, broadly mirroring the spatial pattern of cumulative MHW exposure at depths of 20–30 m. This spatial concordance supports a causal link between subsurface thermal anomalies and increased mortality, particularly when considering the timing of biological sampling in autumn, which captured the integrated effects of preceding summer

and early autumn marine heatwaves. The divergence between stable density and rising mortality highlights a critical demographic mismatch, whereby mortality is increasing but has not yet translated into measurable density decline. Such a pattern is consistent with observations from Mediterranean mass mortality events, where elevated mortality may persist for several years before population-level consequences become apparent (Garrabou et al., 2009; Coma et al., 2009). In solitary corals, this delay may be further amplified by the longevity of skeletal structures and the slow turnover of individuals (Goffredo et al., 2010). Importantly, increased mortality in *L. pruvoti* occurred even in the absence of symbiotic bleaching, reinforcing the notion that azooxanthellate corals are not immune to thermal stress, but instead exhibit alternative stress pathways.

Histological analysis revealed extensive tissue pathology that was frequently not detectable through macroscopic assessment alone. While nearly half of the sampled polyps were initially classified as healthy in the field, microscopic examination confirmed that only a small fraction of samples were truly histologically intact. This discrepancy underscores the limitations of gross morphology as an indicator of coral health, a problem widely recognised in coral pathology (Work, 2004; Work & Aeby, 2006; Hawthorn et al., 2023).

The high prevalence of light to heavy histopathological lesions indicates that a large proportion of the population was experiencing sublethal stress, a condition that may persist for extended periods before culminating in visible tissue loss or mortality. Similar patterns have been described in both tropical and temperate corals exposed to chronic or repeated thermal anomalies, where histology reveals early warning signs of physiological breakdown (Brown et al., 1995; Galloway et al., 2007).

The gastrodermis emerged as the primary target of pathological alteration, with frequent necrotic zones, tissue disintegration, and reduction in cellular density. Gastrodermal vulnerability to thermal stress has been widely documented and is often associated with impaired digestion, nutrient assimilation, and overall energy balance (Brown et al., 1995; Hawthorn et al., 2023). In *L. pruvoti*, the absence of endosymbiotic dinoflagellates excludes classical bleaching mechanisms, indicating that gastrodermal necrosis reflects direct thermal and metabolic stress, rather than symbiont-derived oxidative damage.

Epidermal responses differed between lesion severities. Mildly affected tissues commonly exhibited epithelial hypertrophy and increased mucocyte density, suggesting an adaptive or protective response to prolonged irritation or stress. Comparable epithelial changes have been interpreted as defence mechanisms aimed at enhancing mucus production and barrier function (Galloway et al., 2007; Work & Aeby, 2006). In severely affected polyps, however, epidermal thinning and loss of integrity predominated, reflecting a transition from compensatory to degenerative processes.

The mesoglea generally retained structural continuity, although swelling and reduction were observed, particularly in heavily affected samples. This relative resilience of the mesoglea may provide temporary structural support, delaying complete tissue collapse, but its degradation in advanced lesions suggests that chronic stress ultimately compromises even the most robust tissue compartments.

The presence of gametogenic structures in a substantial proportion of samples, including those with pronounced tissue damage, indicates that reproductive activity may persist despite physiological impairment. Previous studies have shown that reproductive output in *L. pruvoti* is relatively insensitive to temperature gradients across its distribution range (Goffredo et al., 2005). However, the coexistence of gametogenesis with severe histopathology raises important questions regarding energetic trade-offs, gamete quality, and long-term reproductive success. Such separation between reproduction and somatic health has been reported in other corals and may represent a “last-resort” allocation strategy under chronic stress (Caroselli et al., 2019; Carbonne et al., 2024). Whether this strategy enhances population persistence or accelerates exhaustion remains unresolved and warrants further investigation.

The analysis of marine heatwaves at ecologically relevant depths (20 and 30 m) revealed pronounced interannual and depth-specific variability in thermal stress exposure between 2020 and 2023. Subsurface MHWs were detected in all analysed regions (Telašćica, Kornati and Mljet – Rt Lenga), confirming that thermal anomalies repeatedly penetrated into the depth range inhabited by *L. pruvoti*. The cumulative thermal load increased over time, with 2021 representing a low-stress year, while 2020 and 2022 showed moderate but recurrent exposure,

and 2023 emerged as the most thermally stressful year. In 2020, both Telašćica and Kornati experienced two MHW events at 20 m, reaching category III (Severe), including a synchronous regional event in mid-June. At 30 m, thermal stress was less intense overall, although Mljet (Rt Lenga) recorded three events with a cumulative duration exceeding 40 days, indicating prolonged subsurface exposure. In contrast, 2021 was characterised by sporadic, short-lived and low-category MHWs at both depths, providing a relative thermal respite. In 2022, MHW frequency increased again, particularly at 20 m, where Telašćica and Kornati each recorded three events, including a regionally overlapping episode from late May to early June that partially involved Mljet. Although maximum intensities were generally lower (category I–II), repeated exposure early in the warming season increased cumulative stress. At 30 m, fewer events were recorded, but late-season anomalies occurred closer to the sampling period. The most pronounced thermal signal occurred in 2023, when MHWs were frequent, long-lasting and persistent into early autumn. At 20 m, Kornati experienced seven events (≈61 cumulative days), Telašćica four events (≈43 days), and Mljet three events, including category III exposure. At 30 m, both Telašćica and Kornati recorded six to seven events, with cumulative durations of approximately 47–50 days. Importantly, prolonged MHWs extended into September–October, overlapping temporally across multiple locations.

Given that biological sampling was consistently conducted in autumn, the observed morphometric and histological patterns represent post-exposure responses to both late-season MHWs and the cumulative effects of earlier events. This temporal alignment is reflected in the biological data. The absence of density decline, even in years characterised by intense and recurrent marine heatwaves (MHWs), suggests that density alone is a poor proxy for population health in this solitary, non-zooxanthellate coral. Similar distinction between density and physiological stress has been reported for other temperate azooxanthellate corals, where individuals may persist structurally while experiencing progressive tissue impairment (Carbonne et al., 2024; Vuleta, 2024). Therefore, the stability of polyp density observed in this study should not be interpreted as evidence of resistance to thermal stress, but rather as an indication that sublethal impacts precede demographic collapse, a pattern increasingly recognised in benthic invertebrates exposed to climate-driven stressors (Garrabou et al., 2022). While polyp density remained stable across all years, mortality rates increased

significantly towards 2022 and peaked in 2023, coinciding with the escalation in MHW frequency, duration and late-season persistence. Histological analyses further revealed a high prevalence of gastrodermal necrosis, epithelial degradation and microbial colonisation, particularly in years following repeated or prolonged MHW exposure. The combination of stable density, increasing mortality and widespread sublethal tissue damage indicates a progressive erosion of individual health preceding population-level change. Such delayed responses are consistent with previous observations from Mediterranean mass mortality events, where cumulative thermal stress leads to delayed demographic consequences (Garrabou et al., 2009; Coma et al., 2009; Garrabou et al., 2022). The detection of MHWs at both 20 and 30 m further demonstrates that depth does not provide an effective thermal refuge for coralligenous assemblages, supporting recent evidence of increasing subsurface warming in the Mediterranean and Adriatic Seas (da Costa et al., 2024; Darmaraki et al., 2024).

The results demonstrate that *Leptopsammia pruvoti* exhibits a complex response to marine heatwaves, characterised by stable population density, increasing mortality, and widespread sublethal histopathological damage. The integration of morphometric, histological, and thermal data reveals that azooxanthellate corals are highly susceptible to chronic thermal stress, despite the absence of symbiont-mediated bleaching mechanisms. The high prevalence of hidden tissue pathology underscores the importance of histological approaches for detecting early stress signals, particularly in temperate and deep-dwelling corals. As MHWs increase in frequency, duration and depth penetration, such sublethal impacts may progressively undermine population resilience, ultimately leading to delayed but severe demographic consequences.

5.7. Madracis pharensis

Madracis pharensis is a colonial, nodular coral species native to the Mediterranean and eastern Atlantic, often found in dimly lit sublittoral habitats between 10 and 30 m depth. Unlike most shallow-water scleractinians, *M. pharensis* can thrive in mesophotic zones and exhibits a degree of physiological plasticity in its trophic strategy, alternating between autotrophy and

heterotrophy depending on light availability (Fricke et al., 1987; Rosenberg et al., 2019). Despite this adaptability, recent studies have indicated increasing sensitivity of this species to ocean warming and associated MHWs (Rodolfo-Metalpa et al., 2000, 2005, 2006; Garrabou et al., 2009).

Across most investigated stations, *Madracis pharensis* exhibited relatively stable population density over the 2020–2023 period, with no significant interannual differences detected at Ljubačka vrata, Veli Garmenjak, Sestrica Vela, Balun, Mana, Rt Lenga and Hrid Štit. A significant temporal variation was observed only at Mali Obručan, indicating a site-specific response rather than a regional trend. The overall stability of polyp density suggests that recent thermal anomalies did not result in immediate population collapse of *M. pharensis*, even during years characterised by intense marine heatwave activity. This pattern is consistent with previous observations that *M. pharensis* is a structurally persistent species, forming encrusting or nodular colonies tightly attached to the substratum, which may reduce whole colony loss during disturbance events (Morri et al., 2000; Benzoni et al., 2018). Similar differentiation between population persistence and physiological stress has been reported for other temperate and mesophotic scleractinians, where colonies remain present despite substantial tissue-level impairment (Kersting et al., 2013; Carbonne et al., 2024). The significant variation observed at Mali Obručan may therefore reflect local environmental conditions or cumulative stress exposure rather than a species-wide sensitivity.

In contrast to the relative stability of population density, mortality rates increased progressively across stations from 2020 to 2023, with the highest values consistently recorded in the final year of the study. Comparable increases in partial mortality without immediate population loss have been documented in Mediterranean benthic assemblages following prolonged thermal anomalies (Garrabou et al., 2009; Garrabou et al., 2022).

Bleaching rates showed a similar temporal increase but displayed marked spatial and microhabitat-dependent variability. This pattern should be interpreted in light of the facultative symbiotic nature of *M. pharensis*. Colonies inhabiting illuminated microhabitats (vertical walls and overhang edges) commonly host Symbiodiniaceae, whereas colonies located deeper within crevices and caves naturally lack symbionts (Frade et al., 2008;

Bongaerts et al., 2015; Goodbody-Gringley et al., 2024). Consequently, bleaching represents a habitat-specific manifestation of stress and cannot be applied uniformly across all colonies. This ecological trait explains why bleaching rates, although increasing in warmer years, do not directly mirror mortality or population density trends. Similar depth- and light-dependent bleaching responses have been reported in *Madracis* spp. and other corals with flexible symbiotic associations, where bleaching reflects symbiont dysfunction rather than whole-organism failure (Frade et al., 2010; Oakley & Davy, 2018; Helgoe et al., 2024).

Histological analyses revealed that macroscopic appearance substantially underestimated tissue-level degradation in *M. pharensis*. While several colonies appeared healthy in situ, only a small fraction retained intact histological architecture, with the majority exhibiting mild to moderate lesions and a subset showing severe tissue impairment. This discrepancy between external appearance and internal condition highlights the enigmatic nature of stress responses in this species.

The predominance of epidermal lesions, including loss of integrity, hypertrophy and increased mucocyte density, is consistent with non-specific stress responses aimed at maintaining epithelial cohesion and reinforcing the mucus barrier (Galloway et al., 2007; Work, 2004). Mesogleal swelling and the presence of nude mesoglea further indicate compromised tissue mechanics, a feature commonly associated with chronic stress rather than acute disease processes (Hawthorn et al., 2023).

Gastrodermal alterations, including necrotic zones, tissue reduction and changes in symbiont condition, align with histological descriptions of thermal stress and bleaching mechanisms in scleractinian corals (Brown et al., 1995; Oakley & Davy, 2018). The occurrence of darkened, shrunken symbionts and reduced symbiont density, even in the absence of visible bleaching, suggests impaired host–symbiont functioning at the cellular level. Comparable sublethal histopathological responses have been documented in *M. pharensis* exposed to chronic pollution, where tissue degradation precedes overt colony loss (Nardi et al., 2024).

Notably, bacterial presence was sparse and largely restricted to the surface epidermis, with no evidence of invasive infections. This pattern supports the interpretation that tissue

degradation was primarily stress-driven rather than disease-mediated, in line with consensus histopathological frameworks for coral lesions (Work, 2004).

Marine heatwave analysis restricted to 20 and 30 m depths corresponding to the distribution of *Madracis pharensis* revealed pronounced interannual contrasts in cumulative thermal stress. In 2020, cumulative intensity at 20 m reached comparable values in Kornati (11.43) and Telašćica (11.33), while at Mljet (Lenga) cumulative intensity at 30 m was notably higher (19.16), indicating prolonged thermal exposure at depth. In contrast, 2021 represented a low-stress baseline year, with cumulative intensity values ≤3.40 across all regions and depths (e.g. Kornati 30 m: 2.50; Mljet Lenga 20 m: 3.40; Telašćica 20 m: 0.22).

Thermal stress increased again in 2022, with moderate cumulative intensity recorded at 20 m in all regions (Kornati: 6.52; Mljet Lenga: 6.50; Telašćica: 9.57), whereas cumulative intensity at 30 m remained low where data were available (e.g. Telašćica 30 m: 0.80). A marked shift occurred in 2023, which clearly emerged as an extreme year. At 20 m, cumulative intensity reached 29.50 in Kornati (seven MHW events) and 28.82 in Telašćica (four events), while Mljet Lenga reached 10.29. Importantly, elevated cumulative intensity was also recorded at 30 m in the same year (Kornati: 19.80; Telašćica: 18.23; Mljet Lenga: 5.18), demonstrating that intense thermal stress penetrated well into mesophotic habitats.

This temporal pattern offers a methodical interpretation of the observed biological responses of *M. pharensis*. The year 2023, characterised by the highest cumulative intensity at both 20 and 30 m, coincides with the highest recorded mortality and bleaching rates across most stations. In contrast, the low cumulative intensity observed in 2021 corresponds to generally low levels of tissue deterioration. Despite the extreme cumulative thermal stress in 2023, polyp density remained largely stable at most sites, indicating that *M. pharensis* does not respond to marine heatwaves through immediate population collapse, but rather through progressive tissue-level impairment and partial mortality.

Taken together, these results indicate that *Madracis pharensis* exhibits population-level persistence under recent marine heatwave regimes, but at the cost of widespread tissue degradation and increased partial mortality. Its facultative symbiosis likely modulates visible

bleaching responses, reducing acute photoinhibition in cryptic habitats while not preventing direct thermal damage to host tissues. The accumulation of sublethal histopathological lesions over years of high cumulative thermal intensity suggests that continued warming may progressively erode colony function, potentially affecting growth, competitive ability and long-term reproductive output. As such, *M. pharensis* may act as a "cryptic survivor" of marine heatwaves, persisting structurally while undergoing hidden physiological decline, highlighting the importance of integrating histological and thermal data when assessing coral resilience in a warming Mediterranean Sea.

5.8. Comparative analyses of gorgonians

Both *Eunicella cavolini* and *Paramuricea clavata* exhibited a consistent increase through time in colony mortality and in the proportion of affected (degraded) colonies, indicating a shared pattern of progressive colony-level impairment rather than stable conditions punctuated by isolated losses. Such parallel increases in mortality and injury are widely reported for Mediterranean gorgonian forests subjected to recurrent marine heatwaves and are considered characteristic of cumulative thermal stress rather than responses to single extreme events (Garrabou et al., 2022; Gómez-Gras et al., 2021). Long-term field studies have shown that repeated exposure to summer heat anomalies leads to a progressive escalation of both partial tissue loss and colony mortality, particularly when impacts are assessed after the thermal season (Garrabou et al., 2009; Iborra et al., 2022), as in the present study.

In *Eunicella cavolini*, the close alignment between increasing mortality and degradation is consistent with demographic frameworks that interpret visible injury and tissue loss as reliable indicators of disturbance progression at the colony scale (Sini et al., 2015). Experimental and field-based studies further demonstrate that necrosis and subsequent mortality in *Eunicella spp.* are strongly related to the duration and recurrence of thermal stress, with impacts often becoming evident only after repeated summer exposures (Pivotto et al., 2015; Garrabou et al., 2022). In *P. clavata*, although both mortality and degradation increased overall, previous Mediterranean studies indicate that visible degradation can be more unevenly expressed

among sites, even under comparable thermal forcing, reflecting species-specific life-history traits and local environmental modulation of stress expression (Garrabou et al., 2009; Gómez-Gras et al., 2021). Together, these findings support the interpretation of increased death and impacted rates in both species as related but species-specific expressions of chronic thermal stress under periodic marine heatwaves.

Despite differences in ecology and trophic strategy, *Eunicella cavolini* and *Paramuricea clavata* exhibited convergent histopathological signatures indicative of chronic stress, while differing in the intensity and functional implications of tissue impairment. In both species, histological alterations were dominated by epithelial barrier disruption, inflammatory cell infiltration, and extensive gastrodermal damage, a lesion complex widely recognised as a general stress response in corals exposed to prolonged environmental disturbance rather than an acute, pathogen-driven disease (Work and Aeby, 2006; Galloway et al., 2007; Dennis et al., 2020). The high prevalence of amoebocytosis and mesogleal infiltration observed in both species reflects sustained immune activation, consistent with reports of chronic inflammatory states in Mediterranean gorgonians following thermal anomalies (Carella et al., 2014; Gobbato et al., 2024).

However, the functional consequences of these lesions differed between species. In *E. cavolini*, histopathology frequently involved epidermal necrosis, gastrodermal dissociation, and mesogleal tissue loss, but colonies often retained structurally intact regions with apparently functional polyps, suggesting that parts of the colony can retain functional tissue despite repeated thermal stress. Similar patterns of patchy tissue impairment and partial recovery have been described for symbiotic gorgonians, where sublethal damage accumulates over time without immediate colony collapse (Gómez-Gras et al., 2022; Canessa et al., 2024). In contrast, *P. clavata* showed a more common involvement of gastrodermal tissues and axial structures, with widespread gastrodermal necrosis, mesogleal collapse, and frequent alterations of the axial skeleton, indicating deeper impairment of internal transport, feeding, and structural integrity. For an asymbiotic, circalittoral species, such gastrodermal failure likely has disproportionate energetic consequences, as feeding and gastrovascular function

represent the primary sources of energy acquisition and internal resource distribution (Coma et al., 1994; Coma et al., 2009).

Importantly, both species exhibited a marked discrepancy between macroscopic appearance and histological condition, with colonies often appearing externally intact while showing extensive internal pathology. This mismatch has been repeatedly emphasised in coral pathology frameworks as a mark of chronic stress syndromes, where tissue-level dysfunction precedes visible colony degradation or mortality (Work et al., 2014; Traylor-Knowles, 2019). Taken together, the comparative histological evidence shows that although *E. cavolini* and *P. clavata* exhibit similar inflammatory and degenerative responses to repeated thermal stress, the degree to which internal tissue damage affects colony function and survival differs between species, likely due to differences in symbiotic status, energy acquisition, and structural organisation.

5.9. Eunicella cavolini

Eunicella cavolini is a common Mediterranean gorgonian inhabiting coralligenous habitats from 20 to 80 m depth. It plays a key role in structuring benthic assemblages and facilitating biodiversity, but like other octocorals, it is highly susceptible to warming-induced stress. Although often found deeper than *P. clavata*, *E. cavolini* shares similar vulnerabilities due to slow growth, low recruitment, and structural fragility (Cupido et al., 2012; Linares et al., 2008).

Despite the increasing frequency and intensity of MHWs in the Mediterranean Sea, the population density of *Eunicella cavolini* remained stable between 2020 and 2021 across all investigated stations. The absence of significant temporal variation in colony density, regardless of protection status or geographic position, indicates that no acute demographic collapse occurred during the study period. This apparent stability is consistent with the life-history traits of long-lived Mediterranean gorgonians, characterised by slow growth, delayed maturity, and low natural turnover, which may provide substantial demographic stability (Linares et al., 2007; Linares et al., 2008; Garrabou et al., 2009).

In contrast to density, colony-scale indicators revealed a markedly different trajectory. Colony mortality rates increased significantly through time at all stations between 2020 and 2023, with strong temporal effects detected irrespective of site. Importantly, the progressive increase in mortality did not manifest as a reduction in colony abundance, suggesting that mortality was predominantly partial rather than whole-colony. Such partial mortality patterns have been widely reported in Mediterranean gorgonians following thermal anomalies and are recognised as a characteristic of chronic, sublethal stress rather than catastrophic disturbance (Garrabou et al., 2009; Coma et al., 2009; Iborra et al., 2022).

Colony degradation, expressed as the proportion of affected colonies, emerged as the most sensitive morphological indicator. Degradation increased sharply and consistently from 2020 to 2023 at all stations, exceeding the magnitude of change observed in mortality rates. This pattern indicates that structural impairment of colonies precedes both extensive tissue loss and demographic consequences. Similar hierarchies among response variables, where degradation and partial necrosis precede detectable changes in density, have been documented for habitat-forming gorgonians exposed to repeated thermal stress (Gómez-Gras et al., 2021; Capdevila et al., 2025).

Histological analyses revealed that macroscopic assessments substantially underestimated tissue-level impairment. Although over half of the collected colonies were classified as healthy in the field, microscopic examination showed that all analysed samples exhibited histopathological lesions, resulting in the reclassification of every specimen as necrotic to some degree. This mismatch highlights the limitations of visual surveys for detecting early or sublethal stress in gorgonians and underscores the importance of histopathology for accurate health assessment (Galloway et al., 2007; Work and Aeby, 2006; Work et al., 2014).

The dominant histopathological signature in *E. cavolini* consisted of a complex inflammatory and degenerative syndrome affecting multiple tissue compartments. Nearly all samples exhibited coenenchyme epidermal necrosis, indicating widespread compromise of the external epithelial barrier. Gastrodermal alterations were equally prevalent, with dissociation of gastrodermal cells and necrotic transformation into foamy cells observed in the majority of samples. These changes directly impair digestive and absorptive functions and are likely to

reduce feeding efficiency and energy acquisition at the colony level. Comparable gastrodermal degeneration has been reported in Mediterranean gorgonians exposed to thermal stress and is considered a key mechanism underlying sublethal decline (Carella et al., 2014; Gobbato et al., 2024).

Mesogleal tissue loss and expansion of solenia were common, particularly in samples classified as heavily affected, reflecting structural destabilisation of the coenenchyme. In parallel, eosinophilic granular amoebocytes infiltrated the mesoglea in most samples, with higher densities associated with more severe lesions. Such amoebocytosis is widely interpreted as an immune response, reflecting active inflammation rather than passive tissue decay (Galloway et al., 2007; Dennis et al., 2020). Frequent melanisation along the axial skeleton further supports the activation of innate defence mechanisms, consistent with defensive remodelling processes previously described in gorgonians experiencing chronic stress (Carella et al., 2014; Carella et al., 2020).

Although microorganisms were occasionally detected within the axial skeleton—including algae, cyanobacteria, diatoms, and rare bacterial cells—their presence was inconsistent and absent from most samples. This observation suggests that microbial colonisation was largely secondary, facilitated by tissue breakdown and barrier failure, rather than the primary driver of pathology. The lack of evidence for predators, together with the absence of a consistent infectious agent, points towards a non-infectious stressor as the initiating cause of tissue degeneration, in line with previous studies linking thermal stress to similar histological syndromes (Cerrano et al., 2000; Garrabou et al., 2009).

Marine heatwave (MHW) analyses at depths of 20 and 30 m, corresponding to the bathymetric distribution of *Eunicella cavolini*, revealed recurrent and increasingly intense thermal stress in both Kornati and Telašćica between 2020 and 2023. At 20 m depth, MHWs were already present in 2020, including Category III (Severe) events lasting up to 9–10 days, while Category II (Strong) events were recorded at 30 m, with durations reaching up to 11–15 days, indicating that anomalous warming extended well into deeper infralittoral habitats. Thermal exposure intensified in subsequent years, with an increase in both the number and persistence of events. In 2022, three MHWs were recorded at 20 m depth in both areas, whereas 2023

represented the peak of thermal stress, with up to seven MHW events at 20 m and six to seven events at 30 m, including multiple Category II (Strong) MHWs lasting up to 21 days. Notably, several events occurred synchronously across Kornati and Telašćica at both depths, indicating regionally coherent thermal forcing rather than isolated local anomalies. As biological sampling was conducted in autumn, the pronounced increases in colony mortality and degradation observed particularly in 2022 and 2023 reflect post-impact responses to cumulative summer heat stress, rather than immediate effects of single extreme events.

The progressive increase in colony mortality and degradation observed between 2020 and 2023 coincided with a marked rise in the frequency and persistence of marine heatwaves at 20 and 30 m depth, the bathymetric range occupied by *Eunicella cavolini*. Years characterised by a higher number of MHW events and longer event durations were followed by significantly elevated levels of colony degradation and mortality recorded during autumn sampling, indicating a delayed, post-impact response to summer thermal stress. Similar delayed responses to repeated MHW exposure have been reported for Mediterranean gorgonians, where cumulative thermal stress impairs recovery processes even in the absence of single extreme events (Garrabou et al., 2022; Rovira et al., 2024). Furthermore, the occurrence of strong MHWs at infralittoral and upper circalittoral depths supports growing evidence that depth no longer provides reliable thermal refuge during recent warming events (Bramanti et al., 2023; Estaque et al., 2023).

At the tissue level, histopathological alterations observed in *E. cavolini* are consistent with known cellular responses to thermal stress. Elevated temperatures can disrupt epithelial integrity and trigger programmed and necrotic cell death, particularly within metabolically active gastrodermal tissues (Dunn et al., 2004; Traylor-Knowles, 2019). The widespread epidermal necrosis, gastrodermal dissociation, mesogleal tissue loss, and inflammatory responses documented in this study align with these mechanisms, suggesting that repeated thermal anomalies compromise tissue homeostasis rather than inducing acute, pathogen-driven disease. Taken together, the combined morphological and histological evidence indicates that recurrent MHW exposure promotes a progressive weakening of colony structure and function. Compromised epithelial barriers facilitate secondary microbial colonisation,

while sustained inflammation and melanisation reflect chronic immune activation. These tissue-level processes translate macroscopically into partial tissue loss, exposed axial skeleton, and increasing colony degradation. Because colonies retain living tissue and structural continuity, such deterioration is not immediately reflected in population density, thereby masking the extent of physiological decline over short timescales, a pattern previously described as "hidden erosion" in long-lived habitat-forming species exposed to chronic climatic stress (Gómez-Gras et al., 2021; Vergotti et al., 2025).

The results indicate that *E. cavolini* populations in the eastern Adriatic are experiencing sublethal but pervasive degradation driven by repeated thermal stress, despite the absence of immediate demographic collapse. Such conditions may have profound long-term consequences, including reduced reproductive output, increased susceptibility to additional stressors, and limited capacity for recovery following future disturbances. Given the role of *E. cavolini* as a structural and functional component of coralligenous assemblages, ongoing degradation may also translate into broader ecosystem-level effects (Verdura et al., 2019; Piazzi et al., 2021).

5.10. Paramuricea clavata

Gorgonian *Paramuricea clavata* is a habitat-forming gorgonian species that dominates the coralligenous assemblages of the Mediterranean Sea, typically found at depths greater than 30 m and considered as one ot the architect species of the coralligenous biocenosis. Due to its branching morphology, slow growth rate, and low recruitment, *P. clavata* is considered highly sensitive to disturbances, particularly those caused by thermal anomalies. Numerous studies have identified it as one of the most impacted species during marine heatwave (MHW) events across the western and central Mediterranean (Garrabou et al., 2009; Crisci et al., 2023). In the present study, colonies of *P. clavata* were monitored between 30 and 40 m depth, primarily at sites with reduced hydrodynamic exchange and prolonged thermal exposure.

Population density of *Paramuricea clavata* did not statistically differ between 2020 and 2021 at any station, indicating no short-term demographic collapse. This pattern is consistent with

the demographic inertia expected for long-lived, slow-growing Mediterranean gorgonians, where density may remain apparently stable while colony condition progressively deteriorates (Linares et al., 2007; Linares et al., 2008; Garrabou et al., 2009). As an ecosystem engineer with sluggish growth, *P. clavata* is particularly prone to "delayed" population consequences: colony-scale deterioration can accumulate for years before being expressed as reduced abundance (Garrabou et al., 2009; Kipson et al., 2015; Gómez-Gras et al., 2021).

In contrast to density, colony mortality increased strongly between 2020 and 2023 at all stations. The temporal coherence of this trend across both Telašćica and Kornati suggests a regionally shared stress regime rather than a strictly local disturbance, consistent with MHW-driven impacts documented across Mediterranean gorgonian forests (Garrabou et al., 2022; Rovira et al., 2024). Importantly, because sampling occurred in autumn, these mortality estimates represent post-impact outcomes after summer heat stress, a timing that aligns with known delayed responses in temperate benthic communities following thermal anomalies (Garrabou et al., 2009; Coma et al., 2009).

Colony degradation (affected colonies) showed a more spatially heterogeneous response. Degradation increased significantly at Sestrica Vela, Balun and Mana, but not at Mali Obručan. It indicates that increasing mortality can occur even where the proportion of visibly degraded colonies does not rise significantly, suggesting that tissue loss expression may be modulated by site-specific factors (e.g., hydrodynamics, substrate configuration, microhabitat shading, or disturbance history), despite a shared regional thermal forcing. Such within-region heterogeneity in visible impact has been repeatedly observed for Mediterranean mass mortality events, where responses vary markedly among sites exposed to comparable thermal anomalies (Garrabou et al., 2009; Crisci et al., 2017; Iborra et al., 2022). I therefore interpret colony degradation as a spatially heterogeneous response, whereas the consistent increase in mortality across all sites indicates a broad-scale deterioration in colony performance through time.

Histological analyses revealed pervasive tissue impairment that was frequently not apparent macroscopically. Although 12 of 21 collected colonies were initially classified as healthy in the field, only 1 of 20 analysed samples was microscopically confirmed as healthy; the remaining

19 were reclassified as necrotic, with most in moderate histopathology (state 2; 15 samples) and a minority in light histopathology (state 1; 4 samples). This discrepancy reinforces that gross colony appearance can underestimate sublethal impairment, and it underlines the value of structured histopathology for diagnosing stress syndromes in corals (Work and Aeby, 2006; Galloway et al., 2007; Work et al., 2014).

The lesion complex was dominated by (i) surface epithelial necrosis and loss of integrity, (ii) extensive inflammatory responses in the mesoglea (amoebocytosis and basophilic infiltrates, (iii) mesogleal tissue loss and expanded solenia, and (iv) gastrodermal necrosis and dissociation present in all necrotic samples, with severe polyp necrosis. These tissue-level disruptions are consistent with physiological mechanisms expected under repeated thermal stress: elevated temperatures can compromise epithelial integrity and trigger cell death pathways, particularly in metabolically active gastrodermal tissues, leading to loss of internal organisation and reduced functional capacity (Dunn et al., 2004; Traylor-Knowles, 2019). For an asymbiotic gorgonian such as *P. clavata*, gastrodermal failure is especially consequential because it directly undermines feeding, digestion and internal transport via the gastrovascular system, mechanisms that are central to colony maintenance and recovery in summer-stratified conditions (Coma et al., 2009; Coma et al., 1994).

Axial pathology further indicated chronic internal stress and remodelling: black deposits, melanin deposition near the axis, and structural changes/rupture and altered rigidity (reported in the majority of necrotic samples) suggest sustained defence activation and skeletal compromise. The inconsistent detection of potential pathogens supports an interpretation in which tissue breakdown is primarily stress-related, with opportunistic colonisation occurring secondarily rather than a consistent infectious cause, a distinction emphasised in coral lesion-description frameworks (Work and Aeby, 2006; Dennis et al., 2020).

Notably, oocytes were present in many samples, but oocyte resorption was occasionally observed when severe pathology was present. This pattern is consistent with the idea that chronic stress can divert energy away from reproduction or impair gamete viability, contributing to long-term loss of resilience even when colonies persist (Linares et al., 2007;

Sarda et al., 2025). In demographic terms, such sublethal reproductive impacts can be particularly damaging for slow-growing, long-lived habitat-forming species.

Because *P. clavata* is a characteristic circalittoral species (≥30 m), I interpreted thermal forcing using only 30 and 40 m MHW metrics from Kornati and Telašćica. The MHW table shows that thermal anomalies were not confined to shallow water: MHWs occurred repeatedly at both depths, including Category IV (Extreme) event, demonstrating that warming penetrated into habitats traditionally considered more buffered. In 2020, MHWs were already recorded at 30 m in both Kornati (2 events, up to 11 days; Categories I–II) and Telašćica (2 events, up to 15 days; Category II), while at 40 m Telašćica experienced four events (up to 10 days, Categories I–IV) and Kornati two moderate events (up to 7 days). In 2022, Category II (Strong) MHWs occurred at both depths in both areas, including a synchronous event at 40 m (25 September–2 October) immediately preceding autumn sampling. The strongest escalation was observed in 2023, with a sharp increase in event frequency at both depths (30 m: Kornati 7 events, Telašćica 6; 40 m: Kornati 9, Telašćica 4), durations reaching 10–14 days and dominance of Categories I–II. Several 2023 events were synchronous across Kornati and Telašćica at both depths (30 m: 3–12 August and 23–29 September; 40 m: 28 August–2 September), indicating regionally coherent thermal forcing rather than isolated local anomalies. This depth-explicit MHW pattern supports growing evidence that depth is no longer a consistent refuge during recent Mediterranean heat extremes and recurrent MHWs (Bramanti et al., 2023; Estaque et al., 2023; Garrabou et al., 2022; Rovira et al., 2024). The autumn sampling design is therefore particularly powerful here: the elevated colony mortality and (at most stations) increased degradation recorded after 2022–2023 are consistent with cumulative exposure to repeated MHWs at 30–40 m rather than a single episodic event.

These results indicate that *P. clavata* populations in Telašćica and Kornati retained stable density over the short term while showing progressively increasing colony mortality through 2020–2023 and, at most stations, increasing degradation of colony integrity. The MHW record demonstrates that these biological trends developed under recurrent thermal anomalies at 30–40 m, including multiple synchronous events across both areas and an escalation in event frequency in 2023. Histological findings from Kornati provide a tissue-level evidence for the

observed colony-scale deterioration: epithelial barrier failure, gastrodermal collapse, mesogleal tissue loss, and chronic inflammation represent a coherent stress syndrome consistent with repeated thermal exposure, particularly when sampling captures post-summer outcomes.

6. CONCLUSIONS

This doctoral dissertation provides an integrated assessment of the effects of climate-driven thermal anomalies and marine heatwaves on six representative coral species of the eastern Adriatic Sea, combining marine heatwave analyses with morphological, histological, and microbiome-based approaches. The study represents one of the first multi-level investigations linking depth-resolved thermal stress with biological responses of Mediterranean corals across infralittoral and circalittoral habitats in the Adriatic Sea.

All main objectives were accomplished and the proposed hypotheses confirmed: (i) elevated and prolonged seawater temperatures were associated with increased visible morphological deterioration and partial mortality in both scleractinian and gorgonian corals, confirming that thermal anomalies negatively affect coral colony condition; (ii) histological analyses demonstrated widespread tissue pathology, including epithelial disruption, gastrodermal collapse, inflammatory responses, and necrosis linked to repeated thermal exposure, confirming that elevated temperatures induce significant tissue damage even in apparently healthy colonies; and (iii) microbiome analyses revealed pronounced shifts in bacterial community composition and increased microbial heterogeneity in necrotic coral tissues and surrounding seawater, confirming that elevated temperatures influence both coral-associated and environmental microbial assemblages.

The results of this study demonstrate that marine heatwaves represent a dominant structuring force shaping coral condition in the eastern Adriatic, with impacts that extend well beyond surface waters and single extreme events. The depth-resolved MHW analysis reveals a complex thermal landscape in which intermediate depths are increasingly subjected to prolonged cumulative stress, while deeper layers experience episodic but highly anomalous and rapidly developing events. These depth-dependent thermal regimes help to explain the biological patterns observed across coral taxa. The absence of long-term trends in nutrient availability further supports the interpretation that the observed biological deterioration is not confounded by progressive eutrophication, but is primarily driven by thermal forcing and its interaction with local hydrographic conditions.

Across both gorgonian and scleractinian corals, morphological indicators consistently point to a progressive increase in mortality and tissue degradation through time, indicative of chronic rather than episodic disturbance. These changes frequently occurred without obvious declines in colony abundance, suggesting that sublethal deterioration and partial mortality accumulate before demographic collapse becomes detectable. Importantly, these macroscopic patterns are underpinned by widespread histopathological alterations that are frequently present even in colonies appearing externally healthy. The predominance of epithelial barrier disruption, gastrodermal collapse, inflammatory cell infiltration, and mesogleal alteration across species highlights a common stress syndrome associated with repeated thermal exposure. At the same time, differences between species in tissue damage and reproductive condition show that species-specific traits strongly shape their vulnerability to thermal stress.

Microbiome analyses add a further layer to this integrative picture, indicating that tissue degradation is accompanied by a breakdown of host-mediated microbial regulation and a shift towards more heterogeneous, environmentally influenced bacterial assemblages. While host-specific microbial signatures remain detectable, particularly in gorgonian corals, necrotic tissues consistently show increased compositional variability, consistent with microbial dysbiosis under chronic stress. The stronger interaction between seawater and coral-associated microbiomes in semi-enclosed systems such as Veliko jezero further suggests that local hydrographic context can amplify biological responses to thermal anomalies.

Collectively, these findings indicate that Mediterranean corals in the Adriatic are increasingly exposed to a regime of recurrent and vertically extensive marine heatwaves that compress recovery windows, promote sublethal tissue damage, and progressively erode colony function. These findings further demonstrate that depth does not provide a reliable long-term thermal refuge for the investigated coral species, as recurrent MHWs increasingly penetrate into circalittoral habitats traditionally considered buffered from climate extremes. This interpretation is strongly consistent with recent Mediterranean studies showing that recurrent MHWs drive repeated mass mortalities, reduce resilience to subsequent disturbance, compromise reproductive success, and generate long-term sublethal deterioration even in populations previously considered relatively resistant or buffered by depth.

The differences between macroscopic appearance and internal tissue condition highlight the limitations of visual assessments alone and emphasise the importance of integrative, multi-level approaches. Histological and microbial indicators frequently revealed physiological deterioration before severe external colony degradation became evident, demonstrating their value as early warning indicators of chronic thermal stress. By linking depth-resolved thermal extremes with morphological, histological, and microbial responses, this study provides a coherent framework for understanding how chronic thermal stress translates into long-term degradation of coral populations, even in habitats traditionally considered buffered from climate extremes, where any refuge effect may be only partial or temporary.

This dissertation contributes to the understanding of climate-driven coral degradation in the Mediterranean by providing one of the first integrative assessments combining marine heatwave dynamics, histopathology, morphometric indicators, and microbiome analyses across multiple coral taxa and depth ranges in the Adriatic Sea. The results establish baseline knowledge on species-specific vulnerability, hidden tissue deterioration, and microbial dysbiosis associated with chronic thermal stress, thereby improving the capacity to detect early signs of coral decline before irreversible population-level impacts become evident.

Future research should further investigate the long-term ecological consequences of recurrent marine heatwaves on Mediterranean coral assemblages, particularly regarding recovery capacity, reproductive success, and shifts in community structure under continued climate warming. In addition, extended temporal monitoring and experimental approaches integrating thermal exposure, microbial dynamics, and host physiology would improve understanding of the mechanisms underlying resilience and susceptibility among Mediterranean coral species.

7. REFERENCE

Aguirre, J. and Jiménez, A.P. (1998) 'Fossil analogues of present-day *Cladocora caespitosa* coral banks: Sedimentary setting, dwelling community, and taphonomy (Late Pliocene, W Mediterranean)', *Coral Reefs*, 17(3), pp. 203–213. doi:10.1007/s003380050119.

Ainsworth, T. and Hoegh-Guldberg, O. (2009) 'Bacterial communities closely associated with coral tissues vary under experimental and natural reef conditions and thermal stress', *Aquatic Biology*, 4, pp. 289–296. doi:10.3354/ab00102.

Ainsworth, T.D., Fine, M., Blackall, L.L. and Hoegh-Guldberg, O. (2006) 'Fluorescence in situ hybridization and spectral imaging of coral-associated bacterial communities', *Applied and Environmental Microbiology*, 72(4), pp. 3016–3020. doi:10.1128/AEM.72.4.3016-3020.2006.

Ainsworth, T.D., Thurber, R.V. and Gates, R.D. (2010) 'The future of coral reefs: A microbial perspective', *Trends in Ecology & Evolution*, 25(4), pp. 233–240. doi:10.1016/j.tree.2009.11.001.

Aleem, A.A. and Aleem, E.A.A. (1992) '*Balanophyllia europaea* (Risso, 1826): A scleractinian solitary coral in the southeastern Mediterranean', *Journal of the Egyptian German Society of Zoology*, 8, pp. 227–233.

Allemand, D. and Furla, P. (2018) 'How does an animal behave like a plant? Physiological and molecular adaptations of zooxanthellae and their hosts to symbiosis', *Comptes Rendus Biologies*, 341(5), pp. 276–280. doi:10.1016/j.crvi.2018.03.007.

Apprill, A., McNally, S., Parsons, R. and Weber, L. (2015) 'Minor revision to V4 region SSU rRNA 806R gene primer greatly increases detection of SAR11 bacterioplankton', *Aquatic Microbial Ecology*, 75(2), pp. 129–137. doi:10.3354/ame01753.

Arin, L., Guillén, J., Segura-Noguera, M. and Estrada, M. (2013) 'Open sea hydrographic forcing of nutrient and phytoplankton dynamics in a Mediterranean coastal ecosystem', *Estuarine, Coastal and Shelf Science*, 133, pp. 116–128. doi:10.1016/j.ecss.2013.08.018.

Artegiani, A., Bregant, D., Paschini, E., Pinardi, N., Raicich, F. and Russo, A. (1997) 'The Adriatic Sea general circulation. Part I: Air–sea interactions and water mass structure', *Journal of*

Physical Oceanography, 27(8), pp. 1492–1514. doi:10.1175/1520-0485(1997)027<1492:TASGCP>2.0.CO;2.

Avian, M., Boero, F., Mills, C., Rossi, L. and Rottini-Sandrini, L. (1995) 'Cnidaria, Ctenophora', u Minelli, A., Ruffo, S. and La Posta, S. (ur.) *Checklist delle specie della fauna italiana*, Vol. 3. Bologna: Calderini, pp. 1–33.

Baker, A.C., Glynn, P.W. and Riegl, B. (2008) 'Climate change and coral reef bleaching: An ecological assessment of long-term impacts, recovery trends and future outlook', *Estuarine, Coastal and Shelf Science*, 80(4), pp. 435–471. doi:10.1016/j.ecss.2008.09.003.

Ballesteros, E. (2006) 'Mediterranean coralligenous assemblages: a synthesis of present knowledge', *Oceanography and Marine Biology: An Annual Review*, 44, pp. 123–195.

Banin, E., Israely, T., Fine, M., Loya, Y. and Rosenberg, E. (2001) 'Role of endosymbiotic zooxanthellae and coral mucus in the adhesion of the coral-bleaching pathogen *Vibrio shiloi* to its host', *FEMS Microbiology Letters*, 199(1), pp. 33–37. doi:10.1111/j.1574-6968.2001.tb10647.x.

Banin, E., Vassilakos, D., Orr, E., Martinez, R.J. and Rosenberg, E. (2003) 'Superoxide dismutase is a virulence factor produced by the coral bleaching pathogen *Vibrio shiloi*', *Current Microbiology*, 46(6), pp. 418–422. doi:10.1007/s00284-002-3912-5.

Barshis, D.J., Ladner, J.T., Oliver, T.A., Seneca, F.O., Traylor-Knowles, N. and Palumbi, S.R. (2013) 'Genomic basis for coral resilience to climate change', *Proceedings of the National Academy of Sciences of the United States of America*, 110(4), pp. 1387–1392. doi:10.1073/pnas.1210224110.

Bavestrello, G. and Boero, F. (1986) 'Necrosi e rigenerazione in *Eunicella cavolinii* in Mar Ligure', *Bollettino dei Musei e degli Istituti Biologici dell'Università di Genova*, 52, pp. 295–300.

Bavestrello, G., Bertone, S., Cattaneo-Vietti, R., Cerrano, C., Gaino, E. and Zanzi, D. (1994) 'Mass mortality of *Paramuricea clavata* (Anthozoa, Cnidaria) on Portofino Promontory cliffs, Ligurian Sea, Mediterranean Sea', *Marine Life*, 4(1), pp. 15–19.

Bavestrello, G., Cerrano, C., Zanzi, D. and Cattaneo-Vietti, R. (1997) 'Damage by fishing activities in the gorgonian coral *Paramuricea clavata* in the Ligurian Sea', *Aquatic Conservation: Marine and Freshwater Ecosystems*, 7(3), pp. 253–262. doi:10.1002/(SICI)1099-0755(199709)7:3<253::AID-AQC243>3.0.CO;2-1.

Beckmann, A. and Özbek, S. (2012) 'The nematocyst: a molecular map of the cnidarian stinging organelle', *International Journal of Developmental Biology*, 56(6–8), pp. 577–582. doi:10.1387/ijdb.113472ab.

Benović, A., Lučić, D., Onofri, V., Pećarević, M., Caric, M., Njire, J. and Onofri, I. (2000) 'Ecological characteristics of the Mljet Island seawater lakes (South Adriatic Sea) with special reference to their resident populations of medusae', *Scientia Marina*, 64(S1), pp. 197–206. doi:10.3989/scimar.2000.64s1197.

Bensoussan, N., Romano, J.-C., Harmelin, J.-G. and Garrabou, J. (2010) 'High resolution characterization of northwest Mediterranean coastal waters thermal regimes: To better understand responses of benthic communities to climate change', *Estuarine, Coastal and Shelf Science*, 87(3), pp. 431–441. doi:10.1016/j.ecss.2010.01.008.

Benzoni, F., Arrigoni, R., Stefani, F., Reijnen, B.T., Montano, S. and Hoeksema, B.W. (2018) 'Morphological and genetic divergence between Mediterranean and Caribbean populations of *Madracis pharensis* (Heller 1868) (Scleractinia, Pocilloporidae): Too much for one species?', *Zootaxa*, 4471(3), pp. 473–492. doi:10.11646/zootaxa. 4471.3.3.

Bernasconi, M.P., Corselli, C. and Carobene, L. (1997) 'A bank of the scleractinian coral *Cladocora caespitosa* in the Pleistocene of the Crati Valley (Calabria, southern Italy): Growth versus environmental conditions', *Bollettino della Società Paleontologica Italiana*, 36(1–2), pp. 53–62.

Bernasconi, R., Stat, M., Koenders, A. and Huggett, M.J. (2019) 'Global networks of Symbiodinium–bacteria within the coral holobiont', *Microbial Ecology*, 77(3), pp. 794–807. doi:10.1007/s00248-018-1255-4.

Bertucci, A., Moya, A., Tambutté, S., Allemand, D., Supuran, C.T. and Zoccola, D. (2013) 'Carbonic anhydrases in anthozoan corals—a review', *Bioorganic & Medicinal Chemistry*, 21(6), pp. 1437–1450. doi:10.1016/j.bmc.2012.10.024.

Bieri, T., Onishi, M., Xiang, T., Grossman, A.R. and Pringle, J.R. (2016) 'Relative contributions of various cellular mechanisms to loss of algae during cnidarian bleaching', *PLoS ONE*, 11(4), pp. e0152693. doi:10.1371/journal.pone.0152693.

Blackall, L.L., Wilson, B. and van Oppen, M.J.H. (2015) 'Coral—the world's most diverse symbiotic ecosystem', *Molecular Ecology*, 24(21), pp. 5330–5347. doi:10.1111/mec.13400.

Boilard, A., Dubé, C.E., Gruet, C., Mercière, A., Hernandez-Agreda, A. and Derome, N. (2020) 'Defining coral bleaching as a microbial dysbiosis within the coral holobiont', *Microorganisms*, 8(11), pp. 1682. doi:10.3390/microorganisms8111682.

Bongaerts, P., Frade, P.R., Hay, K.B., Englebert, N., Latijnhouwers, K.R.W., Bak, R.P.M., Vermeij, M.J.A., Hoegh-Guldberg, O. *et al.* (2015) 'Deep down on a Caribbean reef: lower mesophotic depths harbor a specialized coral–endosymbiont community', *Scientific Reports*, 5, pp. 7652. doi:10.1038/srep07652.

Bongaerts, P., Riginos, C., Brunner, R., Englebert, N., Smith, S.R. and Hoegh-Guldberg, O. (2017) 'Deep reefs are not universal refuges: Reseeding potential varies among coral species', *Science Advances*, 3(2), pp. e1602373. doi:10.1126/sciadv.1602373.

Bourne, D.G., Iida, Y., Uthicke, S. and Smith-Keune, C. (2008) 'Changes in coral-associated microbial communities during a bleaching event', *The ISME Journal*, 2(4), pp. 350–363. doi:10.1038/ismej.2007.112

Bourne, D.G., Morrow, K.M. and Webster, N.S. (2016) 'Insights into the coral microbiome: underpinning the health and resilience of reef ecosystems', *Annual Review of Microbiology*, 70, pp. 317–340. doi:10.1146/annurev-micro-102215-095440.

Braithwaite, C.J.R. (1973) 'Reefs: Just a problem of semantics?', *American Association of Petroleum Geologists Bulletin*, 57(6), pp. 1100–1116.

Bramanti, L., Manea, E., Giordano, B., Estaque, T., Bianchimani, O., Richaume, J., Mérigot, B., Schull, Q., Sartoretto, S., Garrabou, J. and Guizien, K. (2023) 'The deep vault: a temporary refuge for temperate gorgonian forests facing marine heat waves', *Mediterranean Marine Science*, 24(3), pp. 601–609, doi:10.12681/mms.35564.

Brown, B.E. and Bythell, J.C. (2005) 'Perspectives on mucus secretion in reef corals', *Marine Ecology Progress Series*, 296, pp. 291–309. doi:10.3354/meps296291.

Brown, B.E., Le Tissier, M.D.A. and Bythell, J.C. (1995) 'Mechanisms of bleaching deduced from histological studies of reef corals sampled during a natural bleaching event', *Marine Biology*, 122(4), pp. 655–663. doi:10.1007/BF00350687.

Burriesci, M.S., Raab, T.K. and Pringle, J.R. (2012) 'Evidence that glucose is the major transferred metabolite in dinoflagellate–cnidarian symbiosis', *Journal of Experimental Biology*, 215(19), pp. 3467–3477. doi:10.1242/jeb.070946.

Cairns, S.D. (1999) 'Species richness of recent Scleractinia', *Atoll Research Bulletin*, 459, pp. 1–12. doi:10.5479/si.00775630.459.1.

Callahan, B.J., McMurdie, P.J., Rosen, M.J., Han, A.W., Johnson, A.J.A. and Holmes, S.P. (2016a) 'DADA2: High-resolution sample inference from Illumina amplicon data', *Nature Methods*, 13(7), pp. 581–583. doi:10.1038/nmeth.3869.

Callahan, B.J., Sankaran, K., Fukuyama, J.A., McMurdie, P.J. and Holmes, S.P. (2016b) 'Bioconductor workflow for microbiome data analysis: From raw reads to community analyses', *F1000Research*, 5, pp. 1492. doi:10.12688/f1000research.8986.2.

Capdevila, P., Zentner, Y., Rovira, G., Garrabou, J., Medrano, A. and Linares, C. (2025) 'Mediterranean octocoral populations exposed to marine heatwaves are less resilient to disturbances', *Journal of Animal Ecology*, 94, pp. 1528–1541. doi:10.1111/1365-2656.14147.

Carbonne, C. et al. (2024) 'Response of two temperate scleractinian corals to projected ocean warming and marine heatwaves', *Global Change Biology*, 30, pp. e17023. doi:10.1111/gcb.17023.

Carella, F., Miele, C. and De Vico, G. (2020) 'Nodular-like growth and axial thickening in gorgonians are a defensive response to endolithic cyanobacteria, involving amyloid deposition', *Diseases of Aquatic Organisms*, 138, pp. 155–169. doi:10.3354/dao03451.

Canessa, M., Bertolotto, R., Betti, F., Bo, M., Dagnino, A., Enrichetti, F., Toma, M. and Bavestrello, G. (2024) 'Variation in the health status of the Mediterranean gorgonian forests: The synergistic effect of marine heat waves and fishing activity', *Biology*, 13(8), pp. 642. doi:10.3390/biology13080642.

Cánovas-Molina, A., Sánchez-Tocino, L., Llorens, C., Pascual, M. and Turon, X. (2018) 'From depth to regional spatial genetic differentiation of *Eunicella cavolini* in the NW Mediterranean', *Comptes Rendus Biologies*, 341(9–10), pp. 421–432. doi:10.1016/j.crvi.2018.09.002.

Caputi, N., Kangas, M.I., Denham, A., Feng, M., Pearce, A., Hetzel, Y., Chandrapavan, A. and Penn, J. (2016) 'Management adaptation of invertebrate fisheries to an extreme marine heat wave event at a global warming hot spot', *Ecology and Evolution*, 6(11), pp. 3583–3593. doi:10.1002/ece3.2137.

Carella, F., Aceto, S., Saggiomo, M., Mangoni, O. and De Vico, G. (2014) 'Gorgonian disease outbreak in the Gulf of Naples: pathology reveals cyanobacterial infection linked to elevated sea temperatures', *Diseases of Aquatic Organisms*, 111, pp. 69–80.

Caroselli, E., Prada, F., Pasquini, L., Nonnis Marzano, F., Zaccanti, F., Falini, G., Levy, O., Dubinsky, Z. and Goffredo, S. (2011) 'Environmental implications of skeletal micro-density and porosity variation in two scleractinian corals', *Zoology*, 114(5), pp. 255–264. doi:10.1016/j.zool.2011.04.003.

Cebrian, E., Uriz, M.J., Garrabou, J. and Ballesteros, E. (2011) 'Sponge mass mortalities in a warming Mediterranean sea: Are cyanobacteria-harboring species worse off?', *PLOS ONE*, 6(6), p. e20211. doi:10.1371/journal.pone.0020211.

Cerrano, C., Bavestrello, G., Bianchi, C.N., Cattaneo-Vietti, R., Bava, S., Morganti, C., Morri, C., Picco, P., Sara, G., Schiaparelli, S., Siccardi, A. and Sponga, F. (2000) 'A catastrophic mass-mortality episode of gorgonians and other organisms in the Ligurian Sea (North-western

Mediterranean), summer 1999', *Ecology Letters*, 3(4), pp. 284–293. doi:10.1046/j.1461-0248.2000.00152.x.

Cheung, M.W.M., Hock, K., Skirving, W. and Mumby, P.J. (2021) 'Cumulative bleaching undermines systemic resilience of the Great Barrier Reef', *Current Biology*, 31(23), pp. 5385–5392.e4. doi:10.1016/j.cub.2021.09.078.

Coll, M., Piroddi, C., Kaschner, K., Ben Rais Lasram, F., Steenbeek, J., Aguzzi, J., Ballesteros, E., Bianchi, C.N., Corbera, J., Dailianis, T., Danovaro, R., Estrada, M., Froglia, C., Galil, B.S., Gasol, J.M., Gertwagen, R., Gil, J., Guilhaumon, F., Kesner-Reyes, K., Kitsos, M.S., Koukouras, A., Lampadariou, N., Laxamana, E., López-Fé de la Cuadra, C.M., Lotze, H.K., Martin, D., Mouillot, D., Oro, D., Raicevich, S., Rius-Barile, J., Saiz-Salinas, J.I., San Vicente, C., Somot, S., Templado, J., Turon, X., Vafidis, D., Villanueva, R. and Voultsiadou, E. (2010) 'The biodiversity of the Mediterranean Sea: Estimates, patterns, and threats', *PLOS ONE*, 5(8), p. e11842. doi:10.1371/journal.pone.0011842.

Collins, M., Sutherland, M., Bouwer, L., Cheong, S.M., Frölicher, T., Jacot Des Combes, H., Roxy, M.K., Losada, I., McInnes, K., Ratter, B., Rivera-Arriaga, E., Susanto, R.D., Swingedouw, D., Tibig, L., Bakker, P., Eakin, C.M., Emanuel, K., Grose, M., Hemer, M. and Timmermans, M.L. (2019) 'Extremes, abrupt changes and managing risk', u Pörtner, H.O., Roberts, D., Masson-Delmotte, V., Zhai, P., Tignor, M., Poloczanska, E., Mintenbeck, K., Alegría, A., Nicolai, M., Okem, A., Petzold, J., Rama, B. and Weyer, N.M. (ur.) *IPCC special report on the ocean and cryosphere in a changing climate*. Geneva: Intergovernmental Panel on Climate Change, pp. 589–674.

Coma, R., Gili, J.M., Zabala, M. and Riera, T. (1994) 'Feeding and prey capture cycles in the aposymbiontic gorgonian *Paramuricea clavata*', *Marine Ecology Progress Series*, 115(3), pp. 257–270. doi:10.3354/meps115257.

Coma, R., Pola, E., Ribes, M. and Zabala, M. (2004) 'Long-term assessment of temperate octocoral mortality patterns: Protected vs. unprotected areas', *Ecological Applications*, 14(5), pp. 1466–1478. doi:10.1890/03-5176.

Coma, R., Linares, C., Ribes, M. and Garrabou, J. (2006) 'Consequences of a mass mortality in populations of *Eunicella singularis* (Cnidaria: Octocorallia) in Menorca (NW Mediterranean)', *Marine Ecology Progress Series*, 327, pp. 51–60. doi:10.3354/meps327051.

Coma, R., Ribes, M., Serrano, E., Jiménez, E., Salat, J. and Pascual, J. (2009) 'Global warming-enhanced stratification and mass mortality events in the Mediterranean', *Proceedings of the National Academy of Sciences of the United States of America*, 106(15), pp. 6176–6181. doi:10.1073/pnas.0805801106.

Corinaldesi, C., Tangherlini, M., Luna, G.M., Dell'Anno, A., Morigi, C., Francesco, M., Cerrano, C. and Danovaro, R. (2022) 'Changes in coral forest microbiomes predict the impact of marine heatwaves on habitat-forming species', *Global Change Biology*, 28(2), pp. 393–409. doi:10.1111/gcb.15904.

Crisci, C., Bensoussan, N., Romano, J.C. and Garrabou, J. (2011) 'Temperature anomalies and mortality events in marine communities: Insights on factors behind differential mortality impacts in the NW Mediterranean', *PLOS ONE*, 6(9), p. e23814. doi:10.1371/journal.pone.0023814.

Cushman-Roisin, B., Gačić, M., Poulain, P.-M. and Artegiani, A. (eds) (2001) *Physical Oceanography of the Adriatic Sea: Past, Present and Future*. Dordrecht: Springer. doi:10.1007/978-94-015-9819-4.

Cupido, R., Cocito, S., Barsanti, M., Sgorbini, S., Peirano, A. and Santangelo, G. (2009) 'Unexpected long-term population dynamics in a canopy-forming gorgonian following mass mortality', *Marine Ecology Progress Series*, 394, pp. 195–200. doi:10.3354/meps08260.

Cupido, R., Cocito, S., Sgorbini, S., Peirano, A. and Santangelo, G. (2012) 'Sexual structure of a highly reproductive, recovering gorgonian population: Quantifying reproductive output', *Marine Ecology Progress Series*, 469, pp. 25–36. doi:10.3354/meps09976.

da Costa, V.S., Vilibić, I., Mihanović, H., Šepić, J. and Dunić, N. (2024) 'Marine climate indicators in the Adriatic Sea', *Frontiers in Climate*, 6, p. 1449633. doi:10.3389/fclim.2024.1449633.

Danovaro, R., Umani, S.F. and Pusceddu, A. (2009) 'Climate change and the potential spreading of marine mucilage and microbial pathogens in the Mediterranean Sea', *PLoS ONE*, 4(9), pp. e7006. doi:10.1371/journal.pone.0007006.

Darmaraki, S., Somot, S., Sevault, F., Nabat, P., Cavicchia, L., Djurdjevic, V., Li, L., Sannino, G. and Artale, V. (2019) 'Future evolution of marine heatwaves in the Mediterranean Sea', *Climatic Dynamics*, 53(3–4), pp. 1371–1392. doi:10.1007/s00382-019-04661-z.

Darmaraki, S., Somot, S., Sevault, F., Cavicchia, L., Djurdjevic, V., Li, L., Sannino, G. and Artale, V. (2024) 'Marine heatwaves in the Mediterranean Sea: A literature review', *Mediterranean Marine Science*, 25(3), pp. 586–620. doi:10.12681/mms.38392.

Davy, S.K., Allemand, D. and Weis, V.M. (2012) 'Cell biology of cnidarian–dinoflagellate symbiosis', *Microbiology and Molecular Biology Reviews*, 76(2), pp. 229–261. doi:10.1128/MMBR.05014-11.

DeCarlo, T.M., Gajdzik, L., Ellis, J., Coker, D.J., Roberts, M.B., Hammerman, N.M., Pandolfi, J.M., Monroe, A.A. and Berumen, M.L. (2020) 'Nutrient-supplying ocean currents modulate coral bleaching susceptibility', *Science Advances*, 6(34), pp. eabc5493. doi:10.1126/sciadv.abc5493.

Dennis, M.M., Becker, A.A.M.J. and Freeman, M.A. (2020) 'Pathology of multifocal purple spots, a nonspecific lesion morphology of Caribbean sea fans *Gorgonia* spp.', *Diseases of Aquatic Organisms*, 141, pp. 79–89. doi:10.3354/dao03523.

Di Camillo, C.G., Luna, G.M., Bo, M., Giordano, G., Corinaldesi, C., Bavestrello, G. and Danovaro, R. (2013) 'Sponge disease in the Adriatic Sea', *Marine Ecology*, 34(1), pp. 62–71. doi:10.1111/j.1439-0485.2012.00525.x.

Donovan, M.K., Adam, T.C., Shantz, A.A., Speare, K.E., Munsterman, K.S., Rice, M.M., Schmitt, R.J., Holbrook, S.J. and Burkepile, D.E. (2020) 'Nitrogen pollution interacts with heat stress to increase coral bleaching across the seascape', *Proceedings of the National Academy of Sciences of the United States of America*, 117(10), pp. 5351–5357. doi:10.1073/pnas.1915395117.

Dornbos, S.Q. and Wilson, M.A. (1999) 'Paleoecology of a Pliocene coral reef in Cyprus: Recovery of a marine community from the Messinian Salinity Crisis', *Neues Jahrbuch für*

Geologie und Paläontologie - Abhandlungen, 213(1), pp. 103–118. doi:10.1127/njgpa/213/1999/103.

Downs, C.A., Kramarsky-Winter, E., Fauth, J.E., Segal, R., Bronstein, O., Jeger, R., Loya, Y., Woodley, C.M. and Pennington, P. (2009) 'Symbiophagy as a cellular mechanism for coral bleaching', *Autophagy*, 5(2), pp. 211–216. doi:10.4161/auto.5.2.7405.

Dunn, S.R., Thomason, J.C., Le Tissier, M.D.A. and Bythell, J.C. (2004) 'Heat stress induces different forms of cell death in sea anemones and their endosymbiotic algae depending on temperature and duration', *Cell Death and Differentiation*, 11, pp. 1213–1222. doi:10.1038/sj.cdd.4401484.

Estaque, T., Richaume, J., Bianchimani, O., Schull, Q., Mérigot, B., Bensoussan, N., Sartoretto, S., Monfort, T., Basthard-Bogain, S., Fargetton, M., Gatti, G., Barth, L., Cheminée, A. and Garrabou, J. (2023) 'Marine heatwaves on the rise: One of the strongest ever observed mass mortality event in temperate gorgonians', Global Change Biology, 29(22), pp. 6159–6162. doi:10.1111/gcb.16931.

Fader, M., Giupponi, C., Burak, S., Dakhlaoui, H., Koutroulis, A., Lange, M.A., Llasat, M.C., Pulido-Velazquez, D. and Sanz-Cobeña, A. (2020) 'Water', in Cramer, W., Guiot, J. and Marini, K. (eds.) *Climate and Environmental Change in the Mediterranean Basin – Current Situation and Risks for the Future. First Mediterranean Assessment Report*. Marseille, France: Union for the Mediterranean, Plan Bleu, UNEP/MAP, pp. 181–236. doi:10.5281/zenodo.7101074.

Fautin, D.G. and Mariscal, R.N. (1991) 'Cnidaria: Anthozoa', in Harrison, F.W. and Westfall, J.A. (eds) *Microscopic Anatomy of Invertebrates. Vol. 2: Placozoa, Porifera, Cnidaria, and Ctenophora*. New York: Wiley-Liss, pp. 267–358.

Frade, P.R., de Jongh, F., Vermeulen, F., van Bleijswijk, J. and Bak, R.P.M. (2008) 'Variation in symbiont distribution between closely related coral species over large depth ranges', *Molecular Ecology*, 17, pp. 691–703. doi:10.1111/j.1365-294X.2007.03612.x.

Frade, P.R., Reyes-Nivia, M.C., Faria, J., Kaandorp, J.A., Luttikhuizen, P.C. and Bak, R.P.M. (2010) 'Semi-permeable species boundaries in the coral genus *Madracis*: introgression in a brooding

coral system', *Molecular Phylogenetics and Evolution*, 57(3), pp. 1072–1090. doi:10.1016/j.ympev.2010.09.010.

Fricke, H.W., Vareschi, E. and Schlichter, D. (1987) 'Photoecology of the coral *Leptoseris fragilis* in the Red Sea twilight zone (an experimental study by submersible)', *Oecologia*, 73(3), pp. 371–381. doi:10.1007/BF00385256.

Gaino, E. (1989) 'Ultrastructural evidence of bacterial damage to *Spongia officinalis* fibres (Porifera, Demospongiae)', *Diseases of Aquatic Organisms*, 6, pp. 67–74. doi:10.3354/dao006067.

Gaino, E., Pronzato, R., Corriero, G. and Buffa, P. (1992) 'Mortality of commercial sponges: Incidence in two Mediterranean areas', *Italian Journal of Zoology*, 59(1), pp. 79–85. doi:10.1080/11250009209386652.

Galloway, S.B., Work, T.M., Bochsler, V.S., Harley, R.A., Kramarsky-Winters, E., McLaughlin, S.M., Meteyer, C.U., Morado, J.F., Nicholson, J.H., Parnell, P.G., Peters, E.C., Reynolds, T.L., Rotstein, D.S., Sileo, L. and Woodley, C.M. (2007) 'Coral Disease and Health Workshop: Coral Histopathology II', *NOAA Technical Memorandum NOS NCCOS*, 56 and *NOAA Technical Memorandum CRCP*, 4.

Garren, M. and Azam, F. (2010) 'New method for counting bacteria associated with coral mucus', *Applied and Environmental Microbiology*, 76(18), pp. 6128–6133. doi:10.1128/AEM.01100-10.

Garrabou, J. and Harmelin, J.-G. (2002) 'A 20-year study on life-history traits of a harvested long-lived temperate coral in the NW Mediterranean: Insights into conservation and management needs', *Journal of Animal Ecology*, 71(6), pp. 966–978. doi:10.1046/j.1365-2656.2002.00661.x.

Garrabou, J., Pérez, T., Sartoretto, S. and Harmelin, J.-G. (2001) 'Mass mortality event in red coral *Corallium rubrum* populations in the Provence region (France, NW Mediterranean)', *Marine Ecology Progress Series*, 217, pp. 263–272. doi:10.3354/meps217263.

Garrabou, J., Coma, R., Bensoussan, N., Bally, M., Chevaldonné, P., Cigliano, M., Diaz, D., Harmelin, J.G., Gambi, M.C., Kersting, D.K., Ledoux, J.B., Lejeusne, C., Linares, C., Marschal, C., Pérez, T., Ribes, M., Romano, J.C., Serrano, E., Teixidó, N., Torrents, O., Zabala, M., Zuberer, F. and Cerrano, C. (2009) 'Mass mortality in Northwestern Mediterranean rocky benthic communities: Effects of the 2003 heat wave', Global Change Biology, 15(5), pp. 1090–1103. doi:10.1111/j.1365-2486.2008.01823.x.

Garrabou, J., Ballesteros, E., Linares, C., Hereu, B., Zabala, M., Cebrian, E. and Kersting, D.K. (2014) *Monitoring protocol for reefs – coralligenous community*. MedMPAnet Project. doi:10.13140/2.1.1266.8482.

Garrabou, J. et al. (2019) 'Collaborative database to track mass mortality events in the Mediterranean Sea', *Frontiers in Marine Science*, 6, pp. 707. doi:10.3389/fmars.2019.00707.

Garrabou, J., Gómez-Gras, D., Medrano, A., Cerrano, C., Ponti, M., Schlegel, R., Bensoussan, N., Turicchia, E., Sini, M., Gerovasileiou, V., Teixidó, N., Mirasole, A., Tamburello, L., Cebrian, E., Rilov, G., Ledoux, J.-B., Ben Souissi, J., Khamassi, F., Ghanem, R., Benabdi, M., Grimes, S., Ocaña, O., Bazairi, H., Hereu, B., Linares, C., Kersting, D.K., Rovira, G., Ortega, J., Casals, D., Pagès-Escolà, M., Margarit, N., Capdevila, P., Verdura, J., Ramos, A., Izquierdo, A., Barbera, C., Rubio-Portillo, E., Anton, I., López-Sendino, P., Díaz, D., Vázquez-Luis, M., Duarte, C., Marbà, N., Aspillaga, E., Espinosa, F., Grech, D., Guala, I., Azzurro, E., Farina, S., Gambi, M.C., Chimienti, G., Montefalcone, M., Azzola, A., Pulido Mantas, T., Fraschetti, S., Ceccherelli, G., Kipson, S., Bakran-Petricioli, T., Petricioli, D., Jimenez, C., Katsanevakis, S., Tuney Kizilkaya, I., Kizilkaya, Z., Sartoretto, S., Elodie, R., Ruitton, S., Comeau, S., Gattuso, J.-P. and Harmelin, J.-G. (2022) 'Marine heatwaves drive recurrent mass mortalities in the Mediterranean Sea', *Global Change Biology*, 28(19), pp. 5708–5725. doi:10.1111/gcb.16301.

Fadlallah, Y.H. (1983) 'Population dynamics and life history of a solitary coral, *Balanophyllia elegans*, from central California', *Oecologia*, 58(2), pp. 200–207. doi:10.1007/BF00399218.

Gardner, S.G., Raina, J.B., Nitschke, M.R., Nielsen, D.A., Stat, M., Motti, C.A., Ralph, P.J., Petrou, K. and Bourne, D.G. (2017) 'A multi-trait systems approach reveals a response cascade to bleaching in corals', *BMC Biology*, 15, p. 117. doi:10.1186/s12915-017-0459-2.

Geiser, D.M., Taylor, J.W., Ritchie, K.B. and Smith, G.W. (1998) 'Cause of sea fan death in the West Indies', *Nature*, 394(6689), pp. 137–138. doi:10.1038/28079.

Giovannoni, S.J. and Stingl, U. (2005) 'Molecular diversity and ecology of microbial plankton', *Nature*, 437, pp. 343–348. doi:10.1038/nature04158.

Gissi, E., Manea, E., Mazaris, A.D., Fraschetti, S., Almpanidou, V., Bevilacqua, S., Coll, M., Guarnieri, G., Lloret-Lloret, E., Pascual, M., Petza, D., Rilov, G., Schonwald, M., Stelzenmüller, V. and Katsanevakis, S. (2021) 'A review of the combined effects of climate change and other local human stressors on the marine environment', *Science of the Total Environment*, 755, p. 142564. doi:10.1016/j.scitotenv.2020.142564.

Glasl, B., Bongaerts, P., Elisabeth, N.H., Hoegh-Guldberg, O., Herndl, G.J. and Frade, P.R. (2017) 'Microbiome variation in corals with distinct depth distribution ranges across a shallow–mesophotic gradient (15–85 m)', *Coral Reefs*, 36(2), pp. 447–452. doi:10.1007/s00338-016-1517-x.

Glynn, P.W. (1993) 'Coral reef bleaching: Ecological perspectives', *Coral Reefs*, 12(1), pp. 1–17. doi:10.1007/BF00303779.

Gobbato, J., Work, T.M., Facchinelli, M.P., Siena, F.M., Montalbetti, E., Seveso, D., Louis, Y.D., Galli, P. and Montano, S. (2024) 'Pathology of tissue loss in three key gorgonian species in the Mediterranean Sea', *Journal of Invertebrate Pathology*, 207, pp. 108197, doi:10.1016/j.jip.2024.108197.

Goffredo, S., Arnone, S. and Zaccanti, F. (2002) 'Sexual reproduction in the Mediterranean solitary coral *Balanophyllia europaea*', *Marine Ecology Progress Series*, 229, pp. 83–94. doi:10.3354/meps229083.

Goffredo, S., Telo, T. and Zaccanti, F. (2005) 'Sexual reproduction of the solitary sunset cup coral *Leptopsammia pruvoti* (Scleractinia: Dendrophylliidae) in the Mediterranean. 1. Morphological aspects of gametogenesis and ontogenesis', Marine Biology, 147(2), pp. 485–495. doi:10.1007/s00227-005-1567-z.

Goffredo, S., Telo, T. and Zaccanti, F. (2006) 'Sexual reproduction of the solitary sunset cup coral *Leptopsammia pruvoti* (Scleractinia, Dendrophylliidae) in the Mediterranean. 2. Quantitative aspects of the annual reproductive cycle', Marine Biology, 148(5), pp. 923–931. doi:10.1007/s00227-005-0137-8.

Goffredo, S., Piccinetti, C. and Zaccanti, F. (2007) 'Variation in biometry and population density of solitary corals with solar radiation and sea surface temperature in the Mediterranean Sea', Marine Biology, 152(2), pp. 351–361. doi:10.1007/s00227-007-0695-z.

Goffredo, S., Mattioli, G. and Zaccanti, F. (2008) 'Relationships between growth, population structure and sea surface temperature in the temperate solitary coral *Balanophyllia europaea* (Scleractinia, Dendrophylliidae)', Coral Reefs, 27(3), pp. 623–632. doi:10.1007/s00338-008-0362-y.

Goffredo, S., Caroselli, E., Mattioli, G., Pignotti, E., Dubinsky, Z. and Zaccanti, F. (2009) 'Inferred level of calcification decreases along an increasing temperature gradient in a Mediterranean endemic coral', Limnology and Oceanography, 54(3), pp. 930–937. doi:10.4319/lo.2009.54.3.0930.

Gómez-Gras, D., Linares, C., Ledoux, J.B., Bensoussan, N., López-Sendino, P., Garrabou, J. and Coma, R. (2021) 'Population collapse of habitat-forming species in the Mediterranean: A long-term study of gorgonian populations affected by recurrent marine heatwaves', *Proceedings of the Royal Society B: Biological Sciences*, 288(1965), p. 20212384. doi:10.1098/rspb.2021.2384.

González, J.M., Kiene, R.P. and Moran, M.A. (1999) 'Transformation of sulfur compounds by an abundant lineage of marine bacteria in the α-subclass of the class Proteobacteria', *Applied and Environmental Microbiology*, 65(9), pp. 3810–3819. doi:10.1128/AEM.65.9.3810-3819.1999.

Goodbody-Gringley, G., Martinez, S., Bellworthy, J., Chequer, A., Nativ, H. and Mass, T. (2024) 'Irradiance-driven trophic plasticity in the coral *Madracis pharensis* from the eastern Mediterranean', *Scientific Reports*, 14, pp. 3646. doi:10.1038/s41598-024-54217-3.

Gugliotti, E.F., DeLorenzo, M.E. and Etnoyer, P.J. (2019) 'Depth-dependent temperature variability in the Southern California bight with implications for the cold-water gorgonian

octocoral *Adelogorgia phyllosclera'*, *Journal of Experimental Marine Biology and Ecology*, 514–515, pp. 118–126. doi:10.1016/j.jembe.2019.03.010.

Gutner-Hoch, E., Schneider, K., Stolarski, J., Domart-Coulon, I., Yam, R., Meibom, A., Shemesh, A. and Levy, O. (2016) 'Evidence for rhythmicity pacemaker in the calcification process of scleractinian coral', *Scientific Reports*, 6, pp. 20191. doi:10.1038/srep20191.

Habdija, I., Primc Habdija, B., Radanović, I., Špoljar, M., Matoničkin Kepčija, R., Vujčić Karlo, S., Miliša, M., Ostojić, A. and Sertić Perić, M. (2021) *Protista - Protozoa, Metazoa - Invertebrata*. Zagreb: Alfa d.d.

Hadjioannou, L., Jimenez, C., Rottier, C., Sfenthourakis, S. and Ferrier-Pagès, C. (2019) 'Response of the temperate scleractinian coral *Cladocora caespitosa* to high temperature and long-term nutrient enrichment', *Scientific Reports*, 9, pp. 14229. doi:10.1038/s41598-019-50716-w.

Halpern, B.S., Walbridge, S., Selkoe, K.A., Kappel, C.V., Micheli, F., D'Agrosa, C., Bruno, J.F., Casey, K.S., Ebert, C., Fox, H.E., Fujita, R., Heinemann, D., Lenihan, H.S., Madin, E.M.P., Perry, M.T., Selig, E.R., Spalding, M., Steneck, R. and Watson, R. (2008) 'A global map of human impact on marine ecosystems', *Science*, 319(5865), pp. 948–952. doi:10.1126/science.1149345.

Harmelin, J.G. (1984) 'Biologie du corail rouge: Paramètres de populations, croissance et mortalité. État des connaissances en France', u Charbonnier, D. and Garcia, S. (ur.) *Rapport de consultation technique du CGPM sur les ressources du corail rouge de la Méditerranée occidentale et leur exploitation rationnelle (FAO Rapport sur les pêches No. 306)*. Palma de Mallorca: FAO, pp. 99–103.

Harmelin, J.G. and Marinopoulos, J. (1994) 'Population structure and partial mortality of the gorgonian *Paramuricea clavata* (Risso) in the North-Western Mediterranean (France, Port-Cros Island)', *Marine Life*, 4, pp. 5–13.

Harrison, P.L. (1985) 'Sexual characteristics of scleractinian corals: Systematics and evolutionary implications', u *Proceedings of the 5th International Coral Reef Congress*, Vol. 4, pp. 337–342.

Harrison, P.L. and Wallace, C.C. (1990) ‘Reproduction, dispersal and recruitment of scleractinian corals’, u Dubinsky, Z. (ur.) *Ecosystems of the world: Coral reefs*, Vol. 25. Amsterdam: Elsevier, pp. 133–207.

Harvell, C.D., Jordán-Dahlgren, E., Merkel, S., Rosenberg, E., Raymundo, L., Smith, G., Weil, E. and Willis, B.L. (2007) ‘Coral disease, environmental drivers, and the balance between coral and microbial associates’, *Oceanography*, 20(1), pp. 172–195. doi:10.5670/oceanog.2007.91.

Hawthorn, A., Berzins, I.K., Dennis, M.M., Kiupel, M., Newton, A.L., Peters, E.C., Reyes, V.A. and Work, T.M. (2023) ‘An introduction to lesions and histology of scleractinian corals’, *Veterinary Pathology*, 60(5), pp. 529–546. doi:10.1177/03009858231189289.

Heckel, P.H. (1974) ‘Carbonate buildups in the geological record: A review’, u Laporte, L.F. (ur.) *Reefs in space and time*. *SEPM Special Publication*, 18, pp. 90–154.

Heltzel, P.S. and Babcock, R.C. (2002) ‘Sexual reproduction, larval development and benthic planulae of the solitary coral *Monomyces rubrum* (Scleractinia: Anthozoa)’, *Marine Biology*, 140(4), pp. 659–667. doi:10.1007/s00227-001-0745-3.

Helgoe, J., Davy, S.K., Weis, V.M. and Rodriguez-Lanetty, M. (2024) ‘Triggers, cascades, and endpoints: connecting the dots of coral bleaching mechanisms’, *Biological Reviews*, 99(3), pp. 715–752. doi:10.1111/brv.13042.

Hernandez-Agreda, A., Gates, R.D. and Ainsworth, T.D. (2017) ‘Defining the core microbiome in corals’ microbial soup’, *Trends in Microbiology*, 25, pp. 125–140. doi:10.1016/j.tim.2016.11.003.

Hernandez-Agreda, A., Gates, R.D. and Ainsworth, T.D. (2016) ‘The microbial signature provides insight into the mechanistic basis of coral success across reef habitats’, *mBio*, 7(4), p. e00560-16. doi:10.1128/mBio.00560-16.

Hobday, A.J., Alexander, L.V., Perkins, S.E., Smale, D.A., Straub, S.C., Oliver, E.C.J., Benthuysen, J.A., Burrows, M.T., Donat, M.G., Feng, M., Holbrook, N.J., Moore, P.J., Scannell, H.A., Sen Gupta, A. and Wernberg, T. (2016) ‘A hierarchical approach to defining marine heatwaves’, *Progress in Oceanography*, 141, pp. 227–238. doi:10.1016/j.pocean.2015.12.014.

Hobday, A.J., Oliver, E.C.J., Sen Gupta, A., Benthuysen, J.A., Burrows, M.T., Donat, M.G., Holbrook, N.J., Moore, P.J., Thomsen, M.S., Wernberg, T. and Smale, D.A. (2018) 'Categorizing and naming marine heatwaves', *Oceanography*, 31(2), pp. 162–173. doi:10.5670/oceanog.2018.205.

Houlbrèque, F. and Ferrier-Pagès, C. (2009) 'Heterotrophy in tropical scleractinian corals', *Biological Reviews*, 84(1), pp. 1–17. doi:10.1111/j.1469-185X.2008.00058.x.

Hughes, T.P., Baird, A.H., Bellwood, D.R., Card, M., Connolly, S.R., Folke, C., Grosberg, R., Hoegh-Guldberg, O., Jackson, J.B.C., Kleypas, J., Lough, J.M., Marshall, P., Nyström, M., Palumbi, S.R., Pandolfi, J.M., Rosen, B. and Roughgarden, J. (2003) 'Climate change, human impacts, and the resilience of coral reefs', Science, 301(5635), pp. 929–933. doi:10.1126/science.1085046.

Hughes, T.P., Kerry, J.T., Álvarez-Noriega, M., Álvarez-Romero, J.G., Anderson, K.D., Baird, A.H., Babcock, R.C., Beger, M., Bellwood, D.R. and Berkelmans, R. (2017) 'Global warming and recurrent mass bleaching of corals', *Nature*, 543(7645), pp. 373–377. doi:10.1038/nature21707.

Huggett, M.J. and Apprill, A. (2019) 'Coral microbiome database: Integration of sequences reveals high diversity and relatedness of coral-associated microbes', *Environmental Microbiology Reports*, 11(3), pp. 372–385. doi:10.1111/1758-2229.12686.

Hunt, L.R., Smith, S.M., Downum, K.R., Mydlarz, L.D. and Harvell, C.D. (2012) 'Microbial regulation in gorgonian corals', *Marine Drugs*, 10(6), pp. 1225–1243. doi:10.3390/md10061225.

Iborra, L., Linares, C., Ledoux, J.B., Garrabou, J., Kersting, D.K., Bensoussan, N., Cebrian, E. and Hereu, B. (2022) 'Temporal trends of two iconic Mediterranean gorgonians (*Paramuricea clavata* and *Eunicella cavolini*) in the climate change context', *Journal of Sea Research*, 186, p. 102241. doi:10.1016/j.seares.2022.102241.

Inoue, M., Suwa, R., Suzuki, A., Sakai, K. and Kawahata, H. (2018) 'A simple role of coral–algal symbiosis in coral calcification based on multiple geochemical tracers', *Geochimica et Cosmochimica Acta*, 235, pp. 76–88. doi:10.1016/j.gca.2018.05.016.

Jatkar, A.A., Brown, B.E., Bythell, J.C., Guppy, R., Morris, N.J. and Pearson, J.P. (2010) 'Measuring mucus thickness in reef corals using a technique devised for vertebrate applications', *Marine Biology*, 157(2), pp. 261–267. doi:10.1007/s00227-009-1313-z

Jeffries, M.A. and Lee, C.M. (2007) 'A climatology of the northern Adriatic Sea's response to bora and river forcing', *Journal of Geophysical Research: Oceans*, 112, pp. C03S91. doi:10.1029/2006JC003664.

Jentsch, A., Kreyling, J. and Beierkuhnlein, C. (2007) 'A new generation of climate-change experiments: Events, not trends', *Frontiers in Ecology and the Environment*, 5(7), pp. 365–374. doi:10.1890/1540-9295(2007)5[365:ANGOCE]2.0.CO;2.

Jiménez, C., Kersting, D.K., Bensoussan, N. and Linares, C. (2016) 'Mortality of the scleractinian coral *Cladocora caespitosa* during a warming event in the Levantine Sea (Cyprus)', *Regional Environmental Change*, 16(6), pp. 1963–1973. doi:10.1007/s10113-014-0729-2.

Jones, R.J. (2008) 'Coral bleaching, bleaching-induced mortality, and the adaptive significance of the bleaching response', *Marine Biology*, 154(1), pp. 65–80. doi:10.1007/s00227-007-0900-0.

Kelly, L.W., Williams, G.J., Barott, K.L., Carlson, C.A., Dinsdale, E.A., Edwards, R.A., Haas, A.F., Haynes, M., Lim, Y.W., McDole, T., Nelson, C.E., Sala, E., Sandin, S.A., Smith, J.E., Vermeij, M.J.A., Youle, M. and Rohwer, F. (2014) 'Local genomic adaptation of coral reef-associated microbiomes to gradients of natural variability and anthropogenic stressors', *Proceedings of the National Academy of Sciences of the United States of America*, 111(28), pp. 10227–10232. doi:10.1073/pnas.1403319111.

Kersting, D.K., Bensoussan, N. and Linares, C. (2013) 'Long-term responses of the endemic reef-builder *Cladocora caespitosa* to Mediterranean warming', *PLoS ONE*, 8(8), pp. e70820. doi:10.1371/journal.pone.0070820.

Kersting, D.K., Teixidó, N. and Linares, C. (2014) 'Recruitment and mortality of the temperate coral *Cladocora caespitosa*: implications for the recovery of endangered populations', *Coral Reefs*, 33, pp. 403–407. doi:10.1007/s00338-014-1144-3.

Kersting, D.K., Linares, C., Cebrian, E., Casals, D., Kipson, S. and Garrabou, J. (2015) 'Experimental evidence of the synergistic effects of warming and invasive algae on a temperate reef-builder coral', *Scientific Reports*, 5, p. 18635. doi:10.1038/srep18635.

Kimes, N.E., Johnson, W.R., Torralba, M., Nelson, K.E., Weil, E. and Morris, P.J. (2010) 'Microbial functional structure of *Montastraea faveolata* differs between healthy and yellow-band diseased colonies', *Environmental Microbiology*, 12(2), pp. 541–556. doi:10.1111/j.1462-2920.2009.02113.x.

Knowlton, N. (2001) 'The future of coral reefs', *Proceedings of the National Academy of Sciences of the United States of America*, 98(10), pp. 5419–5425. doi:10.1073/pnas.091092998.

Krediet, C.J., Ritchie, K.B., Paul, V.J. and Teplitski, M. (2013) 'Coral-associated micro-organisms and their roles in promoting coral health and thwarting diseases', *Proceedings of the Royal Society B: Biological Sciences*, 280, p. 20122328. doi:10.1098/rspb.2012.2328.

Kružić, P. (2002) 'Marine fauna of the Mljet National Park (Adriatic Sea, Croatia). 1. Anthozoa', *Natura Croatica*, 11(3), pp. 265–292.

Kružić, P. (2007) 'Anthozoan fauna of Telašćica Nature Park (Adriatic Sea, Croatia)', *Natura Croatica*, 16(4), pp. 233–266.

Kružić, P. and Požar-Domac, A. (2003) 'Banks of the coral *Cladocora caespitosa* (Anthozoa, Scleractinia) in the Adriatic Sea', *Coral Reefs*, 22(4), pp. 536. doi:10.1007/s00338-003-0345-y.

Kružić, P. and Benković, L. (2008) 'Bioconstructional features of the coral *Cladocora caespitosa* in the Adriatic Sea (Croatia)', *Marine Ecology*, 29(1), pp. 125–139. doi:10.1111/j.1439-0485.2008.00220.x.

Kružić, P. and Popijač, A. (2015) 'Mass mortality events of the coral *Balanophyllia europaea* in the Mljet National Park caused by sea temperature anomalies', *Coral Reefs*, 34(1), pp. 109–118. doi:10.1007/s00338-014-1231-5.

Kružić, P. et al. (2014) 'Impact of bleaching on the coral *Cladocora caespitosa* in the eastern Adriatic Sea', *Marine Ecology Progress Series*, 509, pp. 193–202. doi:10.3354/meps10962.

Kružić, P. et al. (2016) 'Impacts of temperature anomalies on mortality of benthic organisms in the Adriatic Sea', *Marine Ecology*, 37(6), pp. 1190–1209. doi:10.1111/maec.12293.

Kružić, P., Sršen, P. and Benković, L. (2012) 'The impact of seawater temperature on coral growth parameters of the colonial coral *Cladocora caespitosa* (Anthozoa, Scleractinia) in the eastern Adriatic Sea', *Facies*, 58(4), pp. 477–491. doi:10.1007/s10347-012-0306-4.

Kružić, P., Zibrowius, H. and Požar-Domac, A. (2002) 'Actiniaria and Scleractinia (Cnidaria, Anthozoa) from the Adriatic Sea (Croatia): First records, confirmed occurrences and significant range extensions of certain species', *Italian Journal of Zoology*, 69(4), pp. 345–353. doi:10.1080/11250000209356480.

La Rivière, M., Garrabou, J. and Bally, M. (2013) 'Transient shifts in bacterial communities associated with the temperate gorgonian *Paramuricea clavata* in the field', *PLoS ONE*, 8(2), pp. e57385. doi:10.1371/journal.pone.0057385.

Lalli, C.M. and Parsons, T.R. (1997) *Biological oceanography: an introduction*. 2nd edn. Oxford: Butterworth-Heinemann.

LaJeunesse, T.C., Parkinson, J.E., Gabrielson, P.W., Jeong, H.J., Reimer, J.D., Voolstra, C.R. and Santos, S.R. (2018) 'Systematic revision of Symbiodiniaceae highlights the antiquity and diversity of coral endosymbionts', *Current Biology*, 28(16), pp. 2570–2580.e6. doi:10.1016/j.cub.2018.07.008.

Lejeusne, C., Chevaldonné, P., Pergent-Martini, C., Boudouresque, C.F. and Pérez, T. (2010) 'Climate change effects on a miniature ocean: the highly diverse, highly impacted Mediterranean Sea', *Trends in Ecology & Evolution*, 25(4), pp. 250–260. doi:10.1016/j.tree.2009.10.009.

Lema, K.A., Willis, B.L. and Bourne, D.G. (2012) 'Corals form characteristic associations with symbiotic nitrogen-fixing bacteria', *Applied and Environmental Microbiology*, 78(9), pp. 3136–3144. doi:10.1128/AEM.07800-11.

Lesser, M.P. (2011) 'Coral bleaching: Causes and mechanisms', in Dubinsky, Z. and Stambler, N. (eds) Coral Reefs: An Ecosystem in Transition. Berlin: Springer, pp. 405–419.

Lesser, M.P., Stat, M. and Gates, R.D. (2013) 'The endosymbiotic dinoflagellates (*Symbiodinium* sp.) of corals are parasites and mutualists', *Coral Reefs*, 32, pp. 603–611. doi:10.1007/s00338-013-1051-z.

Linares, C., Coma, R., Díaz, D., Zabala, M., Hereu, B. and Dantart, L. (2005) 'Immediate and delayed effects of a mass mortality event on gorgonian population dynamics and benthic community structure in the NW Mediterranean Sea', *Marine Ecology Progress Series*, 305, pp. 127–137. doi:10.3354/meps305127.

Linares, C., Doak, D.F., Coma, R., Díaz, D. and Zabala, M. (2007) 'Life history and viability of a long-lived marine invertebrate: The octocoral *Paramuricea clavata*', *Ecology*, 88(4), pp. 918–928. doi:10.1890/05-1931.

Linares, C., Coma, R., Díaz, D., Zabala, M., Hereu, B. and Dantart, L. (2008) 'Size distribution, density and disturbance in two Mediterranean gorgonians: *Paramuricea clavata* and *Eunicella singularis*', *Journal of Applied Ecology*, 45(2), pp. 688–699. doi:10.1111/j.1365-2664.2007.01419.x.

Lipizer, M., Partescano, E., Rabitti, A., Giorgetti, A. and Crise, A. (2014) 'Qualified temperature, salinity and dissolved oxygen climatologies in a changing Adriatic Sea', *Ocean Science*, 10, pp. 771–797. doi:10.5194/os-10-771-2014.

Lowenstam, H.A. (1950) 'Niagaran reefs of the Great Lakes area', *Journal of Geology*, 58(5), pp. 430–487. doi:10.1086/625754.

Magaš, D. (1998) 'Nature Park "Telašćica" on Dugi otok (Croatia) – some aspects of environmental planning', *Geoadria*, 3(1), pp. 81–92. doi:10.15291/geoadria.48.

Maldonado, M., Sánchez-Tocino, L. and Navarro, C. (2010) 'Recurrent disease outbreaks in corneous demosponges of the genus *Ircinia*: Epidemic incidence and defense mechanisms', *Marine Biology*, 157(7), pp. 1577–1590. doi:10.1007/s00227-010-1431-7.

Marini, M., Jones, B.H., Campanelli, A., Grilli, F. and Lee, C.M. (2008) 'Seasonal variability and Po River plume influence on biochemical properties along the western Adriatic coast', *Journal of Geophysical Research: Oceans*, 113, pp. C05S90. doi:10.1029/2007JC004370.

Mescher, A.L. (2013) *Junqueira's Basic Histology: Text and Atlas*. 13th edn. New York: McGraw-Hill Medical.

Meron, D., Rodolfo-Metalpa, R., Cunning, R., Baker, A.C., Fine, M. and Banin, E. (2012) 'Changes in coral microbial communities in response to a natural pH gradient', *The ISME Journal*, 6, pp. 1775–1785. doi:10.1038/ismej.2012.19.

McMurdie, P.J. and Holmes, S. (2013) 'phyloseq: an R package for reproducible interactive analysis and graphics of microbiome census data', *PLoS ONE*, 8(4), pp. e61217. doi:10.1371/journal.pone.0061217.

Mistri, M. and Ceccherelli, V.U. (1996) 'Effect of a mucilage event on the Mediterranean gorgonian *Paramuricea clavata*. I – Short term impacts at the population and colony levels', *Italian Journal of Zoology*, 63(3), pp. 221–230. doi: 10.1080/11250009609356137.

Moberg, F. and Folke, C. (1999) 'Ecological goods and services of coral reef ecosystems', *Ecological Economics*, 29(2), pp. 215–233. doi:10.1016/S0921-8009(99)00009-9.

Morri, C., Peirano, A., Bianchi, C.N. and Sassarini, M. (1994) 'Present-day bioconstructions of the hard coral *Cladocora caespitosa* (L.) (Anthozoa, Scleractinia) in the eastern Ligurian Sea (NW Mediterranean)', *Biologia Marina Mediterranea*, 1, pp. 371–372.

Morri, C., Peirano, A., Bianchi, C.N. and Rodolfo-Metalpa, R. (2000) '*Cladocora caespitosa*: A colonial zooxanthellate Mediterranean coral showing constructional ability', *Reef Encounter*, 27, pp. 22–25.

Morrissey, J.F., Sumich, J.L. and Pinkard-Meier, D.R. (2018) Introduction to the Biology of Marine Life. 11th edn. Burlington, MA: Jones & Bartlett Learning.

Morrow, K.M., Müller, E.M. and Lesser, M.P. (2018) 'How does the coral microbiome cause, respond to, or modulate the bleaching process?', in van Oppen, M.J.H. and Lough, J.M. (eds) *Coral Bleaching*. Cham: Springer, pp. 153–188. doi:10.1007/978-3-319-75393-5_7.

Morrow, K.M., Moss, A.G., Chadwick, N.E. and Liles, M.R. (2012) 'Bacterial associates of two Caribbean coral species reveal species-specific distribution and geographic variability', *Applied and Environmental Microbiology*, 78(18), pp. 6438–6449. doi:10.1128/AEM.01162-12.

Nakajima, R., Tanaka, Y., Yoshida, T., Fujisawa, T., Nakayama, A., Yasuda, A., Yoshinaga, K. and Toda, T. (2015) 'High inorganic phosphate concentration in coral mucus and its utilization by heterotrophic bacteria in a Malaysian coral reef', *Marine Ecology*, 36, pp. 835–841. doi:10.1111/maec.12158.

Nardi A., Resaikos V., Papatheodoulou M., Di Carlo M., Vedhanarayanan H., Regoli F., Gorbi S. and Jimenez C. (2024) 'Cellular adaptations of the scleractinian coral *Madracis pharensis* to chronic oil pollution in a Mediterranean shipwreck', *Frontiers in Marine Science*, 11, p. 1330894. doi:10.3389/fmars.2024.1330894.

National Park Kornati (n.d.) 'List of islands'. Available at: https://www.np-kornati.hr/index.php?option=com_content&view=article&id=58&Itemid=236&lang=en (Accessed: 24 April 2023).

National Park Kornati (n.d.) 'Submarine biology'. Available at: https://www.np-kornati.hr/index.php?option=com_content&view=article&id=61&Itemid=223&lang=en (Accessed: 24 April 2023).

Neave, M.J. et al. (2016) 'Diversity and function of prevalent symbiotic marine bacteria in the genus *Endozoicomonas*', *Applied Microbiology and Biotechnology*, 100(19), pp. 8315–8324. doi:10.1007/s00253-016-7777-0.

Nelson, H.F., Brown, C.W. and Brineman, J.H. (1962) 'Skeletal limestone classification', *American Association of Petroleum Geologists Memoir*, 1, pp. 224–252.

Nielsen, D.A., Petrou, K. and Gates, R.D. (2018) 'Coral bleaching from a single cell perspective', *The ISME Journal*, 12, pp. 1558–1567. doi:10.1038/s41396-018-0080-6.

Oakley, C.A. and Davy, S.K. (2018) 'Cell biology of coral bleaching', in van Oppen, M.J.H. and Lough, J.M. (eds) *Coral Bleaching*. Cham: Springer, pp. 189–211. doi:10.1007/978-3-319-75393-5_8.

O'Brien, P.A., Webster, N.S., Miller, D.J. and Bourne, D.G. (2019) 'Host–microbe coevolution: Applying evidence from model systems to complex marine invertebrate holobionts', *mBio*, 10(1), pp. e02241-18. doi:10.1128/mBio.02241-18.

Oksanen, J., Simpson, G.L., Blanchet, F.G., Kindt, R., Legendre, P., Minchin, P.R., O'Hara, R.B., Solymos, P., Stevens, M.H.H., Szoecs, E., Wagner, H. *et al.* (2026) *vegan: Community Ecology Package*. Available at: https://cran.r-project.org/package=vegan. doi:10.32614/CRAN.package.vegan.

Olson, N.D., Ainsworth, T.D., Gates, R.D. and Takabayashi, M. (2009) 'Diazotrophic bacteria associated with Hawaiian *Montipora* corals: Diversity and abundance in correlation with symbiotic dinoflagellates', *Journal of Experimental Marine Biology and Ecology*, 371(2), pp. 140–146. doi:10.1016/j.jembe.2009.01.012.

Palladino, G., Caroselli, E., Tavella, T., D'Amico, F., Prada, F., Mancuso, A., Franzellitti, S., Rampelli, S., Candela, M., Goffredo, S. and Biagi, E. (2022) 'Metagenomic shifts in mucus, tissue and skeleton of the coral *Balanophyllia europaea* living along a natural CO2 gradient', *ISME Communications*, 2(1), pp. 65. doi:10.1038/s43705-022-00152-1.

Palmer, C.V., Mydlarz, L.D. and Willis, B.L. (2008) 'Evidence of an inflammatory-like response in non-normally pigmented tissues of two scleractinian corals', *Proceedings of the Royal Society B: Biological Sciences*, 275(1652), pp. 2687–2693. doi:10.1098/rspb.2008.0335.

Palmer, C.V. and Traylor-Knowles, N.G. (2012) 'Towards an integrated network of coral immune mechanisms', *Proceedings of the Royal Society B: Biological Sciences*, 279(1745), pp. 4106–4114. doi:10.1098/rspb.2012.1477.

Palmer, C.V., Traylor-Knowles, N.G., Willis, B.L. and Bythell, J.C. (2011) 'Corals use similar immune cells and wound-healing processes as those of higher organisms', *PLoS ONE*, 6(8), pp. e23992. doi:10.1371/journal.pone.0023992.

Palmer, C.V., McGinty, E.S., Cummings, D.J., Smith, S.M., Bartels, E. and Mydlarz, L.D. (2011) 'Patterns of coral ecological immunology: Variation in the responses of Caribbean corals to elevated temperature and a pathogen elicitor', *Journal of Experimental Biology*, 214(24), pp. 4240–4249. doi:10.1242/jeb.061267.

Pantos, O., Bongaerts, P., Dennis, P.G., Tyson, G.W. and Hoegh-Guldberg, O. (2015) 'Habitat-specific environmental conditions primarily control the microbiomes of the coral *Seriatopora hystrix'*, *The ISME Journal*, 9(9), pp. 1916–1927. doi:10.1038/ismej.2015.3.

Parada, A.E., Needham, D.M. and Fuhrman, J.A. (2016) 'Every base matters: Assessing small subunit rRNA primers for marine microbiomes with mock communities, time series and global field samples', *Environmental Microbiology*, 18(5), pp. 1403–1414. doi:10.1111/1462-2920.13023.

Peirano, A., Morri, C., Mastronuzzi, G. and Bianchi, C.N. (1998) 'The coral *Cladocora caespitosa* (Anthozoa, Scleractinia) as a bioherm builder in the Mediterranean Sea', *Memorie Descrittive della Carta Geologica d'Italia*, 52, pp. 59–74.

Peirano, A., Kružić, P. and Mastronuzzi, G. (2009) 'Growth of Mediterranean reef of *Cladocora caespitosa* (L.) in the Late Quaternary and climate inferences', *Facies*, 55(3), pp. 325–333. doi:10.1007/s10347-008-0177-x.

Perez, T., Garrabou, J., Harmelin, J.G., Francour, P., Vacelet, J. and Zabala, M. (2000) 'Mass mortality of marine invertebrates: An unprecedented event in the Northwestern Mediterranean', Comptes Rendus de l'Académie des Sciences - Série III, 323(10), pp. 853–865. doi:10.1016/S0764-4469(00)01237-3.

Peters, E.C. (2016) 'Anatomy', in Woodley, C.M., Downs, C.A., Bruckner, A.W., Porter, J.W. and Galloway, S.B. (eds) *Diseases of Coral*. Hoboken, NJ: Wiley-Blackwell, pp. 85–107.

Piazzi, L., Gennaro, P., Ceccherelli, G., Piazzi, L., Gennaro, P., Ceccherelli, G., and others (2021) 'Animal forest mortality: Following the consequences of a gorgonian coral loss on a Mediterranean coralligenous assemblage', *Diversity*, 13(3), p. 133. doi:10.3390/d13030133.

Pivotto, I.D., Linares, C., Viladrich, N., Priori, C., Tomas, F., Gori, A. and Rossi, S. (2015) 'Highly contrasted responses of Mediterranean octocorals to climate change along a depth gradient', *Royal Society Open Science*, 2(5), p. 140493. doi:10.1098/rsos.140493.

Pjevac, P., Hausmann, B., Schwarz, J., Kohl, G., Herbold, C.W., Loy, A. and Berry, D. (2021) 'An economical and flexible dual barcoding, two-step PCR approach for highly multiplexed

amplicon sequencing', Frontiers in Microbiology, 12, p. 669776. doi:10.3389/fmicb.2021.669776.

Pogoreutz, C., Rädecker, N., Cárdenas, A., Gärdes, A., Wild, C. and Voolstra, C.R. (2018) 'Dominance of *Endozoicomonas* bacteria throughout coral bleaching and mortality suggests structural inflexibility of the *Pocillopora verrucosa* microbiome', *Ecology and Evolution*, 8(4), pp. 2240–2252. doi:10.1002/ece3.3830.

Pogoreutz, C., Rädecker, N., Cárdenas, A., Gärdes, A., Voolstra, C.R. and Wild, C. (2020) 'Adaptive dysbiosis: a new concept for understanding coral bleaching', *Microorganisms*, 8(11), p. 1682. doi:10.3390/microorganisms8111682.

Pollock, F.J., McMinds, R., Smith, S., Bourne, D.G., Willis, B.L., Medina, M., Thurber, R.V. and Zaneveld, J.R. (2018) 'Coral-associated bacteria demonstrate phylosymbiosis and cophylogeny', *Nature Communications*, 9, p. 4921. doi:10.1038/s41467-018-07275-x.

Ponti, M., Perlini, R.A. and Cerrano, C. (2014) 'Ecological shifts in Mediterranean coralligenous assemblages related to gorgonian forest loss', *PLOS ONE*, 9(7), p. e102782. doi:10.1371/journal.pone.0102782.

Pérez, T., Garrabou, J., Sartoretto, S., Harmelin, J.-G., Francour, P. and Vacelet, J. (2000) 'Mass mortality of marine invertebrates: An unprecedented event in the northwestern Mediterranean', *Comptes Rendus de l'Académie des Sciences - Série III*, 323(10), pp. 853–865. doi:10.1016/S0764-4469(00)01237-3.

Rädecker, N., Pogoreutz, C., Voolstra, C.R., Wiedenmann, J. and Wild, C. (2015) 'Nitrogen cycling in corals: the key to understanding holobiont functioning?', *Trends in Microbiology*, 23(8), pp. 490–497. doi:10.1016/j.tim.2015.03.008.

Rädecker, N., Pogoreutz, C., Gegner, H.M., Cárdenas, A., Roth, F., Bougoure, J., Guagliardo, P., Wild, C., Pernice, M., Raina, J.-B., Meibom, A. and Voolstra, C.R. (2021) 'Heat stress destabilizes symbiotic nutrient cycling in corals', *Proceedings of the National Academy of Sciences of the United States of America*, 118(5), pp. e2022653118. doi:10.1073/pnas.2022653118.

Raina, J.-B., Dinsdale, E.A., Willis, B.L. and Bourne, D.G. (2010) 'Do the organic sulfur compounds DMSP and DMS drive coral microbial associations?', *Trends in Microbiology*, 18(3), pp. 101–108. doi:10.1016/j.tim.2009.12.002.

Reynolds, T.L. (2016) 'Gross and microscopic pathology for quantifying responses of coral reefs to remediation efforts', *Veterinary Pathology*, 53(1), pp. 5–6. doi:10.1177/0300985815618434.

Ricci, F., Marcelino, V.R., Blackall, L.L., Kühl, M. and Medina, M. (2019) 'Beneath the surface: Community assembly and functions of the coral skeleton microbiome', *Microbiome*, 7, p. 159. doi:10.1186/s40168-019-0762-y.

Ritchie, K.B. (2006) 'Regulation of microbial populations by coral surface mucus and mucus-associated bacteria', *Marine Ecology Progress Series*, 322, pp. 1–14. doi:10.3354/meps322001.

Rivetti, I., Fraschetti, S., Lionello, P., Zambianchi, E. and Boero, F. (2014) 'Global warming and mass mortalities of benthic invertebrates in the Mediterranean Sea', *PLOS ONE*, 9(12), p. e115655. doi:10.1371/journal.pone.0115655.

Rodolfo-Metalpa, R., Bianchi, C.N., Peirano, A. and Morri, C. (2005) 'Tissue necrosis and mortality of the temperate coral *Cladocora caespitosa*', *Italian Journal of Zoology*, 72(3), pp. 271–276. doi:10.1080/11250000509356685.

Rodolfo-Metalpa, R., Peirano, A., Houlbrèque, F., Abbate, M. and Ferrier-Pagès, C. (2006) 'Coral mortality associated with a warm summer in the Mediterranean Sea', *Marine Biology*, 149(4), pp. 743–754. doi:10.1007/s00227-005-0229-1.

Rodolfo-Metalpa, R., Peirano, A., Houlbrèque, F., Abbate, M. and Ferrier-Pagès, C. (2008) 'Effects of temperature, light and heterotrophy on the growth rate and budding of the temperate coral *Cladocora caespitosa*', *Coral Reefs*, 27(1), pp. 17–25. doi:10.1007/s00338-007-0283-1.

Rohwer, F., Seguritan, V., Azam, F. and Knowlton, N. (2002) 'Diversity and distribution of coral-associated bacteria', *Marine Ecology Progress Series*, 243, pp. 1–10. doi:10.3354/meps243001.

Rose, T.H., Smale, D.A. and Botting, G. (2012) 'The 2011 marine heat wave in Cockburn Sound, southwest Australia', *Ocean Science*, 8(4), pp. 545–550. doi:10.5194/os-8-545-2012.

Rosselló, P., Pascual, A. and Combes, V. (2023) 'Assessing marine heat waves in the Mediterranean Sea: a comparison of fixed and moving baseline methods', *Frontiers in Marine Science*, 10, p. 1168368. doi:10.3389/fmars.2023.1168368.

Rosenberg, E. and Loya, Y. (1999) 'Vibrio shiloi is the etiological (causative) agent of *Oculina patagonica* bleaching: General implications', *Reef Encounters*, 25, pp. 8–10.

Rosenberg, E., Koren, O., Reshef, L., Efrony, R. and Zilber-Rosenberg, I. (2007) 'The role of microorganisms in coral health, disease and evolution', *Nature Reviews Microbiology*, 5(5), pp. 355–362. doi:10.1038/nrmicro1635.

Rossi, S., Bramanti, L., Gori, A. and Orejas, C. (eds) (2017) *Marine Animal Forests: The Ecology of Benthic Biodiversity Hotspots*. Cham: Springer. doi:10.1007/978-3-319-21012-4.

Rovira, G., Capdevila, P., Zentner, Y., Margarit, N., Ortega, J., Casals, D., Figuerola-Ferrando, L., Aspillaga, E., Medrano, A., Pagès-Escolà, M., Hereu, B., Garrabou, J. and Linares, C. (2025) 'When resilience is not enough: 2022 extreme marine heatwave threatens climatic refugia for a habitat-forming Mediterranean octocoral', *Journal of Animal Ecology*, 94(8), pp. 1507–1514. doi:10.1111/1365-2656.14112.

Rubio-Portillo, E., Santos, F., Martínez-García, M., de los Ríos, A., Ascaso, C., Souza-Egipsy, V., Carrascal, L.M., Ríos, P., Antón, J. and Ramos-Esplá, A.A. (2016) 'Structure and temporal dynamics of the bacterial communities associated to microhabitats of the coral *Oculina patagonica*', *Environmental Microbiology*, 18, pp. 4564–4578. doi:10.1111/1462-2920.13548.

Sahin, D., Schoepf, V., Filbee-Dexter, K., Thomson, D.P., Radford, B. and Wernberg, T. (2023) 'Heating rate explains species-specific coral bleaching severity during a simulated marine heatwave', *Marine Ecology Progress Series*, 706, pp. 33–46. doi:10.3354/meps14246.

Salomidi, M., Katsanevakis, S., Borja, Á., Braeckman, U., Damalas, D., Galparsoro, I., Mifsud, R., Mirto, S., Pascual, M., Pipitone, C., Rabaut, M., Todorova, V. and Vassilopoulou, V. (2012) 'Assessment of goods and services, vulnerability, and conservation status of European seabed biotopes: A stepping stone towards ecosystem-based marine spatial management', *Mediterranean Marine Science*, 13(1), pp. 49–88. doi:10.12681/mms.23.

Sarda, J., Gori, A., Donate-Ordóñez, R., Viladrich, N., Costantini, F., Garrabou, J. and Linares, C. (2025) 'Recurrent marine heatwaves compromise the reproduction success and long-term viability of shallow populations of the Mediterranean gorgonian *Eunicella singularis*', *Marine Environmental Research*, 203, pp. 106822. doi:10.1016/j.marenvres.2024.106822.

Schiller, C. (1993) 'Ecology of the symbiotic coral *Cladocora caespitosa* (L.) (Faviidae, Scleractinia) in the Bay of Piran (Adriatic Sea): I. Distribution and biometry', *PSZNI: Marine Ecology*, 14(3), pp. 205–219. doi:10.1111/j.1439-0485.1993.tb00379.x.

Schuhmacher, H. and Zibrowius, H. (1985) 'What is hermatypic? A redefinition of ecological groups in corals and other organisms', *Coral Reefs*, 4(1), pp. 1–9.

Sheppard, C.R.C., Knowlton, N., Lang, J., Fenner, D., Weil, E., Zea, S., Bak, R.P.M., Sanchez, J.A. and Turak, E. (2007) *Coralpedia: A guide to Caribbean corals, octocorals and sponges*. CD-ROM. London: Overseas Territories Environment Programme, Foreign and Commonwealth Office.

Shnit-Orland, M. and Kushmaro, A. (2009) 'Coral mucus-associated bacteria: a possible first line of defence', *FEMS Microbiology Ecology*, 67(3), pp. 371–380. doi:10.1111/j.1574-6941.2008.00644.x.

Sini, M., Kipson, S., Linares, C., Koutsoubas, D., Garrabou, J. and Kizilkaya, Z. (2015) 'The yellow gorgonian *Eunicella cavolini*: Demography and disturbance levels across the Mediterranean Sea', PLoS ONE, 10(5), p. e0126253. doi:10.1371/journal.pone.0126253.

Smale, D.A., Wernberg, T., Oliver, E.C.J. et al. (2019) 'Marine heatwaves threaten global biodiversity and the provision of ecosystem services', *Nature Climate Change*, 9, pp. 306–312. doi:10.1038/s41558-019-0412-1.

Smith, D.J., Suggett, D.J. and Baker, N.R. (2005) 'Is photoinhibition of zooxanthellae photosynthesis the primary cause of thermal bleaching in corals?', *Global Change Biology*, 11(1), pp. 1–11. doi:10.1111/j.1529-8817.2003.00895.x.

Smith, K.E., Burrows, M.T., Hobday, A.J., King, N.G., Moore, P.J., Sen Gupta, A., Thomsen, M.S., Wernberg, T. and Smale, D.A. (2023) 'Biological impacts of marine heatwaves', *Annual Review of Marine Science*, 15, pp. 119–145. doi:10.1146/annurev-marine-032122-121437.

Spalding, M.D., Ravilious, C. and Green, E.P. (2001) World Atlas of Coral Reefs. Berkeley: University of California Press.

Sudek, M., Work, T.M., Aeby, G.S. and Davy, S.K. (2012) 'Histological observations in the Hawaiian reef coral, *Porites compressa*, affected by *Porites* bleaching with tissue loss', *Journal of Invertebrate Pathology*, 111(2), pp. 121–125. doi:10.1016/j.jip.2012.07.004.

Suggett, D.J. and Smith, D.J. (2020) 'Coral bleaching patterns are the outcome of complex biological and environmental networking', *Global Change Biology*, 26(1), pp. 68–79, doi:10.1111/gcb.14871.

Teplitski, M. and Ritchie, K. (2009) 'How feasible is the biological control of coral diseases?', *Trends in Ecology & Evolution*, 24(7), pp. 378–385. doi:10.1016/j.tree.2009.02.008.

Terzić, E., Vilibić, I., Mihanović, H., Šepić, J., Dunić, N. and Tudor, M. (2025) 'Unprecedented warming and salinization observed in the deep Adriatic', *Limnology and Oceanography Letters*, 10(6), pp. 888–898. doi:10.1002/lol2.70051.

Thibaut, T., Pinedo, S., Torras, X. and Ballesteros, E. (2005) 'Long-term decline of the populations of Fucales (*Cystoseira* spp. and *Sargassum* spp.) in the Albères Coast (France, northwestern Mediterranean)', *Marine Pollution Bulletin*, 50(12), pp. 1472–1489. doi:10.1016/j.marpolbul.2005.06.014.

Thomsen, M.S. and South, P.M. (2019) 'Communities and attachment networks associated with primary, secondary and alternative foundation species: A case of stressed and disturbed stands of southern bull kelp', *Diversity*, 11(4), p. 56. doi:10.3390/d11040056.

Thomson, J.A., Burkholder, D.A., Heithaus, M.R., Fourqurean, J.W., Fraser, M.W., Statton, J. and Kendrick, G.A. (2015) 'Extreme temperatures, foundation species, and abrupt ecosystem change: An example from an iconic seagrass ecosystem', *Global Change Biology*, 21(4), pp. 1463–1474. doi:10.1111/gcb.12694.

Thurber, R.V., Barott, K.L., Hall, D., Liu, H., Rodriguez-Mueller, B., Desnues, C., Edwards, R.A., Haynes, M., Angly, F.E., Wegley, L. and Rohwer, F. (2009) 'Metagenomic analysis of stressed

coral holobionts', *Environmental Microbiology*, 11(8), pp. 2148–2163. doi:10.1111/j.1462-2920.2009.01935.x.

Traylor-Knowles, N. (2019) 'Heat stress compromises epithelial integrity in the coral *Acropora hyacinthus*', *PeerJ*, 7, p. e6510. doi:10.7717/peerj.6510.

Tribollet, A. (2008) 'Dissolution of dead corals by euendolithic microorganisms across the Northern Great Barrier Reef (Australia)', *Microbial Ecology*, 55(4), pp. 569–580. doi:10.1007/s00248-007-9298-5.

van de Water, J.A.J.M., Melkonian, R., Junca, H., Voolstra, C.R., Reynaud, S., Allemand, D. and Ferrier-Pagès, C. (2017) 'Comparative assessment of Mediterranean gorgonian-associated microbial communities reveals conserved core and locally variant bacteria', *Microbial Ecology*, 73(2), pp. 466–478. doi:10.1007/s00248-016-0858-x.

van de Water, J.A.J.M., Allemand, D. and Ferrier-Pagès, C. (2018) 'Seasonal stability in the microbiomes of temperate gorgonians and the red coral *Corallium rubrum* across the Mediterranean Sea', *Microbial Ecology*, 75, pp. 274–288. doi:10.1007/s00248-017-1006-y.

van Oppen, M.J.H. and Blackall, L.L. (2019) 'Coral microbiome dynamics, functions and design in a changing world', *Nature Reviews Microbiology*, 17, pp. 557–567. doi:10.1038/s41579-019-0223-4.

Vázquez-Luis, M., Álvarez, E., Barrajón, A., García-March, J.R., Grau, A., Hendriks, I.E., Jiménez, S., Kersting, D.K., Moreno, D., Pérez, M., Ruiz, J.M., Sánchez, J., Villalba, A. and Deudero, S. (2017) 'S.O.S. Pinna nobilis: A mass mortality event in Western Mediterranean Sea', *Frontiers in Marine Science*, 4, p. 220. doi:10.3389/fmars.2017.00220

Verbruggen, H. and Tribollet, A. (2011) 'Boring algae', *Current Biology*, 21(21), pp. R876–R877. doi:10.1016/j.cub.2011.09.047.

Verdura, J., Linares, C., Ballesteros, E., Coma, R., Uriz, M.J., Bensoussan, N., Cebrian, E., Garrabou, J. and Hereu, B. (2019) 'Biodiversity loss in a Mediterranean ecosystem due to an extreme warming event unveils the role of an engineering gorgonian species', *Scientific Reports*, 9, p. 18671. doi:10.1038/s41598-019-41929-0.

Vergotti, M.J., D'Olivo, J.P., Brachert, T.C., Capdevila, P., Garrabou, J., Linares, C., Spreter, P.M. and Kersting, D.K. (2025) 'Reconstruction of long-term sublethal effects of warming on a temperate coral in a climate change hotspot', *Journal of Animal Ecology*, 94, pp. 125–138. doi:10.1111/1365-2656.14225.

Verri, G., Pinardi, N., Oddo, P., Ciliberti, S.A. and Coppini, G. (2018) 'River runoff influences on the central Mediterranean overturning circulation', *Climate Dynamics*, 50(5–6), pp. 1675–1703. doi:10.1007/s00382-017-3715-9.

Vezzulli, L., Previati, M., Pruzzo, C., Marchese, A., Bourne, D.G. and Cerrano, C. (2010) 'Vibrio infections triggering mass mortality events in a warming Mediterranean Sea', *Environmental Microbiology*, 12(7), pp. 2007–2019. doi:10.1111/j.1462-2920.2010.02209.x.

Vilibić, I., Šepić, J. and Proust, N. (2013) 'Weakening thermohaline circulation in the Adriatic Sea', *Climate Research*, 55(3), pp. 217–225. doi:10.3354/cr01128.

Visser, M.E. (2008) 'Keeping up with a warming world: Assessing the rate of adaptation to climate change', *Proceedings of the Royal Society B: Biological Sciences*, 275(1635), pp. 649–659. doi:10.1098/rspb.2007.0997.

Voultsiadou, E., Dailianis, T., Antoniadou, C., Vafidis, D., Dounas, C. and Chintiroglou, C.C. (2011) 'Aegean bath sponges: Historical data and current status', *Reviews in Fisheries Science*, 19(1), pp. 34–51. doi:10.1080/10641262.2010.531794.

Vuleta, S., Nakagawa, S. and Ainsworth, T.D. (2024) 'The global significance of scleractinian corals without photoendosymbiosis', *Scientific Reports*, 14(1), p. 60794. doi:10.1038/s41598-024-60794-0.

Wada, N., Pollock, F.J., Willis, B.L., Ainsworth, T.D., Mano, N. and Bourne, D.G. (2016) 'In situ visualization of bacterial populations in coral tissues: pitfalls and solutions', *PeerJ*, 4, pp. e2424. doi:10.7717/peerj.2424.

Waller, R.G. (2003) 'The reproductive ecology of deep-water scleractinian corals', PhD thesis, University of Southampton.

Waller, R.G., Tyler, P.A. and Smith, C.R. (2018) 'Reproductive ecology of cold-water corals', u Rossi, S., Bramanti, L., Gori, A. and Orejas, C. (ur.) *Marine Animal Forests: The Ecology of Benthic Biodiversity Hotspots*. Cham: Springer, pp. 265–291. doi:10.1007/978-3-319-17001-5_7.

Wells, J.W. (1973) 'New and old scleractinian corals from Jamaica', *Bulletin of Marine Science*, 23(1), pp. 16–55.

Wernberg, T., Bennett, S., Babcock, R.C., de Bettignies, T., Cure, K., Depczynski, M., Dufois, F., Fromont, J., Fulton, C.J., Hovey, R.K., Harvey, E.S., Holmes, T.H., Kendrick, G.A., Radford, B., Santana-Garcon, J., Saunders, B.J., Smale, D.A., Thomsen, M.S., Tuckett, C.A. and Wilson, S. (2016) 'Climate-driven regime shift of a temperate marine ecosystem', *Science*, 353(6295), pp. 169–172. doi:10.1126/science.aad8745.

Wickham, H. (2016) *ggplot2: Elegant Graphics for Data Analysis*. New York: Springer-Verlag. doi:10.1007/978-3-319-24277-4.

Wiedenmann, J., D'Angelo, C., Smith, E.G., Hunt, A.N., Legiret, F.-E., Postle, A.D. and Achterberg, E.P. (2013) 'Nutrient enrichment can increase the susceptibility of reef corals to bleaching', *Nature Climate Change*, 3(2), pp. 160–164. doi:10.1038/nclimate1661.

Wild, C., Rasheed, M., Werner, U., Franke, U., Johnstone, R. and Huettel, M. (2004) 'Degradation and mineralisation of coral mucus in reef environments', *Marine Ecology Progress Series*, 267, pp. 159–171. doi 10.3354/meps267159

Wild, C., Niggl, W., Naumann, M.S. and Haas, A.F. (2010) 'Organic matter release by Red Sea coral reef organisms – potential effects on microbial activity and in situ O_2 availability', *Marine Ecology Progress Series*, 411, pp. 61–71. doi:10.3354/meps08653.

Wild, C., Hoegh-Guldberg, O., Naumann, M.S., Colombo-Pallotta, M.F., Ateweberhan, M., Fitt, W.K., Iglesias-Prieto, R., Palmer, C. and van Woesik, R. (2011) 'Climate change impedes scleractinian corals as primary reef ecosystem engineers', *Marine and Freshwater Research*, 62, pp. 205–215. doi:10.1071/MF10254.

Work, T.M. and Aeby, G.S. (2006) 'Systematically describing gross lesions in corals', *Diseases of Aquatic Organisms*, 70(1–2), pp. 155–160. doi:10.3354/dao070155.

Work, T.M., Aeby, G.S., Lasne, G. and Tribollet, A. (2014) 'Gross and microscopic pathology of hard and soft corals in New Caledonia', *Journal of Invertebrate Pathology*, 120, pp. 50–58, doi:10.1016/j.jip.2014.05.007.

Work, T.M. and Farah, Y. (2014) 'Lectins stain cells differentially in the coral, *Montipora capitata*', *Journal of Invertebrate Pathology*, 117, pp. 42–50. doi:10.1016/j.jip.2014.01.008.

WoRMS Editorial Board (2025) *World Register of Marine Species*. Available at: https://www.marinespecies.org (Accessed: 5 October 2025). doi:10.14284/170.

Wunsam, S., Schmidt, R. and Müller, J. (1999) 'Holocene lake development of two Dalmatian lagoons (Malo and Veliko Jezero, Isle of Mljet) in respect to changes in Adriatic sea level and climate', *Palaeogeography, Palaeoclimatology, Palaeoecology*, 146(1–4), pp. 251–281. doi:10.1016/S0031-0182(98)00147-3.

Zavatarelli, M., Raicich, F., Artegiani, A., Bregant, D. and Russo, A. (1998) 'Climatological biogeochemical characteristics of the Adriatic Sea', *Journal of Marine Systems*, 18(1–3), pp. 227–263. doi:10.1016/S0924-7963(98)00014-1.

Zawada, K.J.A., Dornelas, M. and Madin, J.S. (2019) 'Quantifying coral morphology', *Coral Reefs*, 38(6), pp. 1281–1292. doi:10.1007/s00338-019-01842-4.

Ziegler, M., Seneca, F.O., Yum, L.K., Palumbi, S.R. and Voolstra, C.R. (2017) 'Bacterial community dynamics are linked to patterns of coral heat tolerance', *Nature Communications*, 8, pp. 14213. doi:10.1038/ncomms14213.

Zibrowius, H. (1980) *Les Scléractiniaires de la Méditerranée et de l'Atlantique nord-oriental*, Mémoires de l'Institut Océanographique, 11, pp. 1–284.

Zodrow, J. M., Stegeman, J. J., & Tanguay, R. L. (2004). Histological analysis of acute toxicity of 2,3,7,8-tetrachlorodibenzo-p- dioxin (TCDD) in zebrafish. Aquatic Toxicology, 66(1), 25–38. https://doi.org/10.1016/j.aquatox.2003.07.002

Zunino, S., Pitacco, V., Mavrič, B., Orlando-Bonaca, M., Kružić, P. and Lipej, L. (2018) 'The ecology of the Mediterranean stony coral *Cladocora caespitosa* (Linnaeus, 1767) in the Gulf of Trieste (northern Adriatic Sea): a 30-year long story', *Marine Biology Research*, 14(3), pp. 307–320. doi:10.1080/17451000.2018.1449137.

8. APPENDIX

Table A- 1. Time duration and chemicals used in the tissue dehydration and clearing process

No.	Chemical	Duration (hours)
1.	70% ethanol 1	Min 48
2.	70% ethanol 2	1
3.	96% ethanol	1
4.	100% ethanol 1	1
5.	100% ethanol 2	1
6.	chloroform	Overnight (min 12h)
7.	1:1 chloroform–paraplast	1
8.	Paraplast 1	1
9.	Paraplast 2	1

Table A- 2. Deparaffinization and rehydration protocol for samples prior to histological staining.

No.	Deparaffinization and rehydration	Duration (minutes' and seconds'')
1.	Xylene 1	2'
2.	Xylene 2	2'
3.	Xylene 3	2'
4.	100% ethanol 1	5'
5.	100% ethanol 2	3'
6.	95% ethanol	2'
7.	Distilled water	2'

Table A- 3. Staining protocol for corals with hematoxylin and eosin (Biognost, 2019)

No.	Reagents	Duration (minutes' and seconds '')
1.	Haematoxylin H	3'
2.	Distilled water	2'
3.	95% ethanol	30''
4.	Eozin 0,5%	2'
5.	Rinse under tap water	2'

Table A- 4. Grocott kit staining protocol (Biognost, 2019)

No.	Reagents	Duration (minutes' and seconds '')
1.	Periodic acid, 1%	7'
2.	Rinse in double distilled water	3x 5''
3.	Silver nitrate methenamine borax solution on 62°C	30'
4.	Rinse in double distilled water	3x 5''
5.	Gold chloride, 0,2%	30''
6.	Rinse in double distilled water	3x po 5''
7.	Sodium thiosulfate, 2%	2'
8.	Rinse under tap water	2'
9.	Fast Green F.C.F. contrast reagent	2'
10.	Rinse in double distilled water	2'

Table A- 5. Masson trichrome kit staining protocol (Biognost, 2019)

No.	Dyeing	Duration (minutes' and seconds '')
1.	5 drops Hematoxylin, Weigert A and 5 drops Ferri reagent, Weigert B	20'
2.	Rinse under tap water	3'
3.	Biebrich Scarlet-acid Fuchsin reagent	20'
4.	Rinse in distilled water	until the excessive dye is washed off the section
5.	PTA-PMA reagent	10'
6.	Aniline Blue reagent	7'
7.	Rinse in distilled water	until the excessive dye is washed off the section
8.	Acetic acid, 1%	2''

Table A- 6. Gram kit staining protocol (Biognost, 2019)

No.	Dyeing	Duration (minutes' and seconds '')
1.	Gram Crystal violet, 1% solution	1'
2.	Pour excessive dye off the section.	
3.	Rinse the section carefully using stabilized Gram Lugol solution.	1'
4.	Rinse in distilled water	5''
5.	Treat the preparation using Gram Decolourizer 2 solution	15''
6.	Rinse in distilled water	5''
7.	Treat the preparation using Gram Safranin solution	1'
8.	Rinse in distilled water	5''

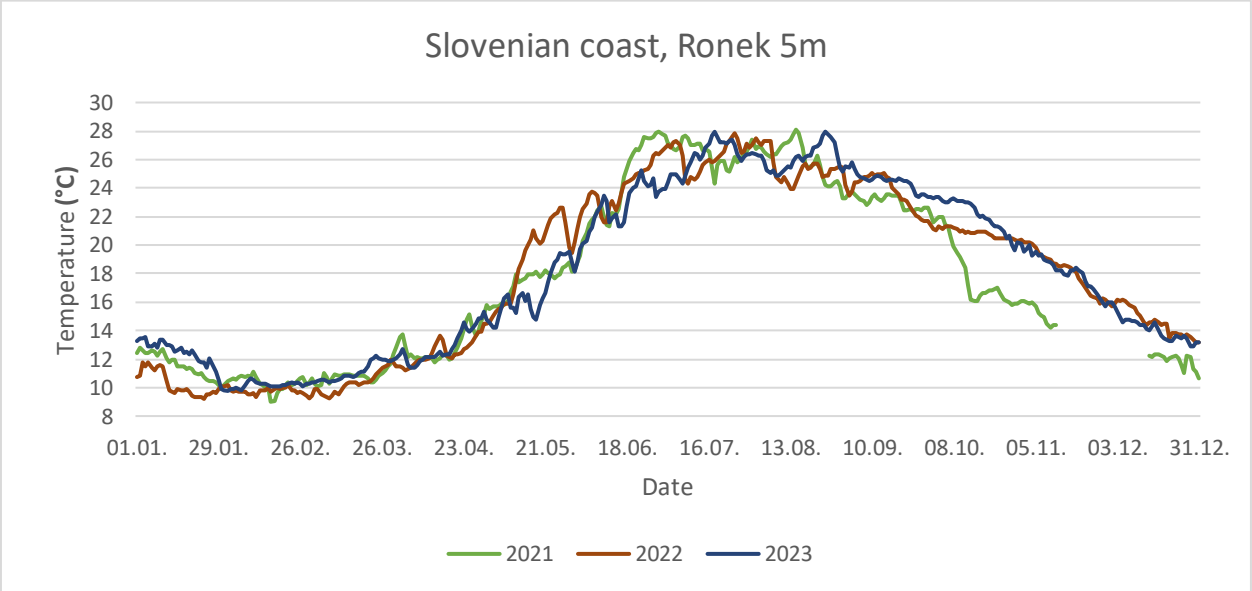

Figure A- 1. Sea temperature values (in °C) at 5 m depth on Ronek station at Slovenian coast over a three-year period from January to December.

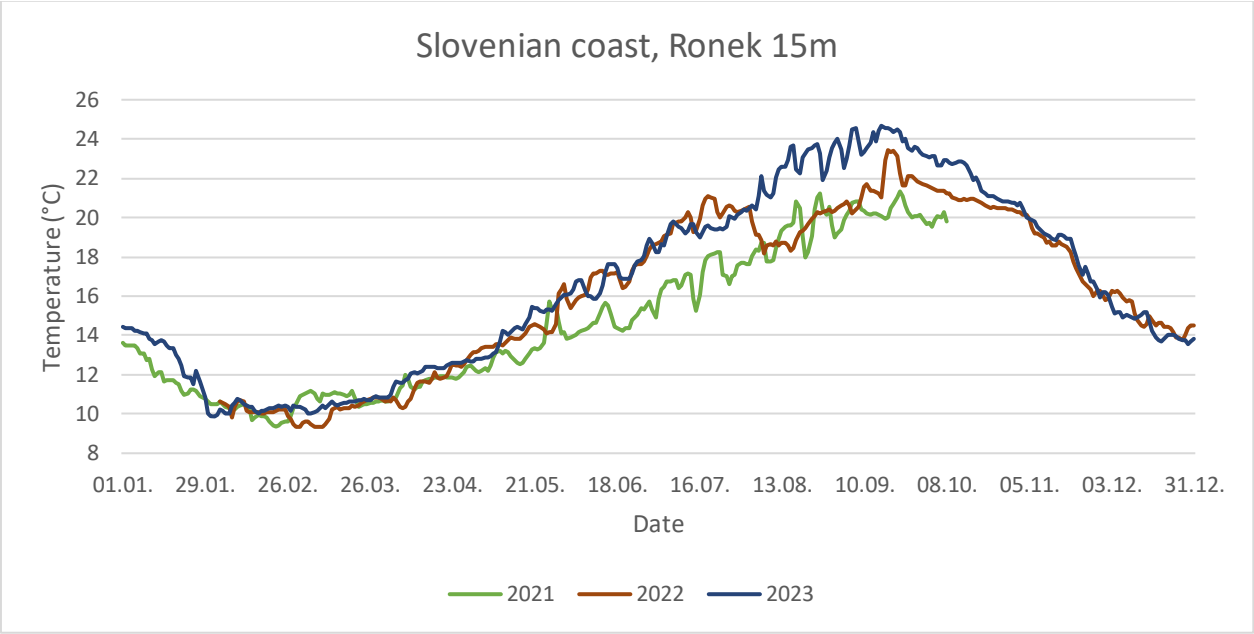

Figure A- 2. Sea temperature values (in °C) at 15 m depth on Ronek station at Slovenian coast over a three-year period from January to December.

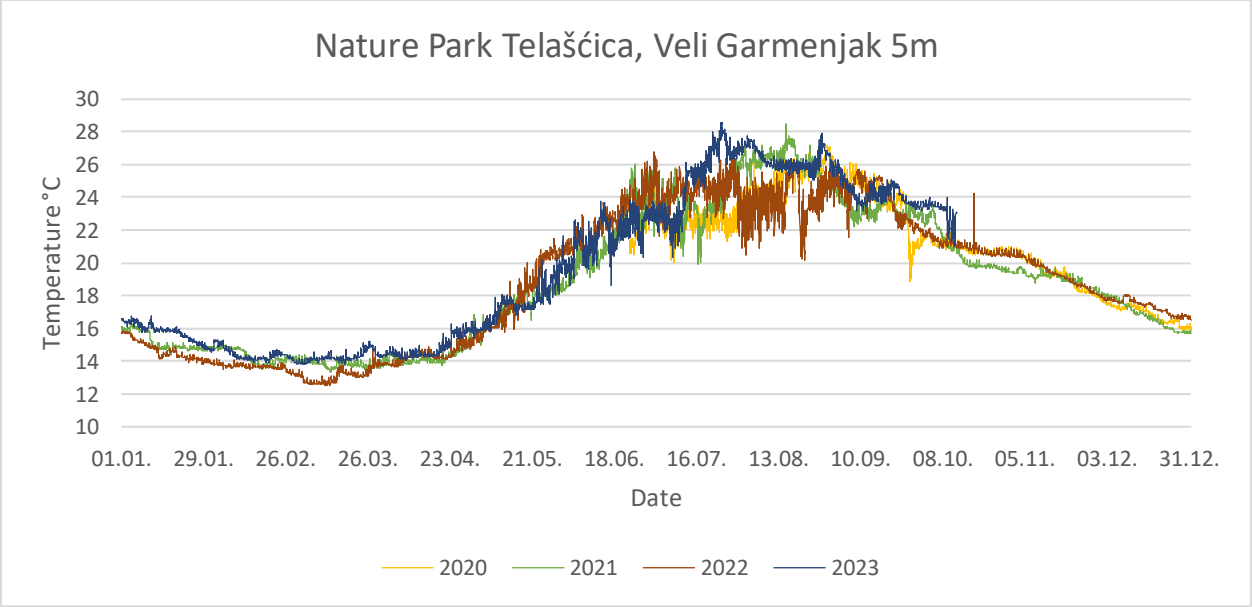

Figure A- 3. Sea temperature values (in °C) at 5 m depth on Veli Garmenjak station at Nature Park Telašćica over a four-year period from January to December.

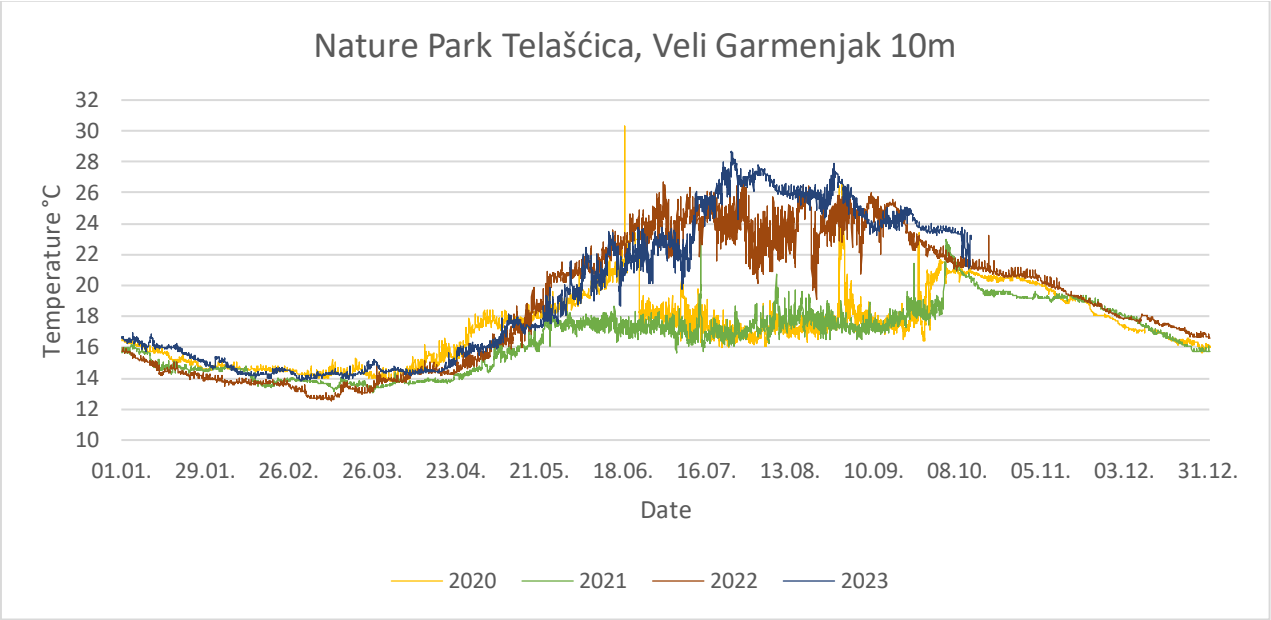

Figure A- 4. Sea temperature values (in °C) at 10 m depth on Veli Garmenjak station at Nature Park Telašćica over a five-year period from January to December.

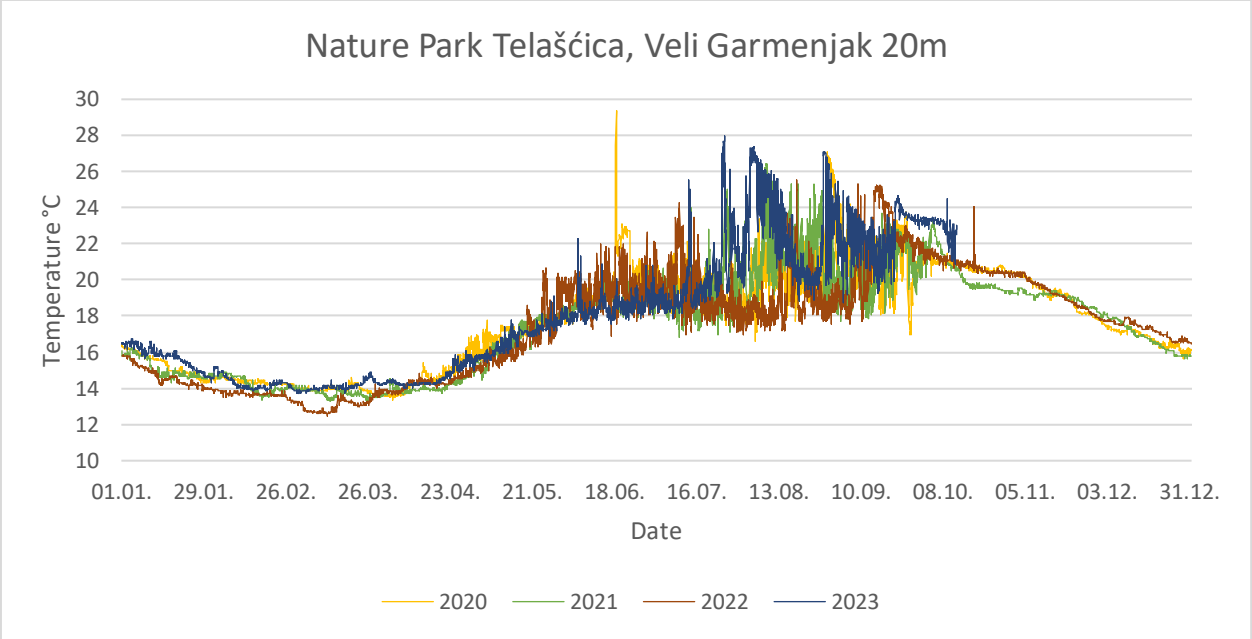

Figure A- 5. Sea temperature values (in °C) at 20 m depth on Veli Garmenjak station at Nature Park Telašćica over a five-year period from January to December.

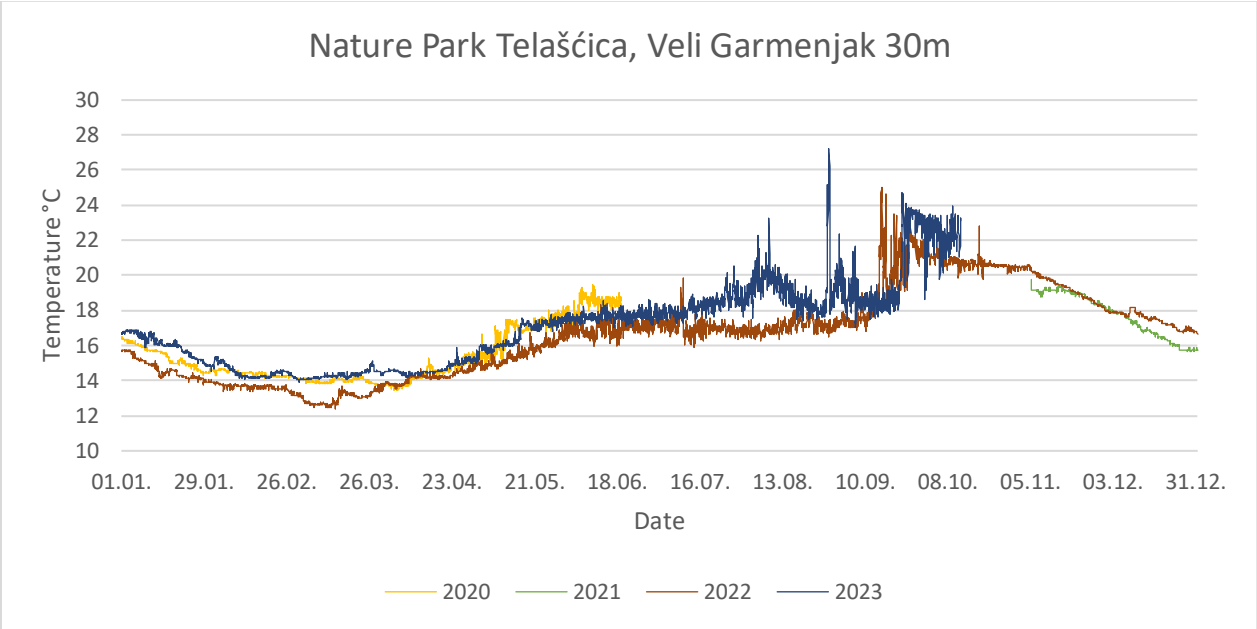

Figure A- 6. Sea temperature values (in °C) at 30 m depth on Veli Garmenjak station at Nature Park Telašćica over a four-year period from January to December.

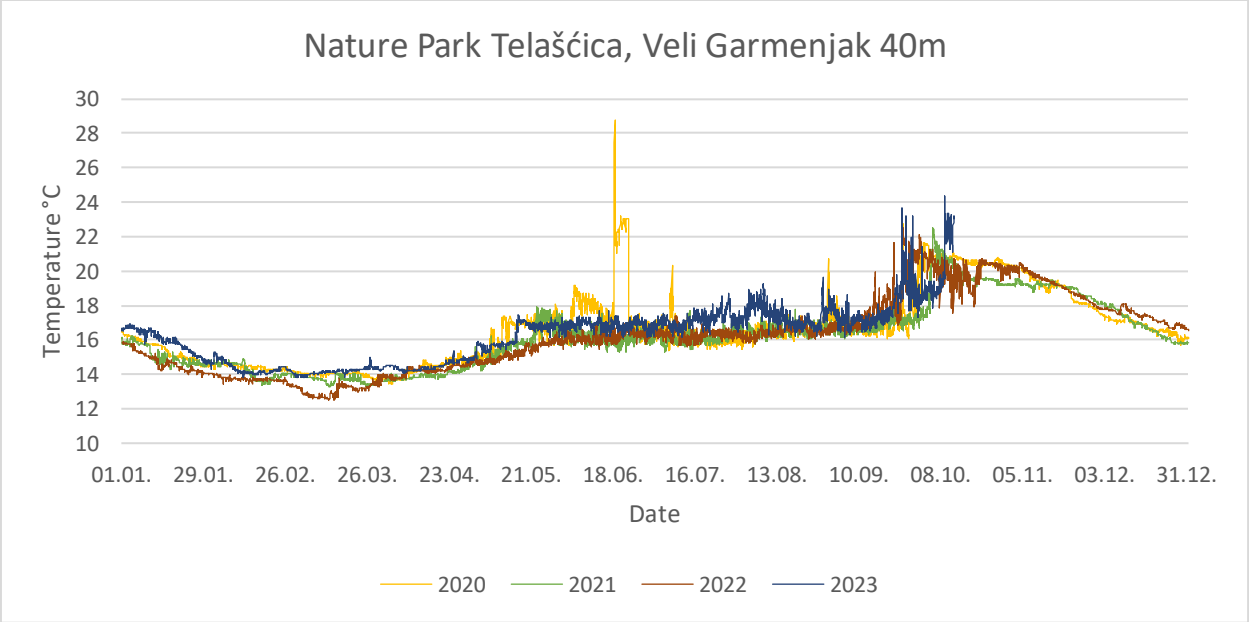

Figure A- 7. Sea temperature values (in °C) at 40 m depth on Veli Garmenjak station at Nature Park Telašćica over a four-year period from January to December.

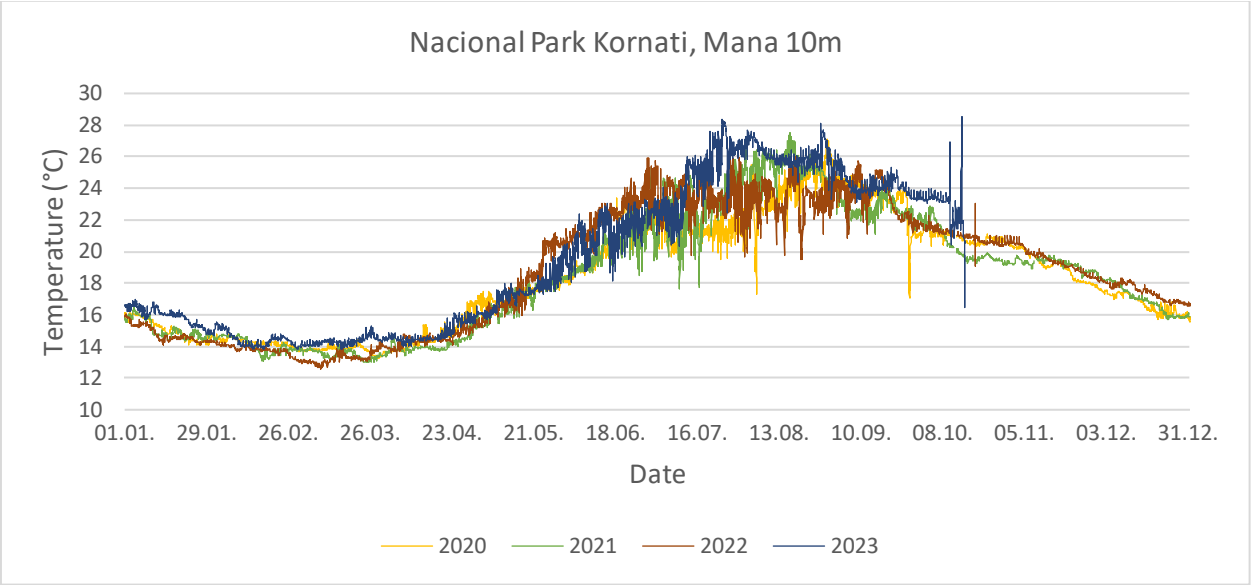

Figure A- 8. Sea temperature temperatures (in °C) at 10 m depth on Mana station at National Park Kornati from January to December over a four-year period.

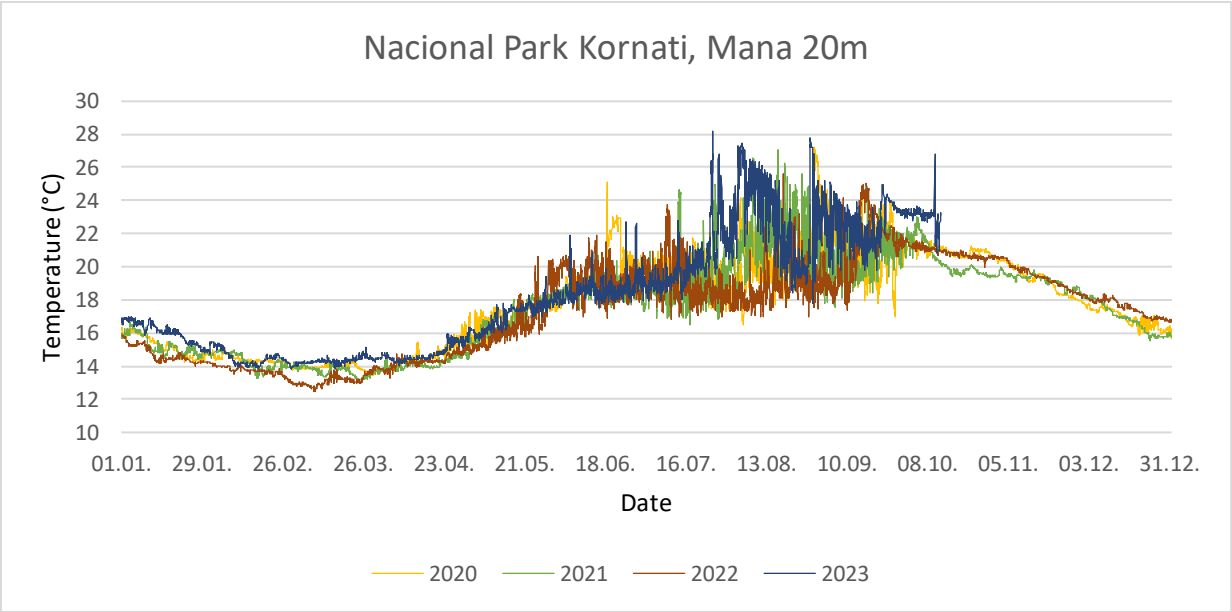

Figure A- 9. Sea temperature temperatures (in °C) at 20 m depth on Mana station at National Park Kornati from January to December over a four-year period.

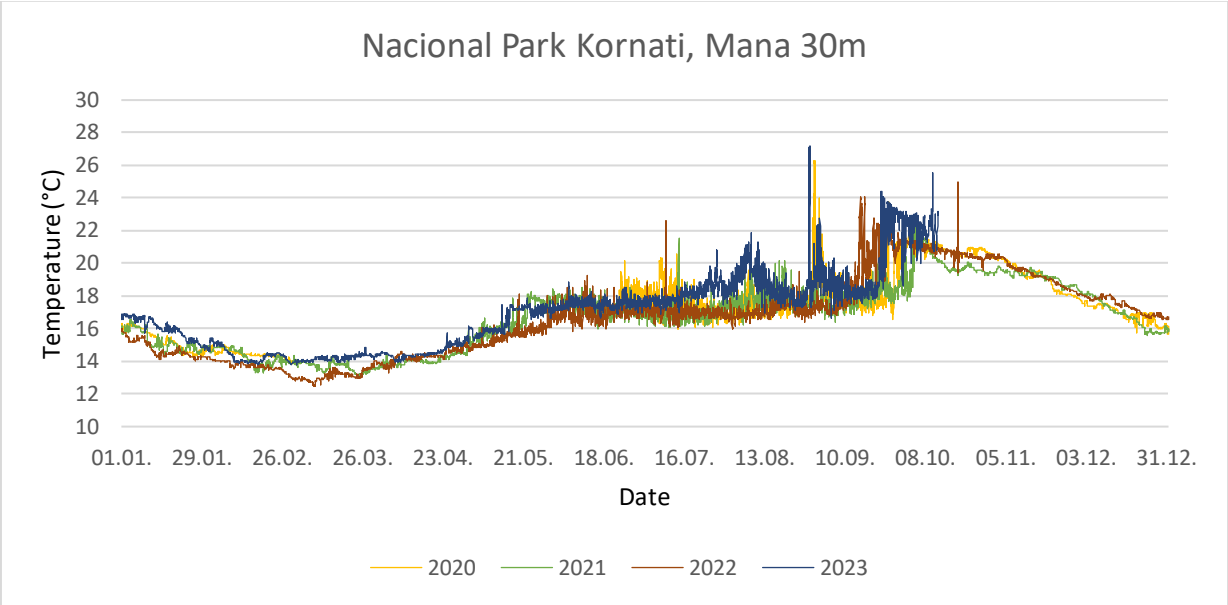

Figure A- 10. Sea temperature temperatures (in °C) at 30 m depth on Mana station at National Park Kornati from January to December over a four-year period.

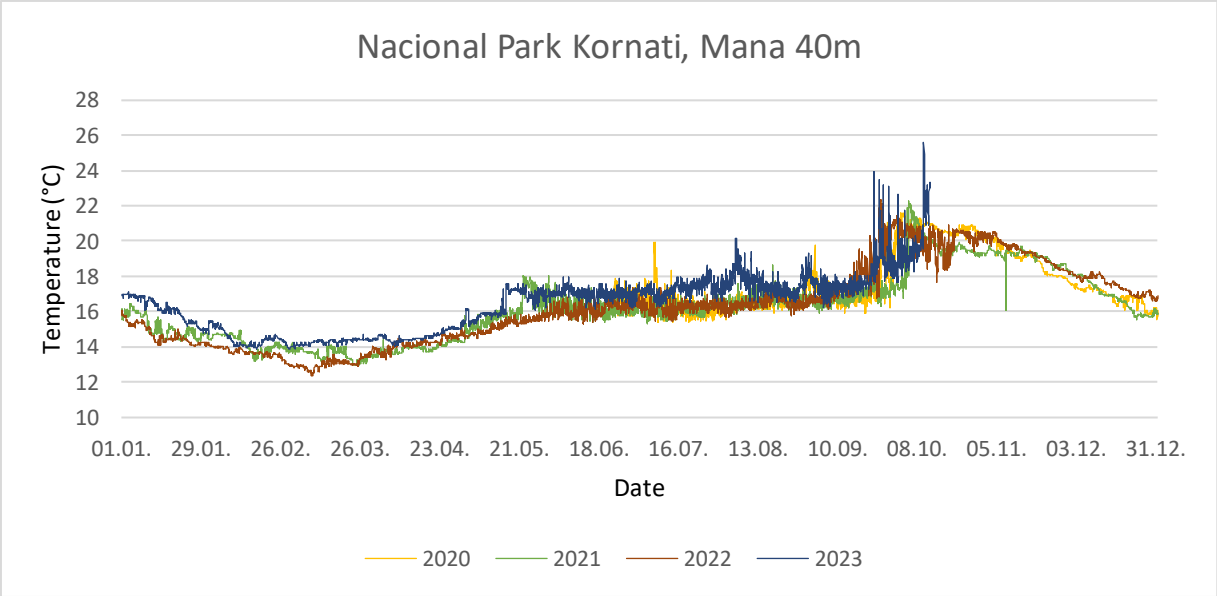

Figure A- 11. Sea temperature temperatures (in °C) at 40 m depth on Mana station at National Park Kornati from January to December over a four-year period.

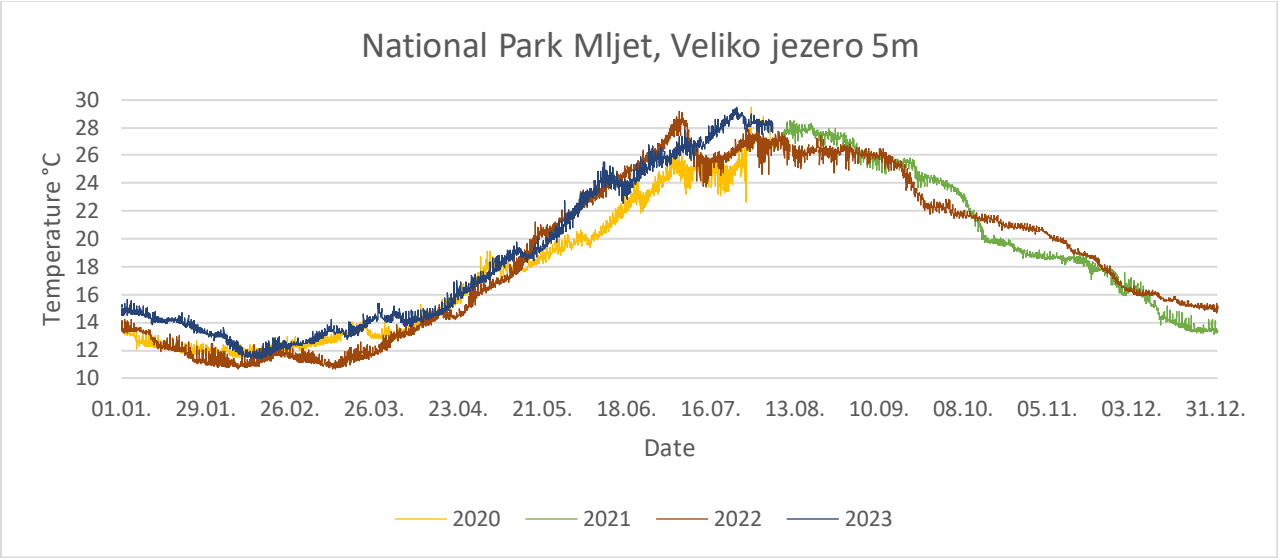

Figure A- 12. Sea temperature values (in °C) at 5 m depth on Veliko jezero station at National Park Mljet over a four-year period from January to December.

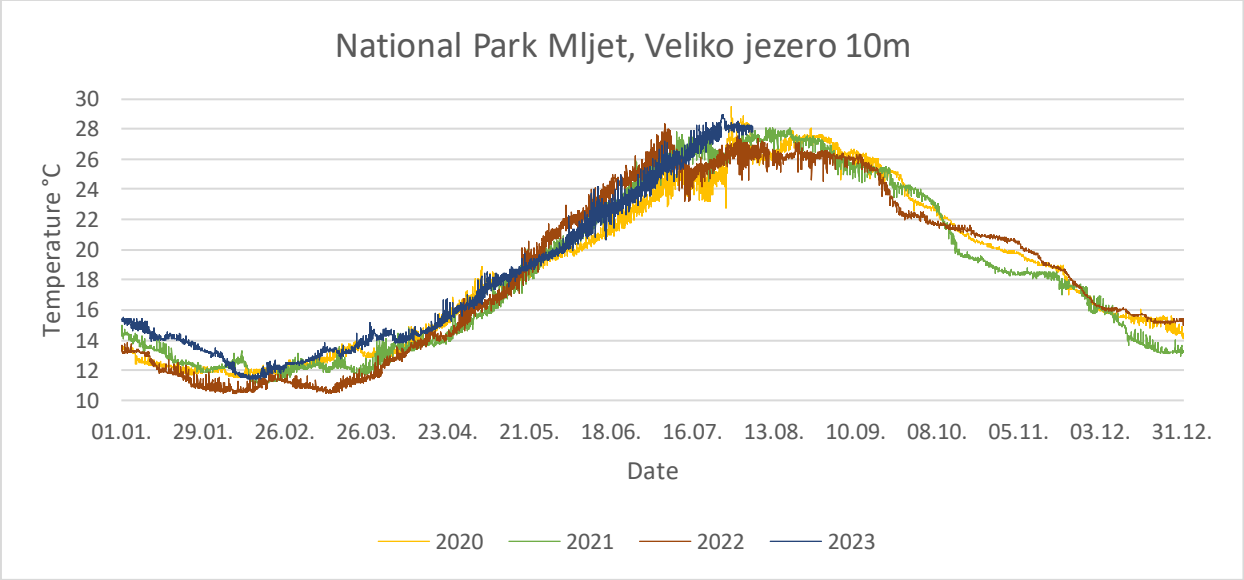

Figure A- 13. Sea temperature values (in °C) at 10 m depth on Veliko jezero station at National Park Mljet over a four-year period from January to December

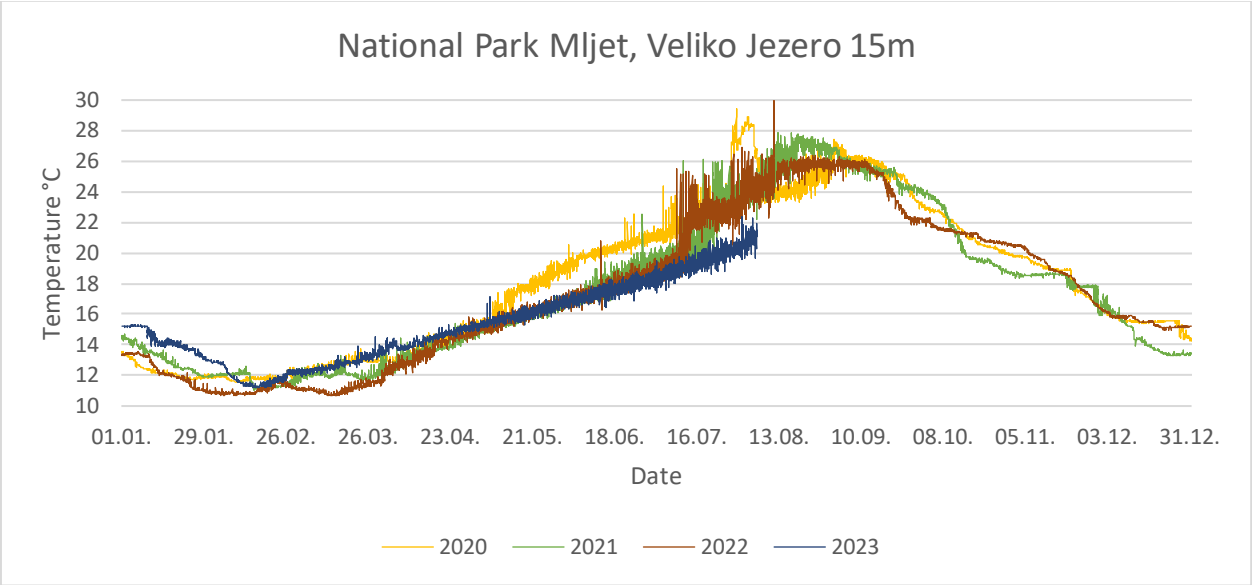

Figure A- 14. Sea temperature values (in °C) at 15 m depth on Veliko jezero station at National Park Mljet over a four-year period from January to December.

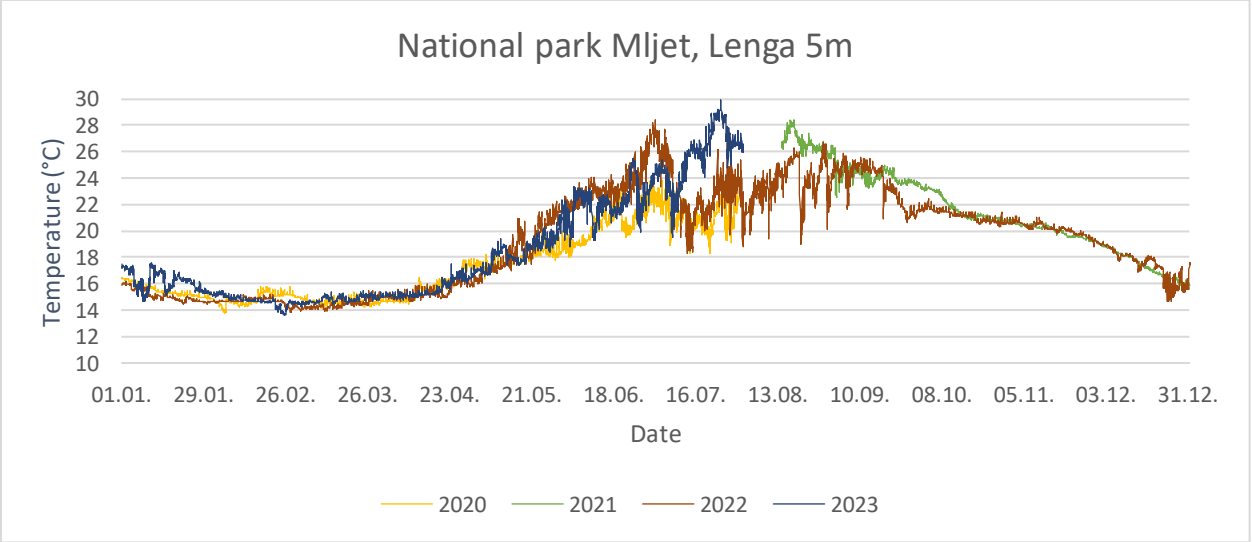

Figure A- 15. Sea temperature values (in °C) at 5 m depth on Lenga station at National Park Mljet over a four-year period from January to December

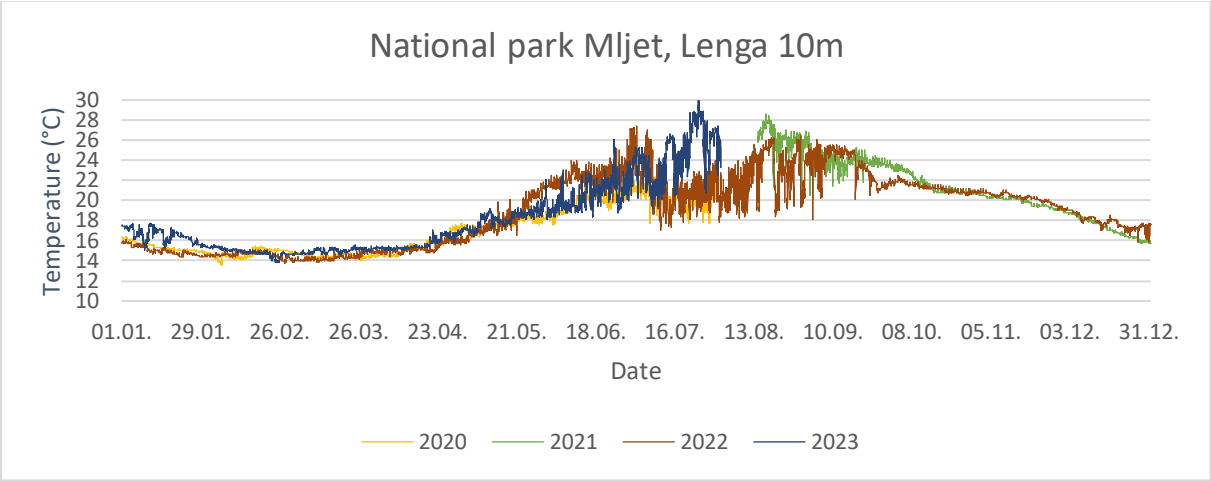

Figure A- 16. Sea temperature values (in °C) at 10 m depth on Lenga station at National Park Mljet over a four-year period from January to December

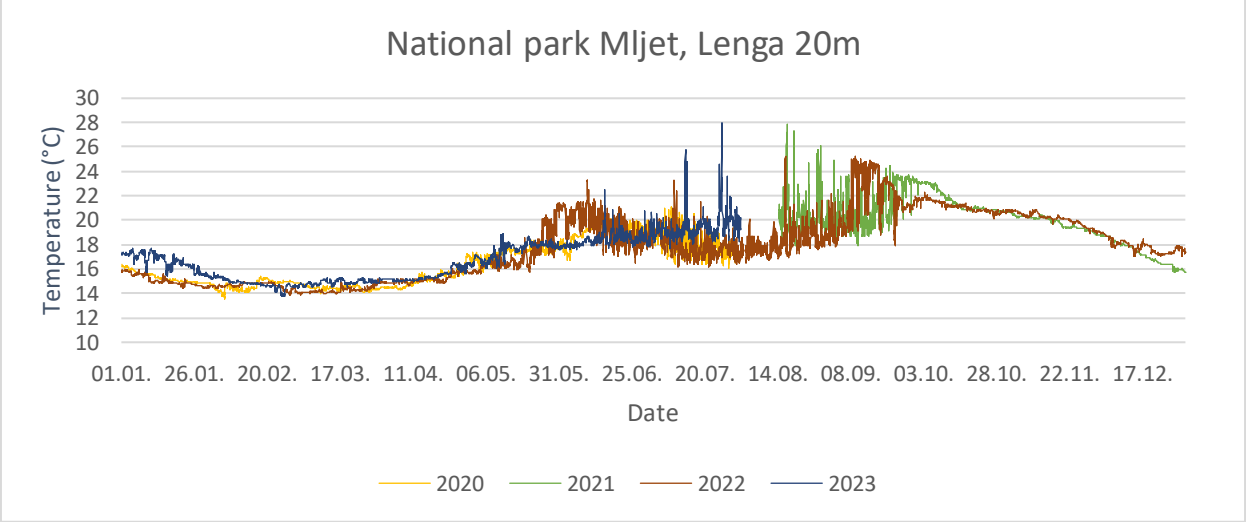

Figure A- 17. Sea temperature values (in °C) at 20 m depth on Lenga station at National Park Mljet over a four-year period from January to December

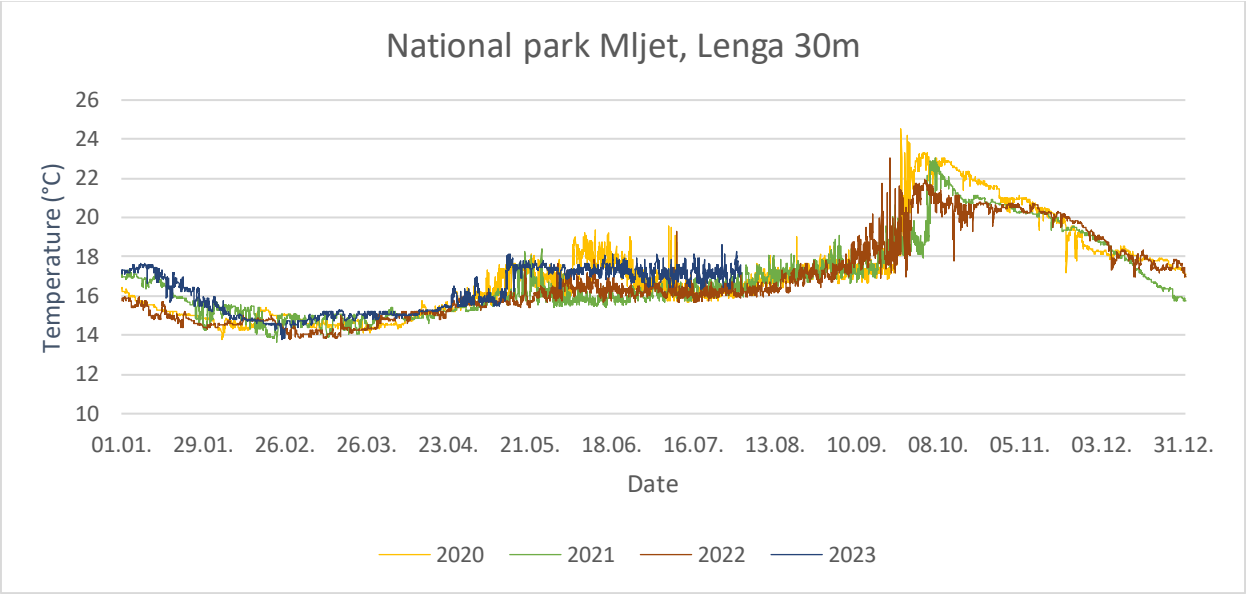

Figure A- 18. Sea temperature values (in °C) at 30 m depth on Lenga station at National Park Mljet over a four-year period from January to December

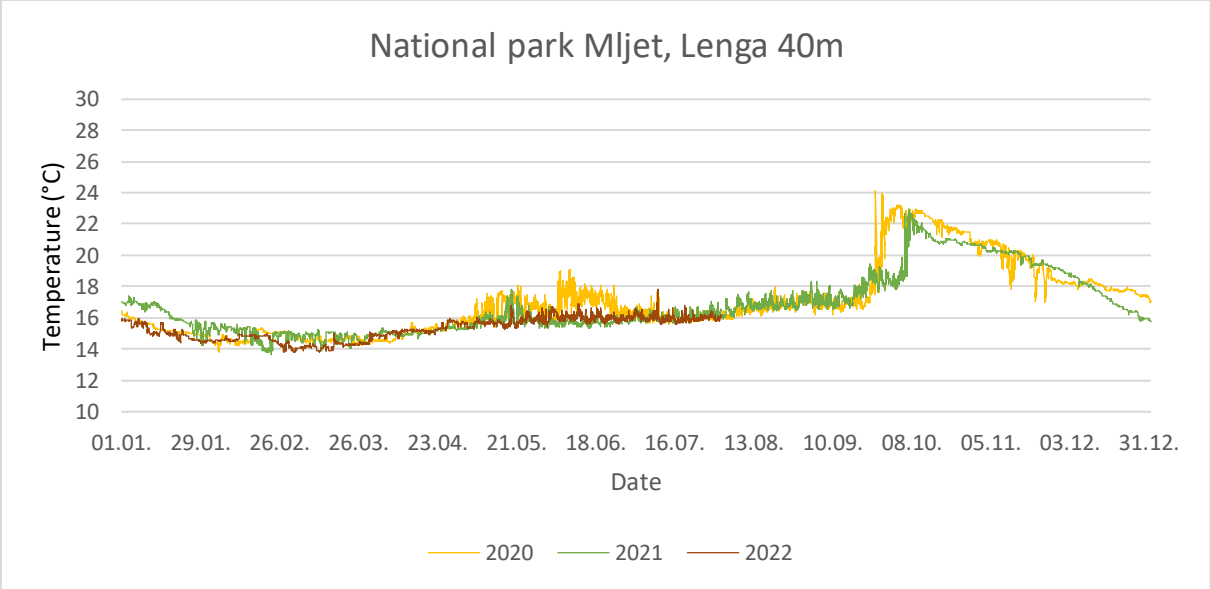

Figure A- 19. Sea temperature values (in °C) at 40 m depth on Lenga station at National Park Mljet over a three-year period from January to December

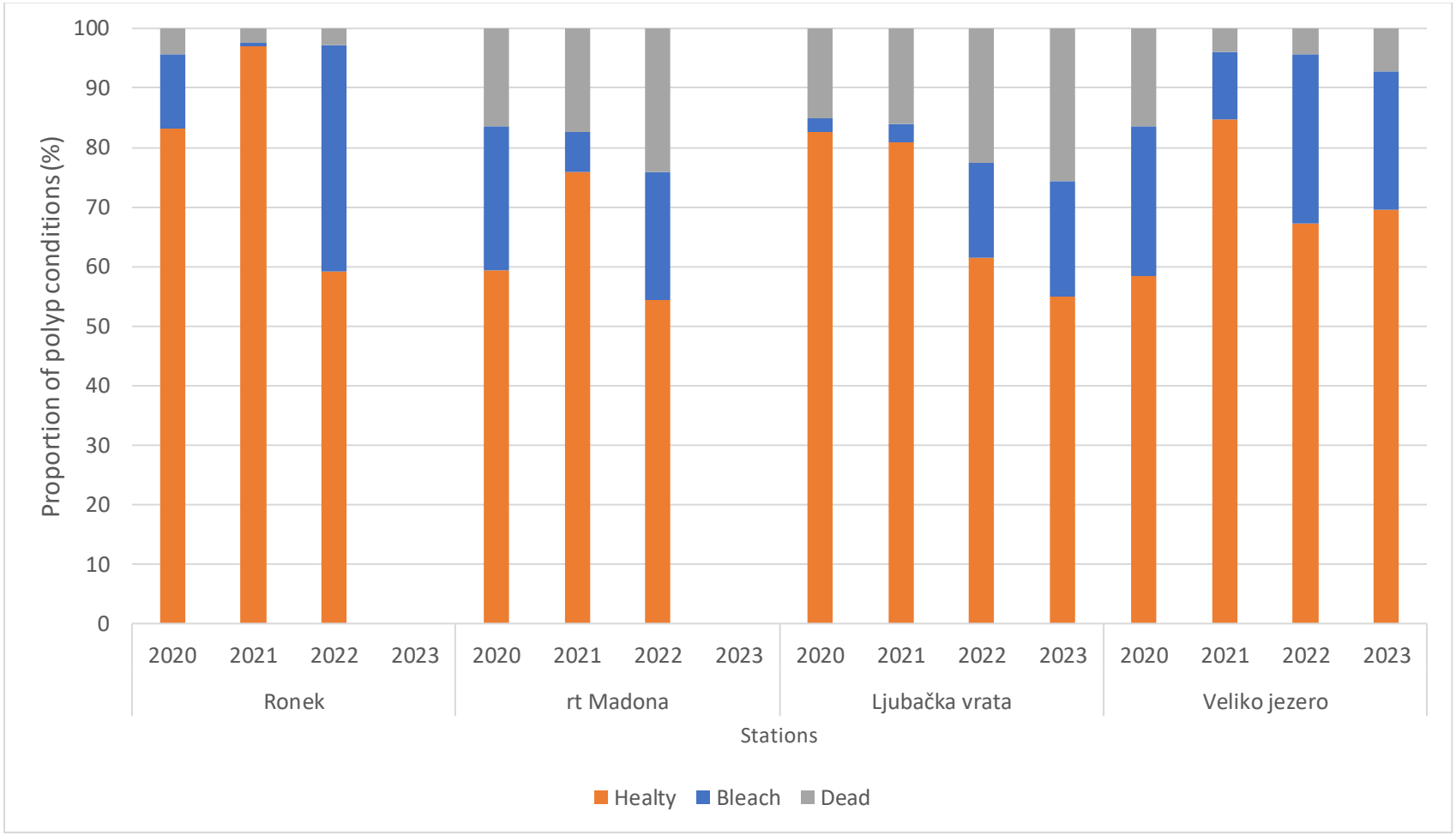

Figure A- 20. Proportion of affected *Cladocora ceaspitosa* colonies on stations: Ronek, rt Madona, Ljubačka vrata and Veliko jezero during period 2020 – 2023. Stacked bar charts show the proportion of affected colonies per year, with blue indicating healthy colonies, orange indicating bleach colonies, and grey indicating dead colonies

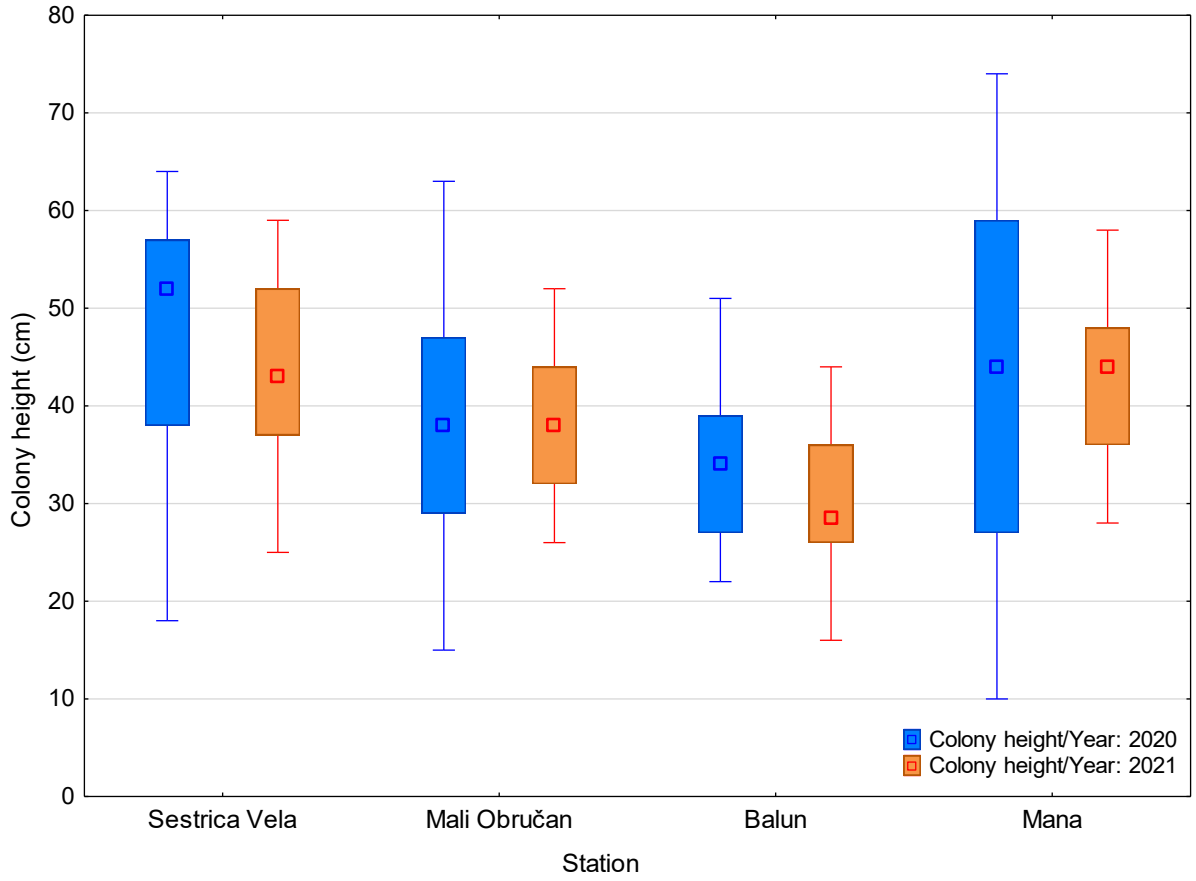

Figure A- 21. Colony height of *Paramuricea clavata* on stations Sestrica Vela [F(1;39) = 2.4662; p = 0.1244], Mali Obručan [F(1;39) = 0.029; p = 0.8656], Balun [F(1;39) = 1.7914; p = 0.1885] and Mana [F(1;50) = 0.0224; p = 0.8815] across period 2020 – 2021

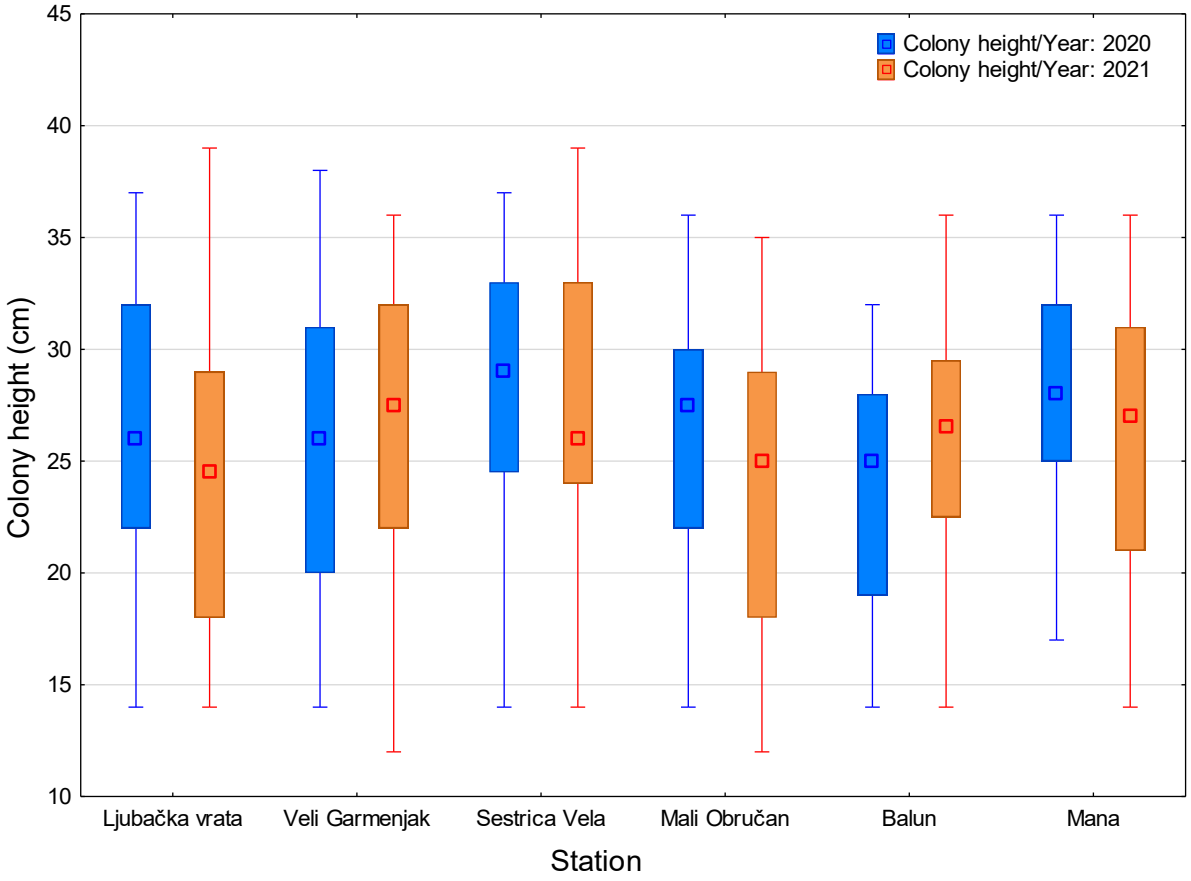

Figure A- 22. Colony height of *Eunicella cavolini* on stations Ljubačka vrata [F(1;51) = 0.7597; p = 0.3875], Veli Garmenjak [F(1;51) = 0.0015; p = 0.9692], Sestrica Vela [F(1;53) = 0.5604; p = 0.4574], Mali Obručan [F(1;51) = 0.7705; p = 0.3842], Balun [F(1;53) = 1.4985; p = 0.2263] and Mana [F(1;52) = 1.4265; p = 0.2378] across period 2020 – 2021

Table A- 7. Seasonal variations of nutrients at investigated stations during research in July and October 2020.

NO_3^- (µmol/L)												
Station	**Veli Garmenjak**		**Mana**		**Rt Lenga**		**Ronek**		**Ljubačka vrata**		**Veliko jezero**	
Depth	July	October	July	October	July	October	July	October	July	October	July	October
5m							0,87	0,61	1,07	1,19	2,17	2,09
10m	0,33	0,35	0,38	0,42	0,31	0,29	0,85	0,51	1,11	1,26	2,12	2,02
15m							0,78	0,54	1,09	1,29	2,14	2,03
20m	0,31	0,33	0,38	0,43	0,30	0,30						
30m	0,31	0,33	0,38	0,42	0,29	0,33						
40m	0,32	0,31	0,36	0,41	0,27	0,31						
NO_2^- (µmol/L)												
Station	**Veli Garmenjak**		**Mana**		**Rt Lenga**		**Ronek**		**Ljubačka vrata**		**Veliko jezero**	
Depth	July	October	July	October	July	October	July	October	July	October	July	October
5m							0,037	0,031	0,036	0,038	0,049	0,037
10m	0,074	0,081	0,076	0,078	0,024	0,019	0,036	0,027	0,032	0,037	0,040	0,042
15m							0,031	0,026	0,031	0,037	0,048	0,040
20m	0,076	0,083	0,075	0,077	0,023	0,022						
30m	0,078	0,086	0,074	0,078	0,024	0,021						
40m	0,064	0,086	0,073	0,076	0,023	0,022						
PO_4^{3-} (µmol/L)												
Station	**Veli Garmenjak**		**Mana**		**Rt Lenga**		**Ronek**		**Ljubačka vrata**		**Veliko jezero**	
Depth	July	October	July	October	July	October	July	October	July	October	July	October
5m							0,012	0,021	0,016	0,019	0,011	0,021
10m	0,039	0,042	0,042	0,041	0,022	0,015	0,011	0,019	0,018	0,021	0,014	0,019
15m							0,008	0,016	0,015	0,018	0,015	0,024
20m	0,039	0,041	0,042	0,043	0,022	0,018						
30m	0,038	0,039	0,041	0,042	0,021	0,019						
40m	0,038	0,037	0,040	0,043	0,020	0,022						
NH_4^+ (µmol/L)												
Station	**Veli Garmenjak**		**Mana**		**Rt Lenga**		**Ronek**		**Ljubačka vrata**		**Veliko jezero**	
Depth	July	October	July	October	July	October	July	October	July	October	July	October
5m							0,08	0,03	0,12	0,19	0,36	0,44
10m	0,033	0,036	0,030	0,036	0,033	0,072	0,09	0,04	0,16	0,18	0,37	0,47
15m							0,09	0,06	0,17	0,19	0,42	0,48
20m	0,033	0,039	0,028	0,034	0,031	0,072						
30m	0,031	0,038	0,028	0,033	0,028	0,073						
40m	0,032	0,036	0,027	0,031	0,025	0,071						

Table A- 8. Values of measured hydrographic parameters at the investigated stations in July and October 2020.

Salinity (‰)												
Station	**Veli Garmenjak**		**Mana**		**Rt Lenga**		**Ronek**		**Ljubačka vrata**		**Veliko jezero**	
Depth	July	October	July	October	July	October	July	October	July	October	July	October
5m							38,5	38,4	38,3	38,1	38,1	37,8
10m	37,9	38,0	38,3	38,2	37,4	37,3	38,5	38,4	38,2	38,1	38,1	37,6
15m							38,3	38,3	38,2	38,2	38,0	37,7
20m	37,9	38,0	38,2	38,2	37,4	37,3						
30m	37,9	38,1	38,2	38,3	37,3	37,4						
40m	38,1	38,3	38,4	38,4	37,6	37,5						
O_2 (mg/L)												
Station	**Veli Garmenjak**		**Mana**		**Rt Lenga**		**Ronek**		**Ljubačka vrata**		**Veliko jezero**	
Depth	July	October	July	October	July	October	July	October	July	October	July	October
5m							7,22	7,09	7,33	7,45	7,41	7,36
10m	8,22	8,09	8,29	8,26	8,07	8,16	7,19	7,08	7,31	7,41	7,38	7,33
15m							7,14	7,05	7,22	7,40	7,36	7,27
20m	8,17	8,06	8,28	8,25	8,05	8,09						
30m	8,12	8,03	8,28	8,21	8,02	8,09						
40m	8,12	7,98	8,19	8,21	8,01	8,06						
pH												
Station	**Veli Garmenjak**		**Mana**		**Rt Lenga**		**Ronek**		**Ljubačka vrata**		**Veliko jezero**	
Depth	July	October	July	October	July	October	July	October	July	October	July	October
5m							8,21	8,28	8,12	8,14	7,93	7,68
10m	8,12	8,10	8,14	8,12	7,90	7,88	8,19	8,27	8,11	8,10	7,90	7,61
15m							8,19	8,27	8,09	8,09	7,89	7,59
20m	8,11	8,10	8,14	8,11	7,91	7,89						
30m	8,12	8,08	8,16	8,11	7,91	7,89						
40m	8,10	8,07	8,16	8,06	7,86	7,88						

Table A- 9. Seasonal variations of nutrients at investigated stations during research in July and October 2021

NO_3^- (µmol/L)												
Station	**Veli Garmenjak**		**Mana**		**Rt Lenga**		**Ronek**		**Ljubačka vrata**		**Veliko jezero**	
Depth	July	October	July	October	July	October	July	October	July	October	July	October
5m							0,53	0,61	0,28	0,36	0,57	0,31
10m	0,39	1,05	0,33	0,27	0,39	0,36	0,52	0,51	0,29	0,32	0,54	0,29
15m							0,52	0,54	0,24	0,31	0,53	0,33
20m	0,39	1,04	0,32	0,26	0,37	0,35						
30m	0,38	1,04	0,31	0,24	0,37	0,36						
40m	0,36	0,95	0,31	0,31	0,36	0,38						
NO_2^- (µmol/L)												
Station	**Veli Garmenjak**		**Mana**		**Rt Lenga**		**Ronek**		**Ljubačka vrata**		**Veliko jezero**	
Depth	July	October	July	October	July	October	July	October	July	October	July	October
5m							0,029	0,031	0,031	0,036	0,044	0,043
10m	0,077	0,92	0,075	0,038	0,072	0,031	0,029	0,029	0,031	0,033	0,047	0,046
15m							0,027	0,028	0,028	0,035	0,047	0,045
20m	0,075	0,82	0,077	0,032	0,070	0,034						
30m	0,074	0,71	0,073	0,036	0,071	0,032						
40m	0,073	0,56	0,063	0,034	0,070	0,034						
PO_4^{3-} (µmol/L)												
Station	**Veli Garmenjak**		**Mana**		**Rt Lenga**		**Ronek**		**Ljubačka vrata**		**Veliko jezero**	
Depth	July	October	July	October	July	October	July	October	July	October	July	October
5m							0,017	0,01	0,022	0,028	0,077	0,052
10m	0,044	0,036	0,040	0,017	0,042	0,035	0,011	0,012	0,021	0,029	0,084	0,053
15m							0,018	0,01	0,022	0,031	0,082	0,051
20m	0,041	0,034	0,041	0,018	0,041	0,034						
30m	0,041	0,034	0,039	0,019	0,041	0,033						
40m	0,040	0,033	0,038	0,017	0,040	0,033						
NH_4^+ (µmol/L)												
Station	**Veli Garmenjak**		**Mana**		**Rt Lenga**		**Ronek**		**Ljubačka vrata**		**Veliko jezero**	
Depth	July	October	July	October	July	October	July	October	July	October	July	October
5m							0,26	0,09	0,14	0,17	0,27	0,36
10m	0,031	0,41	0,035	0,38	0,041	0,44	0,22	0,06	0,15	0,17	0,22	0,34
15m							0,22	0,06	0,15	0,16	0,21	0,35
20m	0,030	0,36	0,033	0,37	0,041	0,43						
30m	0,028	0,33	0,033	0,37	0,039	0,45						
40m	0,027	0,19	0,031	0,21	0,036	0,45						

Table A- 10. Values of measured hydrographic parameters at the investigated stations in July and October 2021.

Salinity (‰)												
Station	**Veli Garmenjak**		**Mana**		**Rt Lenga**		**Ronek**		**Ljubačka vrata**		**Veliko jezero**	
Depth	July	October	July	October	July	October	July	October	July	October	July	October
5m							38,2	38,4	38,2	38,3	38,3	38,1
10m	37,9	38,1	38,3	38,4	38,0	38,4	38,1	38,3	38,1	38,2	38,3	38,1
15m							38,1	38,3	38,1	38,3	38,2	37,9
20m	38,1	38,1	38,1	38,4	38,2	38,3						
30m	38,2	38,3	38,3	38,5	38,2	38,4						
40m	38,4	38,4	38,1	38,6	38,1	38,4						
O_2 (mg/L)												
Station	**Veli Garmenjak**		**Mana**		**Rt Lenga**		**Ronek**		**Ljubačka vrata**		**Veliko jezero**	
Depth	July	October	July	October	July	October	July	October	July	October	July	October
5m							7,09	7,21	7,57	7,41	7,38	7,19
10m	8,27	8,23	8,18	8,09	8,28	8,19	6,94	7,18	7,51	7,43	7,33	7,17
15m							6,72	7,16	7,44	7,38	7,35	7,14
20m	8,29	8,26	8,14	8,05	8,27	8,19						
30m	8,28	8,21	8,10	8,03	8,28	8,21						
40m	8,19	8,21	8,01	7,89	8,26	8,20						
pH												
Station	**Veli Garmenjak**		**Mana**		**Rt Lenga**		**Ronek**		**Ljubačka vrata**		**Veliko jezero**	
Depth	July	October	July	October	July	October	July	October	July	October	July	October
5m							8,23	8,32	8,19	8,17	7,79	7,63
10m	8,17	7,94	8,18	8,16	8,18	8,16	8,25	8,27	8,16	8,16	7,76	7,67
15m							8,24	8,27	8,12	8,15	7,75	7,66
20m	8,16	8,01	8,17	8,15	8,19	8,12						
30m	8,16	8,03	8,19	8,16	8,16	8,14						
40m	8,16	8,06	8,16	8,15	8,15	8,14						

Table A- 11. Seasonal variations of nutrients at investigated stations during research in July and October 2022.

NO_3^- (µmol/L)												
Station	**Veli Garmenjak**		**Mana**		**Rt Lenga**		**Ronek**		**Ljubačka vrata**		**Veliko jezero**	
Depth	July	October	July	October	July	October	July	October	July	October	July	October
5m							0,67	0,53	0,36	0,47	0,68	0,74
10m	0,42	0,34	0,36	0,36	0,42	0,31	0,65	0,54	0,33	0,44	0,63	0,72
15m							0,59	0,51	0,34	0,42	0,69	0,73
20m	0,39	0,37	0,38	0,35	0,40	0,36						
30m	0,37	0,33	0,36	0,33	0,41	0,31						
40m	0,35	0,32	0,33	0,32	0,39	0,32						
NO_2^- (µmol/L)												
Station	**Veli Garmenjak**		**Mana**		**Rt Lenga**		**Ronek**		**Ljubačka vrata**		**Veliko jezero**	
Depth	July	October	July	October	July	October	July	October	July	October	July	October
5m							0,032	0,036	0,056	0,061	0,039	0,056
10m	0,092	0,087	0,068	0,049	0,067	0,053	0,028	0,035	0,048	0,057	0,041	0,059
15m							0,023	0,035	0,047	0,057	0,038	0,057
20m	0,086	0,084	0,066	0,041	0,069	0,054						
30m	0,079	0,079	0,062	0, 042	0,063	0,050						
40m	0,074	0,074	0,058	0,041	0,065	0,051						
PO_4^{3-} (µmol/L)												
Station	**Veli Garmenjak**		**Mana**		**Rt Lenga**		**Ronek**		**Ljubačka vrata**		**Veliko jezero**	
Depth	July	October	July	October	July	October	July	October	July	October	July	October
5m							0,026	0,014	0,048	0,042	0,086	0,096
10m	0,047	0,040	0,046	0,044	0,046	0,037	0,023	0,016	0,045	0,041	0,089	0,098
15m							0,023	0,015	0,049	0,046	0,094	0,105
20m	0,041	0,039	0,045	0,043	0,048	0,038						
30m	0,036	0,035	0,043	0,038	0,050	0,036						
40m	0,038	0,032	0,040	0,035	0,052	0,035						
NH_4^+ (µmol/L)												
Station	**Veli Garmenjak**		**Mana**		**Rt Lenga**		**Ronek**		**Ljubačka vrata**		**Veliko jezero**	
Depth	July	October	July	October	July	October	July	October	July	October	July	October
5m							0,34	0,26	0,16	0,28	0,44	0,81
10m	0,068	1,050	0,082	0,961	0,048	0,59	0,32	0,21	0,18	0,25	0,39	0,94
15m							0,31	0,24	0,19	0,25	0,36	0,89
20m	0,063	0,832	0,084	0,733	0,042	0,55						
30m	0,054	0,437	0,071	0,608	0,033	0,54						
40m	0,048	0,121	0,066	0,387	0,035	0,12						

Table A- 12. Values of measured hydrographic parameters at the investigated stations in July and October 2022.

Salinity (‰)												
Station	**Veli Garmenjak**		**Mana**		**Rt Lenga**		**Piran**		**Ljubačka vrata**		**Veliko jezero**	
Depth	July	October	July	October	July	October	July	October	July	October	July	October
5m							38,3	38,5	38,3	38,5	38,5	38,6
10m	38,1	38,3	38,1	38,3	38,4	38,5	38,4	38,5	38,4	38,3	38,4	38,6
15m							38,2	38,4	38,3	38,3	38,2	38,5
20m	38,2	38,2	38,1	38,4	38,3	38,4						
30m	38,0	38,3	38,1	38,3	38,3	38,3						
40m	38,3	38,4	38,1	38,4	38,2	38,3						
O_2 (mg/L)												
Station	**Veli Garmenjak**		**Mana**		**Rt Lenga**		**Piran**		**Ljubačka vrata**		**Veliko jezero**	
Depth	July	October	July	October	July	October	July	October	July	October	July	October
5m							7,16	7,27	7,46	7,36	7,44	7,07
10m	8,36	8,18	8,29	8,19	8,31	8,14	7,23	7,24	7,47	7,38	7,42	7,09
15m							7,22	7,22	7,42	7,37	7,39	7,09
20m	8,38	8,16	8,31	8,21	8,36	8,11						
30m	8,37	8,17	8,32	8,22	8,33	8,12						
40m	8,32	8,15	8,30	8,17	8,28	8,15						
pH												
Station	**Veli Garmenjak**		**Mana**		**Rt Lenga**		**Piran**		**Ljubačka vrata**		**Veliko jezero**	
Depth	July	October	July	October	July	October	July	October	July	October	July	October
5m							8,18	8,26	8,23	8,24	7,94	7,74
10m	8,21	8,12	8,24	8,18	8,21	8,12	8,21	8,24	8,22	8,23	7,93	7,72
15m							8,22	8,24	8,19	8,23	7,89	7,75
20m	8,19	8,14	8,21	8,15	8,23	8,11						
30m	8,17	8,14	8,21	8,17	8,20	8,10						
40m	8,17	8,12	8,19	8,18	8,19	8,11						

9. CURRICULUM VITAE

Pavel Ankon (MBZ: 387943, ORCID: 0009-0002-1382-751X), master in Ecology and Nature Preservation, research and teaching assistant at Department of Biology, Faculty of Science, University of Zagreb.

Graduated in 2017 from Biology Department of the Faculty of Science. From 2018 to 2020 he worked as a project manager at the Ministry of Science and education on the project *Support for the Implementation of the Comprehensive Curriculum Reform*. In 2020, he enrolled in Doctoral programme of the Biology at the University of Zagreb, Faculty of Science, Department of Biology on the topic "The effect of temperature anomalies on the corals (Anthozoa) in the Adriatic sea". The same year he has been employed as an research and teaching assistant at the Department of Biology, Faculty of Science, University of Zagreb, actively teaching practical work in subjects: Invertebrates, Biological oceanography, Marine biodiversity, Field course in marine biodiversity, Marine resourch management and conservation. He is currently engaged in ecological research of the macroinvertebrates of Adriatic sea, with focus on morfometrical, histopathological and immunological assessments of the corals. He is the co-author of 3 scientific papers, with being first author in one of them. He actively participated in several international professional and scientific congresses with posters and oral presentations. As a member of the organizing committee, he has organized two symposia and one congress. In 2022 he spent two weeks on University of Copenhagen, GLOBE Institute, on education in the processing and analysis of ancient DNA. In 2025 he took "Coral bleaching automated stress system workshop" in Maldives, Faafu atoll, Magoodhoo learning about termal stress in corals. Since 2011 he has been actively diving instructor (NAUI 53423) and scientific diver.

Publications:

Kružić, Petar; Guić, Rita; Lipej, Lovrenc; Mavrič, Borut; Gračan, Romana; **Ankon, Pavel**
A Cladocora caespitosa bank (National Park Mljet, Adriatic Sea) under climate and anthropogenic impacts: a 20-year survey // Mediterranean Marine Science, 26 (2025), 1; 156-174. doi: 10.12681/mms.37029

Ankon, Pavel; Burić, Vida; Đikić, Domagoj; Gračan, Romana; Landeka Jurčević, Irena; Beljan, Silvestar; Kružić, Petar
Effects of heat stress on Mediterranean endemic and endangered reef-building coral Cladocora caespitosa: study on physiological and histological markers // Hydrobiologia, 0 (2025), 0; 0-0. doi: 10.1007/s10750-025-05806-4

Sanna, Daria; Azzena, Ilenia; Locci, Chiara; **Ankon, Pavel**; Kružić, Petar; Manfrin, Chiara; Pallavicini, Alberto; Ciriaco, Saul; Segarich, Marco; Batistini, Edoardo et al.
Reconstructing the Evolutionary History of Pinna nobilis: New Genetic Signals from the Past of a

Species on the Brink of Extinction // Animals, 14 (2024), 1; 114, 31. doi: 10.3390/ani14010114

Participations in congresses:

Ankon,Pavel; Kružić,Petar; Gračan,Romana
Dinamika morskih toplinskih valova na različitim dubinama u istočnom Jadranu (202.-2023.) // Zbornik sažetaka 15. hrvatskog biološkog kongresa / Bosak, Sunčica; Gračan, Romana; Korač, Petra (ur.).
Zagreb: Hrvatsko biološko društvo, 2025. str. 101-102

Gračan, Romana; Ankon, Pavel; Kružić, Petar
Histopatološki pokazatelji okolišnog stresa u dvije gorgonije u Jadranu // Zbornik sažetaka 15. hrvatskog biološkog kongresa / Bosak, Sunčica; Gračan, Romana; Korač, Petra (ur.).
Zagreb: Hrvatsko biološko društvo, 2025. str. 151-152

Kružić, Petar; Guić, Rita; Lipej, Lovrenc; Mavrič, Borut; Gračan, Romana; Ankon, Pavel
Greben koralja *Cladocora caespitosa* (Nacionalni park Mljet, Jadransko more) - 25 godina istraživanja // Zbornik sažetaka 15. hrvatskog biološkog kongresa / Bosak, Sunčica; Gračan, Romana; Korač, Petra (ur.).
Zagreb: Hrvatsko biološko društvo, 2025. str. 40-41

Trinajstić, Daria; Vladimir, Klara; Diana, Kegelj; Filipović, Gracija; Vacka, Majda; Batan, Marina; Ankon, Pavel; Čižmek, Hrvoje
Morski vrtić - vagilna epifauna morskih cvjetnica u Novigradskom i Karinskom moru // Zbornik sažetaka 15. hrvatskog biološkog kongresa / Bosak, Sunčica; Gračan, Romana; Korač, Petra (ur.).
Zagreb: Hrvatsko biološko društvo, 2025. str. 246-247

Burić, Vida; Ankon, Pavel; Đikić, Domagoj; Gračan, Romana; Landeka Jurčević, Irena; Beljan, Silvestar; Kružić, Petar
Impact of temperature stress on physiological and histological changes in the tissue of the Adriatic Sea corals (Hexacorallia, Anthozoa) // Knjiga sažetaka V. znanstveno-stručnog skupa Prilagodbe na klimatske promjene i očuvanje morskih ekosustava Jadranskog mora s međunarodnim sudjelovanjem, Zadar, 2024. / Čolak, Slavica; Šarić, Tomislav; Milošević, Rina (ur.).
Zadar: Sveučilište u Zadru, 2024. str. 109-110

Kružić, Petar; Gračan, Romana; Lipej, Lovrenc; Mavrič, Borut; Ankon, Pavel; Čačković, Andrea
Klimatske promjene i ugroženost crvene gorgonije (*Paramuricea clavata* (Risso, 1826)) u istočnom Jadranu // Knjiga sažetaka V. znanstveno-stručnog skupa Prilagodbe na klimatske promjene i očuvanje morskih ekosustava Jadranskog mora s međunarodnim sudjelovanjem, Zadar, 2024. / Čolak, Slavica; Šarić, Tomislav; Milošević, Rina (ur.).
Zadar: Sveučilište u Zadru, 2024. str. 37-38

Ankon, Pavel; Čačković, Andrea; Gračan, Romana; Orlić, Sandi; Kružić, Petar
What is the impact of changes in sea temperatures on corals in the Adriatic sea? // 8th Faculty of Science PhD Student Symposium: Book of Abstracts / Posarić, Laura; Gmižić, Daria; Ostojić, Tea et al. (ur.).
Zagreb: Faculty of Science, University of Zagreb, Zagreb, Croatia, 2024. str. 11-11

Kružić, Petar ; Pikelj, Kristina ; Bezik, Dolores ; Ankon, Pavel ; Carević, Dalibor
Procjena utjecaja nadohrane plaža na morski okoliš // Zbornik sažetaka 14. Hrvatskog biološkog kongresa.
Zagreb: Hrvatsko biološko društvo, 2022. str. 44-46

Kružić, Petar: Gračan, Romana ; Lipej, Lovrenc ; Mavrič, Borut ; Ankon, Pavel ; Čačković, Andrea ; Prohaska, Ana
Utjecaj marikulture na bentos uz otok Rava. dvadeset godina istraživanja // Zbornik sažetaka 14. hrvatskog biološkog kongresa s međunarodnim sudjelovanjem = Book of abstracts of the 14th Croatian biological congress with International Participation.
Zagreb: Hrvatsko biološko društvo, 2022. str. 43-44

Čačković, Andrea ; Ankon, Pavel ; Kružić, Petar ; Orlić, Sandi
Relationship status: it's complicated - the love story of corals and microbes // Zbornik sažetaka 14. hrvatskog biološkog kongresa = Book of abstracts of the 14th Croatian biological congress.
Zagreb: Hrvatsko biološko društvo, 2022. str. 152-153

Kružić, Petar ; Gračan, Romana ; Ankon, Pavel ; Kovačev, Agata
Stanje populacija crvenog koralja u istočnom dijelu jadranskog mora // Zbornik sažetaka 14. Hrvatskog biološkog kongresa.
Zagreb: Hrvatsko biološko društvo, 2022. str. 34-35

Ankon, Pavel ; Guić, Rita ; Kružić, Petar ; Gračan, Romana
Sos s Mljeta – hoćemo li ostati bez najvećeg koraljnog grebena u Sredozemnom moru? // Zbornik sažetaka 14. Hrvatskog biološkog kongresa.
Zagreb: Hrvatsko biološko društvo, 2022. str. 190-191

Kružić, Petar ; Gračan, Romana ; Lipej, Lovrenc ; Mavrič, Borut ; Ankon, Pavel ; Čačković, Andrea
Klimatske promjene i stanje crvene gorgonije (*Paramuricea clavata* (Risso, 1826)) u zaštićenim područjima istočnog Jadrana // Zbornik sažetaka 14. hrvatskog biološkog kongresa s međunarodnim sudjelovanjem.
Zagreb: Hrvatsko biološko društvo, 2022. str. 42-43

Kružić, Petar ; Ankon, Pavel ; Gračan, Romana
Depth distribution of the invasive alga *Caulerpa cylindracea* sonder in the marine protected areas in

the eastern Adriatic sea // 4. Hrvatski simpozij o invazivnim vrstama s međunarodnim sudjelovanjem.
Zagreb: Hrvatsko ekološko društvo, 2021. str. 92-92

Čižmek, Hrvoje; Ankon, Pavel
Gustoća i struktura populacije plemenite periske – Pinna nobilis u malom jezeru u NP Mljet // 13. Hrvatski biološki kongres s međunarodnim sudjelovanjem, zbornik sažetaka / Kružić, Petar (ur.).
Zagreb: Hrvatsko biološko društvo, 2018. str. 83-84

Kružić, Petar ; Rodić, Petra ; Popijač, Aleksandar ; Vučković, Karla ; Ankon, Pavel ; Matas, Vanja ; Cetinić, Katarina ; Sviben, Sonja ; Kovačev, Agata ; Moraj Nikola
Depth distribution of corals in the coralligenous of the eastern Adriatic Sea // 12. Hrvatski biološki kongres - zbornik sažetaka.
Zagreb: Hrvatsko biološko društvo, 2015. str. 204-205

Ostoić, Ivana; Bauk, Nataša; Ankon, Pavel; Hrubi, Hrvoje; Vohalski, Igor; Vohalski, Tanja; Senjanović, Ivan
Preliminarno istraživanje bentosa uz otočje Palagruža // 10. hrvatski biološki kongres s međunarodnim sudjelovanjem : zbornik sažetaka / Besendorfer, Višnja ; Kopjar, Nevenka ; Vidaković-Cifrek, Željka et al. (ur.).
Zagreb: Hrvatsko biološko društvo, 2009. str. 242-243